PhD Thesis

Chemical Reactions on the Surface of Quantum Dots

by

Satyapriya Bhandari

Department of Chemistry
Indian Institute of Technology Guwahati

June 2015

Chemical Reactions on the Surface of Quantum Dots

A thesis submitted by

Satyapriya Bhandari

Roll No. 10612225

to

Indian Institute of Technology Guwahati

for the award of the degree of

Doctor of Philosophy

Department of Chemistry

Indian Institute of Technology Guwahati
Guwahati – 781039
India

June 2015

Abstract

Understanding the chemistry of the surface of the zero-dimensional semiconductor nanocrystals - otherwise known as quantum dots (Qdots) - and their manipulation are critically important to achieve their desired applications, following optimization of their remarkable optical properties. However, little attention has been given to exploiting chemical reactions performed on the surface of the Qdots following their syntheses. It is expected that altering the structure of the surface or generating new species on the surface would provide a new way of achieving enhanced physicochemical properties of Qdots. The present thesis focuses mainly on two types of chemical reactions; one is ion-exchange reaction and the other one is complexation reaction involving the Qdots. We sincerely hope this will bring a new paradigm in terms of achieving the best of the optical properties of Qdots and thus improving their potential applications.

Specifically, the present thesis addresses the following issues.

(i) What is the role of surface ions in the emission properties of Qdots, which were synthesized at comparatively low temperatures?

(ii) How do the surface labile metal ions of Qdot react to form inorganic complexes with an external organic ligand and what are the consequent influences on the optical and thermal properties and solubility of Qdots following complexation reaction?

(iii) How will the Qdots - following complexation on their surface –be made useful for devices such as light emitting devices and in biological imaging over their independent constituents' precursors (Qdots and bare inorganic complexes)?

The present thesis is divided into seven chapters. Brief discussion of each chapter is given below.

Chapter 1 includes the introduction and the literature review. This will provide a brief and general idea about the Qdots, the importance of their surface followed by manipulation using various chemical means/reactions in order to achieve the desired

optical properties, for making them more advantageous in optoelectronic devices and biodiagnostic applications.

Chapter 2 describes the role of surface ions in the emission characteristics of the Qdots (synthesized at comparatively lower temperature) as probed from the results of a simple cation exchange reaction.

Chapter 3 reports the complexation reaction on the surface of a Qdot with an external organic ligand leading to formation of a new species - called herein as quantum dot complex (QDC) – which exhibited high quantum yield (QY), longer emission life time and extraordinary thermal stability in comparison to bare inorganic complexes.

Chapter 4 demonstrates a new, rapid and facile phase transfer process of hydrophobic Qdots from nonpolar to polar medium, following formation of light emitting inorganic complexes on the surface of Qdots out of the biphasic medium.

Chapter 5 reports the formation of a single component, redox active, thermally stable QDC nanocomposite - which exhibited independent double channel emissions and has excitation dependent tunability in chromaticity color coordinates.

Chapter 6 describes the fabrication of a new magnetofluorescent nanocomposite – composed of a super paramagnetic iron oxide nanoparticle (SPION) and QDC –which exhibited higher QY, photostability, stability in human blood serum and sufficient magnetism and also their magnet guided cell imaging application.

Chapter 7 contains an overview of the thesis and future prospects.

Statement

This thesis entitled "***Chemical Reactions on the Surface of Quantum Dots***" is a work of research and investigation carried out by me under the supervision of Dr. Arun Chattopadhyay, Professor, Department of Chemistry, Indian Institute of Technology Guwahati. This thesis has been submitted by me to the Department of Chemistry, Indian Institute of Technology Guwahati for the award of the degree of Doctor of Philosophy. I further declare that this work has not been submitted anywhere else for any degree, diploma, associateship or membership etc. of any Institute or University to the best of my knowledge.

_____

Satyapriya Bhandari
Department of Chemistry
IIT Guwahati,
Guwahati-781039, Assam
India
Date:
Place: Guwahati, Assam

Certificate

It is certified that the thesis entitled **"*Chemical Reactions on the Surface of Quantum Dots*"** being submitted to the Indian Institute of Technology Guwahati by Satyapriya Bhandari (Roll. No. 10612225) for the award of the degree of Doctor of Philosophy in Chemistry, is a bonafide record of research work carried out by him. The information and data reported by him are solely the results of his original findings. He has meticulously carried out the investigations and followed the guidelines of the laboratory. This work has not been submitted elsewhere for any degree or diploma.

_____

Arun Chattopadhyay
Thesis Supervisor
Professor,
Department of Chemistry,
IIT Guwahati,
Guwahati-781039, Assam,
India.
Date:
Place: Guwahati, Assam

Dedicated to my

Grandmother, Parents and Sister

Acknowledgements

I would like to express my deepest gratitude to the man, who not only introducing me to the glamorous world of Science but also helped in shaping my academic career with his invaluable guidance and expert advice. The man is none other than my PhD advisor Prof. Arun Chattopadhyay. I am blessed by GOD to have him as my guru and also feel very lucky to be a part of his vibrant research group. Thank you Sir.

I would like to thank my doctoral committee members for their valuable suggestions and comments regarding research works. Also, I would like to express my gratitude to all the faculty and staff members of Department of Chemistry, Centre for Nanotechnology and CIF for their support.

A special thanks goes to CSIR (New Delhi) for providing me the scholarship and CIF (IIT Guwahati) for allowing me to use the sophisticated instruments facility.

I would like to thank all my collaborators for their support and valuable discussions. I would also like to acknowledge all my past and present lab members for providing me a healthy and friendly atmosphere in the lab.

Next, I would like to acknowledge all of my friends (inside and outside IITG) for their constant support and care.

At last, I would like to thank my family members for their endless support and unconditional love and care.

Thanks for being in my life.

Satya

Table of Contents

Chapter 1

Introduction

"Everything starts from a dot"- Wassily Kandinsky, the famous early 20th century Russian artist who believed in the spiritual power of a "dot" in the canvas to start off great work of art.[1-2] Yes! The belief of Kandinsky is quite relevant today when the term "dot" - composed of zero-dimensional semiconductor materials with quantum confinement effect - appeared in the field of nanoscience and nanotechnology. From the time of their discovery to present era, the zero-dimensional semiconductor nanocrystals – otherwise known as quantum dots (Qdots) - continuously dominated the nanoscience research with their remarkable optical properties even though the various other nanostructured materials have been emerged. The tremendous optical value of Qdots has made significant impact in a variety of applications such as biological imaging, sensing and drug delivery, catalysis, solar cells and light emitting devices. Not only in the nanoscience, but also the usefulness of the Qdots has been extended from basic science to engineering stream. Till date, the Qdots have played a vital role across different disciplines of science and engineering and their contribution towards the progress of multidisciplinary science is really laudable.

1.1 Quantum Dots

1.1.1 The Definition

A Qdot is a colloidal semiconductor nanocrystallite (size of 1-10 nm) that confines the motion of the bound pairs of the charge carriers (conduction band electrons and valence band holes) in all three spatial directions.[3-7] In other words, the defining features of Qdot are:

(i) Qdot is a zero dimensional semiconductor nanostructure.

(ii) Qdots have sizes in the range of 1-10 nm.

(iii) Specifically, the motion of the excitons (i.e. the bound pairs of conduction band electrons and valence band holes) is confined in Qdot.

These three distinct features of Qdots make them to exhibit unique optical properties -which are absent in the bulk form of the material. The properties results in their application potential in the fields ranging from optoelectronic devices to biological purposes.

1.1.2 The History

In 1981, the Russian physicist Alexey Ekimov discovered semiconductor nanocrystals in a glass matrix for the first time.[5] Then, in 1985, Louis E. Brus first discovered cadmium sulphide (CdS) semiconductor nanocrystals in colloidal dispersion.[6] But, the true beginning of the word "quantum dot" happened in 1988 following the observation of discrete electronic states of quantum dots by Mark Reed.[7]

1.1.3 The Quantum Confinement Effect

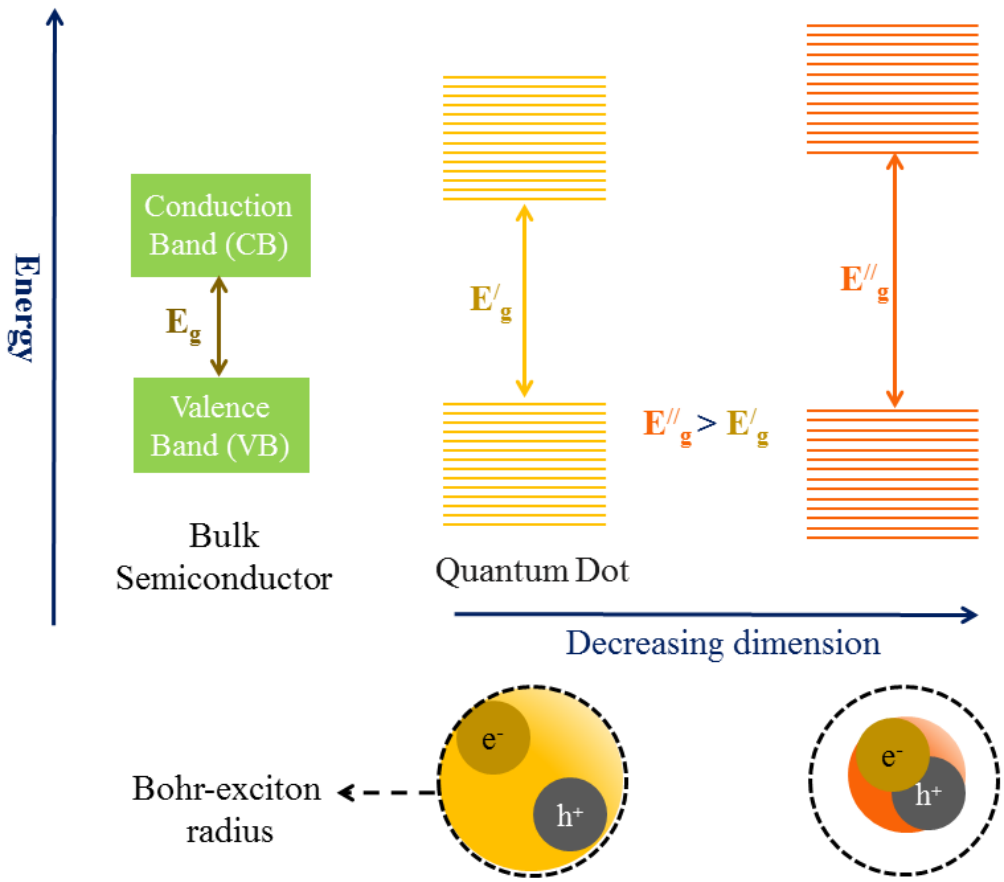

Figure 1.1. Schematic representation of quantum confinement effect resulting in the discretization of the energy levels based on the reduced dimension of the bulk semiconductor.

The quantum confinement effect arises when the size of the bulk semiconductor materials is reduced into nanometer regime and is comparable with the excitonic Bohr radius of the materials.[4, 8-11] This results in the discretization of the energy levels and restriction in the motion of the bound pair of electron and hole (otherwise known as exciton) in all three spatial dimensions of the nanocrystal upon photo-irradiation (Figure 1.1). The exciton in a Qdot behaves like a particle in 1D box (of H-atom) where the degree of confinement depends upon the spacing of the energy levels. [4, 8-11] In Qdot the degree of confinement of exciton increases as the size of the Qdot is decreased and thus increase in their band gap (the energy gap between the valence and conduction bands; Figure 1.1). Due to the nature of the Qdot, they are often called as "artificial atoms". The electronic structure of the Qdot is neither like a band of bulk semiconductor material nor like a bond of a molecule, and is intermediate between bands and bonds (Figure 1.1). The quantum confinement effect of Qdot based on the size makes them to exhibit extraordinary optical properties and opens up a new avenue to tune the electronic structure by size to get desired optical characteristics needed for specific purpose of their use.

1.1.4 Types

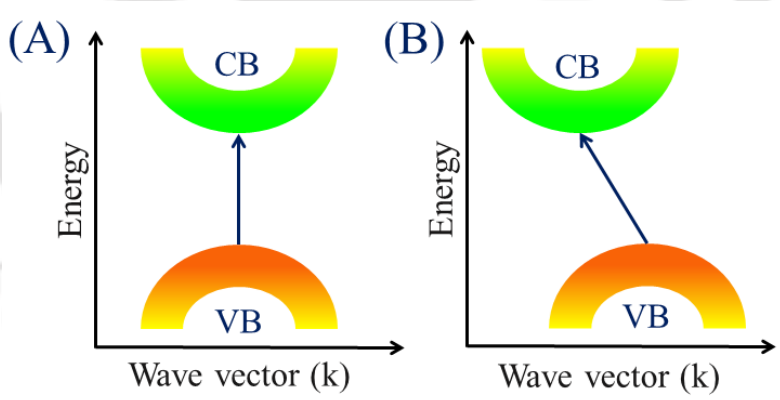

Figure 1.2. Schematic representation of the electronic band structure of (A) direct and (B) indirect semiconductors at their lowest transitions. Where CB and VB stands for conduction band and valence band respectively.

There are two types of Qdots – (i) direct and (ii) indirect band gap - depending upon the nature of the wave vector (*k*) during the lowest transition of electron from valence band to conduction upon excitation.[3] Schematic representation shows (Figure 1.2) how the electronic transition affects the wave vector (k) to categorize the Qdots.

Wave Vector (k) is defined as $k = \frac{2\pi}{\lambda}$ (considering free electron model) and thus in the Schrodinger equation; $E = \frac{h^2 k^2}{8\pi^2 m}$, where E and m are the energy and mass of an electron and h is the Planck's constant .[3]

If there is no change in the value of wave vector, then Qdots can be called as direct band gap Qdots, while indirect band gap Qdots have change in their wave vector parameter during electronic transition.[3] For example, the combinations of group III-V and II-VI of the periodic table lead to formation of direct band gap semiconductors; among them GaN, InP, ZnO, ZnS, CdS, CdSe, HgTe are well known. On the other hand, Si and Ge are known as indirect band gap Qdots.

1.1.5 The Unique Optical Properties Qdots and Their Tailoring

The most important feature of the Qdots is their unique and tunable optical properties. The tunability in their optical properties relies on three important parameters – (i) size; (ii) dopant impurity and (iii) the surface. These three controlling factors not only tune the optical features especially emission of Qdots but also make them appropriate to have their desired applications in the field ranging from biodiagnostics to optoelectronics. How the three parameters affect the emission of Qdot are described as follows.

1.1.5.1 Size

The "size" of the Qdot plays a vital role to achieve the tunability in their band gap - arising due to the quantum confinement effect - which results different optical absorption and emission properties from of a Qdot composed of the same material.[3, 12-21] As is clear from "Brus equation" that band gap energy of the Qdot is inversely proportional to the size of the Qdot, hence the size can effectively tune the band gap energy and thus their optical characteristics.[3, 21] In other words, as the size of the Qdot increases, the energy of the band gap decreases and the emission from the Qdot becomes redder, while blue emission from Qdot arises when the size of the Qdot becomes smaller. For example, the different optical properties like emission color and absorbance of the CdSe Qdots can be observed by varying their size (Figure 1.3 A)[12]

and similarly with the change in the size, different photoluminescence quantum yield (PLQY) of PbS Qdots can also be achieved (Figure 1.3 B).[15]

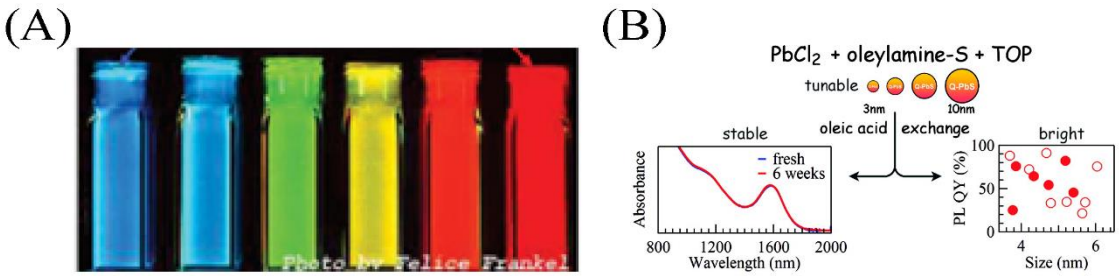

Figure 1.3. (A) Fluorescence image of Qdots as a function of size (left to right based on increasing size of Qdots). Reprinted with permission from Reference [12]. Copyright *J. Phys. Chem. B* 1997 American Chemical Society) and **(B)** schematic representation of PLQY and colloidal stability of the PbS Qdots with the variation of their size (Reprinted with permission from Reference [15]. Copyright *ACS Nano* 2011 American Chemical Society).

1.1.5.2 Incorporation of Impurity

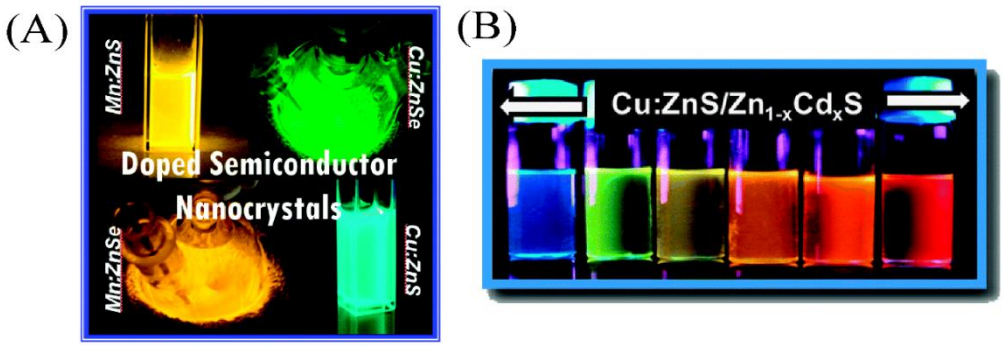

Figure 1.4. Schematic representation of **(A)** different emission colors of ZnE (where E= S or Se) Qdots resulted followed by doping of Mn^{2+} or Cu^{2+} ions (Reprinted with permission from Reference [24]. Copyright *J. Phys. Chem. Lett.* 2010 American Chemical Society) and **(B)** doping of Cu in the alloyed Qdots such as $ZnS/Zn_xCd_{1-x}S$ core/shell leading to different emission color over a wide range of wavelength (Reprinted with permission from Reference [25]. Copyright *J. Am. Chem. Soc.* 2011 American Chemical Society).

The incorporation of atomic impurities (otherwise known as doping) into Qdot provides a new strategy to control their optical, magnetic and electrical properties and thus their usefulness for various applications.[22-37] To dope impurities in the lattice of Qdot, Mn and Cu metal ions have been extensively used and the resulted doped Qdots have become advanced materials compared to undoped Qdots for biomedical labeling and spintronic. For example, doping of transition metal ions like Mn^{2+} and Cu^{2+} into the crystal lattice of group II-VI Qdots such as ZnS, ZnSe and $ZnS/Zn_xCd_{1-x}S$ resulted

intense photoluminescence emission over a wide range of wavelength (Figure 1.4 A-B).[24-25]

1.1.5.3 Surface

The "surface" of the Qdots is critically important in order to have control in their emission properties, without altering their size and shape.[38-70] Earlier studies reported that at small length scale of Qdots, the ratio of surface atoms to core atoms increases and that resulted in the dominating nature of the surface atoms for the entire nanocrystal.[38] Importantly, the chemical nature of the surface atoms is different from the core ones because of the termination of the lattice structure and consequently those (surface atoms) have unsaturated coordination - which are known as "dangling bonds". The chemical reactivity of the surface of Qdots is mainly dependent on the nature of the unbonded orbitals (dangling bonds) present on the surface and their coordinating behavior with different organic, inorganic or bio molecules to obtain saturation in terms of coordination – that is called as "surface passivation". Surface passivation of the dangling bonds can be achieved through different strategies; among them the formation of inorganic shell and reaction with organic or bio molecules are well known. Through the surface passivation strategies, one can have control over the unique optical properties of Qdots even after their synthesis and can specifically modify the emission properties like quantum yield, emission maxima etc. for the desired application potential.

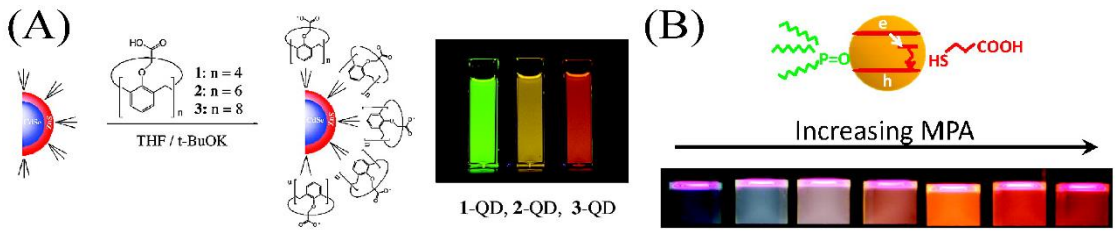

Figure 1.5. Schematic representation of **(A)** the control of the optical properties of Qdots by surface coating with calix[*n*]arene carboxylic acids (Reprinted with permission from Reference [45]. Copyright *J. Am. Chem. Soc.* 2006 American Chemical Society) and **(B)** MPA assisted surface modification of CdSe Qdots and tuning their emission color based on the concentration of MPA (Reprinted with permission from Reference [46]. Copyright *Langmuir* 2010 American Chemical Society).

For example, the emission color of the CdSe/ZnS can be controlled through the modification of their surface by varying the oligomer size of the Calix[*n*]arene

carboxylic acids by replacing the original ligand (Figure 1.5 A).[45] On the other hand, ligand exchange of trioctylphosphineoxide/dodecylamine-capped CdSe Qdots with 3-mercaptopropionic acid (MPA) resulted in their different emission colors, depending upon the concentration of MPA (Figure 1.5 B).[46]

1.1.6 The Applications

The advantageous optical properties especially exceptional resistance to photo bleaching and high quantum efficiency of colloidal Qdots – in addition to their versatile surface functionality - make them ideal candidates for replacement of traditional organic dyes in the field of biomedical imaging, detection, sensing and theranostics.[72-79] On the other hand, the recent advances in the combination of Qdots with photovoltaic and light emitting devices have created enormous excitement and developed new devices which can be advantageous in terms of their cost and uses.[80-82] Apart from their biological and optoelectronic uses, the Qdots can also be used in catalysis of chemical reaction.[83-84]

1.2 Chemical Functionalization of Qdots

While innumerable aspects of Qdots exist for the biomedical and optoelectronic applications, the chief necessity is the functionalization of their surface to make them either biologically amenable or suitable for fabrication processes.[85-133] In other words, functionalization of the surface of the Qdots is the prime condition to achieve the diversity in their uses. The term “surface functionalization” is generally described for the process through which the outer layer of the Qdots is being modified using various chemical means, either during or following their synthesis, while the core structure remains unaltered. Importantly, the functionalization of the surface of the Qdots provides several advantages in terms of their physical and chemical properties through reduction of surface traps (or defects), prevention of agglomeration, oxidation, leaching of ions and photochemical degradation, enhanced solubility and stability. These are all about the functionalization of the surface of Qdots during synthesis. On the other hand, following synthesis Qdots can also be modified through the surface re-functionalization to have more advantageous optical characteristics like enhancement of the quantum yield, changes in emission color and other parameters - in addition to solving the issue of solubility of Qdots for their use in biological activities and device fabrication

procedure. In this regard, several strategies are well known to functionalize the surface of the Qdots following their synthesis and make them appropriate for their specific utilization. A brief discussion of these strategies is given below.

1.2.1 Ligand Exchange

The replacement of the existing ligand of the Qdots following their synthesis with an external ligand - that provides Qdots with superior properties such as solubility and improved optical properties especially quantum efficiency – is termed as the ligand exchange strategy.[85-99] Importantly, the surface ligands govern physicochemical properties of Qdots and thus their desired performances under specific applications. For instance, the long hydrocarbon chains of the ligand present on the surface of the Qdots make hydrophobic Qdots suitable for device fabrication, while their biological uses are restricted due to their insolubility in aqueous medium. But the same hydrophobic Qdots following ligand exchange with hydrophilic ligands can have their biological activities without any change in their morphology and other parameters. Moreover, the modified Qdots through proper ligand exchange have been particularly useful for probing cellular pH, as markers of diseases and as imaging probe in targeted drug delivery. Therefore, the ligand exchange has become an important and popular strategy for the alteration of the properties of the Qdots and thus for their specific applications.

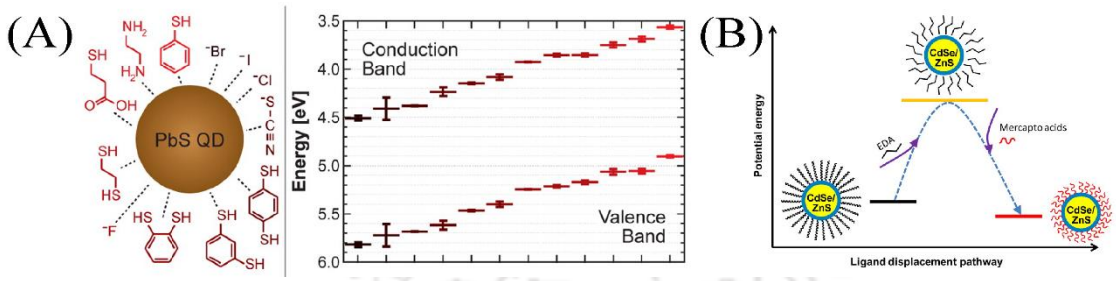

Figure 1.6. Schematic representation of **(A)** the energy level modification in lead sulfide Qdot through ligand exchange. (Reprinted with permission from Reference [89]. Copyright *ACS Nano* 2014 American Chemical Society) and **(B)** ethylenediamine mediated ligand exchange and phase transfer of hydrophobic Qdots following the preservation of their original photoluminescence (Reprinted with permission from Reference [90]. Copyright *Chem. Mater.* 2013 American Chemical Society).

For example, ligand exchange on lead sulphide (PbS) Qdots led to shifts in their band gap and thus their performance optimization in optoelectronic devices (Figure 1.6 A)[89]

while on the other hand, the transfer of olephilic CdSe/ZnS Qdots into water followed by preservation of their original photoluminescence can also be possible through ethylene diamine assisted ligand exchange (Figure 1.6 B).[90]

1.2.2 Conjugate Formation

Apart from the ligand exchange strategy, there is another way to modify the surface of the Qdots in which no replacement of existing stabilizer is required. This can be achieved by conjugating different types of chemical or biological molecules based on their mutual interactions with the existing stabilizer.[100-108] Earlier studies demonstrated that the specific biomolecules such as DNA, peptides, antibodies and proteins have the ability to conjugate with the organic surface of the Qdots and make them water soluble to have the promising applications in cellular imaging, assay, labelling, sensing heavier metal ions and pH, detection of diseases, and as efficient fluorescence resonance energy transfer (FRET) donors. Not only that, conjugation of the Qdots with a molecule based on the FRET mechanism also provides a new aspect toward the development of their utilities in the solar cells and light emitting devices.

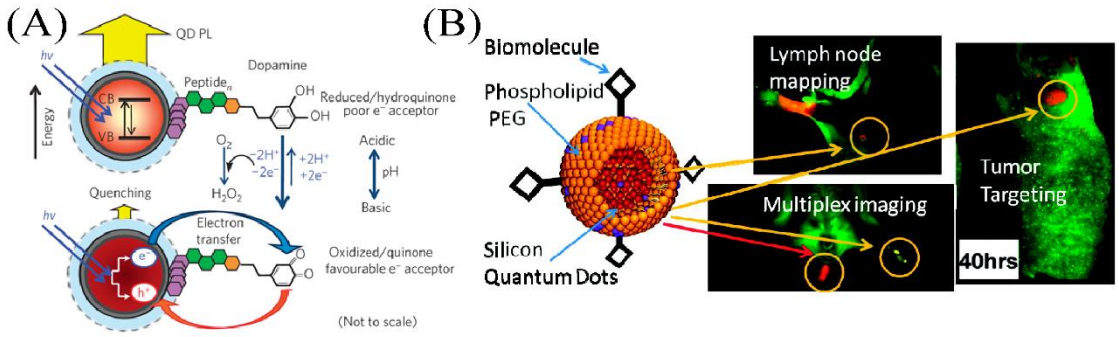

Figure 1.7. Schematic representation of **(A)** Qdot/dopamine bioconjugates act as redox coupled assemblies for *in vitro* and intracellular pH sensing (Reprinted with permission from Reference [104]. Copyright *Nat. Mater*. 2010 Nature publishing group) and **(B)** silicon (Si) Qdots following bioconjugation with PEG and phospholipid for i*n vivo* targeted cancer imaging, sentinel lymph node mapping and multi-channel imaging (Reprinted with permission from Reference [105]. Copyright *ACS Nano* 2011 American Chemical Society).

For example, the Qdot bioconjugates like CdSe-ZnS/dopamine and PEGylated (polyethylene glycolylated), phospholipid conjugated and micelle encapsulated Si Qdots can be used as *in vitro* and intracellular pH sensor (Figure 1.7 A)[104] and in *in Vivo* targeted cancer imaging (along with sentinel lymph node mapping and multi-channel imaging; Figure 1.7 B), respectively.[105]

1.2.3 Other strategies

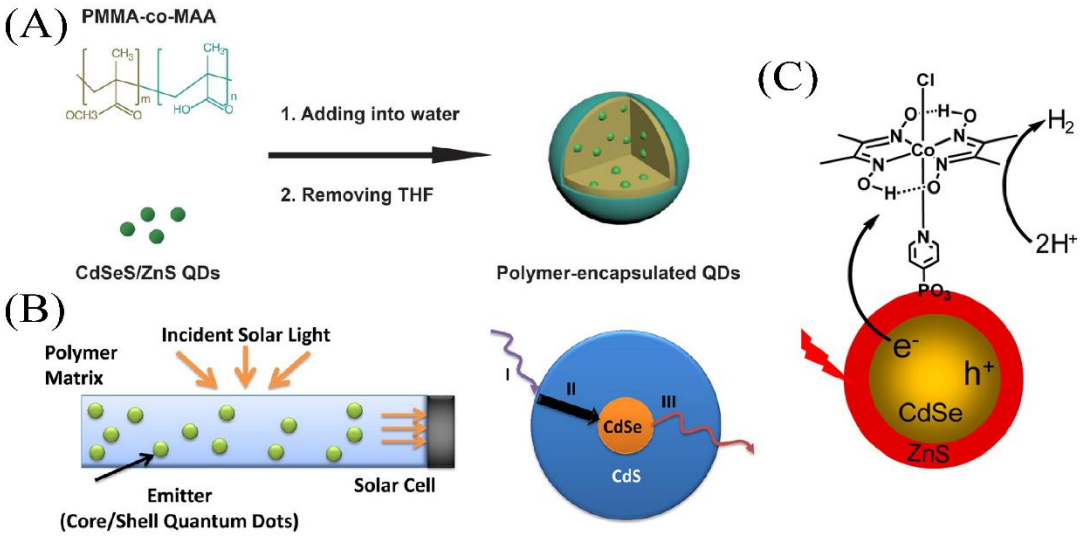

Figure 1.8. Schematic representation of **(A)** polymer encapsulation of CdSeS/ZnS Qdots making them extremely high bright for two-photon cellular and deep-tissue imaging (Reprinted with permission from Reference [131]. Copyright *Sci. Rep.* 2014 Nature publishing group); **(B)** CdSe/CdS core/shell Qdot based luminescent solar concentrators with reduced reabsorption and enhanced efficiency (Reprinted with permission from Reference [132]. Copyright *Nano Letter* 2014 American Chemical Society) and **(C)** CdSe/ZnS Qdot - cobaloxime hybrid based on energy transfer process for efficient hydrogen production (Reprinted with permission from Reference [133]. Copyright *J. Am. Chem. Soc.* 2012 American Chemical Society).

Cross linking the outer organic surface of the Qdots by using chemical means like amphilic polymers not only functionalize the Qdots but also provides extraordinary chemical stability to them.[109-112] Encapsulation of the small sized Qdots into larger size particles like silica, phospholipid micelles and liposomes without exchange of their outer surface can also lead to the changes in their optical properties and solubility.[113-115] The process like encapsulation of Qdots in silica matrix or coating the Qdots with polymer have become advantageous strategies for solving the problem related to their toxicity issue.[109-115] On the other hand, formation of the shell to the core Qdots has gained popularity in terms of their surface functionalization and their consequent changes in the optical properties, stability and toxicity.[116-119] Interestingly, the ability of the Qdots to participate in various energy transfer processes with light harvesting proteins, organic dyes, redox active metal complexes brings new interest towards the development of the bio sensing and light emitting applications of Qdots.[120-125] All the above described strategies of the chemical functionalization of the surface of Qdots afforded a versatile dimension for the applications of the Qdots.[109-133] For example,

encapsulation of CdSeS/ZnS Qdots in the polymer matrix of poly(methyl methacrylate-co-methacrylic acid) (PMMA-co-MAA) resulted high QY of the Qdots and made them suitable for two-photon cellular and deep-tissue imaging (Figure 1.8 A).[131] Similarly, the enhancement of the QY – can also be possible through formation of core/shell Qdots – with better efficacy of the solar cells (Figure 1.8 B).[132] On the other hand, the hybrid system, based on the mutual photo driven charge transfer of CdSe/ZnS Qdot and cobaloxime complex, can function as catalyst for efficient hydrogen production (Figure 1.8 C).[133]

1.3 Chemical Reactions

Chemical reactions - the process through which reactants interact to form new products - happens every moment in the world around us.[134] From the growing nature of our body to our daily life in the food that we eat, in the clothes that we wear and the air that we breathe etc. it's all about the chemical reactions and literally one cannot think about his/her day successful without having a single chemical reaction. On the other hand, the beauty of materials (especially Qdots) at their small length scale has also emerged as a gift for the development of the human society in terms of their applications in disease diagnostics, to cure dangerous disease like cancer, in solar cells and light emitting devices. Therefore, the aspect of chemical reactions on the surface of small materials like Qdots has become an important issue in order to have much more advantageous effect out of their combination. The present thesis describes the chemical reactions mainly based on ion exchange and complexation reactions on the surface of Qdots and also envisions the advantages of having chemical reactions on the surface of Qdots. Hope this will bring a newer avenue towards the development of desired applications of Qdots and may initiate new chemistry for future research activities. The following reactions have been chosen to describe the consequences of the "Chemical Reactions on the Surface of Qdots."

1.3.1 Ion Exchange Reaction

The ion exchange reaction - the process involving replacement of one or more ionic parts between two chemical substances - plays a vital role in the analytical and industrial purposes such as purification of water, chemical staining and sensing.[135-145] Importantly, when the ion exchange reaction especially cation exchange occurs with

particles like Qdots, it not only offers the possibility to tune the optical characteristics of the Qdots by preserving their anionic lattice but also provides a promising way for new and high-quality Qdot synthesis, device fabrication, and chemical sensing. The exchange of cations at the nanoscale leads to the unique attributes like rapid kinetics involving Qdots (compared to their bulk form) at room temperature and modulation of reactivity following the control of size, shape and surface of the Qdots. These features make the cation exchange reaction part of a convenient toolkit for the development of next generation photonic, optoelectronic and catalytic applications of the Qdots following modification of their surface composition and morphology. Further, the stoichiometric control of the ions - which may not be readily accessible during their synthesis - enables the formation of the Qdots with desired compositions, morphology and crystal phase. Hence, the better understanding and control of the surface of the Qdots based on simple cation exchange route will open up a new path for the specific applications in biological uses and device fabrications. Further study in this area should continue to synthesize a library of Qdots and mechanistic understanding of the role of the surface (mostly the surface ions) in the optical properties of the Qdots following their synthesis. To date, various examples of cation exchange reactions of Qdots are well known and some of the examples are discussed below.

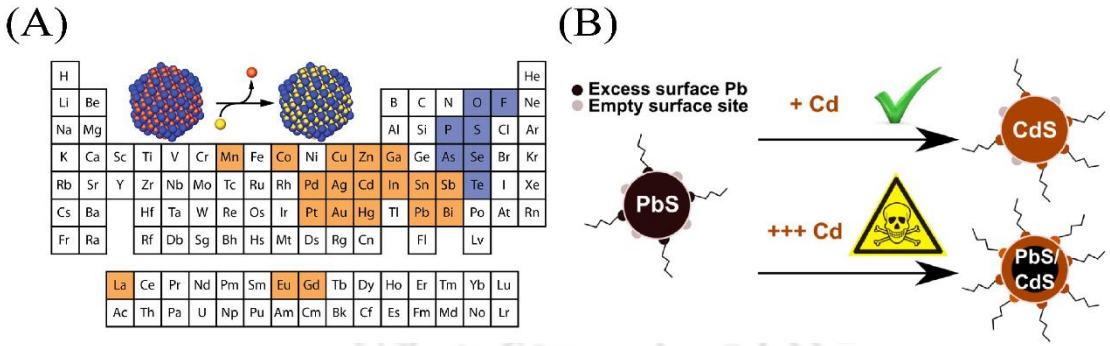

Figure 1.9. Schematic representation of **(A)** cation exchange reaction for the synthesis of various Qdots. (Reprinted with permission from Reference [136] Copyright *J. Phys. Chem. C* 2013 American Chemical Society) and **(B)** chemical transformation of PbS to CdS Qdots based on the cation exchange of Pb^{2+} of PbS Qdots with external Cd^{2+} ions (Reprinted with permission from Reference [143]. Copyright *ACS Nano* 2014 American Chemical Society).

For example, post-synthetic transformation of Qdots through cation exchange reactions has become a robust way to achieve desired Qdots for the development of the next generation photonic, optoelectronic, and catalytic applications (Figure 1.9 A).[136]

On the other hand, the complete transformation of PbS to CdS Qdots can be made followed by understanding their concentration dependent cation exchange behavior (Figure 1.9 B).[143]

1.3.1.1 Cation exchange resin Bead (CB)

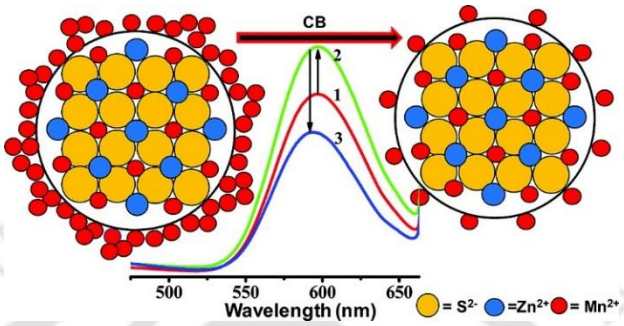

Figure 1.10. Schematic representation of the engineering the surface of Mn^{2+}-Doped ZnS Qdots and thus by their optical properties alteration using ion-exchange resins (Reprinted with permission from Reference [146]. Copyright *Langmuir* 2012 American Chemical Society).

The acid activated form of the commercially available Amberlite IR 120 Na resin bead – which composed of sulfonated polystyrene anionic skeleton and exchangeable cationic part – is called herein as cation exchange resin bead (CB). Apart from the use of the industrial water treatment applications, CB also has additional activities in scientific research due to their different binding affinity of the metal ions of the periodic table. In other words, CBs have different affinity towards metal ions of same charge and that make them suitable for their use to tune the optical characteristics of Qdots following selective engineering of the surface metal ions. Recently, CB was used to tune the emission characteristics especially the quantum yield of the Mn^{2+} doped ZnS Qdots following their synthesis (Figure 1.10).[146] Hence it seems a challenging task to describe the role of the surface ions of Qdots, synthesized at comparatively lower temperature in non-aqueous medium, based on their optical changes following by preferential removal of the surface ions with the help of CB.

1.3.2 Complexation Reaction

The complexation reaction is the process through which ligands react with metal to form coordination complexes. In the late nineteenth century, the famous inorganic chemist Alfred Warner first discovered the coordination complex "hexamminecobalt(III) chloride" using complexation reaction.[147] From the discovery of

the first metal complex to recent times, the complexation reaction holds the key of the success of the field of inorganic chemistry and continuously intrigued researcher with their diversities in applications and simplicities in formation. However, there is few or no reports on the study of the complexation reaction with particles at relatively small length scale like Qdots. Earlier studies reported that the inorganic complexes like metal chalcogenide complexes (MCCs) - can serve as convenient stabilizer for Qdots followed by replacing the existing ligands of the Qdots.[148-151] Interestingly, the MCCs such as AsS_3^{3-}, $Sn_2S_6^{4-}$, $SnTe_4^{4-}$ etc. provide colloidal stabilization to Qdots and enable strong electronic coupling in their solid form – which is important for solid state device applications of Qdots (Figure 1.11 A-B).[148, 151] Hence, researchers have used as-synthesized inorganic complexes as stabilizer of the Qdots following exchange reactions.

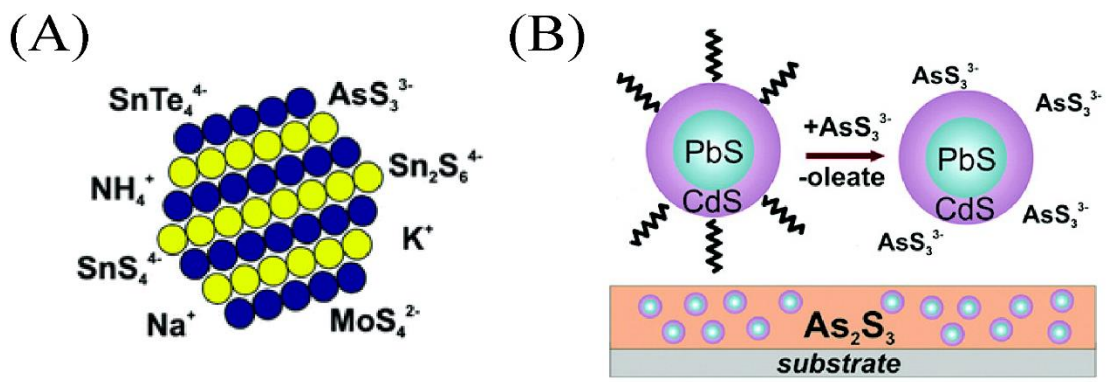

Figure 1.11. Schematic representation of **(A)** molecular metal chalcogenide (MCC) complexes acts as capping agents for expanding the chemical versatility of Qdots (Reprinted with permission from Reference [148]. Copyright *J. Am. Chem. Soc.* 2010 American Chemical Society) and **(B)** inorganically functionalized PbS–CdS Qdots and their integration into amorphous chalcogenide glass (Reprinted with permission from Reference [151]. Copyright *J. Am. Chem. Soc.* 2012 American Chemical Society).

But none of the reports have describe the formation of inorganic complexes on the surface of Qdots following complexation reaction - between Qdot and external organic ligand – which is far different and unique with regard to simple chelation of the ligand to the surface of Qdots. The formation and attachment of the inorganic complexes on the surface of Qdots completely depends upon the nature of the ligand and for that purpose 8-hydroxyquinoline, has been selectively chosen to perform complexation on the surface of Qdots (mainly ZnS and CdS lattice), the details of which are described below.

1.3.2.1 8-hydroxyquinoline (HQ)

8-hydroxyquinoline (HQ; otherwise known as oxine) is an extraordinary complexing agent, a bi-dentate ligand, occupies a unique place in analytical and inorganic chemistry as the second most important chelating ligand after ethylenediaminetetraacetic acid (EDTA) and due to its facile formation of stable metal complexes with most of the metal ions of the periodic table.[152-159] Upon chelation with metal ions like Al^{3+}, Zn^{2+} and Cd^{2+}, HQ forms highly stable electroluminescent metal quinolate complexes (AlQ_3, ZnQ_2 and CdQ_2) which have importance in prototypical electron transport and organic light emitting diodes (OLEDs). For example, AlQ_3 has been extensively used as a primary emitting material for OLED devices, while in recent times, their drawback like restricted performance of OLED at comparatively lower operating voltage has also been solved by using their Zn^{2+} (i.e ZnQ_2) analogue instead of Al. On the other hand, the derivatives of HQ also has diverse pharmacological and biological activities such as being antiseptic, antimicrobial, antibacterial and anticancer agents. However, the formation of the metal quinolate complexes – which is very different form simple chelation[95-99] - with the labile metal ions present over the surface of the Qdots is not yet fully understood. The present thesis will describe the formation of the metal quinolate complexes on the surface of Qdots and the consequences in terms of the changes in optical characteristics and solubility of Qdots. Further, the utilization of having the metal quinolate complexes on the surface of Qdots is also demonstrated following their use as phase transfer agents, for creating a double channel emitting platform of white light generation and as an excellent bio imaging probe – in combination with super paramagnetic iron oxide nanoparticle (SPION) - for targeted cellular applications. Finally, it is hoped that the concept "complexation on the surface of Qdots" will bring a new paradigm in the applications of the Qdots and may initiate a new chemistry for better understanding of the surface of the Qdots.

Chapter 2

Role of Surface Ion in the Emission Characteristics of Quantum Dots

Oleate capped Zn doped CdS ($Zn_xCd_{1-x}S$) colloidal nanocrystal exhibited dual emission, which was tunable by selective removal of the cations, over its surface and in its immediate vicinity, using cation exchange resin beads (CB). The near band gap emission disappeared more rapidly in comparison to deep level emission, the peak wavelength of which shifted by as much as 25 nm, while both exhibited increasingly faster decay.

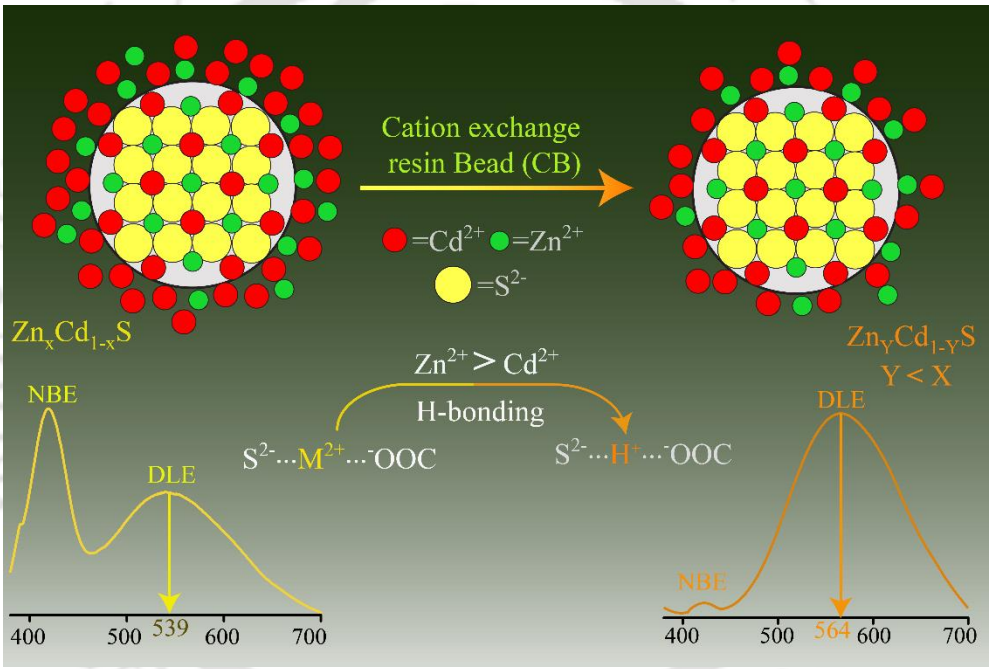

***[Bhandari et al. *RSC Adv.*, 2013, *3*, 2885-2888] - Reproduced by permission of The Royal Society of Chemistry. http://pubs.rsc.org/en/Content/ArticleLanding/2013/RA/c2ra22447j#!divAbstract**

2.1. Experimental Section

2.1.1. Materials. Cadmium acetate dihydrate ($Cd(CH3COO)_2.2H_2O$, 99%), zinc acetate dihydrate ($Zn(CH_3COO)_2.2H_2O$, 99%), sodium sulphide ($Na_2S.9H_2O$, 58%), sodium oleate ($C_{18}H_{33}O_2Na$), amberlite IR-120 cation exchange resin beads (CB), hydrochloric acid, quinine sulphate, sulphuric acid and hexane were of analytical grade and used without further purification. They were purchased from the Merck Limited, Mumbai, India. Mili-Q grade water was used for the synthesis.

2.1.2. Synthesis of $Zn_xCd_{1-x}S$ Nanocrystals. For a typical preparation of $Zn_xCd_{1-x}S$ nanocrystals (NCs), cadmium acetate (5.0 mM) followed by zinc acetate (2.5 mM) were added to the 50 mL Mili-Q grade water under constant stirring and heating. After 5 min, 5.0 mM sodium oleate was added to the mixture upon which the solution became milky white. The milky white solution turned into greenish yellow when sodium sulphide (5.0 mM) was added to it, 5 minutes after sodium oleate addition. Since it is already reported that the distribution, growth kinetics and the composition of Zn and Cd in the resulting $Zn_XCd_{1-X}S$ NCs are sensitive to feed Zn-Cd-S ratios[160], the ratio of Zn, Cd and S was fixed at 1:2:2, for better post synthesis fluorescence tuning of the NCs. The whole mixture was allowed to reflux for 5-6 hours (to avoid discontinuous growth) [161] at 100 ^{0}C with constant stirring. After half an hour, greenish yellow solid particles were found to be floating over the aqueous solution. After 6 hours of reflux, the resulting greenish yellow mixture was centrifuged at 25000 rpm for 15 min and the pellet was thoroughly washed with Mili-Q water. This was followed by ultra-sonication of the redispersion to remove unreacted salts. The mixture was centrifuged again for 15 minutes. The pellet was dried under IR lamp and then kept at room temperature. To monitor the spectroscopic properties of the NCs, dispersions of the NCs were prepared in hexane.[162-163]

2.1.3. Preparation of activated Cation exchange Resin Beads (CB). To activate the polymeric resin beads, 3.0 g of Amberlite IR-120 cation exchange resin beads (sulfonated polystyrene divinylbenzene co-polymer) was first washed with Mili-Q grade water and then added to a 15.0 mL of 3.0 M HCl and was kept for 3 h. After activation, resin beads were washed with copious amount of Mili Q water to remove the excess HCl and washing was continued until the pH of the activated resin beads (CB) medium was 6-7. The beads were then dried under IR lamp for further use.[164]

2.1.4. Sample preparation for Experimental measurements. $Zn_xCd_{1-x}S$ NCs dispersion prepared in hexane (1.0mg/10.0mL) was used for (UV-Vis, photoluminescence, FTIR, time-resolved photoluminescence and atomic absorption) spectroscopic as well as TEM measurement. For spectroscopic and TEM measurements, different amounts of CB were added to 10.0 mL of hexane dispersion of NCs. Solid NCs were used to measure XRD, FTIR. For quantum yield measurement, reference quinine sulphate solution was prepared in 0.1 M H_2SO_4 solution.[165] For preparing atomic absorption spectroscopic (AAS) measurement samples, dispersions of Qdots and different amount of CB treated Qdots (after removing CB) in hexane, were evaporated over hot plate (> 80°C) until the mixture was completely dried. After that 30.0 μL of 12 M HCl was added to each of the dried samples followed by sonication and finally the volume of the each HCl added sample was adjusted to 10.0 mL with Milli-Q water. Then, AAS measurements were performed for the samples using standard solutions of cadmium acetate and zinc acetate salts as the references.

2.2. Results and Discussion

2.2.1. Characterization of $Zn_xCd_{1-x}S$ Qdots.

The powder X-ray diffraction (XRD) pattern of the precipitate exhibited three prominent peaks at 26.9°, 44.8° and 51.9° (Figure 2.1.A). The three characteristic peaks are due to (002), (110) and (112) planes of the hexagonal wurtzite CdS NCs.[166] Transmission electron microscopy (TEM) images of the sample (Figure 2.1.B and Figure 2.1.C), exhibited uniform spherical structures of the NCs with average diameter 3.0 $\pm$ 0.3 nm. High-resolution TEM (HRTEM, Figure 2.1.D and Table A.2.1, Appendix) image of the NCs consisting of clear lattice fringes further confirmed their crystalline nature. Also, the observed d-spacing (d_{sp} = 0.32 nm) of (002) plane supported formation of wurtzite CdS NC structure.[166] Further, selected area electron diffraction (SAED) pattern showed the crystallinity of the as-synthesized NCs (Figure 2.1.E). The XRD patterns and the inter-planar distances as measured in the HRTEM of the crystals, proved the formation of CdS, possibly doped with Zn and thus ruling out the formation of separate nucleation of ZnS and CdS as well as their phase separated crystals. Figure 2.1.F shows the absorption and emission spectra of a dispersion of the NCs in hexane. The absorption spectrum consisted of an edge at 400 nm, while the

emission spectrum (λ_{ex}- 369 nm) exhibited dominant, sharp NBE at 420 nm, with considerably weak and broad DLE at 539 nm.

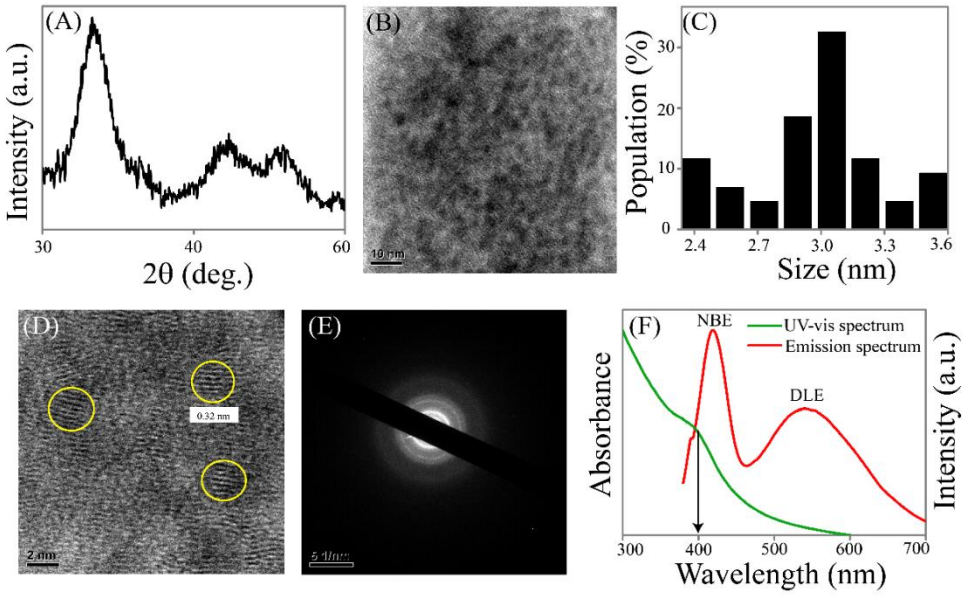

Figure 2.1. (A) Powder x-ray diffraction pattern; **(B and C)** transmission electron microscopic (TEM) image and corresponding particle size distribution; (D) high resolution TEM image **(E)** selected area electron diffraction (SAED) image and **(F)** absorption and emission spectra (λ_{ex}- 369 nm) of $Zn_xCd_{1-x}S$ nanocrystals.

2.2.2. Treatment of CB to $Zn_XCd_{1-X}S$ Qdots.

Further, when the hexane-dispersion of $Zn_xCd_{1-x}S$ NCs was treated with different amounts of cation exchange resin bead (CB) there was a systematic decrease in intensities of the emission at both the peaks (Figure 2.2.A and Figure 2.2.B); however, no significant change (in terms of λ_{max}) was observed in the UV-Vis and excitation spectra (Figure 2.2.C and Figure 2.2.D). On the other hand, it was further observed that the intensity of the peak at 420 nm (NBE) decreased more rapidly than that at 539 nm (DLE). For example, for an addition of 120 mg of CB, the intensity ratio of NBE/DLE at 420 nm decreased from 1.61 (of as-synthesized crystals) to 0.24. Interestingly, a plot of emission with intensity of the peaks normalized at the value of DLE peak indicated significant red-shift, which was by as much as 25 nm (Figure 2.2 B and Figure A.2.1, Appendix). Figure 2.3.A shows the plots of NBE/DLE peak intensity ratio and shift of λ_{max} of DLE peak versus the amount of CB added. Both the plots indicated step-wise changes with the additions of CB. It may be mentioned here that use of 150 mg beads per 10 mL of dispersion resulted in the disappearance of the peak at 420 nm (i.e. NBE

peak). On the other hand, further addition of beads led to precipitation and thus was not pursued.

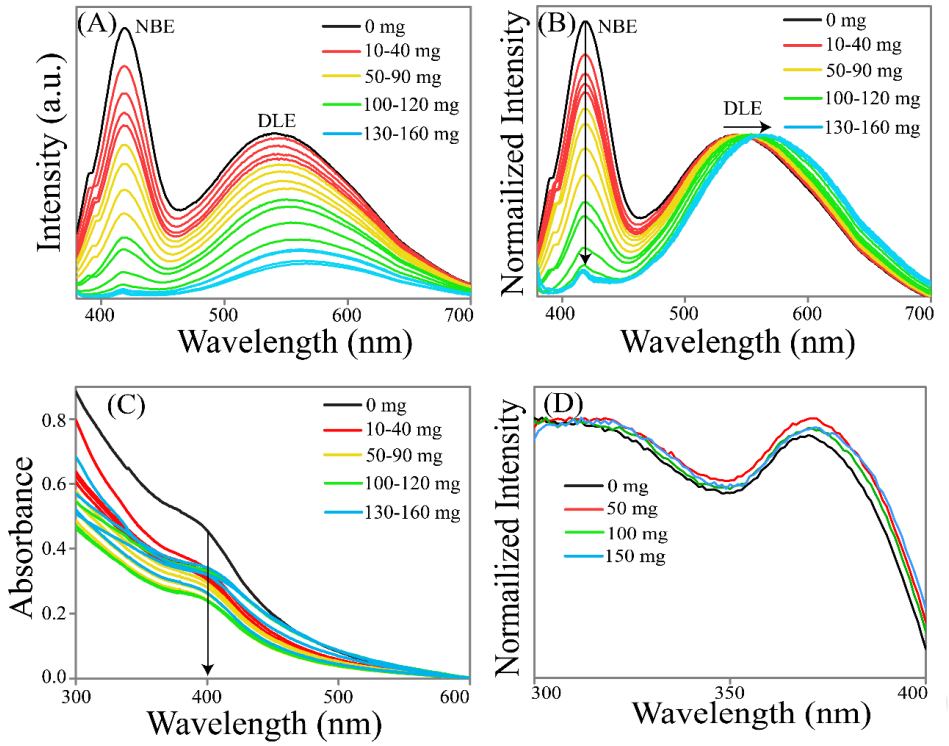

Figure 2.2. (A) Room temperature emission (λ_{ex}- 369 nm) spectra of $Zn_xCd_{1-x}S$ NCs dispersion (in hexane) in the presence of 10–160 mg CB (after 30 min of incubation); **(B)** corresponding normalized emission **(C)** uv-vis and **(D)** normalized excitation (λ_{em}- 539 nm) spectra .

The quantum yield (QY) of the as-synthesized NCs, at an excitation wavelength of 369 nm, was determined to be 12%, using quinine sulphate as a standard (QY-54%). The results of QY of the NCs upon addition of various amounts of CB are shown in Figure 2.3.B (and Table A.2.2, Appendix). As is clear from the figure 2.3.B and the table A.2.2, QY decreased systematically upon addition of increasing amounts of CB. Further, the diagram indicated a step-wise decrease in QY, which was similar to the changes in emission intensity ratio and λ_{max} shift of the DLE peak. For example, for 10–50 mg of beads the QY was between 10.4–7.3%, while for 60–100 mg of beads the value was between 6.3–4.5%. Similarly, the value of QY was between 4.3–1.7% for 110–150 mg of CB.

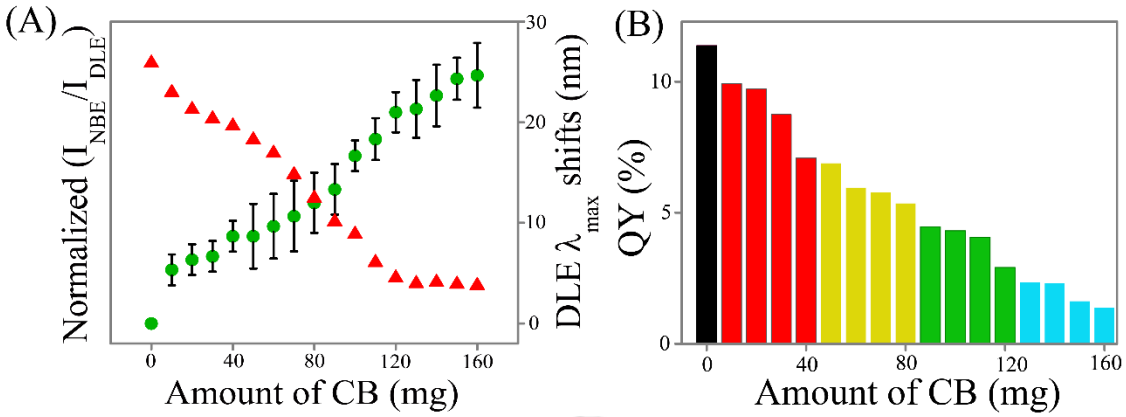

Figure 2.3. Dependence of **(A)** NBE/DLE intensity ratio and shifts of DLE λ_{max} on the amount of CB beads added to NC dispersion (in hexane) and **(B)** quantum yield (%) of the NCs on CB amount.

Figure 2.4 shows the results of TRPL for the as-synthesized NCs and those in the presence of two different amounts of beads, for both NBE and DLE peaks. The photoluminescence decay profile for both the emissions could be fitted with tri-exponential decay. Results also indicated a decrease in the average life time (τ_{av}) for both the peaks in the presence of CB, with lowered the value of τ_{av} at higher bead amount. For example, for the NBE peak τ_{av} of the as-synthesized NCs was 192 ns, which became 176 ns and 103 ns after addition of 50 mg and 150 mg of CB respectively. Similarly, for the DLE peak the τ_{av} of the as-synthesized NCs was 583 ns, which became 543 ns and 499 ns in the presence of 50 mg and 150 mg of CB respectively. The results also indicated that the average lifetime of NBE decreased more rapidly than that of DLE, with the increased amount of CB (Figure A.2.2 and Table A.2.3, Appendix). Wang et al. have reported that for CdS Qdots the broad red-shifted emission decays with significantly longer lifetime (244–360 ns) than the band edge emission (40–61 ns).[167] On the other hand, Kim et al. reported that tri-exponential behaviour of $Zn_xCd_{1-x}S$ NC emission corresponds to having three distinct lifetimes.[166] The three decay times have been assigned to be occurring due to transfer of the electron from (i) the conduction band to shallow traps, (ii) shallow traps to deep traps and (iii) deep traps to surface traps. Also, it has been reported that the mean lifetime increases with the compositional increase of Zn.[166] The observed TRPL results indicated the ion population dependent PL behaviour of the engineered NCs and also revealed that NBE was more sensitive towards CB in hexane than DLE.

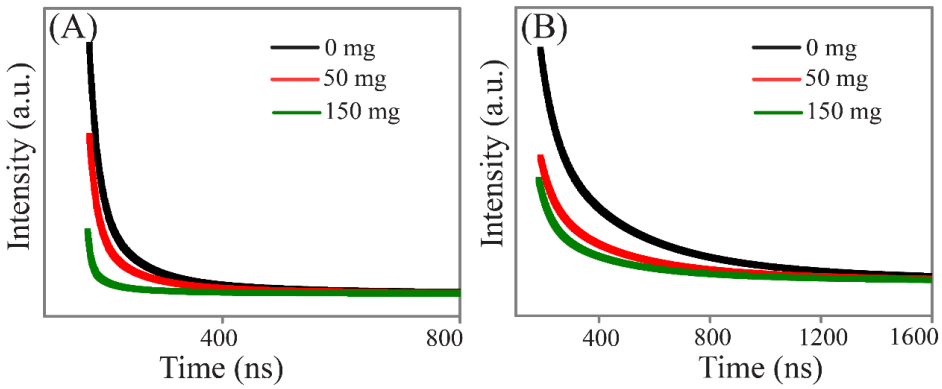

Figure 2.4. Decay kinetic profiles of $Zn_xCd_{1-x}S$ NCs and the NCs in the presence of different amounts of CB for **(A)** NBE and **(B)** DLE. Emission was monitored at their respective emission peak (λ_{max}).

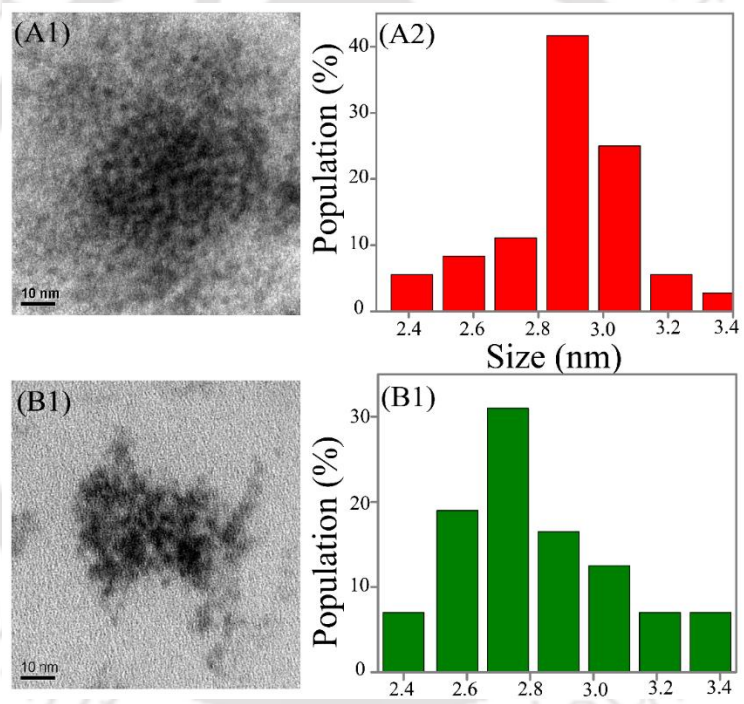

Figure 2.5. TEM image and corresponding particle size distribution of **(A)** 50 mg and **(B)** 150 mg of CB treated NCs.

As mentioned before, TEM analysis of the as-synthesized NCs, revealed average particle size of 3.0±0.3 nm (Figure 2.1). When the particles were treated with 50 mg of beads then the average particle size was found to be 2.9 ± 0.2 nm (Figure 2.5 A). Additionally, treatment of 150 mg CB to the NCs resulted in average particle size of 2.8 ± 0.3 nm (Figure 2.5 B). The results suggested that there was no major change of particle size upon treatment of the NCs with CB. This possibly indicated that surface ions were removed from the NCs without much change in their sizes.

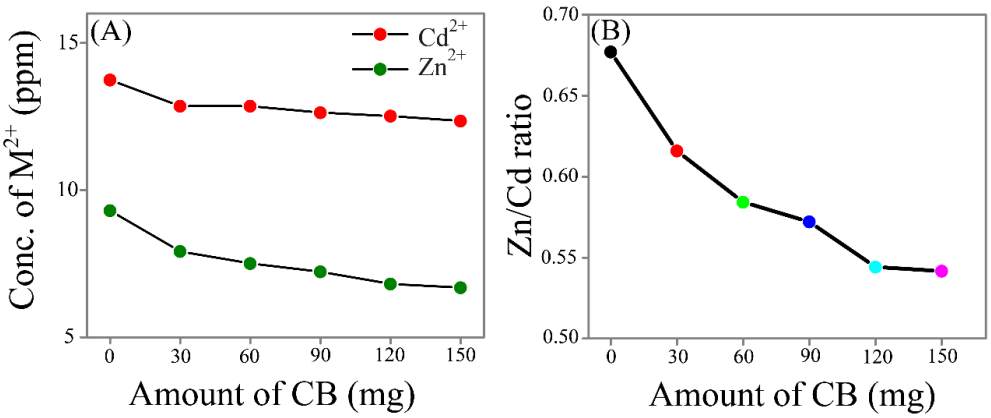

Figure 2.5. Variation of **(A)** individual metal ion (Zn^{2+} and Cd^{2+}) concentration and **(B)** their molar ratio with respect to the amount of CB added to $Zn_xCd_{1-x}S$ NC dispersion.

Atomic absorption spectroscopy (AAS) measurements indicated the presence of Zn and Cd in the crystals. Thus crystals consisted of Zn^{2+}-doped CdS. Also, AAS measurements indicated that with increasing amount of CB, the concentration of the both metal ions decreased. However, the extent of removal of Zn^{2+} was higher than that of Cd2+ (Figure 2.6 A). For example, analysis of the 150 mg CB treated NC dispersion showed that the concentration of Zn^{2+} in the Qdots decreased by 28%; whereas the decrease in Cd^{2+} concentration was by 10%. In other words, the Zn/Cd molar ratio in the Qdots decreased as the amount of CB treating the NC dispersion was increased (Figure 2.6 B). The results clearly evidenced the preferential removal of Zn^{2+} over Cd^{2+} ions by CB and also supported the observed spectroscopic changes. It may also be concluded that preferential removal of Zn^{2+}, accompanied by possible H-bonding with sulphide, led to more sensitive change of NBE than DLE.

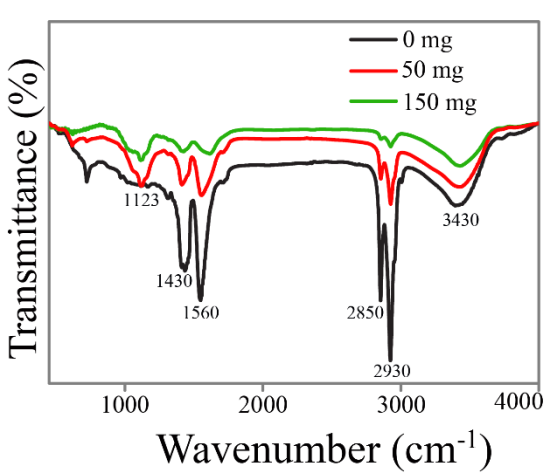

Figure 2.6. FTIR spectra of different amounts (50 mg and 150 mg) of CB added $Zn_xCd_{1-x}S$ NCs.

Fourier transform IR spectra of oleate, oleate capped NCs before and after incubation with different amounts of CB showed that all of the spectra consisted of main characteristic peaks of the functional groups –C–H (2930, 2850 and 1440 cm^{-1}),–COO2 (1560 cm^{-1}), –C–O (1123 cm^{-1}) and –O–H (3430 cm^{-1}) (Figure 2.6, Figure A.2.3 and Table A.2.4, Appendix).[168] Thus FTIR studies indicated the presence of oleate on the surface of NCs before and after the treatment of CB. In other words, ion removal from the outer surface of the NCs did not deplete the stabilizing oleate.

The results presented above indicated that $Zn_xCd_{1-x}S$ NCs interacted with CB and as a result the PL characteristics changed.

Also, the interactions between the NCs and the CB led to removal of cations – with preference for Zn^{2+} over Cd^{2+} ions. It is known that Zn^{2+} has higher affinity for exchange with H^+ of CB than Cd^{2+}, which is consistent with the results.[163] It is possible that cation exchange was accompanied by attachment of H^+ to the S^{2-} of the crystals. Also, this might be favoured by the formation of H-bonding with other S^{2-} ions as the hydrophobic solvent may not host the H^+ released from the CB.[170] Experiments with different solvents (such as chloroform, dichloromethane, acetone and propanol) indicated that in the solvent with higher H-bonding possibility i.e. more polar and protic solvent, the effect on the PL was higher (Figure 2.7 A-B). In this regard, propanol had the highest influence with both changes in ratio of fluorescence intensities of NBE/DLE and red-shift of the DLE peak (Figure 2.7 C-D). However, the red-shift in emission was much less pronounced than that in the presence of CB. It thus can be concluded that treatment of the NCs with CB had two consequences. The cations of the NCs, with preference for Zn^{2+}, could be systematically removed by the CB. This would be accompanied by exchange of H^+, which would preferably bind with the sulphide of the crystals. It has been demonstrated earlier that NBE is sensitive to the H-bonding ability of the solvent or any solute present in the medium (especially when NCs are dispersed in non-aqueous medium).[163] It is also dependent on the surface composition of the NC.[160] On the other hand, DLE depends upon ratio of the cations present on the surface of the NCs. Further, Resch et al. reported that complete suppression of excitonic emission of CdS NCs in non-aqueous solvent can be achieved by the addition of any molecule or solvent which is capable of forming H bonds with the sulphide ions of the NCs.[163] In the present case, the experiments were performed in hydrophobic solvent hexane in the presence of CB. Thus while ion removal had influence on the

emission intensities of both the peaks, the H-bonding with the surface sulphide ions of the NCs resulted in further change in NBE. Hence NBE was observed to be more sensitive to CB than DLE. The results also imply that surface ions played important role in the emission characteristics of the NCs. Thus by their systematic removal the emission characteristics could be changed. That the NBE could be completely suppressed preferentially implicated the role of surface defects and the ratio of Zn^{2+}/Cd^{2+} ions present on the surface of the NC. Further, surface cations and their ratio also decided intensity and peak shift of the DLE peak. Additionally, since the experiments were performed in hydrophobic hexane (used as solvent), it may be that pH had no or little influence in the change in the properties of the NCs. That the ions exchanged and thus removed from the crystals played the sole role in the modification of the emission was clearly demonstrated by AAS results. This was further supported by TEM analyses indicating little change in the particle size.

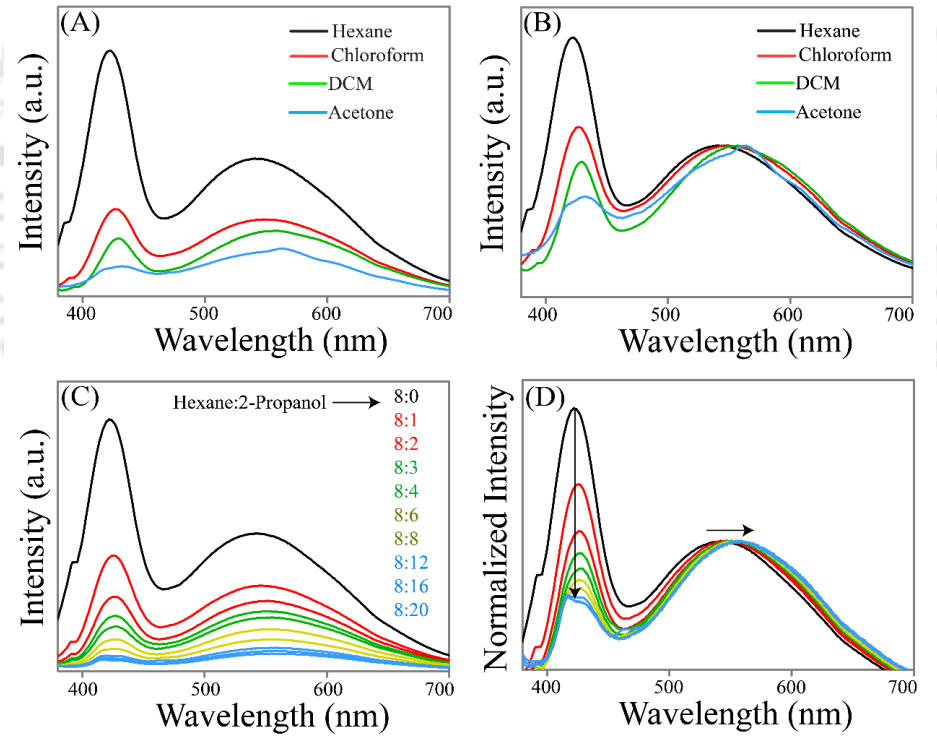

Figure 2.7. (A) Emission spectra (λ_{ex} = 369 nm) of $Zn_xCd_{1-x}S$ NCs in different organic solvents and **(B)** corresponding normalized (to DLE maximum) emission spectra. **(C)** Emission spectra (λ_{ex} = 369 nm) of $Zn_xCd_{1-x}S$ NCs in hexane at different volume of 2-propanol (V/V) and **(D)** corresponding normalized (to DLE maximum) emission spectra.

2.3. Conclusion

Finally, the results reported herein demonstrated the role of surface ions in determining the overall emission characteristics of NCs synthesized in aqueous medium and at comparatively low temperature. The observations made herein also indicated that engineering the surface of Qdots following synthesis is possible and this may be pivotal in modifying their properties, which is important for their useful applications.

Chapter 3

Complexation on the Surface of Quantum dot

Reaction between colloidal ZnS nanocrystals (NCs) and 8-hydroxy quinoline (HQ) led to complexation on the surface of the NCs. The quantum dot complex (QDC), with ZnQ_2 attached to the surface of the NC, has a longer emissive lifetime, higher fluorescence quantum yield and enhanced thermal stability, making it a better LED material than ZnQ_2.

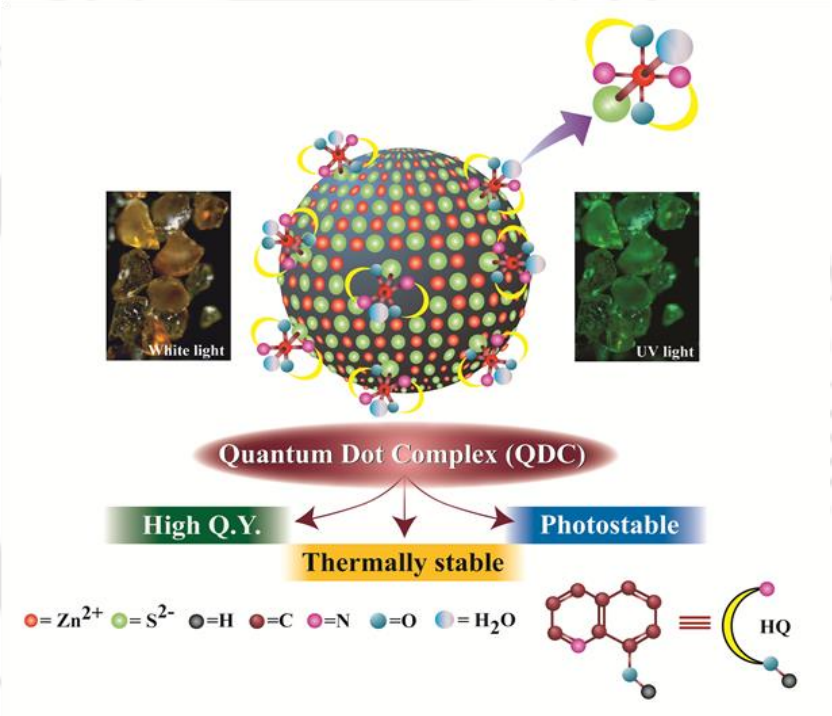

***[Bhandari et al. *RSC Adv.*, 2014, *4*, 24217-24221] - Reproduced by permission of The Royal Society of Chemistry. http://pubs.rsc.org/en/Content/ArticleLanding/2014/RA/c4ra03341h#!divAbstract.**

3.1. Experimental Section

3.1.1. Materials. 8-Hydroxyquinoline (HQ, Merck), zinc acetate dihydrate (99%, Merck), sodium sulphide (58%, Merck), sodium hydroxide (Merck), L- cysteine hydrochloride (Loba Chemie, India), methanol (Merck), methanol (HPLC), potassium bromide (Sigma Aldrich), quinine sulphate were used as received without further purification. Mili-Q grade water was used in all experiments.

3.1.2. Synthesis and characterization of ZnS quantum dots. L-cysteine stabilized ZnS quantum dots (Qdots) were synthesized by an aqueous chemical precipitation method. To synthesize the Qdots, 5.0 mM of zinc acetate dihydrate, 5.0 mM of sodium sulphide and 5.0 mM of L-cysteine hydrochloride were taken in a round bottom flask containing 50.0 mL of Mili Q grade water. At first, zinc acetate dihydrate was dissolved in 30.0 mL of water and to that solution 10.0 mL of 25.0 mM sodium sulphide and 10.0 mL of 25.0 mM cysteine hydrochloride solution (with pH adjusted to ~11 by adding 0.8 M NaOH) were added simultaneously under constant stirring. The resulting mixture turned milky white in color and was refluxed for 3 h under constant stirring at 100 ^{o}C. Finally, the milky white colloidal dispersion so obtained was centrifuged at a speed of 25,000 rpm for 15 min; the pellet was washed with water, redispersed in 50 mL water and the same cycle was repeated. The pellet obtained (after centrifugation twice) was dispersed in 100.0 mL water following sonication for 10 min. The dispersion was used for further experiments. The same procedure was followed to synthesize uncapped ZnS Qdots instead of using cysteine (except that the mixture was refluxed for half an hour at 100 ^{0}C in order to avoid much agglomeration).The details of which is described in Figure A.3.1, Appendix. The synthesized Qdots were characterized using X-ray diffraction (XRD), transmission electron microscopy (TEM), high resolution TEM (HRTEM), UV-Vis, photoluminescence (PL) and FTIR spectroscopy.

3.1.3. Preparation of Ligand (HQ) Solutions. 5.0 mM 8-hydroxy quinoline (HQ) solution in methanol was prepared using sonication.

3.1.4. Synthesis and Characterization of $ZnQ_2.2H_2O$ Complex. The $ZnQ_2.2H_2O$ complex was prepared by using a sonochemical method. 5.0 mM HQ was dissolved in 10.0 mL of methanol and then it was added drop-wise to 10.0 mM of 10.0 mL zinc acetate solution (in water) which was followed by sonication for an hour.[152]

Finally, the yellowish green precipitate so obtained was filtered out and repeatedly washed with MiliQ water and hexane to remove unreacted metal salts and ligand respectively. The final products were dried under room temperature and were used for further experiments. The synthesized complex was characterized using XRD, UV-Vis, FTIR and PL spectroscopy, SEM and optical microscopic analysis.

3.1.5. Synthesis and characterization of QDCs. Room temperature synthesis of QDC was carried out by the following two steps.

A) To 2.0 mL of cysteine capped ZnS (pH-6.6) Qdot water dispersion (with an absorption value of 0.03 at 361 nm), 2.0 μL methanolic solution of 5.0 mM HQ was added step-wise. The fluorescence spectrum of the Qdots in the presence of the ligand was monitored with spectrofluorimeter. The optimum concentration of ligand was taken as the concentration at which the resultant mixture showed maximum emission intensity at its peak. (Figure A.3.2, Appendix) Similar fluorometric titration was carried out using 0.5 mM methanolic solution of $ZnQ_2.2H_2O$ complex. (Figure A.3.3, Appendix) The optimum amount of ligand and complex added to 2.0 mL Qdots dispersion were 30.0 μL and 100.0 μL, respectively.

B) After separate addition of optimum amount of ligand and complex to 2.0 mL of Qdot dispersions, the resulting solutions were centrifuged with a speed of 25000 rpm for 15 min. The obtained supernatant and pellet (after being redispersed into same amount of solvent) were used for PL spectroscopy to check the attachment behavior of HQ and complex. The cycle of centrifugation and redispersion of the dispersion from pellet was repeated until supernatant was nonfluorescent at the same excitation wavelength. The final pellet was collected and was redispersed into the same amount of solvent (2.0 mL) which was then used for UV-Vis, PL, TRPL spectroscopic measurements and TEM analysis. The pH of the medium of both the QDC dispersions (either from HQ added or ZnQ_2 added Qdots) before and after centrifugation remained unchanged from the dispersion of as-synthesized Qdots (pH-6.6). The powder XRD, TGA, DSC, FTIR and optical microscopic analysis of QDCs were carried out using solid pellet obtained similarly. The PL quantum yields (QY) was measured using quinine sulphate solution (in 0.1 M H_2SO_4) as reference. The photostabilty of QDC was measured under continuous irradiation of light, using rhodamine 6G as standard dye solutions.

3.1.6. Control experiments.

A) Formation of QDCs with uncapped ZnS. To 2.0 mL of uncapped ZnS Qdot dispersion in water, 30.0 μL of 5.0 mM HQ (in methanol) and 0.5 mM $ZnQ_2.2H_2O$ complex in methanol were separately added and the resulting mixtures were centrifuged. The pellet obtained after centrifugation was redispersed into the same amount of solvent to monitor the spectroscopic changes in UV-Vis and PL.

B) Effect of sulphide ions and solvent on the optical properties of $ZnQ_2.2H_2O$ complex. To 2.0 mL of 0.5 mM methanolic $ZnQ_2.2H_2O$ solution, a pinch of solid Na_2S dissolved in methanol was added. Separately, different amount of 0.5 mM methanolic $ZnQ_2.2H_2O$ was added to 2.0 mL of water. For both the solutions, UV-Vis and fluorescence measurements were made in order to observe spectroscopic changes.

C) Effect of benzoquinone (BQ) on Qdots/ QDC/ $ZnQ_2.2H_2O$ complex. To 2.0 mL of cysteine capped ZnS Qdot dispersion in water, 30.0 μL of 5.0 mM BQ (in methanol) was added, followed by addition of 30.0 μL of 5.0 mM HQ (in methanol). Separately, to 2.0 mL of cysteine capped ZnS Qdot dispersion in water, 30.0 μL of 5.0 mM HQ (in methanol) was added first and then 30.0 μL of 5.0 mM BQ (in methanol) was added. The resulting mixtures were used to monitor the spectroscopic changes in fluorescence. Similarly, to 2 mL of 0.5 mM methanolic $ZnQ_2.2H_2O$ solution, 30.0 μL and 60.0 μL of 5.0 mM BQ (in methanol) were added to observe the effect of BQ on the fluorescence of the complex.

3.1.7. Effect of heating on the luminescence properties of $ZnQ_2.H_2O$ complex and QDCs through microscopic analysis and PL spectroscopy.

Solid $ZnQ_2.2H_2O$ complex and QDCs were placed on glass slides, heated above 270 ^oC over a hot plate for 10 min and then cooled to room temperature. The changes in PL due to heating were observed using optical microscopy (under white and UV light). Then the solids were redispersed into water using sonication in order to measure their PL spectroscopic properties.

3.2. Results and Discussion

3.2.1. Characterization of ZnS Qdots.

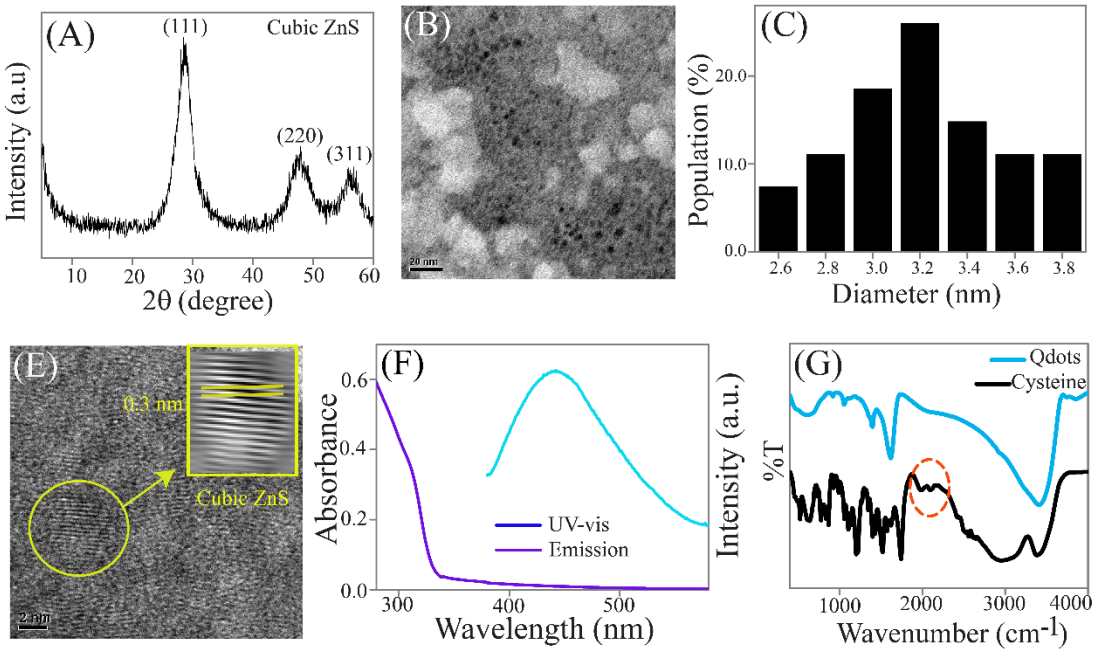

Figure 3.1. **(A)** Powder X-ray diffraction pattern, **(B)** transmission electron microscopic (TEM) image (scale bar -20 nm), **(C)** corresponding particle size distribution, **(E)** high resolution TEM image (scale bar - 20 nm), **(F)** uv-vis and emission (λ_{ex}-322 nm; in water) of cysteine capped ZnS Qdots. **(G)** Fourier transform infrared (FTIR) spectra of cysteine capped ZnS Qdots and cysteine.

The powder X-ray diffraction (XRD) pattern of the as-synthesized precipitates of both capped and uncapped Qdots exhibited three prominent peaks at 28.6º, 47.9º and 56.5º (Figure 3.1A). The three characteristic peaks are due to the (111), (220) and (311) planes of the cubic ZnS Qdots.[145, 170] The morphology of ZnS Qdots can be observed on TEM images in Figure 3.1B and 3.1C with average particle size 3.2 $\pm$ 0.5 nm (for capped Qdots) and 4.0 $\pm$ 0.5 nm (for uncapped Qdots). Further, selected area electron diffraction (SAED) confirmed the crystalline nature of the Qdots (Figure 3.1 D). The internal lattice fringes (d_{sp} = 0.3 nm; indicating 111 plane of ZnS) observed for capped Qdots in HRTEM (Figure 3.1E) also confirmed the formation of cubic ZnS Qdots. [145, 170] Figure 3.1 F-G shows absorption and emission spectra of ZnS Qdot dispersion. While absorption spectrum showed an edge at 308 nm for the capped one and at 318 nm for uncapped one, the emission spectrum (λ_{ex} = 322 nm) exhibited broad emission

band centered at 440 nm for both Qdots. [145, 170] Presence of cysteine on the surface of the Qdots was confirmed by FTIR spectroscopy and absence of –S-H bands in Qdots confirmed that cysteine binds the Qdots through –S atom of thiol group of cysteine for capped ZnS Qdots (Figure 3.1 H).

3.2.2. Characterization of ZnQ_2, $2H_2O$ complexes.

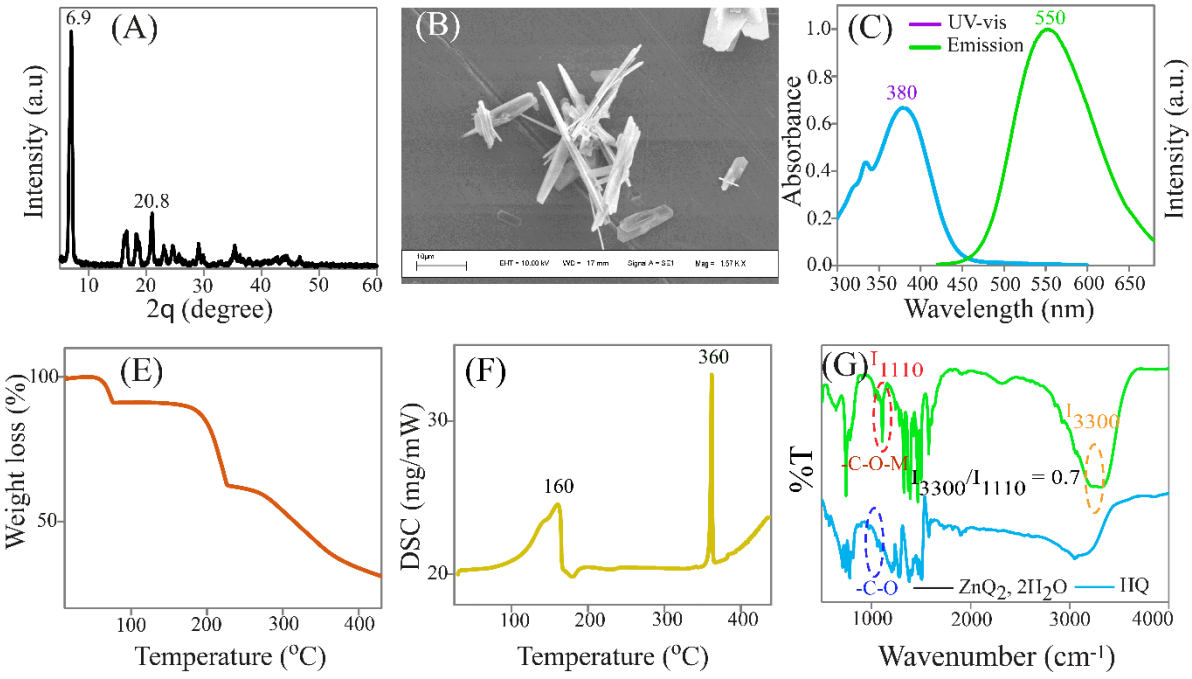

Figure 3.2. **(A)** Powder X-ray diffraction pattern, **(B)** scanning electron microscopic (SEM) image (scale bar -10 μM), **(C)** uv-vis and emission (λ_{ex}-361 nm; in methanol) **(E)** thermo-gravimetric and **(F)** differential scanning calorimetric analyses of FTIR spectra of ZnQ_2, $2H_2O$. **(G)** Fourier transform infrared (FTIR) spectra of ZnQ_2, $2H_2O$ and HQ.

The powder XRD pattern of the as-synthesized precipitates exhibited two strongest peaks at 6.9° and 20.8°, which indicated the formation of $ZnQ_2.2H_2O$ complex (Figure 3.2A). Scanning electron microscopic analysis revealed known rod-like shape of the complex (Figure 3.2B).[152, 171] Figure 3.2C shows the optical absorption and emission spectra of complex in methanol. ZnQ_2. $2H_2O$ complex shows broad absorption maximum at 380 nm which arises from efficient ligand to metal transfer and its broadness depends upon the transition populating ligand centered excited states. On the other hand, emission of the complex was observed at 550 nm and is due to a transition from electron rich phenoxide ring (HOMO; highest occupied molecular orbital) to the electron deficient pyridyl ring (LUMO; lowest occupied molecular

orbital). The nature of photoluminescence of complex depends upon the coordination and angle of the ligand and presence of additional functional group. As for example, introduction of electron withdrawing groups in phenoxide and pyridyl ring causes blue shifts and red shifts respectively in the emission of the AlQ_3 complex while electron donating groups shows the reverse effect. [154-155] Figure 3.3D-3.3E shows the TGA and DSC results of the complex. In TGA, two step weight loss was observed; first one occurred from 120 ^oC upto 150 ^oC and second one at 450 ^oC, while DSC curve shows endothermic peaks at 160 ^oC and at 360 ^oC. The first weight loss is ascribed to loss of coordinated two water molecules while second one indicates the decomposition of the complex in the TGA curve (Figure 3.3D). Water loss and decomposition of the complex were further confirmed by observing two endothermic peaks - one at 160 ^oC and another sharp peak at 360 ^oC respectively in the DSC curve (Figure 3.3E).[152] The presented results clearly indicated the formation of $ZnQ_2.2H_2O$.The presence of HQ and water of hydration in the zinc quinolato complex was verified by FTIR spectroscopy (Figure 3.3F). The C-O stretching frequency observed in the free oxine molecule at 1095 cm^{-1}, shifted to higher frequencies in all the metal complexes giving a strong absorption band at 1110 cm^{-1} (-C-O-M) (Figure 3.3F). This clearly indicates the coordination of HQ to Zn^{2+} ion in these complexes.[152] The bands at 1605, 1577, 1391 and 1328 cm^{-1} are assigned to the quinoline group of ZnQ_2. The pyridyl and phenyl groups in ZnQ_2 are easily identified by presence of 1500 cm^{-1} and 1468 cm^{-1} bands respectively. Specifically, the presence of C-C/C-N stretching, C-H bending peaks at 1500, 1465, 1322 cm^{-1}, C-H out plane wagging at 822, 800, 742 cm^{-1} and in-plane ring deformation at 742, 642 and 605 cm^{-1} in the ZnQ_2 indicated that HQ was successfully coordinated to Zn^{2+} ion to form complex.[3] (Figure 3.3F) Moreover, it is earlier reported that the intensity ratio of 3333 cm^{-1} (3μ) band to 1110 cm^{-1} (9μ) is commonly used to identify the number of water molecules in metal quinolates. The intensity ratio (3333 cm^{-1} /1110 cm^{-1}) is 0.30 $\pm$ 0.05 for one and 0.60 $\pm$ 0.05 for two molecules of water per molecule of quinolate.[152, 172] Here, the intensity ratio was found to be 0.70 which is slightly higher than the expected value for presence of two molecules of water for ZnQ_2 complex, which indicates the possible presence of two water molecules in the complex. This indicates that the formation of $ZnQ_2.2H_2O$ complex.

3.2.3 Complexation Reaction.

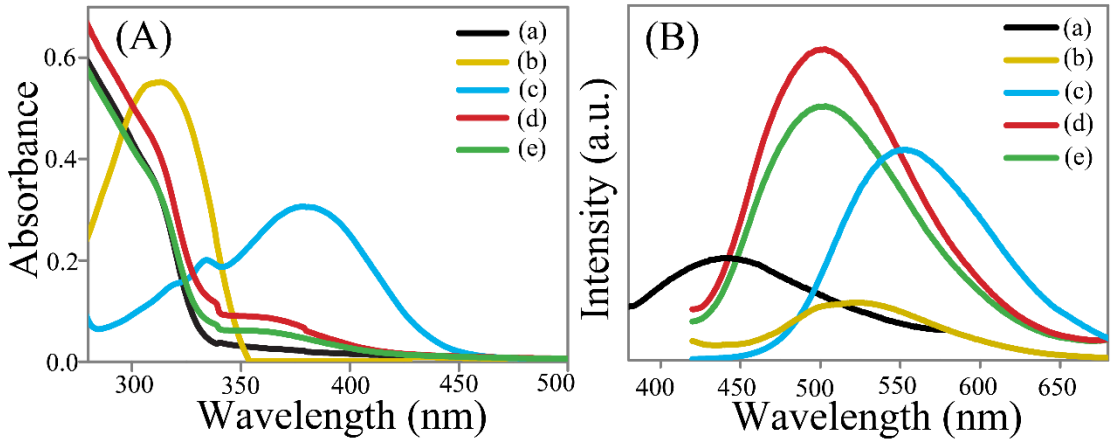

Figure 3.3. (A) UV-vis and **(B)** emission spectra of (a) cysteine capped ZnS Qdots (pH-6.6); (b) HQ; (c) ZnQ_2; (d) HQ added ZnS Qdots (pH-6.6) and (e) ZnQ_2 added ZnS Qdots (pH-6.6). For the emission spectral measurements, the excitation wavelength was set at 322 nm (Qdots) and 361 nm (others).

Experimentally, the UV-vis absorption spectrum of cysteine stabilized 3.2 nm ZnS Qdots consisted of a peak at 308 nm, as is represented in Fig. 3.3A. The absorption spectrum of HQ consisted of a peak at 316 nm (Fig. 3.3A). Further, the absorption spectrum of ZnQ_2 consisted of a peak at 380 nm (Fig. 3.3A). On the other hand, when an aqueous dispersion of cysteine-stabilized 3.2 nm ZnS Qdots was treated with HQ (in MeOH), a second peak in the UV-vis absorption spectrum appeared at 361 nm, in addition to the original peak due to the Qdots at 308 nm (Fig. 3.3A). The absorption spectrum of ZnQ_2 added Qdots (Fig. 3.3A) had the same feature as that of HQ added Qdots. The appearance of a new peak is indicative of interaction between the Qdots and HQ as well as ZnQ_2, leading to the formation of a new species. The identical absorption spectral peak in both the cases pointed toward formation of the same species. Further, when the samples were centrifuged and redispersed in water the absorption spectra remained the same, indicating that indeed there was product formation out of a reaction between the Qdots and HQ as well as ZnQ_2 (Figure A.3.4, Appendix). Fluorescence spectrum of HQ-treated Qdots consisted of a single peak at 500 nm with QY of 3.2%, when excited at 361 nm and that of 0.16% following excitation at 322 nm. ZnQ_2 treated Qdots had the same spectrum with QY of 3.0% and 0.14%, under excitation at 361 nm and 308 nm, respectively (Figure 3.3B and Table A.3.1, Appendix). Fluorescence spectrum of ZnQ_2 consisted of a peak at 550 nm (QY-0.9%), while that of HQ had a

weak peak at 520 nm (QY-0.2%), both of them being excited at 361 nm (Figure 3.3B and Table A.3.1, Appendix). Further, when the dispersions were centrifuged and the solids so obtained were redispersed similar fluorescence spectra were obtained for the samples (Figure A.3.5, Appendix). Fluorescence excitation spectrum of the HQ as well as ZnQ_2 treated Qdots consisted of a single peak with maximum at 361 nm (Figure A.3.6, Appendix).

The above results indicated that interaction between HQ and ZnS Qdot led to the reaction resulting in possible complexation on the surface of the Qdot. Thus while the fluorescence due to the Qdot was quenched, the new fluorescence could be attributed to the formation of a complex on the Qdot (Figure A.3.7, Appendix). That addition of ZnQ_2 to Qdot also resulted in similar spectral behaviour further supported the formation of a complex on the surface, as ZnQ_2 upon functionalizing the surface could have produced similar structure. Control experiment with addition of water to the methanol medium containing ZnQ_2 complex resulted in weakening of emission without change in the peak wavelength, discounting the role of water only in changing the emission spectrum (Figure A.3.8, Appendix). The significant blue shift observed in the emission spectrum in the presence of Qdots could be due to the presence of S^{2-} ions on the surface of the Qdots. Moreover, there was no change in pH, during formation of QDCs from Qdots (pH 6.6), which ruled out the possibility of pH effect on the emission properties of ZnQ_2 complex. This was further substantiated by the observation that when solid Na_2S was added to ZnQ_2 (in MeOH) the peak at 550 nm blue-shifted to 525 nm (Figure A.3.9, Appendix). The absorption spectrum was also blue-shifted from 380 nm to 368 nm in the presence of Na_2S (Figure A.3.9, Appendix). It is important to mention here that when all of the above experiments were carried out with ZnS Qdots, which were synthesized without the use of any stabilizer; the results were similar, indicating that interactions between the Qdots and HQ or ZnQ_2 indeed led to complexation on the surface (Figure A.3.10, Appendix). Further, addition of benzoquinone (BQ) – an electron quencher – to ZnS Qdots led to the quenching of luminescence, which was recovered following addition of HQ.[173] On the other hand, when BQ was added to QDC generated from either of the reaction there was no change in fluorescence (Figure A.3.11, Appendix). Further, BQ had no influence on the fluorescence of ZnQ_2 (Figure A.3.12, Appendix). The results clearly support the

formation of a stable fluorescent complex on the Qdot, notwithstanding the presence of a quencher (BQ) of the Qdot.

Time-resolved fluorescence measurements indicated that the average life-time of fluorescence increased under excitation at 375 nm (with respect to ZnQ_2 complex) and decreased under excitation at 308 nm (with respect to Qdots) following complexation (Figure A.3.13, Appendix). For example, the life-time for ZnQ_2 was found to be 2.5 ns, whereas HQ treated and ZnQ_2 treated samples had average life-time of 10.5 and 11.5 ns respectively with excitation at 375 nm while reverse was observed with excitation at 308 nm (Table A.3.4, Appendix). The increase in average life-time was commensurate with increase in QY as mentioned above. In addition, enhanced photostabilty of the QDCs formed from either of the reactions, with a fluorescence decrease rate (I/I_o) of 0.003% s^{-1} versus 0.013% s^{-1} for rhodamine 6G dye, indicated superior application potential of the new material (Figure 3.4A). It may further be mentioned here that photostabilty of the QDC was as good as that of ZnQ_2 (0.004% s^{-1}), indicating preservation of photochemical stability of the complex even when present on the surface of the Qdot (Table A.3.5, Appendix).

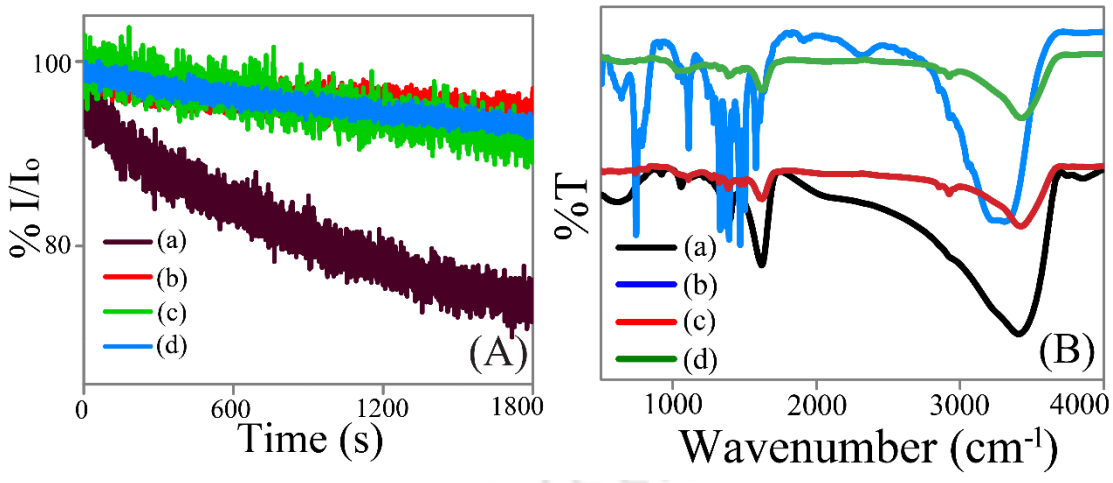

Figure 3.4. (A) Effect of photo irradiation with time on the emission (λ_{ex} = 361nm) intensity of (a) conventional dye (Rhodamine- 6G); (b) HQ-added ZnS Qdots and (c) ZnQ_2 added ZnS Qdots and (d) ZnQ_2 monitored at their respective emission maximum. The same light was used for irradiation and monitoring of the spectra. **(B)** FTIR spectra of (a) cysteine capped ZnS Qdots; (b) ZnQ_2; (c) HQ added ZnS Qdots (d) ZnQ_2 added ZnS Qdots.

The formation of Zn^{2+}–quinolato complex on the surface of the Qdots was further substantiated by FTIR spectroscopic results. The presence of C–C/C–N

stretching, C–H bending peaks at 1605, 1577, 1500, 1468 and 1322 cm^{-1}, C–H out plane wagging at 822, 800 and 742 cm^{-1} and in-plane ring deformation at 742, 642 and 605 cm^{-1} in the QDCs indicated that HQ was successfully coordinated to the surface Zn^{2+} ion or ZnQ_2 was attached to the surface (Figure 3.4B and expanded version in Figure A.3.14-A.3.16, Appendix). [152, 172] Importantly, the QDC had a strong absorption band at 1110 cm^{-1}- due to C−O stretching of metal coordinated oxine - which was absent in the Qdots (Figure A.3.15, Appendix). The intensity ratio of the two prominent bands at 3333 cm^{-1} and 1110 cm^{-1} was measured to be 0.7, pointing toward the formation of a complex similar to the dihyrdate complex (Figure 3.4B and Tables A.3.6, Appendix). However, considering the observed role of surface S^{2-} ions a proposal could be made where a water molecule of the hexa-coordinated complex is replaced by S^{2-} ions, which is simultaneously bound to the surface of the Qdot via dangling bond.

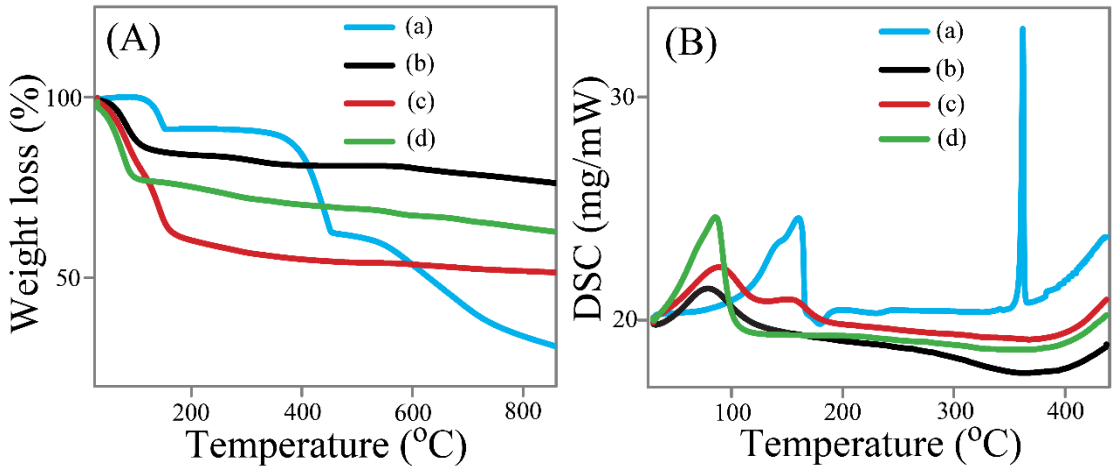

Figure 3.5. (A) Thermo-gravimetric and **(B)** differential scanning calorimetric analyses of (a) ZnQ_2; (b) cysteine capped ZnS Qdots; (c) HQ added ZnS Qdots and (d) ZnQ_2 added ZnS Qdots.

Thermo-gravimetric analysis (TGA) showed weight loss (15– 20%) for Qdots and QDCs up to 95 °C and there was no further change till 850 °C. These weight losses could be due to loss of surface adsorbed water. [152] On the other hand, ZnQ_2 exhibited two weight losses – one at 120 °C, while the other major one at 450 °C, which could be due to decomposition of the sample (Figure 3.4A).[152] Differential scanning calorimetry (DSC) studies similarly showed that the major endothermic change observed for ZnQ_2 at 360 °C was absent for QDC obtained from both the sources, indicating superior stability of the complex on the surface of the Qdots (Figure 3.4B). It is plausible that

the peak at 360 ^{o}C is due to melting of the ZnQ_2 crystal which was absent in the QDC, also supporting superior thermal stability of the complex when incorporated in the Qdots.

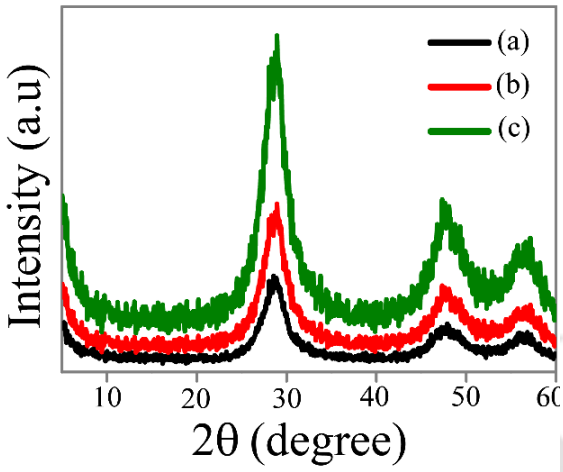

Figure 3.5. Powder X-ray diffraction pattern of (a) cysteine capped ZnS Qdots; (b) HQ added ZnS Qdots and (c) ZnQ_2 added ZnS Qdots.

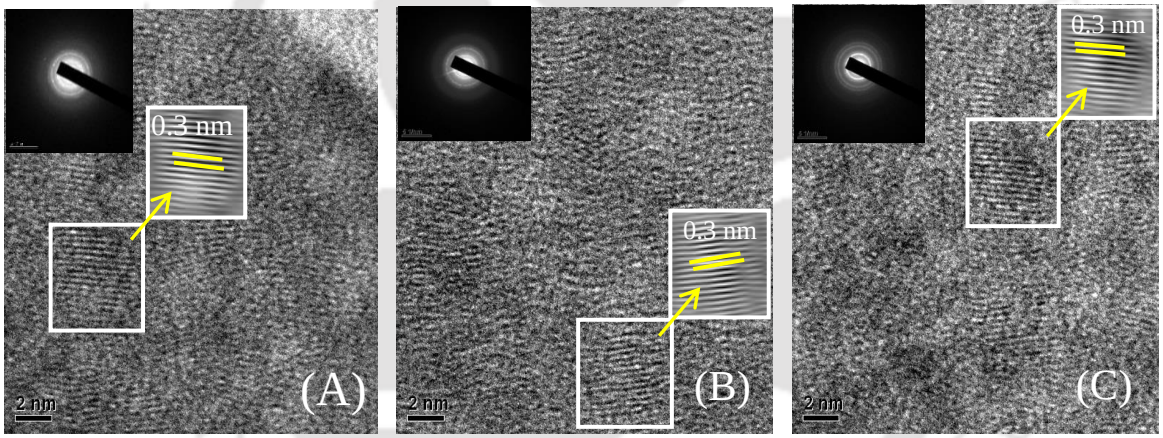

Figure 3.6. HRTEM (scale bar- 2 nm) and corresponding IFFT (in boxes) and SAED (inset; scale bar- 5 nm^{-1}) images of (A) cysteine capped ZnS Qdots, (B) HQ added ZnS Qdots and (C) ZnQ_2 added ZnS Qdots.

The powder X-ray diffraction (XRD) pattern and high resolution transmission electron microscopy (HRTEM) analyses of QDCs generated from both the sources had the characteristics of as synthesized Qdots, which indicated that there was no significant structural changes of cubic ZnS Qdots (Figure 3.5-3.6). Further, TEM analysis results (Figure 3.7) revealed that the average particle size of the spherical structures remained unaffected following complexation.

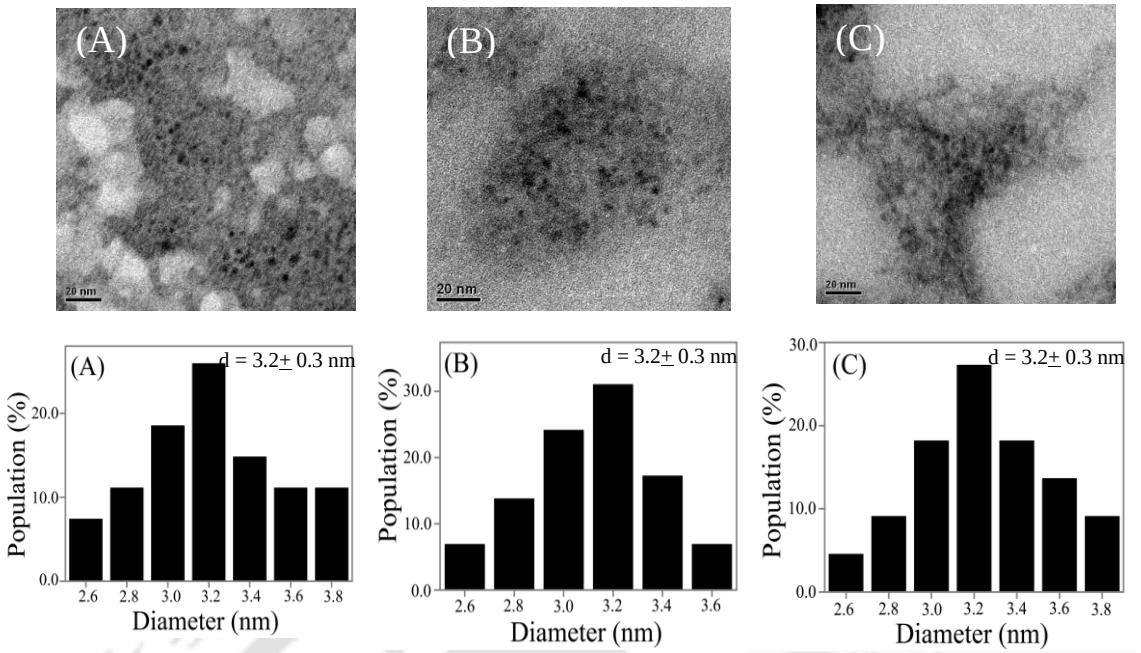

Figure 3.7. TEM images and corresponding particle size distribution of **(A)** as-synthesized cysteine capped ZnS Qdots; **(B)** HQ added ZnS Qdots and **(C)** ZnQ_2 added ZnS Qdots.

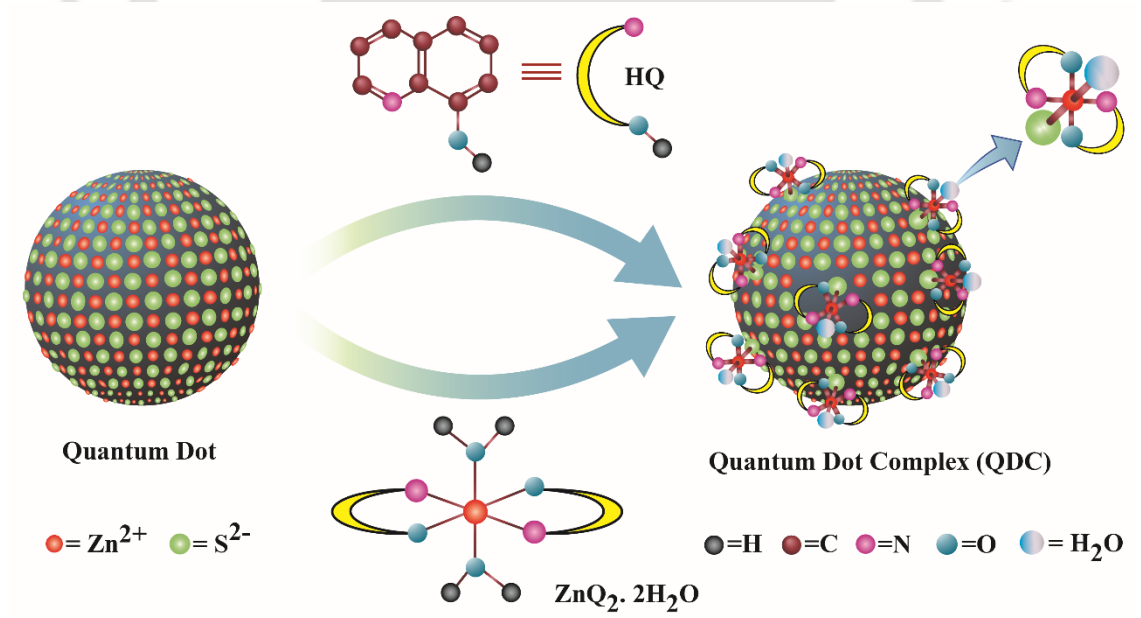

Figure 3.8. Schematic representation of quantum dot complex (QDC) formation on the surface of cysteine capped as well as uncapped ZnS Qdot following its reaction with either HQ (ligand) or ZnQ_2 (complex).

A schematic representation in Figure 3.8 captures the proposed formation of QDC, based on the reaction of Qdot with either HQ or ZnQ_2, $2H_2O$. The surface of Qdot is expected to have sufficient concentrations of Zn^{2+} and S^{2-} ions bound to the crystal via dangling bonds. Such Zn^{2+} ions would preferentially react with HQ forming QDC. In the process of complex formation, the ions may be removed from the surface and the whole complex would bind on the surface instead, also acting as a stabilizer for the Qdot. The facile removal of Zn^{2+} ions is commensurate with the literature reports of surface ion removal and ion-exchange reactions as mentioned above. The S^{2-} ions present on the surface may bind with ZnQ_2 along with another water molecule in the opposite axial position forming an octahedral complex on the surface. Similarly, ZnQ_2, $2H_2O$ may lose one coordinating water molecule and bind with S^{2-} in order to form similar complex on the surface. The octahedral ZnQ_2, $2H_2O$ complex with two water molecules in axial positions is stable at room temperature. Here, in both the QDCs, one of the axial positions of the complex may be occupied by S^{2-} – replacing a water molecule, while the sulphide ion itself would be bound to the Qdot through dangling bond, providing stability to the complex and the Qdot as well in exchange. On the other hand, the HOMO–LUMO band-gap energy of 3.26 eV of ZnQ_2, $2H_2O$ changed to 3.43 eV in QDC formed from both the reactions. The role of S^{2-} in tuning of the energy gap of the complex is established by the observation of increase in the gap to 3.37 eV in the presence of the anion. The observation of significant change in the energy gap following the formation of QDC indicates role of Qdot in tuning the energy level of the complex. Further, the presence of a single excitation spectrum of QDC with the peak at 361 nm indicated that the formation of the complex led to quenching of fluorescence due to Qdot, while the new fluorescence is entirely due to the complex present on the surface of the Qdot, even though the absorption peak due to the Qdot was retained in the QDC.

The octahedral ZnQ_2, $2H_2O$ has its two axial positions occupied by H_2O. On the other hand, when the complex is attached to the surface of the Qdot, it is proposed that one of the H_2O molecules is exchanged with bonding to a surface dangling sulphide ion. This provides not only chemical stability to the complex but also change in its optical property such as blue shift of the emission maximum and increase in QY and thermal stability. This conclusion is further supported by the observation that when

Na_2S was added to the ZnQ_2, $2H_2O$ (in methanol) there was a blue shift in emission maximum accompanied by an enhancement in QY.

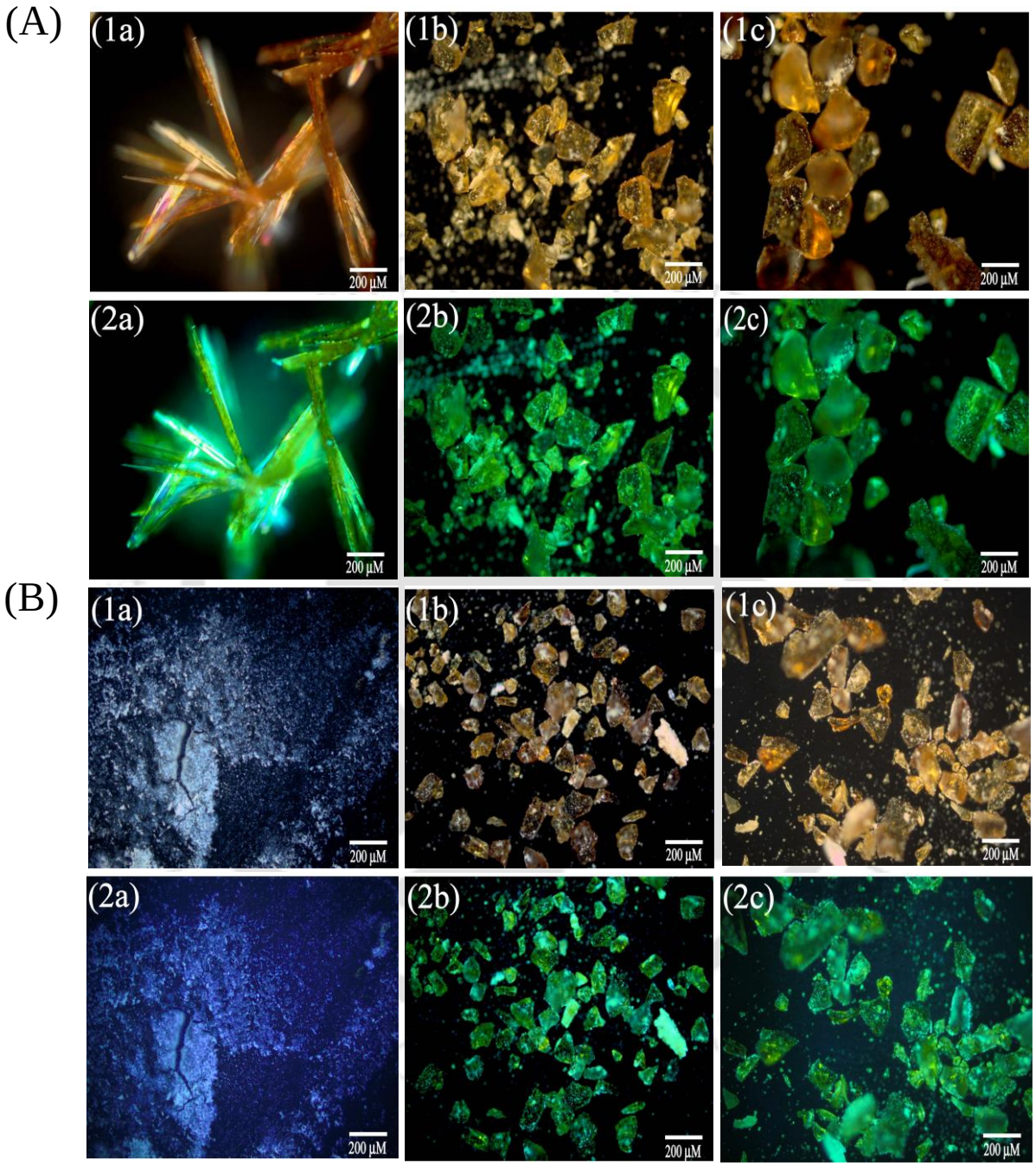

Figure 3.9. Microscopic images of solid samples **(A)** before and **(B)** after heating (at 370 ^{0}C) in presence of (1) white and (2) UV light (λ_{ex}-350 nm); (a) ZnQ_2, (b) HQ added ZnS Qdots and (c) ZnQ_2 added ZnS Qdots.

Finally, ZnQ_2, $2H_2O$ is popular as an active material for light emitting diodes (LEDs).[153, 158-159] Thus any potential application of the new QDC would require ease of processing and stability. We observed that the QDCs generated from both the processes could be turned into solid powder with the retention of their properties. Figure 3.9 A shows the optical micrographs of the powders of ZnQ_2, $2H_2O$ and QDCs, which are brown under visible light and green under UV light, the characteristic fluorescent colour of the complex. In contrast, the colour of solid powder of the Qdots appeared colourless under white light and blue under UV light (Figure A.3.17, Appendix). More importantly, the green fluorescent colour of the free complex vanished upon heating for 10 min at 370 ^oC. On the other hand, the crystalline solid form with retention of fluorescence of QDCs could clearly be observed, indicating their superior thermal stability (Figure 3.9 B). It may be mentioned here that when the heat-treated solids were redispersed in methanol, the fluorescence spectra of the QDCs were retained (Figure 3.10); however, the fluorescence spectrum of the dispersion of the solid, obtained from heat treated complex, did not exhibit any characteristic fluorescence indicating loss of the structure.

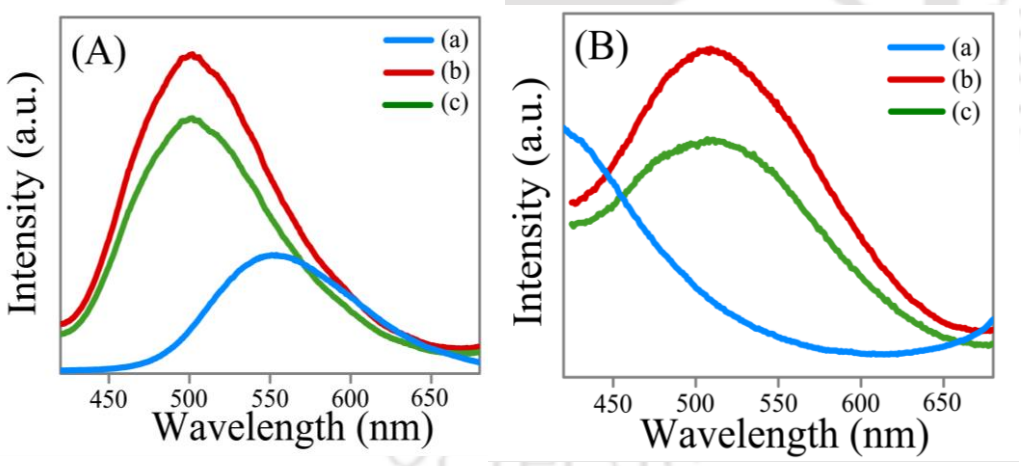

Figure 3.10. . Emission spectra (λ_{ex}=361 nm) (A) before and (B) after heating at 350^{0}C of (a) ZnQ_2, (b) HQ added ZnS Qdots and (c) ZnQ_2 added ZnS Qdots.

3.3. Conclusion

In conclusion, a new material following complexation of Qdots leading to the formation of ZnQ_2 species on the surface has been reported. The high fluorescence QY, longer fluorescence lifetime and enhanced thermal stability of the QDCs are important indicators of their potential in light emitting and other applications. The role of surface ions in the formation and stability of the complex brings out a new chemistry which may usher in a new approach to inorganic complexes. Our observations of formation of similar complexes from reaction of HQ with $Zn_xCd_{1-x}S$ and Mn^{2+} doped ZnS nanocrystals indicated generality of the approach and future prospects of a new field.

Chapter 4

Surface Complexation Reaction for Phase Transfer of Hydrophobic Quantum Dot from Nonpolar to Polar Medium

Chemical reaction between oleate-capped $Zn_xCd_{1-x}S$ quantum dots (Qdots) and 8-hydroxyquinoline (HQ) led to formation of a surface complex, which was accompanied by transfer of hydrophobic Qdots from nonpolar (hexane) to polar (water) medium with high efficiency. The stability of the complex on the surface was achieved via involvement of dangling sulfide bonds. Moreover, the transferred hydrophilic Qdots - herein called as quantum dot complex (QDC) - exhibited new and superior optical properties in comparison to bare inorganic complexes with retention of the dimension and core structure of the Qdots. Finally, the new and superior optical properties of water-soluble QDC make them potentially useful for biological-in addition to light emitting device (LED) - applications.

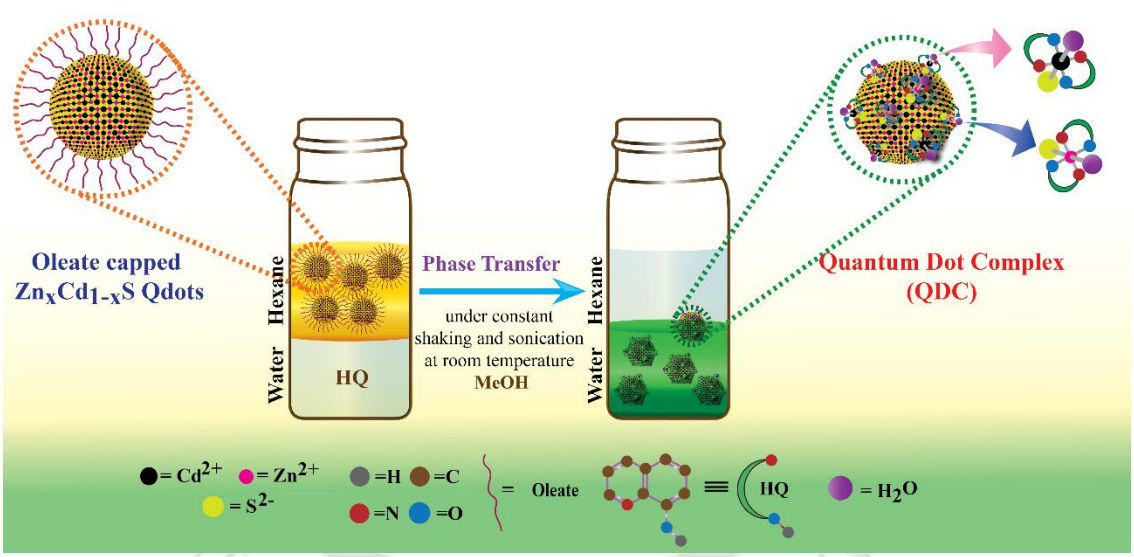

*** "Reprinted with permission from (Bhandari et al. *Langmuir,* 2014, *30,* 10760-10765). Copyright 2014 American Chemical Society." http://pubs.acs.org/doi/abs/10.1021/la502764a**

4.1. Experimental Section

4.1.1. Materials. 8-Hydroxyquinoline (HQ, Merck), cadmium acetate dihydrate (99%, Merck), zinc acetate dihydrate (99%, Merck), sodium sulfide (58%, Merck), sodium oleate (Loba Chemie), methanol (HPLC, Merck), potassium bromide (Sigma-Aldrich), quinine sulfate (Sigma-Aldrich), sulfuric acid (Merck), and hexane (Merck) were of analytical grade and used without further purification. Milli-Q grade (>18 MΩ cm, Millipore) water was used for the synthesis and in all experiments.

4.1.2. Synthesis and Characterization of $Zn_xCd_{1-x}S$ Quantum Dots. Oleate-capped Zn doped CdS quantum dots (Qdots) were synthesized following an established procedure from our laboratory ($Zn_xCd_{1-x}S$, where x = 0.35 ± 0.05, as reported in our earlier work).[174] In brief, 5.0 mM sodium oleate was added to a solution containing cadmium acetate (5.0 mM) and zinc acetate (2.5 mM) in 50 mL of Milli-Q grade water under constant stirring and heating. The colorless solution of metal ions turned to milky white upon addition of sodium oleate. Further, when sodium sulfide (5.0 mM) was added, the solution became greenish-yellow, and solid particles could be observed floating over the water surface, which indicated the formation of hydrophobic Qdots. In order to avoid discontinuous growth, the solution was refluxed for 6 h at 100 °C, under constant stirring. After that, the resulting mixture was centrifuged with a speed of 25 000 rpm for 15 min, and the so-obtained pellet was repeatedly washed with Milli-Q water. The sample was redispersed in water, and the same cycle of experiments was repeated. Finally, the pellet was dried at room temperature, and in order to perform experiments the Qdots were dispersed in a hydrophobic solvent (in hexane).

4.1.3. Preparation of Ligand (HQ) Solutions. 5.0 mM 8-hydroxyquinoline (HQ) solution in methanol was prepared using sonication.

4.1.4. Synthesis and Characterization of $MQ_2{\cdot}2H_2O$ Complex (M =Zn or Cd). Our previously reported sonochemical method was used for the synthesis of the complex $ZnQ_2{\cdot}2H_2O$.[175] A 10.0 mL methanolic solution of 5.0 mM HQ was dropwise added to a solution containing 10.0 mM of 10.0 mL zinc acetate solution (in water) under constant sonication for an hour at room temperature. The resulting yellowish green mixture was filtered out followed by repeatedly washing with Milli-Q water and hexane, in order to remove unreacted precursors. Finally, the precipitates were dried at

room temperature and recrystallized in methanol. The resulting crystals were dispersed into methanol for further experiments.[152]

Similarly, the $CdQ_2 \cdot 2H_2O$ complex was synthesized using the above procedure. In order to perform photoluminescence (PL) experiments, the obtained CdQ_2 complexes were filtered, washed with methanol four to five times, and then dried at 50 °C for 2 h. 0.5 g of the product was dissolved in 100 mL of methanol. The UV−vis and PL spectra (Figure A.4.1, Appendix) and powder XRD, TGA (thermogravimetric analysis), and FTIR (Figure A.4.2, Appendix) were used to characterize the $CdQ_2 \cdot 2H_2O$ complex.[176]

4.1.5. Phase Transfer Reaction Procedure. The complexation reaction based phase transfer of oleate-capped $Zn_xCd_{1-x}S$ Qdots from hexane to water was carried out using HQ as complexation agent and methanol as the mediating agent. In brief, 5 mL of oleate-capped $Zn_xCd_{1-x}S$ Qdots (2.0 mg/10 mL) in hexane was mixed with an equal volume of solution containing 4.0 mL of Milli-Q water and 1 mL of methanol, at varying concentrations of HQ. The resulting biphasic mixture was ultrasonicated for 10 min at room temperature followed by vigorous shaking until the top hexane solution showed minimum absorbance at the absorption edge of the Qdot (at 400 nm), in order to achieve the maximum depletion (%) of Qdots from hexane. After that, the top greenish-yellow phase in hexane became colorless while the colorless bottom aqueous part appeared as colloidal pale white, and the water-soluble part was separated from the biphasic solution. The obtained colloidal dispersion was then centrifuged at 25 000 rpm for 15 min, and the pellet was thoroughly washed with water and redispersed into the same amount of water for further experiments. The details of the system are tabulated in Table A.4.1, Appendix.

Calculation of Depletion (%). The phase transfer efficiency was calculated using the indirect parameter depletion (%) in the original organic layer (here hexane), and the following equation was used for that:[57]

$$\text{Depletion percentage (\%)} = 100 \times (A_1 - A_2)/A_1$$

where A_1 is the absorbance of Qdots at 400 nm in hexane before phase transfer and A_2 the absorbance of Qdots at 400 nm in hexane after phase transfer (Table A.4.1, Appendix).

It was found that the depletion (%) value was different for different concentration of HQ in the bottom water phase and as the concentration of HQ increase the depletion in hexane layer increased. All the transferred Qdots in water phase (i.e., quantum dot complex or QDC) was used for PL measurements following centrifugation. The optimum value of HQ concentration was 1.0 mM HQ, which showed maximum depletion (%), and this was used for QDC formation via biphasic reaction following centrifugation (with a speed of 25000 rpm for 15 min). The water dispersion of QDC was used for further experiments like white and UV (365 nm) light photo capturing, PL, UV−vis, QY, lifetime, photostabilty, TEM, HRTEM, and SAED analyses, while the solid particles, obtained from optimum amount of HQ, were used for FTIR and powder XRD analyses.

4.1.6. Control Experiments.

(**A**) A similar phase transfer reaction was performed with 1.0 mL of methanolic solution of 0.1 mM ZnQ_2 complex or 0.1 mM CdQ_2 complex separately instead of 1.0 mL of 5.0 mM of HQ (in methanol). In addition, we have performed phase transfer reaction with the water phase containing both the complexes with equal concentrations (i.e., 1.0 mL of methanolic solution containing 0.05 mM ZnQ_2 + 0.05 mM CdQ_2). These solutions were used to measure the PL and depletion (%) following UV−vis analysis. The details of the phase transfer system are tabulated in Table A. 4.2.

(**B**) The reaction of HQ with oleate capped $Zn_xCd_{1-x}S$ Qdots was also performed in hexane medium via the fluorometric titration method, in order to confirm the involvement of both the metal ions in complexation reaction and also to rule out the effect of solvent throughout the biphasic reaction. In brief, sequentially 1.0 and 5.0 mM HQ (in hexane) was separately added to 2.0 mL of $Zn_xCd_{1-x}S$ Qdots (in hexane), and the PL change was monitored at an excitation wavelength of 369 nm.

4.2. Results and Discussion

The hydrophobic 3.0 nm sized Zn-doped CdS ($Zn_xCd_{1-x}S$: $0 \leq x \leq 1$) Qdots were synthesized following an established protocol with oleate as the capping agent.[174] The colors of the Qdots in hexane under white and UV light (365 nm) were greenish-yellow and bright yellow, respectively (Figure 4.1 A, B). On the other hand, shaking the Qdot dispersion in hexane in the presence of a 4:1 mixture of water and MeOH containing HQ for 10 min, under sonication at room temperature, led to loss of color in the hexane

medium, while the colors of the water medium were yellowish-white and bright green in the presence of white and UV light, respectively (Figure 4.1 A, B). The details of phase transfer experiments are given in Tables A.4.1 and A.4.2, Appendix. The absorption spectrum of the Qdots in hexane consisted of an edge at 400 nm (Figure 4.1 C a), while they exhibited dual emission consisting of a sharp and dominant peak at 420 nm, due to near band edge emission (NBE), and relatively weak and broad peak at 539 nm, due to deep level edge emission (DLE) (Figure 4.1 D a). The starting water phase containing HQ exhibited a strong absorbance at 316 nm (Figure 4.1 C b) and negligible fluorescence (Figure 4.1 D b). When the Qdots were transferred from hexane to water following reaction with HQ, the absorption edge broadened from 400 to 350 nm (Figure 4.1 C c) while the dual emission turned into a single peak at 505 nm (Figure 4.1 D c). In addition, the remainder in hexane showed a dominant absorbance at 316 nm (Figure 4.1 C d), while the solution exhibited negligible fluorescence (Figure 4.1 D d). The loss of absorbance at 400 nm and fluorescence in the hexane medium and appearance of absorbance and fluorescence in water medium indicated that the Qdots were transferred to aqueous medium efficiently. In addition, the excitation spectrum of transferred Qdots showed two prominent peaks at 338 and 364 nm which were absent in as synthesized Qdots (Figure A.4.3, Appendix). Interestingly, when $ZnQ_2{\cdot}2H_2O$, $CdQ_2{\cdot}2H_2O$, or a mixture of the two complexes were added to the hexane medium, similar results were obtained in terms of absorption and emission characteristics (Figure A.4.4, Appendix), thus indicating similar nature of product formation. Further, when Qdots (in hexane) were titrated against different concentrations of HQ (in hexane), a similar change was observed in their emission property, which indirectly supports the formation of same product as obtained via phase transfer and clearly ruled out the effect of solvent and pH on the luminescent properties of the product (Figure A.4.5, Appendix). Further, the surface complexation reaction for Qdots either with HQ or with MQ_2 (M = Zn or Cd) led to quenching of the emission of Qdots. This was accompanied by broadening of absorption band of the Qdots and the appearance of a new emission, following their transfer from hexane to water, indicating the formation of a new luminescent species on the surface of the Qdots.

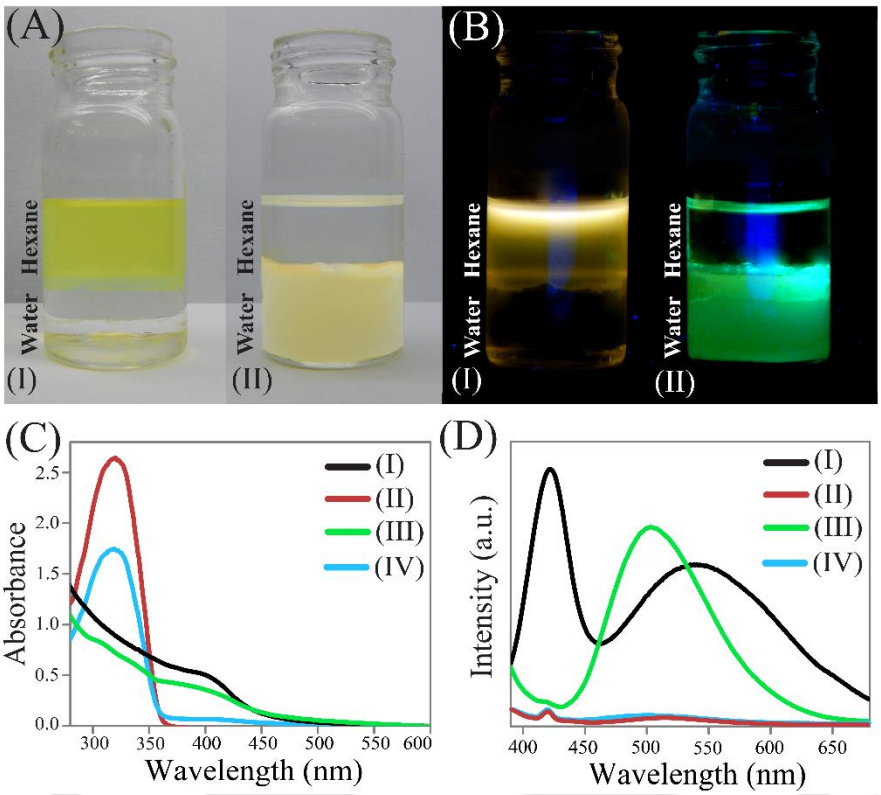

Figure 4.1. Photographs in presence of (**A**) white and (**B**) UV (365 nm) light of oleate capped $Zn_xCd_{1-x}S$ Qdots (a) before and (b) after phase transfer of from hexane to water following complexation reaction with HQ, **(C)** uv-vis and **(D)** emission spectra of (a) oleate capped $Zn_xCd_{1-x}S$ Qdots (in hexane at λ_{ex} =369 nm) (b) water phase containing HQ (in methanol) (c) centrifuged phase transferred Qdots(in water; pH 5.7 at λ_{ex} =365 nm) following complexation with HQ and (d) dispersion left after phase transfer in hexane(at λ_{ex} =369 nm).

HQ (in methanol) exhibited absorption peak at 316 nm, while ZnQ_2 and CdQ_2 complexes (in methanol) showed peaks at comparatively longer wavelengths of 380 and 383 nm, respectively (Figure A.4.1, Appendix). The emission spectrum of HQ (in methanol) showed a weak peak at 520 nm, while ZnQ_2 and CdQ_2 complexes (in methanol) exhibited strong fluorescence peaks at 550 and 545 nm, respectively (Figure A.4.1, Appendix). The excitation spectra (Figure A.4.1, Appendix) of the complexes consisted of two peaks at 340 and 365 nm (relatively broad), while HQ showed a single peak at 375 nm.

Further evidence for the transfer of the Qdots came from transmission electron microscopy (TEM) and X-ray diffraction measurements. The average size (value) of the Qdot was also retained (Figure 4.2 A, B).[174] High resolution TEM (HRTEM) and inverse fast Fourier transform (IFFT) images of the sample prepared from the water

medium exhibited the presence of nanocrystals with d-spacing value of 0.32 nm, corresponding to the wurtzite crystal lattice of CdS (Figure 4.2 C), which is the same as the sample in hexane medium.[174] Selected area diffraction (SAED) analysis also evidenced the phase transfer of the Qdots (Figure 4.2 D). Additionally, powder X-ray diffraction (XRD) patterns of the samples in hexane and water media had three main peaks at 26.1°, 43.9°, and 51.0°, which are the characteristics peaks due to (002), (110), and (112) planes of hexagonal wurtzite CdS lattice (Figure 4.3).[174] The results clearly proved that Qdots were transferred from the hexane medium to water medium without change in their dimension or core structure and also supported that the so obtained new optical properties out of the biphasic reaction was due to MQ_2 complexes attached to the surface of the Qdots.

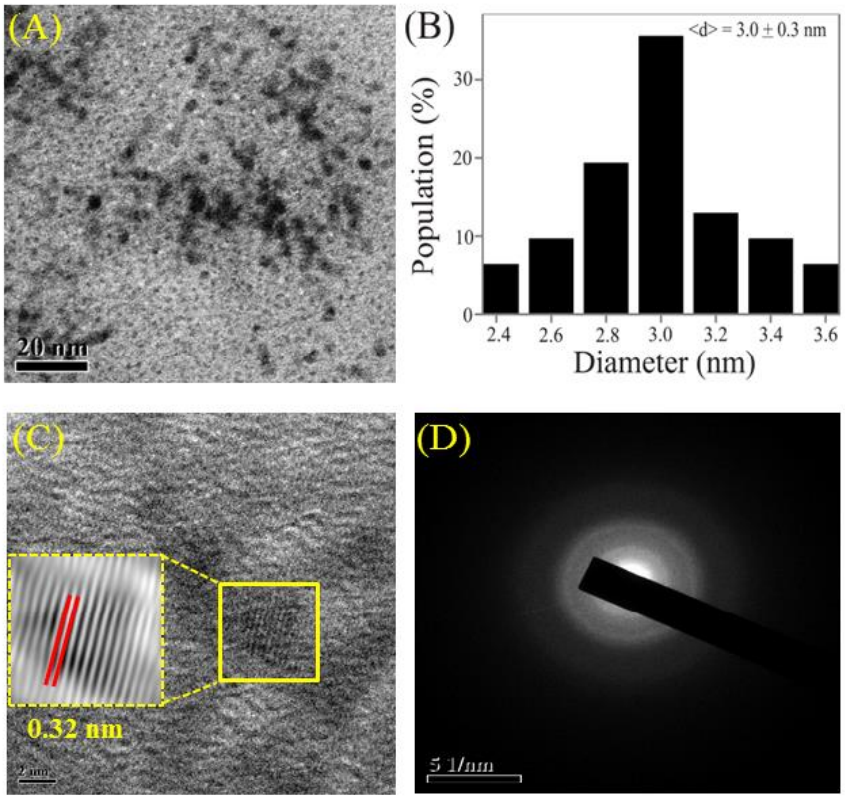

Figure 4.2. **(A)** TEM (scale bar-20 nm) image, **(B)** corresponding particle size distribution, (C) high resolution TEM (HRTEM) and (D) selected area electron diffraction (SAED) pattern (scale bar: 5 nm^{-1}) of the transferred Qdots (in water) following complexation.

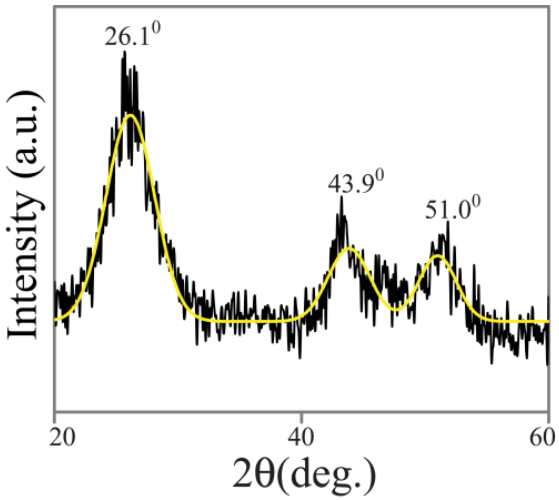

Figure 4.3. Powder X-ray diffraction pattern of solid transferred Qdots following complexation.

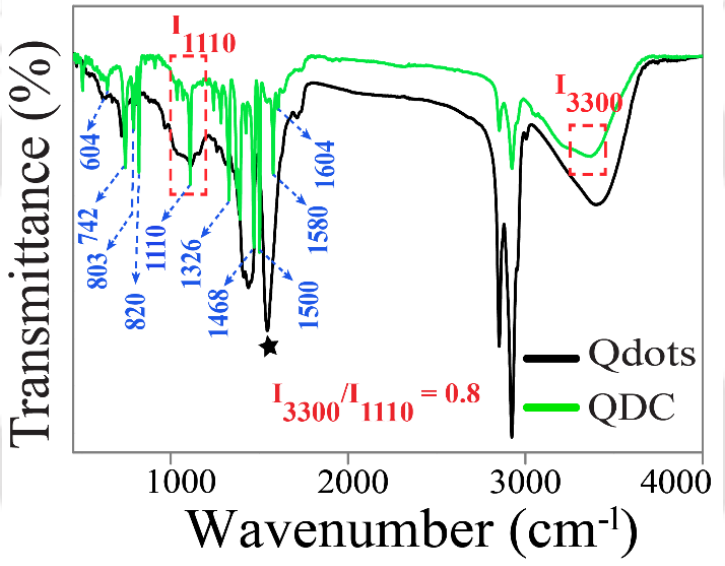

Figure 4.4. FTIR spectra of (a) oleate capped $Zn_xCd_{1-x}S$ Qdots and (b) transferred Qdots following complexation with HQ.

Fourier transform infrared (FTIR) spectroscopy results indicated the appearance of a new peak at 1110 cm^{-1}, following reaction of HQ with Qdot (the sample being collected from the aqueous medium). The intensity of the peak (Figure 4.4)– which is due to C−O−M stretching - was 0.8 of that at 3300 cm^{-1}, indicating formation of octahedral complex ($MQ_2 \cdot 2H_2O$), for which the ratio is generally 0.65 or higher.[152, 175] Further, the presence of in-plane ring deformation (at 604 and 742 cm^{-1}), C−H out-of-plane wagging (at 742, 803, and 820 cm^{-1}), C−H bending peaks (at 1326 cm^{-1}), pyridyl and phenyl peaks (at 1500 and 1468 cm^{-1}), and C−C/ C−N stretching peak (at 1580 and 1604 cm^{-1}) supported the incorporation of MQ_2 on the surface of Qdot (Figure 4.4).[152,

[175]The absence of the main characteristic peak of −COO− functional group (at 1540 cm^{-1}) in transferred Qdots further supported the removal and replacement of oleate following attachment of MQ_2 complexes.

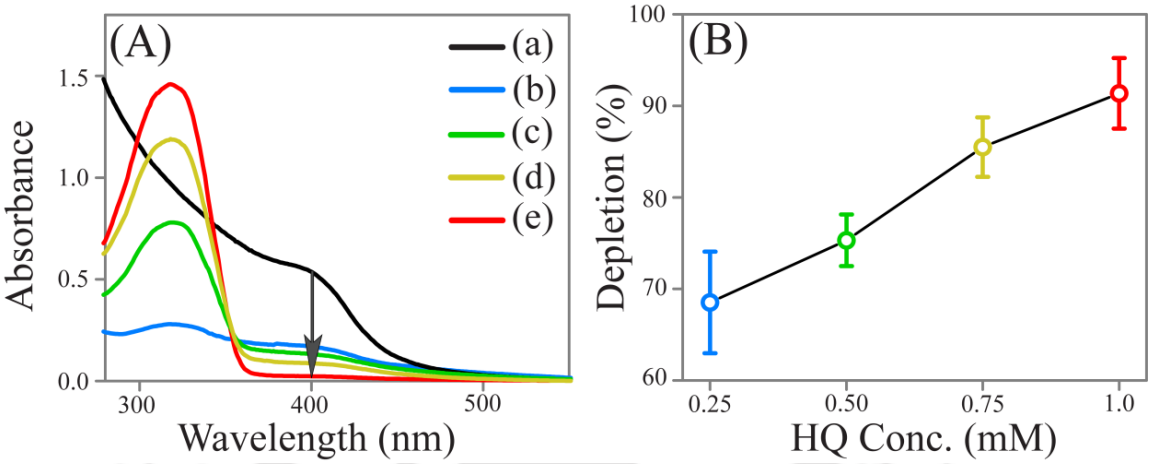

Figure 4.5. (**A**) UV-Vis spectra of (a) oleate capped $Zn_xCd_{1-x}S$ Qdots (in hexane) and the rest part in hexane after phase transfer of Qdots into water following complexation with (b) 0.25 mM, (c) 0.5 mM, (d) 0.75 mM, and (e) 1.0 mM of HQ in water phase (with which the reaction was started), (**B**) variation of depletion (%) of Qdots in hexane with concentration of HQ used during the biphasic reaction.

The transfer efficiency of Qdots from the hexane phase depended upon the concentration of HQ. As is clear from Figure 4.5, the depletion (%) of Qdots increased with HQ amount with an optimum concentration of 1 mM, in order to achieve the maximum depletion (>90%) of Qdots (with absorption 0.54) from hexane. The depletion was calculated using the UV−vis technique by monitoring the absorbance at 400 nm (Figure 4.5 and Table A.4.3, Appendix).[57] On the other hand, when the biphasic reactions were carried out with bare ZnQ_2 or CdQ_2 complexes separately and also with their mixture instead of HQ, the variations in depletion (%) were noticed (Figure A.4.6 and Table A.4.4, Appendix). For example, biphasic reaction with ZnQ_2 and CdQ_2 showed maximum of 72% and 83% depletion, respectively, while their mixture showed 78% depletion. Additionally, the transfer of Qdots by HQ or by MQ_2 complex (Figure 4.1 and Figure A.4.7, Appendix) resulted in emission maximum at 505 nm in water medium, and the emission intensity was found to depend upon the amount of HQ or the complex which was used during phase transfer. This indirectly suggested the formation of similar complexes starting with either HQ or the MQ_2 complex for the phase transfer.

The change in QY and average excited state lifetime also supported the transfer of Qdots from hexane to water following replacement of oleate via attachment of MQ_2 complexes. For example, Qdots (in hexane) and phase transferred MQ_2 attached Qdots (in water) had QY 10.8% and 4.9%, respectively, while the QY of MQ_2 attached Qdots was 3−4 times more than that of the bare MQ_2 complexes (Table A.4.5, Appendix). On the other hand, tri-exponentially fitted decay pattern of MQ_2 attached Qdots had 14.8 ns average lifetime, which is much lower than the reported average lifetime of Qdots (based on NBE and DLE);[174] however, significantly higher than bare MQ_2 complexes (Figure A.4.8 and Table A.4.6, Appendix). In addition, the photostabilty of MQ_2 attached Qdots under continuous irradiation of light was 10 times more than that of an organic dye, while the photostabilty of Qdots and individual complexes were preserved in QDC (Figure A.4.9 and Table A.4.7, Appendix).

The experimental observations reported herein indicated that Qdots were transferred from hexane medium to water medium. This was accompanied by change in their optical properties, which were closer to those of complexes than to original Qdots. It is plausible that reaction of HQ with oleate-stabilized Qdots led to formation of ZnQ_2 and CdQ_2 complexes, which were bound to the surface labile S^{2-} ions.[175] The source of Zn^{2+} and Cd^{2+} could be surface labile ions which may react with the ligand leading to formation of the complex. One of the axial coordinations of the complex may be with the formation of metal−S^{2-} bond, through which the complex would remain attached to the Qdot. The sixth coordination position could be occupied by H_2O. Our previous results indicated distinct possibility of such complex formation, which provide stability in aqueous medium and enhanced optical properties.[175] Similar complexes could be formed on the surface from reaction with ZnQ_2 or CdQ_2. It may be mentioned here that since the optical properties of the two complexes even on the surface would be close to each other, it would not possible to clearly decipher whether both the complexes were formed simultaneously. However, since similar results were obtained from all the reactions it is likely that both the complexes were formed. Overall, the reaction of the Qdots with HQ led to the formation of surface complexes which quenched the emission of the Qdots. This was further substantiated by the observation that addition of ZnQ_2, CdQ_2, or a mixture of the two also quenched the fluorescence of the Qdots. On the other hand, the peak originating from the emission due to ZnQ_2 or CdQ_2 complexes was shifted to lower wavelength (505 nm) with enhanced QY, upon incorporation on

the surface of the Qdots. The change has been attributed to the bonding of the complex with dangling sulfide ion present on the surface of the Qdots.[175] We call this new species as quantum dot complex (QDC), where an inorganic complex is formed on the surface of a quantum dot resulting in distinct optical properties. A schematic of the reaction leading to QDC formation is shown in Figure 4.6.

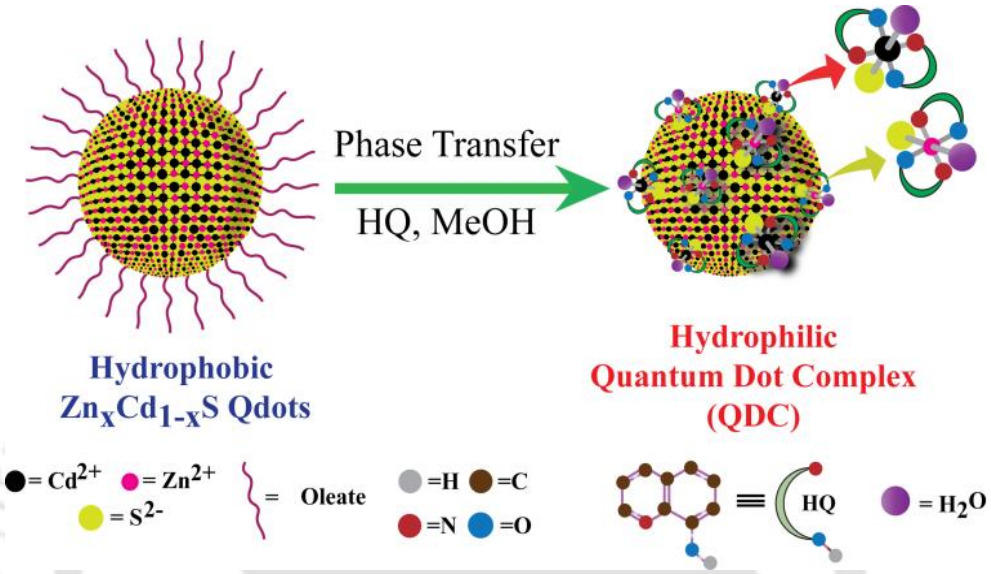

Figure 4.6. Schematic representation of quantum dot complex (QDC) formation on the surface of hydrophobic oleate capped $Zn_xCd_{1-x}S$ Qdots involving surface Cd^{2+} and Zn^{2+} ions and organic ligand (HQ) following phase transfer reaction from hexane to water.

4.3. Conclusion

In summary, a new and simple complexation reaction based approach for transferring oleate-capped $Zn_xCd_{1-x}S$ Qdots from nonpolar to polar medium is reported. This was achieved through formation of MQ_2 (M = Zn or Cd) complexes which were attached to the Qdot surface through dangling sulfide ions, rendering them water-soluble. The phase transfer process had high transfer efficiency without any precipitation at the phase boundary. In addition, the morphology and dimension of Qdots were preserved. The MQ_2 attached Qdots - called as quantum dot complex (QDC) - had high QY and longer emission lifetime compared to MQ_2 complexes. The reported complexation based phase transfer process can be considered as a new strategy to make hydrophobic Qdot water-soluble and also to provide a new material (QDC) with superior optical properties, which may be useful in LED as well as in biomedical applications.

Chapter 5

Double Channel Emission from a Redox Active Single Component Quantum Dot Complex

Herein we report the generation and control of double channel emission from a single component system following a facile complexation reaction between a Mn^{2+} doped ZnS colloidal quantum dot (Qdot) and an organic ligand (8-hydroxy quinoline; HQ). The double channel emission of the complexed quantum dot- called the quantum dot complex (QDC) - originates from two independent pathways: one from the complex (ZnQ_2) formed on the surface of the Qdot and the other from the dopant Mn^{2+} ions of the Qdot. Importantly, reaction of $ZnQ_2 \cdot 2H_2O$ with the Qdot resulted in the same QDC formation. The emission at 500 nm with an excitation maximum at 364 nm is assigned to the surface complex involving ZnQ_2 and a dangling sulfide bond. On the other hand, the emission at 588 nm - with an excitation maximum at 330 nm - which is redox tunable, is ascribed to Mn^{2+} dopant. The ZnQ_2 complex while present in QDC has superior thermal stability in comparison to the bare complex. Interestingly, while the emission of Mn^{2+} was quenched by an electron quencher (benzoquinone), that due to the surface complex remained unaffected. Further, excitation wavelength dependent tunability in chromaticity color coordinates makes the QDC a potential candidate for fabricating a light emitting device of desired color output.

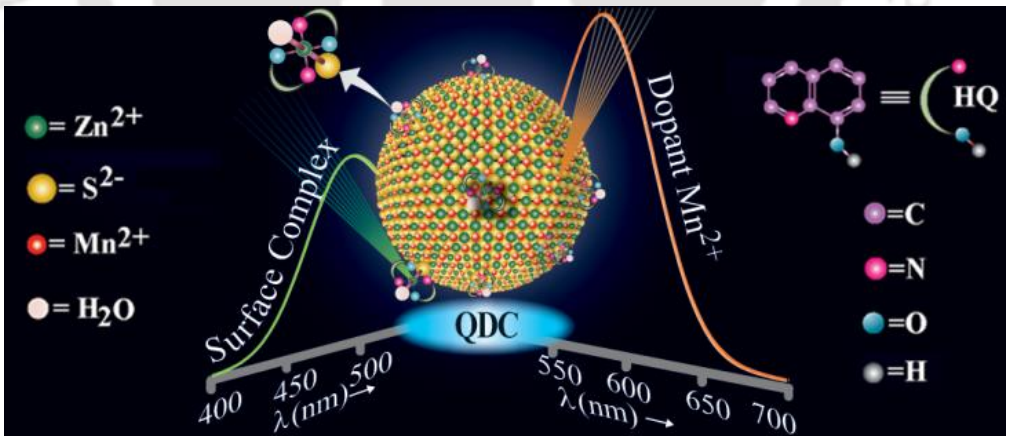

*** "Reprinted with permission from (Bhandari et al. *Langmuir*, 2015, *31*, 551–561). Copyright 2015 American Chemical Society." http://pubs.acs.org/doi/abs/10.1021/la504139m**

5.1. Experimental Section

5.1.1. Materials. 8-Hydroxyquinoline (HQ, Merck), zinc acetate dihydrate (99%, Merck), manganese acetate tetrahydrate (99%, Merck), sodium sulphide flakes (58%, Merck), sodium hydroxide (Merck), acetyl acetone (AcAc, Merck), tri-sodium citrate (99%, Merck), chitosan (medium mol. wt., Sigma Aldrich), benzoquinone (99%, Sigma Aldrich), potassium peroxodisulphate (KPS; 99% Merck), Sodium borohydride (NaBH4, 98% Acros), methanol (HPLC), potassium bromide (Sigma Aldrich), quinine sulphate, rhodamine 6G (98%, Sigma), sodium hydroxide (Merck, NaOH), hydrochloric acid (Merck), sulphuric acid (Merck) were used as received without further purification. Mili-Q grade water was used in all experiments.

5.1.2. Synthesis and characterization of Mn^{2+} doped ZnS quantum dots. A simple and aqueous based chemical precipitation method has been employed to synthesize the acetyl acetone (AcAc) capped 5.6% Mn^{2+} doped ZnS Qdots. In brief, 400.0 μL of acetyl acetone was added following the simultaneous addition of 5.0 mM zinc acetate dihydrate and 2.5 mM manganese acetate tetrahydrate in 50 mL of water under constant stirring and heating at 70-80 ^{o}C.[146] To that solution after 5 min, 5.0 mM solid sodium sulphide was added and the resulting mixture was refluxed for 3 h with constant stirring and heating at 100^{o}C. The resulting colloidal dispersion so obtained was centrifuged at a speed of 25,000 rpm for 10 min; the pellet was washed repeatedly with water, redispersed in 50.0 mL water and the same cycle was repeated. After centrifugation twice, the pellet was further redispersed into 200.0 mL of Mili Q grade water under sonication for half an hour and the redispersion was used for further experiments.[146] The same procedure was followed to synthesize AcAc capped 3.4% and 2.7% Mn^{2+} doped ZnS Qdots using 0.5 mM and 0.1 mM of manganese acetate during the synthesis.

Similar procedure was used to synthesize uncapped 5-6% Mn^{2+} doped ZnS Qdots except that no capping agent was used during the synthesis. For the synthesis of citrate capped and chitosan capped 5-6% Mn^{2+} doped ZnS Qdots, 5.0 mM tri-sodium citrate and 5.0 mM chitosan (in presence of 50.0 μL acetic acid) were used separately instead of AcAc during the syntheses and the rest of the procedure was as same as above. The synthesized Qdots were characterized using X-ray diffraction (XRD), transmission electron microscopy (TEM), high resolution TEM (HRTEM), UV-Vis,

photoluminescence (PL) and FTIR spectroscopy. The dopant mol% of the samples was calculated by using atomic absorption spectroscopic analysis.

5.1.3. Preparation of Ligand (HQ) Solutions. 5.0 mM 8-hydroxy quinoline (HQ) was dissolved in methanol under sonication for further experiments.

5.1.4. Synthesis and Characterization of $MQ_2{\cdot}2H_2O$ Complex (M =Zn or Mn).

(I) **ZnQ_2, $2H_2O$ Complex**. A simple sonochemical method was used to synthesize $ZnQ_2.2H_2O$ complex. At first, 10.0 mL of 5.0 mM HQ (in methanol) was added dropwise to a solution containing 5.0 mM of 10.0 mL zinc acetate solution (in water) under sonication for an hour.[152] The resulting yellowish green precipitate so obtained was filtered out and repeatedly washed with MiliQ water and hexane to remove unreacted zinc salts and ligand, respectively, from the mixture. The final precipitates were dried under room temperature and were redispersed into methanol for further experiments.[152]

(II) **MnQ_2,$2H_2O$ Complex**. Similar method was used to synthesize $MnQ_2.2H_2O$ complex using manganese tetrahydrate as precursor salt instead of zinc acetate. The as synthesized MnQ_2 (in methanol) was used for UV-Vis and PL analysis.

5.1.5. Synthesis and Characterization of QDCs Using Mn^{2+} Doped ZnS Qdots with Different Surface Environments.

I. Synthesis and Characterization of QDCs from AcAc Capped 5.6% Mn^{2+} Doped ZnS Qdots. The synthesis of Mn^{2+} doped ZnS Qdots was carried out using an established procedure from our laboratory. [69, 146] During the synthesis of QDC, the emission spectrum of the Qdot in the presence of ligand was monitored using 330 and 364 nm excitation wavelengths. In brief, to a 2.0 mL water dispersion of as synthesized AcAc capped 5.6% Mn^{2+} doped ZnS Qdots (with absorption values of 0.15 and 0.06 at 330 and 364 nm, respectively), 5.0 µL of 5.0 mM HQ was added sequentially, until the resultant mixture reached the maximum emission intensity at 500 nm. The optimum amount of ligand added to 2.0 mL of Qdot was found to be 30.0 µL. Further, an excess of ligand (100.0 µL) was added in order to check the saturation in complexation. The resulting mixtures of optimum and excess ligand added Qdot dispersions were centrifuged at a speed of 25000 rpm for 20 min. The supernatant was found to be

nonfluorescent (or very weakly fluorescent) at both of the excitation wavelengths (for both of the samples). The centrifuged pellets were washed with water, which were further redispersed into the same amount of solvent, and it was observed that adding excess ligand had no effect after the maximum in emission intensity at 500 nm was achieved. However, to avoid the incomplete complexation due to a lesser amount of ligand, we have used excess ligand for preparation of QDCs. The final redispersion (pH 5.8; similar to as synthesized Qdots) of the pellet was used for UV−vis, PL, time-resolved PL (TRPL), quantum yield (using quinine sulfate in 0.1 M H2SO4 as the standard), photostabilty (using rhodamine 6G as the standard dye solution), spectroscopic measurements, transmission electron microscopy (TEM), and zeta potential analysis. The solid form of QDC was used for X-ray diffraction (XRD), thermogravimetric analysis (TGA), differential scanning calorimetry (DSC), FTIR, optical microscopy, and electron paramagnetic resonance (EPR) measurements.

II. Synthesis of QDCs from AcAc Capped Mn^{2+} Doped ZnS Qdots with Different Dopant Concentrations. The method for synthesis of QDCs was the same as above except that we have used different amounts of Mn^{2+} as the precursor during the synthesis of Qdots, keeping AcAc as the stabilizer. In brief, to 2.0 mL of AcAc capped 3.4 and 2.7% Mn^{2+} doped ZnS Qdot dispersions in water, an excess (100.0 μL) of 5.0 mM HQ (in methanol) was added separately and the resulting mixtures were centrifuged and washed. Then, the pellets were redispersed into the same amount of solvents and the changes in PL, TEM based size distribution, and zeta potential values were monitored.

III. Synthesis of QDCs from 5.0−6.0% Mn^{2+} Doped ZnS Qdots with Different Capping Environments. Similarly, QDCs were synthesized using the above procedure except that, in one case, we have used no stabilizer and in other samples different stabilizers (e.g., citrate and chitosan) were used during the synthesis of Qdots, keeping the same Mn^{2+} dopant concentration (5.0−6.0%). In brief, to 2.0 mL of differently capped 5.0−6.0% Mn^{2+} doped ZnS Qdot dispersions in water, an excess (100.0 μL) of 5.0 mM HQ (in methanol) was added separately and the resulting mixtures were centrifuged. Then, the centrifuged pellets (following washing with water) were redispersed into the same amount of solvents and the changes in PL, TEM based size distribution, and zeta potential values were monitored. The powder form of the pellet was used for FTIR analysis.

5.1.6. Control experiments: Formation of QDC between $ZnQ_2.2H_2O$ complex and AcAc capped 5.6% Mn^{2+} doped ZnS Qdot. To check the attachment of parent inorganic complex ZnQ_2, we have used the same procedure for QDCs formation, except that instead of ligand we have added 200.0 μL of previously synthesized 0.5 mM ZnQ_2 complex (in methanol) to 2.0 mL of AcAc capped 5.6% Mn^{2+} doped ZnS Qdot dispersion following the step-wise titration. The resulting pellet obtained after the centrifugation and washing was further redispersed to observe the attachment of complex with fluorescence and UV-Vis.

5.1.7. Effect of Oxidizing Agent (Potassium Peroxodisulphate; KPS) and Then Reducing Agent ($NaBH_4$) on the Luminescence Properties of QDCs. To check the dopant (Mn^{2+}) oxidation state dependent emission behavior of Qdots in QDCs, at first 60.0 μL of 2.0 mM KPS (in water) was added into a 3.0 mL water dispersion of the QDC under heating at 70−80°C for 5−7 min and the resulting mixture was then brought to room temperature and was centrifuged. The obtained pellet was redispersed into the same amount of solvent and was used to observe the changes in fluorescence. In the next step, to 3.0 mL water dispersion of KPS added QDC, 60.0 μL of 13.2 mM $NaBH_4$ (in water) was added and centrifuged. The pellet was redispersed into the same amount of solvent and was used to monitor the spectroscopic changes in fluorescence. To avoid the pH effect on the luminescence of QDC during oxidation and reduction, the pH's of the medium of KPS treated QDC and $NaBH_4$ treated QDC (followed by KPS treatment) were adjusted appropriately. Further, the same cycle was performed more than once. Similarly, in order to observe the effect of pH on the luminescence of QDCs during KPS and $NaBH_4$ treatment, the pH's of the QDC solutions were adjusted to the pH's of KPS added QDC and $NaBH_4$ added QDC (followed by KPS treatment).

5.18. Formation of QDC following addition of electron quencher e.g. following benzoquinone (BQ) and Cu^{2+} addition to Qdots. At first water dispersion of 2.0 mL of AcAc capped 5.6% Mn^{2+} doped ZnS Qdot was treated with 30.0 μL of 5.0 mM BQ (in methanol)- which resulted in the quenching of dopant emission and which persisted following centrifugation and redispersion into same amount of solvent. Then the resulting mixture (redispersion) was further treated with 30.0 μL of 5.0 mM HQ (in methanol) and was again centrifuged. The pellet was redispersed into same amount of solvent and the redispersion was used to monitor the

spectroscopic changes in UV absorption and fluorescence. Similar experiment was performed using 5.0 mM Cu^{2+} instead of BQ.

5.1.9. Stability of QDCs in liquid medium and in presence of chemical means (Hg^{2+} ions). The stability of QDCs was followed by observing their UV-vis and emission spectra in water medium at different time interval. On the other hand, the chemical stability of QDCs was checked in the presence of different concentration of Hg^{2+} ions, which has higher affinity towards ligand over Zn^{2+}, according to Irving-Williams series.

5.1.10. Effect of Heating on the Luminescence Properties of QDCs as Observed through Microscopic Analysis and PL Spectroscopy. Solid QDCs were used to monitor the loss of fluorescence - if any - due to heating at high temperature, using optical microscopy. In brief, solid QDCs (placed on glass slides) were heated above 370 °C over a hot plate for 10 min and then were cooled to room temperature. The resulting solids were used to monitor PL changes (if any) using optical microscopy (under white and UV light). Further, the solids were redispersed into methanol using sonication to record the PL spectrum.

5.1.11. CIE Chromaticity Coordinates Calculation. The determination of the color point in the CIE (1931) diagram was performed with the use of "go cie" software following instructions.

5.2. Results and Discussion

Experimentally, acetyl acetonate (AcAc) stabilized 5.6% Mn^{2+} doped ZnS NCs were synthesized in an aqueous medium, based on an established procedure, and the details are described in the Supporting Information. [69, 146] The absorption spectrum of the Qdots consisted of a peak at 330 nm (Figure 5.1A). When HQ (in MeOH) was added to the dispersion, the main peak (at 330 nm) did not significantly change; however, there was a clear increase in absorption at higher wavelengths (at 364 nm in Figure 5.1A). The solid Qdots appeared pale yellowish green in visible light, and they appeared orange in the presence of UV light (inset of Figure 5.1A). On the other hand, HQ-treated Qdots appeared light brown and yellowish green in the presence of visible and UV light, respectively. The as synthesized Qdots had an emission at 588 nm when excited by 330 nm light (Figure 5.1B). Now, the sequential addition of HQ (in MeOH) to the water dispersion of Qdots led to the gradual decrease in intensity due to Mn^{2+}

emission to a value of 40% of that of the as-synthesized Qdots. There was no decrease upon further addition of HQ. On the other hand, an additional peak in the emission spectrum appeared at 500 nm, the intensity of which increased with HQ concentration to a maximum value commensurate with the decrease at 588 nm (Figure 5.1B). Further, the excitation spectrum corresponding to emission at 588 nm (of as-synthesized Qdots) consisted of a single peak at 330 nm (Figure 5.1C). On the other hand, the same for the HQ-added Qdots consisted of two peaks - one at 330 nm and another one appearing at 364 nm. Interestingly, when probed at 500 nm (emission), the excitation spectrum consisted of a single peak at 364 nm. The emission peak at 500 nm with an excitation maximum at 364 nm is blue-shifted compared to that of ZnQ_2.[175] The presence of an isosbestic point at 540 nm indicated a reaction between HQ and the Qdots. It could be that HQ addition led to ZnQ_2 formation which was attached to the surface of the Qdots. The source of Zn^{2+} could primarily be the surface ions which are more labile than those at the core. The attached ZnQ_2 had luminescence with the emission maximum at 500 nm having an excitation peak at 364 nm, whereas the emission due to Mn was quenched by the same species (ZnQ_2). The extent of quenching was limited to the concentration of ZnQ_2 present on the surface of the Qdot. Addition of excess HQ led to quenching of PL at 500 nm. Thus, the optimum amount of HQ was calculated by monitoring the emission at 500 nm with an excitation wavelength of 364 nm (Figure A.5.1, Appendix). Further, when the dispersions of optimum and excess HQ treated Qdots were centrifuged and the solids obtained were redispersed, similar PL spectra were obtained for both of the cases (Figure A.5.2, Appendix), which clearly indicated that the unbound HQ has no effect other than self-absorption. Similarly, UV−vis spectra of excess HQ treated Qdots showed that excess HQ was removed as supernatant during centrifugation (Figure A.5.3, Appendix). However, for further experiments - in order to avoid incomplete formation of the new species - we have used an excess amount of HQ followed by centrifugation of the product. The HQ treated Qdots exhibited dual emission, i.e., a new emission due to formation of a new luminescent species on the surface of the Qdots - akin to that of ZnQ_2 -in addition to partially quenched identical emission of Qdots. In the emission spectrum, the dopant emission became stronger over new luminescent species at 330 nm excitation, while the reverse was observed for 364 nm excitation (Figure 5.1D).

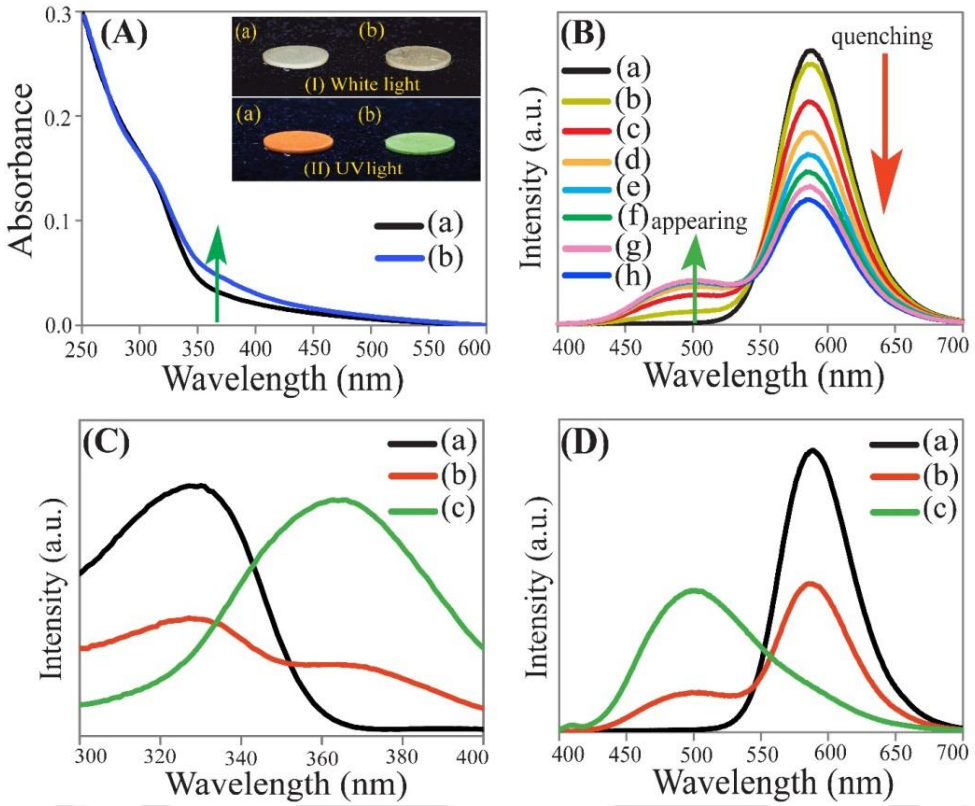

Figure 5.1. (A) UV−vis spectra and (inset) images in the presence of (I) white and (II) UV (365 nm) light of (a) the AcAc capped 5.6% Mn^{2+} doped ZnS Qdot and (b) the HQ added AcAc capped 5.6% Mn^{2+} doped ZnS Qdot (QDC). (B) Emission spectra with excitation at λ_{ex} = 330 nm of different amounts; (a) 0.0 µL, (b) 5.0 µL, (c) 10.0 µL, (d) 15.0 µL, (e) 20.0 µL, (f) 25.0 µL, (g) 30.0 µL, and (h) 35.0 µL of 5.0 mM HQ (in methanol) added to a 2.0 mL aqueous dispersion of Qdots (with absorbance at 330 nm being 0.15). (C) Excitation spectra of (a) the Qdot (λ_{em} = 588 nm) and that of the QDC at (b) λ_{em} = 588 nm and (c) λ_{em} = 500 nm. The QDC was redispersed following centrifugation of the as-synthesized sample. (D) Emission spectra of (a) the Qdot (λ_{ex} = 330 nm) and that of the QDC at (b) λ_{ex} = 330 nm and (c) λ_{ex} = 365 nm.

Importantly, the absorption as well as emission spectrum of ZnQ_2 added Qdots had the same characteristics as the HQ treated Qdots, indicating the formation of the same species either way (Figure A.5.4, Appendix). On the other hand, the absorption spectrum of HQ exhibited a peak at 316 nm, which further shifted to 380 and 384 nm following formation of ZnQ_2 and MnQ_2, respectively (Figure A.5.5 A, Appendix).[177-178] The PL spectrum of HQ showed a weak peak at 520 nm, while ZnQ_2 consisted of a strong PL peak at 550 nm and MnQ_2 was found to be negligibly fluorescent (Figure A.5.5 B, Appendix). [177-178] The observed blue shifts in absorption and emission for HQ or ZnQ_2 treated Qdots compared to ZnQ_2 indicated the formation of a new species structurally - QDC - exhibiting a dual emission over the entire visible window. It is

plausible that in the QDC, ZnQ_2 is attached to the Qdot through the surface dangling sulfide bond. Further, the extent of quenching of the Qdot PL depended on the extent of dopant present in the crystal. For example, at the highest concentration of HQ addition, when the concentration of the dopant was 5.6% the QY reduced from 6.2 to 3.0%, with retention of the peak of Mn (although with diminished intensity) (Table A.5.1, Appendix). On the other hand, when the concentration was 2−3%, the peak was solely due to the product from the reaction and the peak due to Mn was no longer prominent. It may be that when the concentration of Mn in the Qdot was low then ZnQ_2 formed on the surface completely quenched its PL and the emission was purely due to the surface complex. At higher concentration of the dopant - which means more Mn^{2+} present on the surface and thus a lower concentration of ZnQ_2 - the extent of quenching was not sufficient to diminish the PL of the doped Qdot completely. The results are shown in Figure A.5.6 (Appendix). The results indicated that formation of ZnQ_2 on the surface of the Qdots not only quenches the PL of Mn^{2+} emission of Qdots but also leads to appearance of a new PL at 500 nm, the intensity of which was commensurate with the free Zn^{2+} available on the surface. It may also be possible that MnQ_2 was formed on the surface which too contributed to the overall changes in PL due to the complex. This is suggested by the observation that MnQ_2 has an absorption spectrum with a peak at 384 nm and its emission spectrum has the same characteristic as that due to ZnQ_2 - although with much lowered QY (Figure A.5.5, Appendix). A literature report suggests that HQ forms more stable metal complexes over acetyl acetone (AcAc), for any given metal ion.28 Hence, the greater stability of metal complexes of HQ over AcAc may lead to formation of MnQ_2 -in addition to ZnQ_2 formation - on the surface of Mn^{2+} doped ZnS Qdots, notwithstanding the presence of AcAc as the stabilizer on the surface of the Qdots.

Results also indicated that the extent of quenching of PL of the dopant was dependent on the nature of stabilizers used in the synthesis of the Qdot (Figure A.5.7, Appendix). For example, for Qdots with no organic stabilizers when reacted with HQ, the QY diminished from 9.2 to 3.3% (λ_{ex} at 330 nm); for Qdots with citrate stabilizer, the extent was from 25.4 to 4.8% (λ_{ex} at 330 nm); and for chitosan stabilized Qdots, the QY reduced from 16.6 to 10.2% (λ_{ex} at 330 nm; Table A.5.1, Appendix). It may be that for the first two cases (in addition to the previous AcAc stabilized case) the formation of ZnQ_2 led to the complete coverage of the surface with the complex (accompanied by

complete replacement of the ligand in the second instance). On the other hand, in the case of biopolymer chitosan, incomplete coverage of the surface by ZnQ_2 (due to the surface area occupied by the polymer) led to quenching to a lesser extent. Further time-resolved PL of HQ treated Qdots showed tri-exponential decay irrespective of dopant concentration (Figure A.5.8, Appendix) and also of the stabilizer used during the synthesis of Qdots (Figure A.5.8, Appendix). The results (Table A.5.2, Appendix) further indicated that the PL of HQ treated Qdots had an average lifetime (τ_{av}) in the range 7.2−13.2 ns, irrespective of the dopant amount and the stabilizer used. The similar QY (with excitation at 364 nm) value (Table A.5.1, Appendix) for different amounts of dopants with the same stabilizer and similar ratios of QY of HQ treated Qdots (at 364 nm) and Qdots (at 330 nm) (Table A.5.1, Appendix) and average lifetime (Table A.5.2, Appendix) of HQ treated Qdots (without stabilizer) and Qdots for different stabilizers with the same dopant concentration indicated that similar or the same luminescent species might have been formed in all cases. In other words, in all cases, ZnQ_2 might have been formed on the surface of the Qdot, which is the emitting species, and an identical structure of the complex might be existent in all cases. Moreover, the newly formed species following addition of HQ to Qdots exhibited a high quantum yield (with excitation at 364 nm) and a longer lifetime than that of parent ZnQ_2, indicating its superior luminescent behaviour. As is clear from Table A.5.3 (Appendix), there is no significant change in pH between HQ treated Qdots and as prepared Qdots irrespective of the stabilizer used during the synthesis of Qdots, which ruled out the effect of pH on the luminescence of the product formed out of the reaction between HQ and Qdots.

Interestingly, zeta potential measurements of HQ treated Qdots prepared with different extents of dopants and stabilizers exhibited similar values of the product, which were in the range 23.8−27.4 mV (Figure A.5.9 - A.5.10, Appendix). For example, the zeta potential of AcAc capped doped ZnS Qdots with different Mn^{2+} concentrations changed from 17.2 to 26.8 mV for 5.6% Mn^{2+}, 19.9 to 26.2 mV for 3.4% Mn^{2+}, and 18.8 to 25.8 mV for 2.7% Mn^{2+} following HQ addition (Figure A.5.9, Appendix and Table A.5.4, Appendix). On the other hand, the zeta potential of 5.0−6.0% Mn^{2+} doped ZnS Qdots with different stabilizers varied from 17.1 to 27.4 mV for uncapped, 8.1 to 23.8 mV for citrate capped, and 38.3 to 24.8 mV for chitosan stabilized, following a reaction with HQ (Figure A.5.10 and Table A.5.4, Appendix). In

addition, the mobility of Qdots was modified in a similar way, which further supports that similar kinds of species were formed out of a reaction between HQ and Qdots, even in different surface environments (Table A.5.4, Appendix). Moreover, all the QDCs formed from Qdots with different surface environments exhibited similar zeta potential values close to 25 mV, indicating excellent stability of the colloidal dispersion over respective Qdots.[179] The results clearly indicated that the surface of Qdots was modified in the same way for all cases. In brief, the zeta potential measurements further supported the results that reaction of ZnS Qdots with HQ or ZnQ_2 results in the formation of the same species (QDC) and the final products are stable in the dispersion media.

Atomic absorption spectroscopy (AAS) measurements indicated that following reaction with HQ there was no significant change in the ratio of metal ion concentrations (in mol%) in any of the Qdots (with different ratios of Mn^{2+}/Zn^{2+}) tested (Table A.5.5, Appendix). In other words, the individual metal ion concentrations (Mn^{2+} and Zn^{2+}) and their ratio in the Qdots remained unaltered before and after complexation. Also, as earlier[175, 180] and current experimental results suggest, even if there was etching of the metal ions, the complex so formed upon reaction with HQ (even in the liquid medium) would be bonded to the surface sulfide ions. Thus, the concentration of metal ions on the Qdots would remain the same.

Further, transmission electron microscopy (TEM) studies revealed that following reactions with HQ the average sizes remained unchanged for uncapped and differently capped Qdots (Figures A.5.11-A.5.12 and Tables A.5.6-A.5.7, Appendix). On the other hand, the characteristic peaks in powder X-ray diffraction (XRD) patterns corresponding to (111), (220), and (311) planes and the lattice spacing (0.3 nm) of the (111) plane in high resolution TEM (HRTEM) of cubic ZnS remained the same before and after HQ treatment to Qdot (Figure A.5.13 and A.5.14, Appendix). [69, 146, 175] Similar observations were made with respect to selected area electron diffraction (SAED) studies (Figure A.5.15). [69, 146, 175] These clearly indicate that there was no morphological change in the cubic ZnS lattice of Qdots following complexation with HQ.

Fourier transform IR (FTIR) spectroscopy studies indicated the peaks characteristic of ZnQ_2, especially the functional groups (of the aromatic quinoline ring) corresponding to C− C/C−N stretching (at 1605 and 1577 cm^{-1}), pyridyl and phenyl (at

1500 and 1468 cm^{-1}), C−H bending peaks (at 1328 cm^{-1}), C−H out-of-plane wagging (at 822, 800, and 742 cm^{-1}), and in-plane ring deformation (at 742, 642, and 605 cm^{-1}), were present in the spectra of the product of reaction of HQ and AcAc capped 5.6% Mn^{2+} doped ZnS Qdots (Figure A.5.16 and Table A.5.8-A.5.9, Appendix). [152, 175] Importantly, the QDC had a strong absorption band at 1110 cm^{-1}- due to C−O stretching of metal coordinated oxine - which was absent in the Qdots. This clearly indicates the formation of a metal - oxinate complex on the surface of the Qdots. [152, 175] Similar results were obtained for other samples capped with different reagents (Figure A.5.17 and Table A.5.8-A.5.9, Appendix). Further, the formation of an octahedral ZnQ_2 complex was confirmed by monitoring the intensity ratio of the two characteristic bands at 3333 and 1110 cm^{-1}. [152, 175] The intensity ratios were found to be equal or more than 0.7 for all the QDCs obtained from Qdots with different stabilizers, which clearly indicated the formation of a complex like dihydrate ZnQ_2 (Table A.5.10, Appendix).

The results presented above suggest the formation of a new species (QDC) having dual emissive behavior - following a complexation reaction between HQ and surface Zn^{2+} ions of Mn^{2+} doped ZnS Qdots. In addition, the formation of MnQ_2 on the surface cannot be ruled out; however, its weak PL may not contribute significantly to the optical property of the QDC. We were further interested in probing the optical properties of the QDC in the presence of a redox environment. Recent work from our laboratory demonstrated that the emission characteristics of AcAc capped Mn^{2+} doped ZnS Qdots can be controlled via partial oxidation and reduction of the population of emitting dopant Mn^{2+} ions of Qdots.[69] Interestingly, in the present case, the emission at 588 nm due to Mn^{2+} dopant in QDC could also be controlled reversibly through partial oxidation and reduction. In brief, addition of an oxidizing agent (here KPS: potassium peroxodisulfate) to QDCs partially quenched the emission intensity at 588 nm (when excited at 330 nm), with little decrease in the emission intensity at 500 nm (Figure 5.2). On the other hand, addition of a strong reducing agent ($NaBH_4$) to the KPS treated QDCs fully recovered the dopant emission intensity. In addition, the emission due to the dopant (Mn^{2+}) in the QDC could be reversibly switched by redox reaction and this was possible for more than one cycle (Figure 5.2).

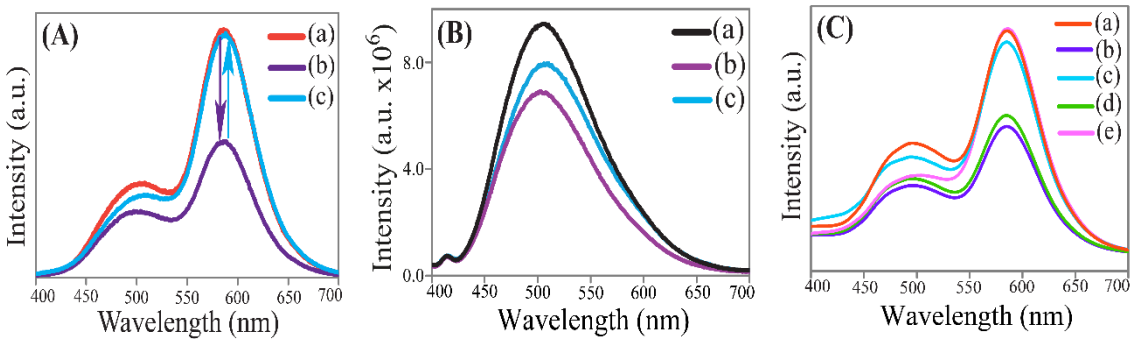

Figure 5.2. Emission spectra with λ_{ex} at **(A)** 330 and **(B)** 364 nm of (a) the HQ added AcAc capped 5.6% Mn^{2+} doped ZnS Qdot (QDC), (b) the QDC in the presence of KPS and heat, and (c) the KPS treated QDC in the presence of $NaBH_4$. All samples were centrifuged following addition of a reagent and then redispersed before recording of the spectra. **(C)** Emission spectra with λ_{ex} = 330 nm of (a) QDC; (b) QDC in presence of KPS and heat and (c) KPS treated QDC in presence of $NaBH_4$ (d) QDC followed by one cycle redox reaction in presence of KPS second time and (e) QDC followed by one cycle redox reaction and second time KPS treatment in presence of $NaBH_4$ again.

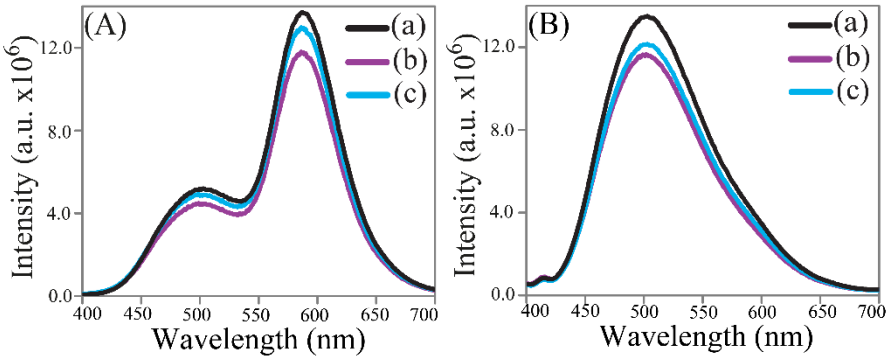

Figure 5.3. Emission spectra (A) with λ_{ex} = 330 nm and (B) with λ_{ex} = 364 nm of centrifuged excess HQ added AcAc capped 5.6% Mn^{2+}doped ZnS Qdots at pH (a) 5.8, (b) 5.3 and (c) 5.7 respectively. It is important to mention here that pH 5.3 and 5.7 were pH of the medium obtained following addition of KPS to QDC and then $NaBH_4$ to that medium, respectively. The results show weak dependence on pH of the medium in comparison to reaction with oxidizing or reducing agent.

The minor difference from the original spectrum is due to an increase in the pH of the medium following addition of $NaBH_4$. Further, by adjusting the pH of the QDCs to the observed pH of KPS treated QDCs and $NaBH_4$ added KPS treated QDCs, changes in emission intensity at 500 nm due to changes in the pH of the medium were noticed while the emission intensity at 588 nm does not show any significant changes at both of the excitation wavelengths, which clearly ruled out the effect of pH on the

observed changes in emission intensity of QDCs during KPS and $NaBH_4$ treatment (Figure 5.3).

Further, it was deemed important to identify the excitation source related to emission at 500 nm due to the ZnQ_2 complex on the surface of the Qdot. For this, the complexation reaction on the surface of Qdots was pursued in the presence of electron quenchers, i.e., benzoquinone (BQ) and Cu^{2+} ions, separately.[173] Thus, when BQ was added to the Qdots, there was no apparent change in the absorption spectrum, while the emission at 588 nm (with excitation at 330 nm) was significantly reduced (Figure 5.4). Also, the excitation spectrum corresponding to the emission at 588 nm changed, with a less prominent peak due to the Qdot. The results indicate quenching of PL of the Qdots by BQ. Now, upon addition of HQ to the medium, a new absorption peak at 364 nm appeared (in addition to that at 330 nm due to the Qdots), which was accompanied by the occurrence of a new emission peak at 500 nm. The new excitation peak at 364 nm did not have any signature of the original peak at 330 nm. Also, the emission peak at 588 nm did not reappear even with excitation at 330 nm. The results are shown in Figure 5.4. Similar results were obtained following treatment of QDC with BQ (Figure 5.4). That the loss of PL at 588 nm was due to the presence of quencher and not due to any other phenomenon (such as loss of light due to absorption by BQ having a peak at 291 nm - which is highly unlikely as per Figure 5.4) was further tested by using Cu^{2+} ions in the medium as the quencher. The results, as presented in Figure 5.5, were similar to those in the presence of BQ. For example, the loss of emission intensity at 588 nm was significant in comparison to that at 500 nm (when excited by 330 nm light). Similar observations were made when Cu^{2+} ions were added to the medium following formation of QDC (i.e., HQ was added to Qdots before addition of Cu^{2+}; Figure 5.5). It may be mentioned here that addition of Cu^{2+} ions to the medium led to brown coloration and subsequent precipitation with time, making it difficult to have observation over a longer period of time.[145, 181] The above results thus indicated independence of emission (and possibly absorption) of ZnQ_2 in the QDC from that of the Qdot. In other words, it is plausible that emission at 500 nm due to ZnQ_2 is from the excited state of the complex attached to the surface of the Qdot. However, the emission at 588 nm is still due to Mn^{2+} present in the Qdots and results from the excitation of Qdot at 330 nm. The emission of ZnQ_2 in a liquid medium did not get significantly affected by an electron quencher, such as BQ or Cu^{2+} in the QDC. This also supports

the independent nature of emission of two channels in QDC - one from the complex and the other from the Qdot.

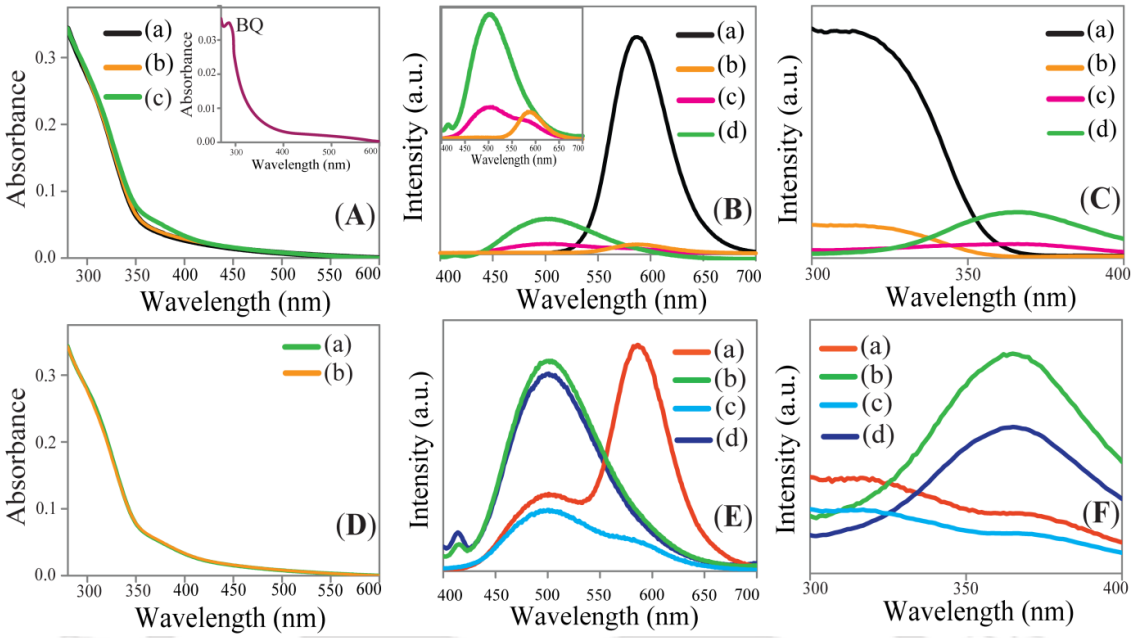

Figure 5.4. (A) UV-Vis spectra of (a) Qdots, (b) BQ treated Qdots following centrifugation and (c) BQ-treated Qdots to which HQ was added (following centrifugation), (inset- absorption spectrum of BQ); **(B)** emission spectra of (a) Qdots (λ_{ex} = 330 nm) (b) BQ treated Qdots (with λ_{ex} = 330 nm) following centrifugation; BQ-treated Qdots (as in (b)) to which HQ was added following centrifugation; monitored with (c) λ_{ex} =330 nm and (d) λ_{ex} =364 nm; **(C)** excitation spectra of (a) Qdots (λ_{em} = 588 nm) (b) BQ treated Qdots (with λ_{em} = 588 nm) following centrifugation; BQ-treated Qdots (as in (b)) to which HQ was added following centrifugation; monitored with (c) λ_{em} =588 nm and (d) λ_{em} =500 nm; **(D)** UV-Vis spectra of (a) QDC, (b) BQ treated QDC following centrifugation; **(E)** emission spectra of QDC monitored with (a) λ_{ex} = 330 nm and (b) λ_{ex} = 364 nm; BQ treated QDC following centrifugation monitored with (c) λ_{ex} = 330 nm and (d) λ_{ex} = 364 nm; **(F)** excitation spectra of QDC monitored with (a) λ_{em} = 588 nm and (b) λ_{em} = 500 nm; BQ treated QDC following centrifugation monitored with (c) λ_{em} = 588 nm and (d) λ_{em} = 500 nm.

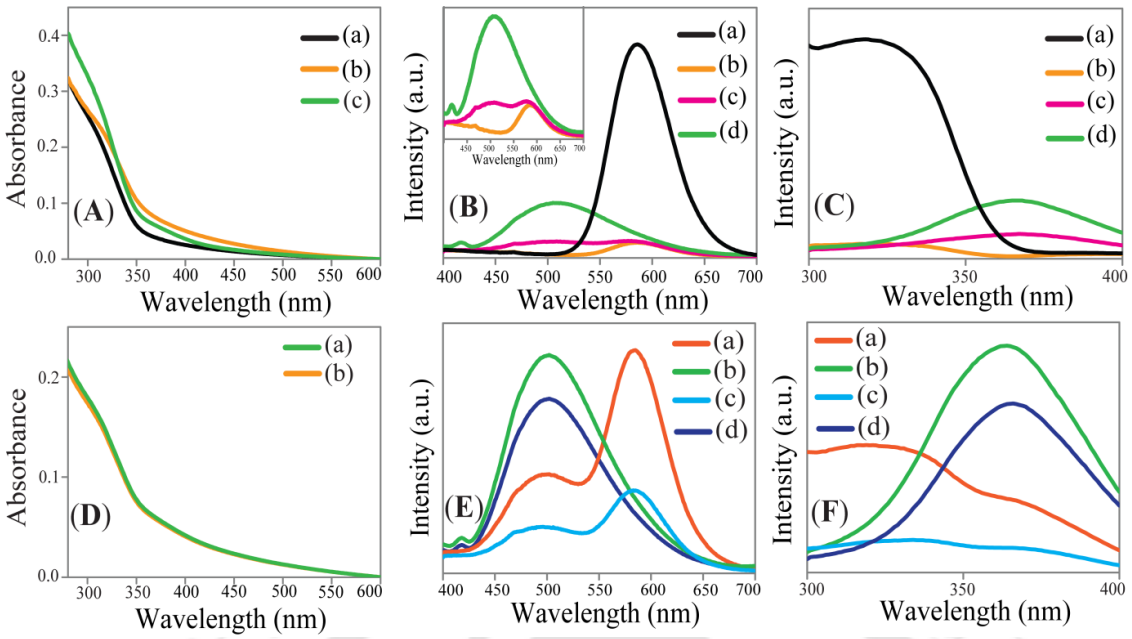

Figure 5.5. (A) UV-Vis spectra of (a) Qdots, (b) Cu^{2+}- treated Qdots following centrifugation and (c) Cu^{2+}- treated Qdots to which HQ was added (following centrifugation); **(B)** emission spectra of (a) Qdots (λ_{ex} = 330 nm) (b) Cu^{2+}- treated Qdots (with λ_{ex} = 330 nm) following centrifugation; Cu^{2+}- treated Qdots (as in (b)) to which HQ was added following centrifugation; monitored with (c) λ_{ex} =330 nm and (d) λ_{ex} =364 nm; **(C)** excitation spectra of (a) Qdots (λ_{em} = 588 nm) (b) Cu^{2+}- treated Qdots (with λ_{em} = 588 nm) following centrifugation; Cu^{2+}- treated Qdots (as in (b)) to which HQ was added following centrifugation; monitored with (c) λ_{em} =588 nm and (d) λ_{em} =500 nm; **(D)** UV-Vis spectra of (a) QDC, (b) Cu^{2+}- treated QDC following centrifugation; **(E)** emission spectra of QDC monitored with (a) λ_{ex} = 330 nm and (b) λ_{ex} = 364 nm; then Cu^{2+} was added to QDC following centrifugation and monitored with (c) λ_{ex} = 330 nm and (d) λ_{ex} = 364 nm; **(F)** excitation spectra of QDC monitored with (a) λ_{em} = 588 nm and (b) λ_{em} = 500 nm; Cu^{2+} treated QDC following centrifugation and monitored with (c) λ_{em} = 588 nm and (d) λ_{em} = 500 nm.

The electron paramagnetic resonance (EPR) spectrum, as shown in Figure 5.6, of the solid as-synthesized AcAc stabilized 5.6% Mn^{2+} doped ZnS Qdots consists of six sharp major peaks arising due to allowed M_S = −1/2 to M_S = +1/2 transition, with splitting via hyperfine interactions with the Mn^{2+} nucleus (MI = +5/2).[69, 146] The coordination of Mn in the lattice follows two types of geometry, one is tetrahedral in the core and the other is octahedral near the surface of the crystal, which can easily be identified through EPR studies.[26, 69, 146] Interestingly, the weak peaks at the edges of the sextuplet EPR spectrum of Qdot became more prominent when Qdot reacted with HQ. This clearly indicates that treatment with HQ reduced the dipolar Mn^{2+}–Mn^{2+}

interaction due to clustering of ions and the presence of a Mn^{2+} occupying octahedral geometry on the surface of Qdots. [26, 69, 146] Hence, it may also be possible that the observed changes in EPR occurred due to formation of MnQ_2 which was attached to the Qdot like ZnQ_2.

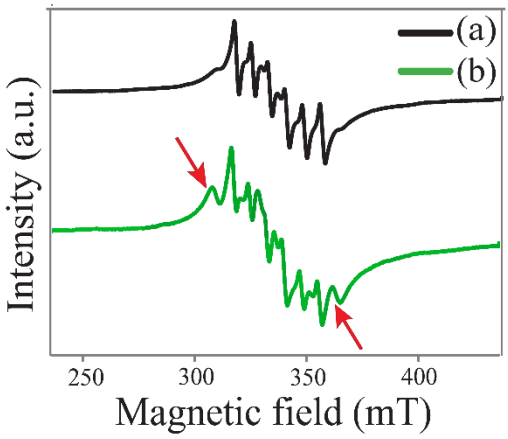

Figure 5.6. Electron paramagnetic resonance (EPR) spectra of (a) Qdots and (b) QDC.

The photostabilty of the ZnQ_2 complex as well as that of the AcAc capped 5.6 % Mn^{2+} doped ZnS Qdot was retained in the QDC, for both excitation at 330 nm (excitation maximum of the Qdot) and at 364 nm (excitation maximum of the complex). It was also observed that the photostabilty of the complex was 3.7 times that of an organic dye (Figure 5.7 and Table A.5.11). For example, the change in luminescence of the QDC was found to be 0.03%/s, whereas that of rhodamine 6G was 0.11%/s.

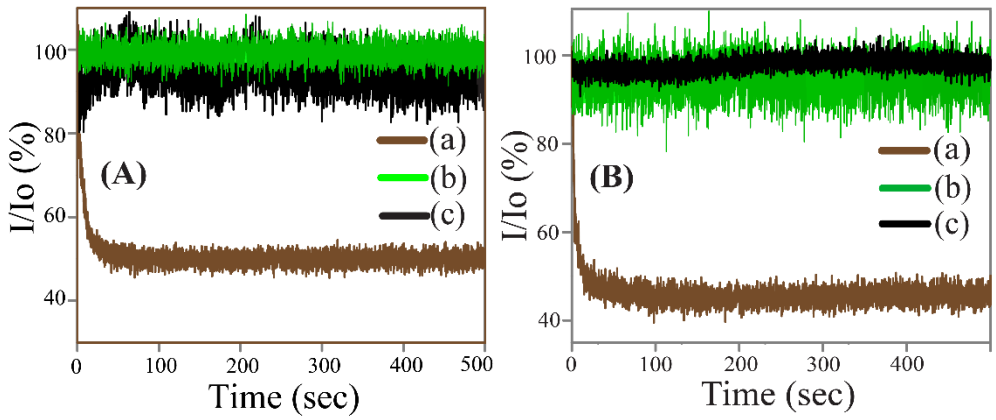

Figure 5.7. Photochemical stability under continuous irradiation of light of **(A)** λ_{ex} - 330 and **(B)** λ_{ex} - 364 nm of (a) organic dye (rhodamine 6G), (b) QDC, and (c) Qdots.

Thermogravimetric analysis (TGA) of Qdots and QDCs showed similar kinds of weight loss (15−20%) up to 90 °C due to removal of the surface adsorbed water. [152]

There was no significant weight loss up to 550 °C (Figure 5.8). The absence of weight loss at 440 °C in QDCs revealed the enhancement of the thermal stability of the ZnQ_2 complex on the surface of Qdots. The parent ZnQ_2 complex showed major weight loss at around 440 °C due to loss of its structure.[152] Similarly, the major endothermic peak at 360 °C for melting of the ZnQ_2 complex in the differential scanning calorimetric (DSC) curve was absent in QDCs obtained from Qdots, which further supported the extraordinary thermal stability of the ZnQ_2 complex on the surface of the Qdots (Figure A.5.18, Appendix). [152]

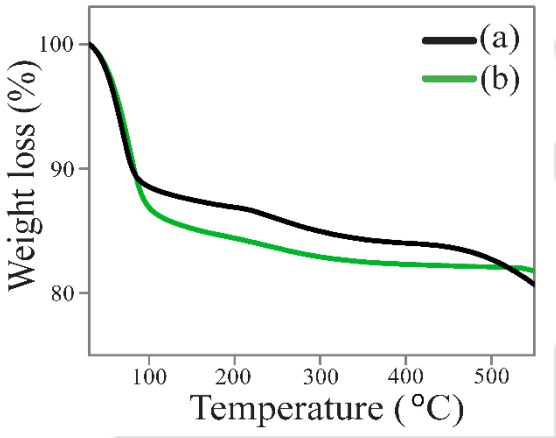

Figure 5.8. Thermogravimetric analysis of (a) Qdots and (b) QDC.

The results described above point to chemical reaction between the Qdots and HQ leading to the formation of a new and luminescent species. The QDC emits in the visible region with two independent sources of excitation and emission. A schematic representation in Figure 5.9A depicts the double channel emission in QDCs, following a complexation reaction between HQ and Mn^{2+} doped ZnS Qdots. PL emission of Mn^{2+} doped ZnS Qdots at 588 nm is due to the transition $^4T_1$–$^6A_1$ of dopant Mn^{2+}.[69, 146, 182] Recently, we have observed that the surface Mn^{2+} ions of Mn^{2+} doped ZnS Qdots synthesized in aqueous medium at comparatively low temperature are also responsible for the emission. [69, 146] On the other hand, emission form the surface ZnQ_2 complex originates from the optical transition from the electron rich phenoxide ring (HOMO; highest occupied molecular orbital) to the electron deficient pyridyl ring (LUMO; lowest occupied molecular orbital) and the nature of the emission depends upon the coordination of the ligand and the presence of an additional functional group in the ligand.[154-155,175] The above observations are in concordance with the literature, where introduction of electron withdrawing groups in phenoxide and the pyridyl ring of AlQ_3

complexes cause blue shifts and red shifts, respectively, in their emission maximum, while the reverse case was observed in the case of electron donating groups.[154-155] It is well-known that the surface metal ions (here Zn^{2+} and Mn^{2+}) and anions (S^{2-}) -bonded to the Qdot via dangling bonds - are prone to binding to an external ligand. Among the two metal ions on the surface of Qdots, Zn^{2+} may bind to HQ preferentially over Mn^{2+} to form QDCs according to Irving-Williams series.33 In addition, Mn^{2+} may also be involved in forming MnQ_2 in QDCs but in competitive complexation Zn^{2+} forms a complex preferentially. During the formation of QDCs, the metal ions may be removed from the surface, followed by formation of a complex with HQ (ZnQ_2) and then the complex is attached to the surface. The complex (ZnQ_2) may be bound to the Qdot through a dangling sulfide bond of the Qdot and by replacing one of the water molecules of the $ZnQ_2{\cdot}2H_2O$ complex. The so formed complex replaces the stabilizer of Qdots and acts as a stabilizer in QDCs. This may be the reason for the chemical stability of the complex and also the observed changes in optical parameters like absorption and emission maxima, QY, average lifetime, and enhancement of the thermal stability on the surface of Qdots in comparison to the bare $ZnQ_2{\cdot}2H_2O$ complex.[175] For example, the absorption and emission maxima of surface ZnQ_2 are blue-shifted compared to bare ZnQ_2. There may be several such complexes formed on the surface of the same Qdot. The QDC contains an attached ZnQ_2 complex and Mn^{2+} ions as emissive species, thereby generating two independent channels of emissions (and absorption) from a single species.

Results of our previous experiments and current observations suggest that an octahedral complex is formed on the surface of a Qdot. For example, our observations following addition of HQ as well as a ZnQ_2 complex to ZnS, $Zn_xCd_{1-x}S$, and Mn^{2+} doped CdS (both with and without a stabilizer for all the Qdots) indicated that the complexes formed on the surface of all of them (Qdots) are the same as their optical properties and the signatures from FTIR spectroscopy are the same.[175, 180] Similar results were obtained following addition of CdQ_2 to $Zn_xCd_{1-x}S$ Qdots. [180] Additionally, when Na_2S was added to ZnQ_2, the PL results were similar to those of the QDC. [175] Further, our observations based on exchange of ligand (HQ) with hydrophobic $Zn_xCd_{1-x}S$ Qdots, leading to their phase transfer, indicated similarly structured complex formation on the surface.[180] What we have proposed is that ZnQ_2 and CdQ_2 complexes are octahedral in nature with two axial positions occupied by water. However, in the presence of sulfide

ions, one of the positions or both of the positions may be occupied by S^{2-}. In the case of a complex formed on the surface of the Qdots, one of the positions will probably be occupied by S^{2-} an ion, which itself is connected to the Qdot via a dangling bond. Thus, the evidence is convincing enough to propose the current model. Figure 5.9B depicts the dependence of the emission intensity of QDC on the excitation wavelength in the range 330−365 nm. The three-dimensional plot clearly shows that for excitation at 330 nm the dopant emission (at 588 nm) becomes stronger over surface complex emission (at 500 nm). As the excitation wavelength is increased toward 364 nm, the stronger dopant emission becomes weaker while the surface complex emission becomes stronger. Similarly, the contour plot of the excitation−emission matrix (EEM) (Figure 5.9C) indicates the independent nature of dopant and surface complex emissions in QDCs. For example, the intensity zone becomes higher in value (red in color) at 588 nm with excitation at 330 nm and at 500 nm with excitation at 364 nm. Hence, the nature of two independent emissions in double channel emission of a single emitting species depends upon the wavelength of excitation. In Figure 5.9D, the individual band gaps of the constituent species (Qdots and surface ZnQ_2 complex) in QDC exhibit two different pathways for the double channel emission. Thus, at the band gap excitation of Qdots, the dopant emission becomes stronger and the surface complex emission becomes weaker while the case is reversed at the band gap of the surface ZnQ_2 complex. Thus, it may be concluded that two different species (Mn^{2+} dopant and surface ZnQ_2) follow different paths to generate emission in QDCs.

Optical microscopic results (Figure 5.10 A-B) indicated that following formation of the QDC the color of the Qdot changed from pale yellowish green to dark brown, which is the characteristic color of $ZnQ_2{\cdot}2H_2O$. The same samples when observed under UV light were orange and green (characteristics of doped Qdot and complex, respectively), which further supported the formation of the QDC. Interestingly, when the solid QDC was heated over 370 °C for 10 min (and then cooled to room temperature), the color in white and UV lights was the same as before heating (Figure 5.10 C), which supported the retention of PL behavior following heating at a higher temperature. This is in contrast to $ZnQ_2{\cdot}2H_2O$, which loses its PL upon heating at 370 °C due to loss of its structure. Further, dispersion of QDC (in methanol; Figure 5.19, Appendix) - following heating - exhibited the PL of the sample before heating, pointing to enhanced stability of the complex upon incorporation in the Qdot.

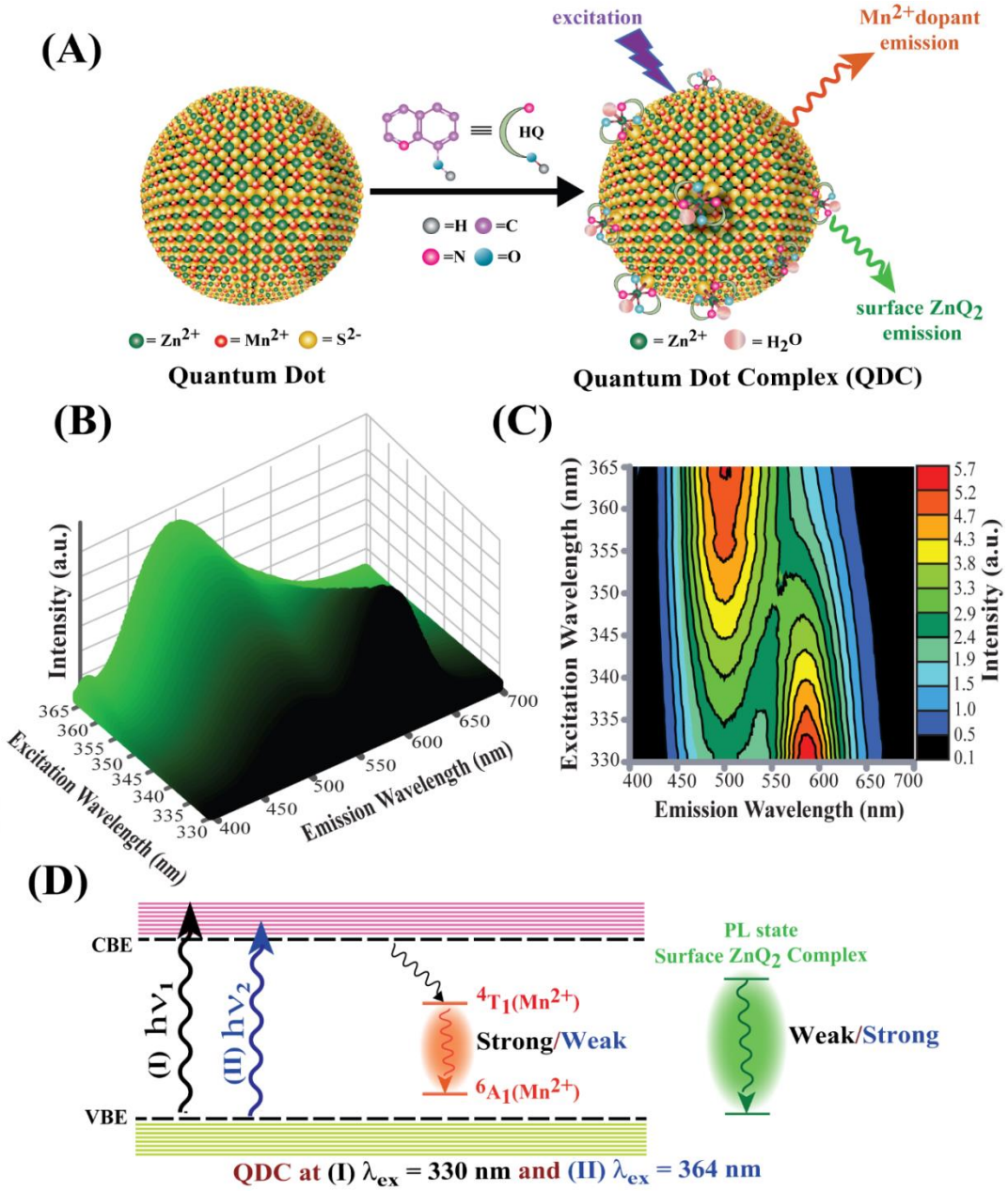

Figure 5.9. (A) Schematic representation of quantum dot complex (QDC) formation on the surface of Mn^{2+} doped ZnS Qdots involving surface Zn^{2+} ions and organic ligand (HQ). (B) Three-dimensional (3D) representation of excitation dependent emission spectra and (C) the corresponding excitation−emission matrix (EEM) contour plot of the QDC. (D) Energy level diagram illustrating the energy gaps corresponding to two different emission channels at two different excitations in the quantum dot complex (QDC).

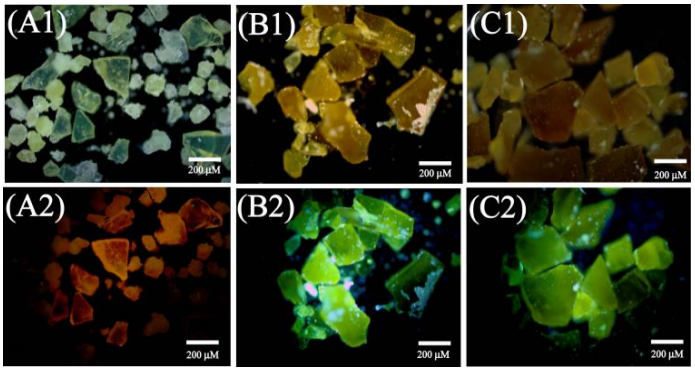

Figure 5.10. Microscopic images of solid samples of **(A)** AcAc capped 5.6% Mn^{2+} doped ZnS Qdot, **(B)** HQ added AcAc capped Mn^{2+} doped ZnS Qdot (QDC) and **(C)** QDC after heating at 370 °C. The images were recorded in presence of (1) white and (2) UV light (λ_{ex} = 350 nm). The samples were prepared by centrifugation of the QDC. The samples were then placed on glass microscope slides for imaging as well as heating.

On the other hand, no significant change was observed in the absorption and emission behavior of QDCs in liquid medium (in water) up to 24 h (Figure A.5.20, Appendix), which clearly indicated the stability of QDCs in the liquid medium. Further, in order to test the chemical stability of the QDC, its water dispersion was treated with Hg^{2+} ions of different concentrations, which led to the quenching of emission at two different excitation wavelengths (330 and 365 nm, Figure A.5.21A-B, Appendix), followed by yellow colored precipitation (inset, Figure 5.21A, Appendix). Similar observations were made when the Qdots were treated with Hg^{2+} (Figure A.5.21C, Appendix). Our earlier observation indicated reaction between ZnS Qdots and Hg^{2+}, leading to formation of HgS (yellow in color).[145] Thus, it would not be possible to clearly demonstrate chemical stability of the surface complexes in the presence of metal ions like Hg^{2+}- which has a higher affinity toward the ligand HQ over Zn^{2+}, according to Irving−Williams series.

Further, the differences in CIE (Commission Internationale del'Eclairage 1931) chromaticity color coordinates were observed when the bare ZnQ_2 complex (or HQ) reacted with Qdots to form a single component system QDC, which was purified by centrifugation. As is clear from Figure 5.11A-B and Table 5.1, at an excitation wavelength of 330 nm, the chromaticity coordinates of Qdots changed from (0.55, 0.45) to (0.42, 0.43) and similarly, at an excitation wavelength of 365 nm, the chromaticity coordinates of bare ZnQ_2 changed from (0.41, 0.54) to (0.24, 0.40) following the complexation reaction. The shifts in chromaticity coordinates also

supported the formation of a new single component luminescent species, following complexation between Qdots and ZnQ_2 (or HQ). In addition to the excitation dependent emissive behaviour of QDCs (Figure 5.12C), the tunability in their chromaticity coordinates in the CIE diagram was observed (Figure 5.11D, Table 5.1) and some of the chromaticity coordinates were falling into the near white light region.[29, 183-184] For example, points c, d, and e (Figure 5.11D, Table 5.1) exhibited (0.37, 0.42), (0.34, 0.41), and (0.30, 0.41) chromaticity coordinates, respectively, which are close to perfect white light chromaticity coordinates (0.333, 0.333).40−42 Hence, the precise control over the chromaticity coordinates of single component QDCs in CIE color output - in addition to their excitation dependent double channel emissions - not only brings a new paradigm for solid state lighting but also makes a successful step toward fabricating devices of desired color output.

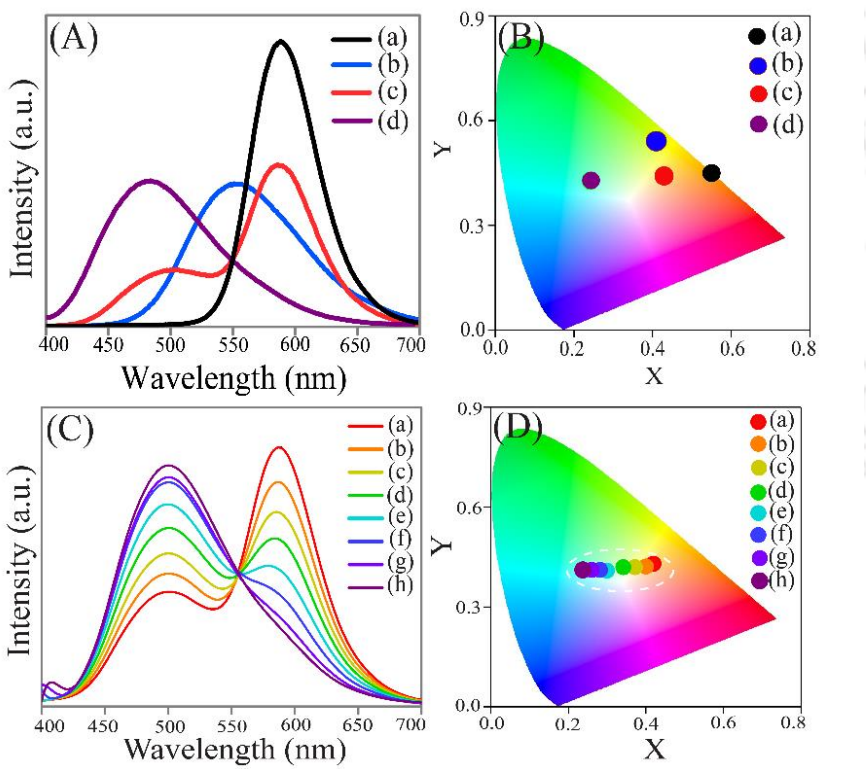

Figure 5.11. (A) Emission spectra of (a) acac capped 5.6% Mn^{2+} doped ZnS Qdots (λ_{ex} -330 nm), (b) bare ZnQ_2 complexes (λ_{ex} -365 nm) (c) QDC (λ_{ex} -330 nm) and (d) QDC (λ_{ex} -365 nm) following complexation between Qdots and HQ and **(B)** their corresponding CIE coordinates. **(C)** Emission spectra and **(D)** corresponding CIE chromaticity diagram of QDCs at the excitation wavelengths of (a) 330 nm, (b) 335 nm, (c) 340 nm, (d) 345 nm, (e) 350 nm, (f) 355 nm, (g) 360 nm and (h) 365 nm.

Sample	λ_{ex} (nm)	CIE Coordinates	
		X	Y
(a) Qdots	330	0.55	0.45
(b) ZnQ_2	365	0.41	0.54
(c) QDC	330	0.42	0.43
	335	0.40	0.42
	340	0.37	0.42
	345	0.34	0.42
	350	0.30	0.41
	355	0.28	0.41
	360	0.26	0.41
	365	0.24	0.40

Table 5.1. CIE chromaticity coordinates value of (a) acac capped 5.6% Mn^{2+} doped ZnS Qdots (λ_{ex} -330 nm), (b) bare ZnQ_2 complexes (λ_{ex} -365 nm) (c) QDC at different excitation wavelengths.

Recent literature reports suggest that the drawbacks of a multicomponent system such as color aging, complicated processing technique, self-absorption, scattering, nonradiative energy transfer, and undesirable changes in chromaticity coordinates for fabricating light emitting devices can easily be overcome by using a single component system composed of different emitters over the entire visible window.[183, 185] Although Mn^{2+} doped ZnS Qdots and bare ZnQ_2 complexes were used in fabricating devices, they also suffered from problems due to processing, thermal and optical stability, blinking, and chemical degradation.[175, 184] In this regard, QDC may be able to overcome some of these issues and may have importance over their individual components in solid state lighting. Finally, tuning the chromaticity color coordinates in the CIE diagram of light harvesting material is important for fabricating devices of desired color output - in addition to generating white light emission.[185] Thus, it is important to achieve a change in the chromaticity coordinates of Qdots following their synthesis, which is otherwise achieved during synthesis such as in Mn doped ZnSe.40 This will not only avoid the uncertainties of exact chromaticity coordinate variations but may also be important for solid state lighting.

5.3. Conclusion

In brief, we have reported new surface reactions of HQ with Mn^{2+} doped ZnS Qdots to create a QDC that displays independent dual-channel emissions. Further, the retention of redox behavior of the emitting Mn^{2+} species and without affecting the emission of the ZnQ_2 surface complex provides a new regime in the optical properties involving Qdots and metal complexes. That the emission could be quenched selectively is important for sensing chemical species in liquid medium. Finally, the thermally stable complex on the Qdot provides a new LED material with enhanced emissivity both in terms of wavelength and intensity. This is expected to open new avenues in optical materials with superior roles of principles of chemistry. Further, the excitation dependent tunability in chromaticity color coordinates of QDCs not only makes them advantageous over their components toward the development of LED material of desired color output but also provides control over chromaticity of the material following their synthesis.

Chapter 6

Surface Complexation Based Biocompatible Magnetofluorescent Nanoprobe for Targeted Cellular Imaging

We report the synthesis of a magnetofluorescent biocompatible nanoprobe – following room temperature complexation reaction between Fe_3O_4-ZnS nanocomposite and 8-hydroxyquinoline (HQ). The composite nanoprobe exhibited high luminescence quantum yield, low rate of photobleaching, reasonable excited-state life time, luminescence stability especially in human blood serum, superparamgnetism and no apparent cytotoxicity. Moreover, the nanoprobe could be used for spatio-controlled cell labeling in the presence of an external magnetic field. The ease of synthesis and cell labeling in vitro make it a suitable candidate for targeted bioimaging applications.

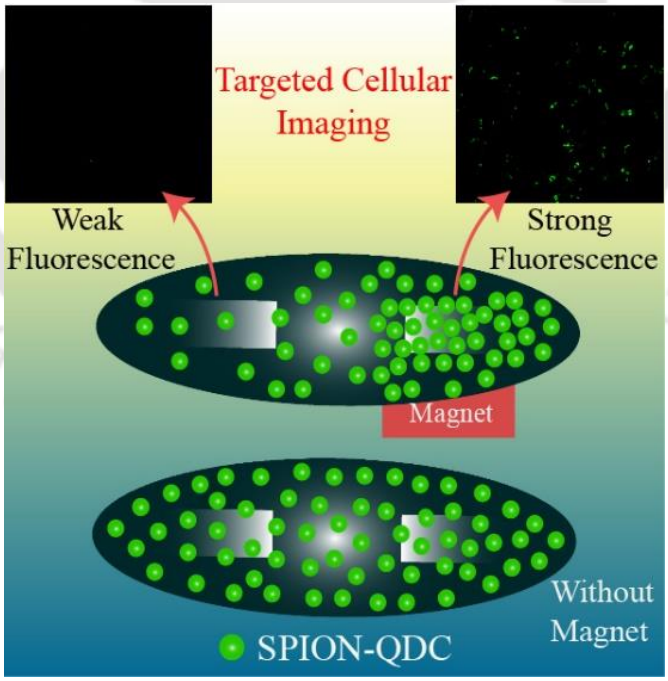

6.1. Experimental Section

6.1.1. Materials. 8-Hydroxyquinoline (HQ, Merck), iron chloride hexahydrate (Sigma Aldrich), sodium oleate (Merck), oleylamine (CDH), oleic acid (Merck), tetramethylammonium hydroxide (Spectrochem), zinc acetate dihydrate (Merck), sodium sulphide (58%, Merck), L- cysteine hydrochloride (Loba Chemie, India), sodium hydroxide (Merck), quinine sulphate (Sigma Aldrich), rhodamine 6G (Sigma Aldrich), hexane (Merck) and ethanol (Merck) were purchased and used without further purification. Mili-Q grade water was used for the synthesis and in all other experiments.

6.1.2. Synthesis and characterization of SPION-QDC (HQ treated Fe_3O_4-ZnS composite)

6.1.2.1. Synthesis of Fe_3O_4 nanoparticles. The water dispersible Fe_3O_4 nanoparticles were synthesized in three steps: (1) firstly, Fe-oleate complex was synthesized; (2) which was then used to synthesize water insoluble Fe_3O_4 nanoparticles and (3) finally, the water insoluble Fe_3O_4 nanoparticles were transferred to water using phase transfer agent, based on reported protocols.[186-187] To synthesize Fe-oleate complexes, 3.24 g of iron chloride hexahydrate and 18.25 g sodium oleate were mixed in a solvent mixture of hexane (18.0 mL), water (15.0 mL) and ethanol (8.0 mL) and the resulting solution was heated at 70 $^{\circ}$C under constant stirring and refluxing. After 4 h, a dark brown crystalline precipitate separated out into the upper hexane layer, which was collected by filtration, followed by washing with water-ethanol mixture (4-5 times).[1-2] Following this, 300.0 mg of the as-synthesized crystalline Fe-oleate complex was added into a mixture of oleylamine and oleic acid (3:1) and was refluxed for 1 h at 120 $^{\circ}$C until the solution became black.[186-187] Then the temperature was raised from 120 °C to 200 °C and immediately nitrogen gas was blown through the reaction mixture. Then the temperature was further raised to 300 °C and the solution was allowed to heat for another 2 h under constant stirring. After the completion of the reaction, ethanol was added to precipitate out the product from the solution and then the precipitate was further washed with hexane-ethanol mixture to remove excess oleic acid and oleyl amine.[186-187] Finally, the precipitate was transferred into water medium by dissolving in 1 M tetramethylammonium hydroxide (TMAOH) under constant sonication.[186-187] The transferred product was collected using a magnet, which was followed by washing with

Milli-Q water for 3 times to remove excess ligand. Finally, the precipitate was dispersed in 500 mL Milli-Q water for further characterization and other experiments.

6.1.2.2. Synthesis and characterization of Fe_3O_4-ZnS composite. Fe_3O_4-ZnS composite was synthesized using the as prepared the Fe_3O_4 nanoparticles as seeds and then following our earlier (reported) method of synthesis of cysteine capped ZnS Qdots.[175] At first, 5.0 mM zinc acetate dihydrate was added to a solution containing 10.0 mL of as synthesized Fe_3O_4 in Mili-Q water (dark brown in color) in a round bottom flask and then the volume of the solution was made up to 30.0 mL with water under constant stirring. To that mixture, 10.0 mL of 25.0 mM cysteine hydrochloride solution (pH-11.0) and 10.0 mL of 25.0 mM sodium sulphide (in water) were added under constant stirring and kept that for another 3 h at 100 ^{0}C under reflux condition. After half an hour, the dark brown color of the solution became light brown. After 3 h, the resulting light brown color solution was centrifuged with a speed of 20000 r.c.f. for 10 min, in order to remove the unreacted salts; the so obtained pellet was repeatedly washed with water. Then the pellet was redispersed into the same amount of water and kept in presence of an external magnet. With the help of the magnetic field, the unbound ZnS Qdots were removed and the particles accumulated towards the magnet were collected. The particles were further dispersed and then centrifuged and the same cycle was repeated. Finally, the particles were dispersed in water for further characterization and experiments.

6.1.2.3. Preparation of ligand (HQ) solution. The solid powder of 5.0 mM 8-hydroxy quinoline (HQ) was dissolved in ethanol using sonication.

6.1.2.4. Synthesis and characterization of the SPION-QDC composite. The emission spectrum (λ_{ex}-365 nm) of as synthesized Fe_3O_4-ZnS in the presence of HQ was used to monitor and to confirm the completeness of the complexation reaction. In brief, sequentially 2.0 μL portions of 5.0 mM HQ was added to 2.0 mL aqueous dispersion of as-synthesized Fe_3O_4-ZnS (with an absorption value of 0.2-0.25 at 320 nm) until the resulting mixture showed the maximum emission intensity at 500 nm. Then the resulting mixture was centrifuged at a speed of 20000 rcf for 20 min. It was found that the supernatant had negligible emission intensity at 500 nm. Finally, the so obtained pellet was washed with water and further redispersed into the same amount of water for further characterization and experiments.

The resulted aqueous dispersion of the pellet in water was used for recording visual images in absence and presence of an external magnet under white and UV light (365 nm), UV–vis and photoluminescence (PL) spectra, quantum yield (using quinine sulfate in 0.1 M H_2SO_4 as the standard), time-resolved PL (TRPL) spectra, photostability (using rhodamine 6G as the reference dye solution), transmission electron microscopy (TEM), high resolution TEM (HRTEM), selected area electron diffraction (SAED) and atomic absorption spectroscopic (AAS) measurements. The solid form of the pellet was used for optical microscopy, Fourier transform infrared (FTIR) and X-ray diffraction (XRD).

6.1.3. Control experiments. Similar complexation reaction was carried out between 2.0 mL aqueous dispersion of as prepared Fe_3O_4 nanoparticles and 30.0 μL of 5.0 mM HQ (in ethanol). The resulting mixture was subjected through centrifugation and redispersion, which was used to measure the PL.

6.1.4. Study of Stability (using luminescence) of the SPION-QDC in human blood serum. Blood sample was collected from a healthy volunteer, as per the guidelines of Indian Institute of Technology Guwahati (India) and the serum was separated from the coagulated blood by centrifugation. Then 0.05 mg mL^{-1} amount of the SPION-QDC was incubated with 2.0 mL serum sample and the change in emission intensity at 500 nm was monitored with regular time interval (until 24 h).

6.1.5. Cell viability assay. HeLa cells, procured from National Center for Cell Sciences (NCCS), Pune, India, were cultured in Dulbecco's modified Eagle's medium, supplemented with L-glutamine (4 mM), penicillin (50 units mL^{-1}), streptomycin (50 mg mL^{-1}) and 10 % (v/v) fetal bovine serum. Cells were maintained in 5 % CO_2 humidified incubator at 37 °C. 10^4 HeLa cells/well were seeded in a 96 well microplate and grown overnight. Then, the medium was removed and fresh medium containing different concentrations of SPION-QDC (0.07 mg mL^{-1} – 0.36 mg mL^{-1}) was added to the cells and incubated for 24 h, in a humidified atmosphere containing 5% CO_2 at 37 °C. Following this, the cells were washed with PBS for several times and finally MTT (3-(4,5-dimethylthiazolyl-2)-2,5-diphenyltetrazolium bromide) based cell viability assay was carried out in triplicates, according to the established protocol.

6.1.6. Recording of luminescence of HeLa cells incubated with SPION-QDC, in the presence and absence of an external magnetic field. 2×10^5 HeLa cells were seeded onto two coverslips placed inside 35 mm cell culture petri plate and the cells were allowed to grow overnight. Then the medium was removed and a fresh medium containing SPION-QDC (0.05 mg mL^{-1}) was added to the cells. A rare earth magnet was placed below the petri plate such that one coverslip was just above the magnet and the other one was away from magnet (Figure S14). After 4 h of incubation, the cells were washed with PBS for several times and then were fixed with freshly prepared 4% formaldehyde solution for 15 min at room temperature. The cells were washed again and finally mounted on a glass microscopic slide with a drop of mounting agent. The coverslips were sealed and then the samples were visualized under epi-fluorescence microscope (Nikon Eclipse TS100, Tokyo, using Qdot 525 nm filter). The cells were similarly incubated with SPION-QDC in the absence of the magnet and were processed as above for other analyses. Following similar incubation process, the cells (with SPION-QDC) were also imaged under Leica TCS SP8 STED (using 405 nm diode laser) microscope.

6.2. Results and Discussion

Experimentally, cysteine-capped Fe_3O_4-ZnS composite was synthesized using 7.7 ± 3.2 nm Fe_3O_4 NP as seed and onto which cysteine capped ZnS Qdots were grown, based on an earlier method, (Figure 6.1).[175, 188-189] The powder x-ray diffraction (XRD) pattern of the solid Fe_3O_4-ZnS composite (obtained following magnetic separation) showed diffraction patterns due to the cubic inverse spinel Fe_3O_4 and cubic ZnS, thus confirming the formation of composite material (Figure 6.2). [175, 188-189] Also, as is clear from the high resolution TEM image, 3.2 $\pm$ 0.6 nm ZnS Qdots were formed surrounding the Fe_3O_4 NPs. The formation of moiré pattern (Figure 6.3) also indicated the presence of overlapping crystals of similar lattice parameters i.e. cubic inverse spinel Fe_3O_4 (0.28 nm) and cubic ZnS (0.3 nm). [175, 188-189] In a similar vein, the selected area electron diffraction (SAED) analysis of the composite also supported the presence of both the crystals (SI, Figure S3B).The growth of ZnS nanocrystals on the surface of the Fe_3O_4 NPs was accompanied by the change in zeta potential from –52.0 $\pm$ 0.5 mV (for Fe_3O_4 NPs) to –31.1 $\pm$ 0.1 mV (for the composite, Table A.6.1, Appendix).

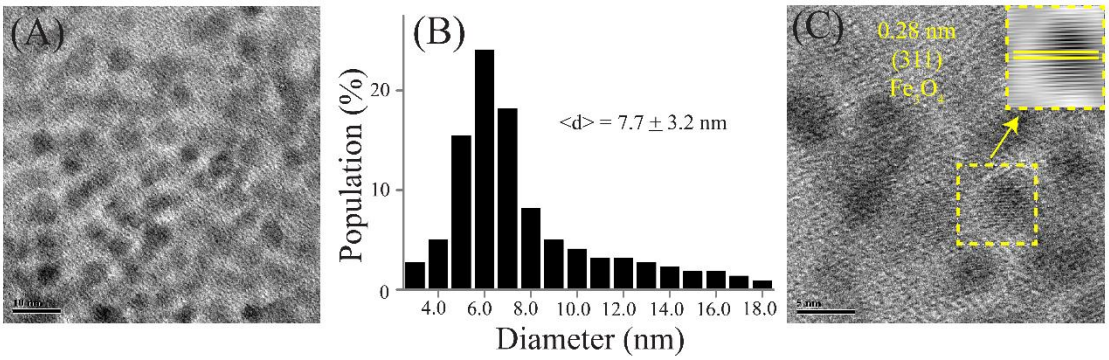

Figure 6.1. (**A**) Representative TEM (scale bar-10 nm) image, (**B**) corresponding particle size distribution and (**C**) high resolution TEM image (scale bar- 5 nm) of the aqueous dispersion of as synthesized Fe_3O_4 nanoparticles. The 0.28 nm lattice fringes correspond to (311) plane of inverse spinel Fe_3O_4 nanoparticles.[175, 186-189]

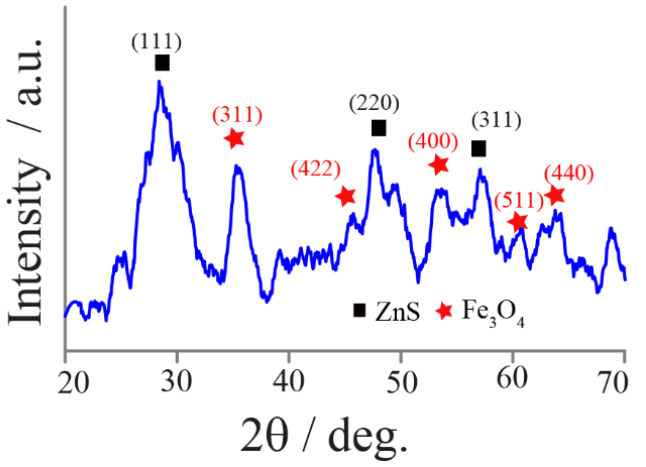

Figure 6.2. Powder x-ray diffraction (XRD) pattern of the solid particles of Fe_3O_4-ZnS.The powder x-ray diffraction pattern showed the presence of the characteristic peaks of cubic inverse spinel Fe_3O_4 with diffractions at 35.6º, 45.2º, 53.5º, 60.4º and 66.2º, corresponding to (311), (400), (422), (511) and (440) planes (marked as red star) and cubic ZnS with diffractions at 28.8º, 48.2º and 57.0º, corresponding to (111), (220) and (311) planes (marked as black square boxes). [186-190]

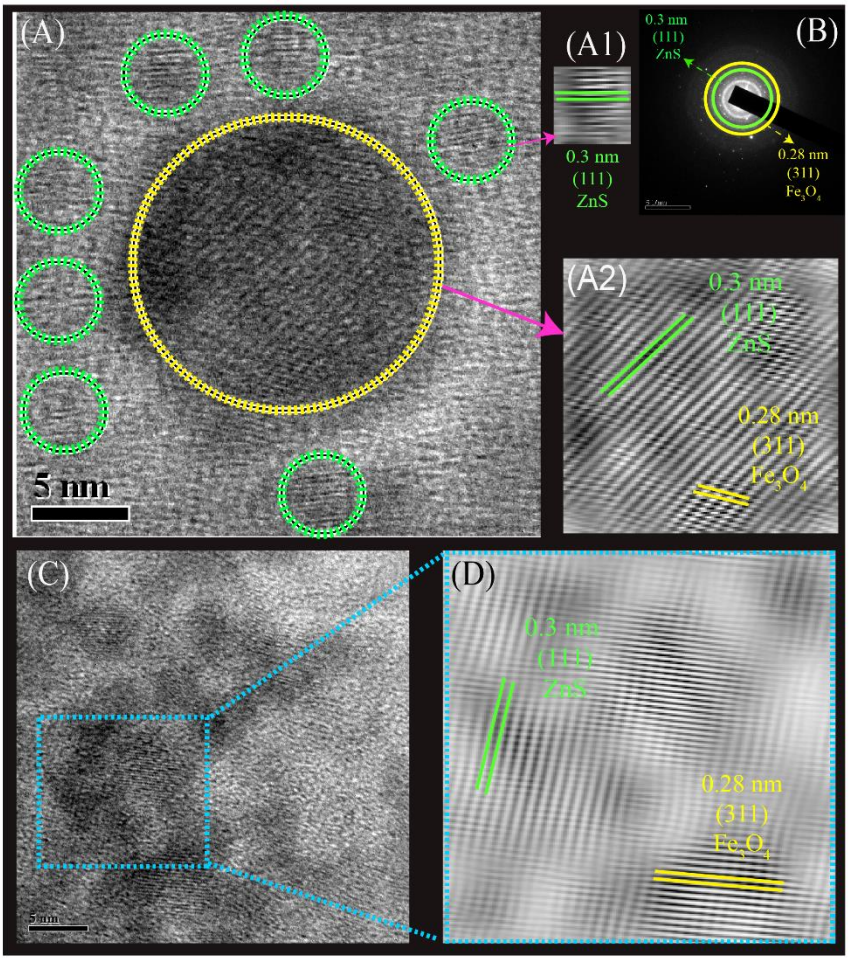

Figure 6.3. (**A**) High resolution TEM (HRTEM; scale bar-5 nm), (1, 2) corresponding inverse fast Fourier transform (IFFT) images and (**B**) selected area electron diffraction (SAED) pattern (scale bar: 5 nm^{-1}) of the aqueous dispersion of Fe_3O_4-ZnS composite obtained following focusing on the Fe_3O_4 nanoparticle which has size greater than 10 nm, so that 3.2 nm ZnS Qdots could easily be observed simultaneously; (**C**) high resolution TEM (HRTEM; scale bar-5 nm) and (**D**) corresponding inverse fast Fourier transform (IFFT) images of the Fe_3O_4-ZnS composite obtained following focusing on another zone, where Fe_3O_4 nanoparticles and ZnS Qdots have similar sizes. The high resolution TEM images and the IFFT patterns in Figure S3A clearly showed the presence of ZnS Qdots surrounding the Fe_3O_4 nanoparticles (>10 nm), while it is very hard to clearly distinguish the ZnS Qdots and Fe_3O_4 nanoparticles when they are of similar sizes (Figure S3B). [175, 186-192] Interestingly, the presence of moiré pattern – which occurred due to the overlap of similar lattice fringes of (311) plane of inverse spinel Fe_3O_4 nanoparticles and (111) plane of cubic ZnS Qdots (0.3 nm) - irrespective of the size of the Fe_3O_4 nanoparticles and ZnS Qdots in the composite, clearly indicated the presence of both the crystals in the Fe_3O_4-ZnS composite.

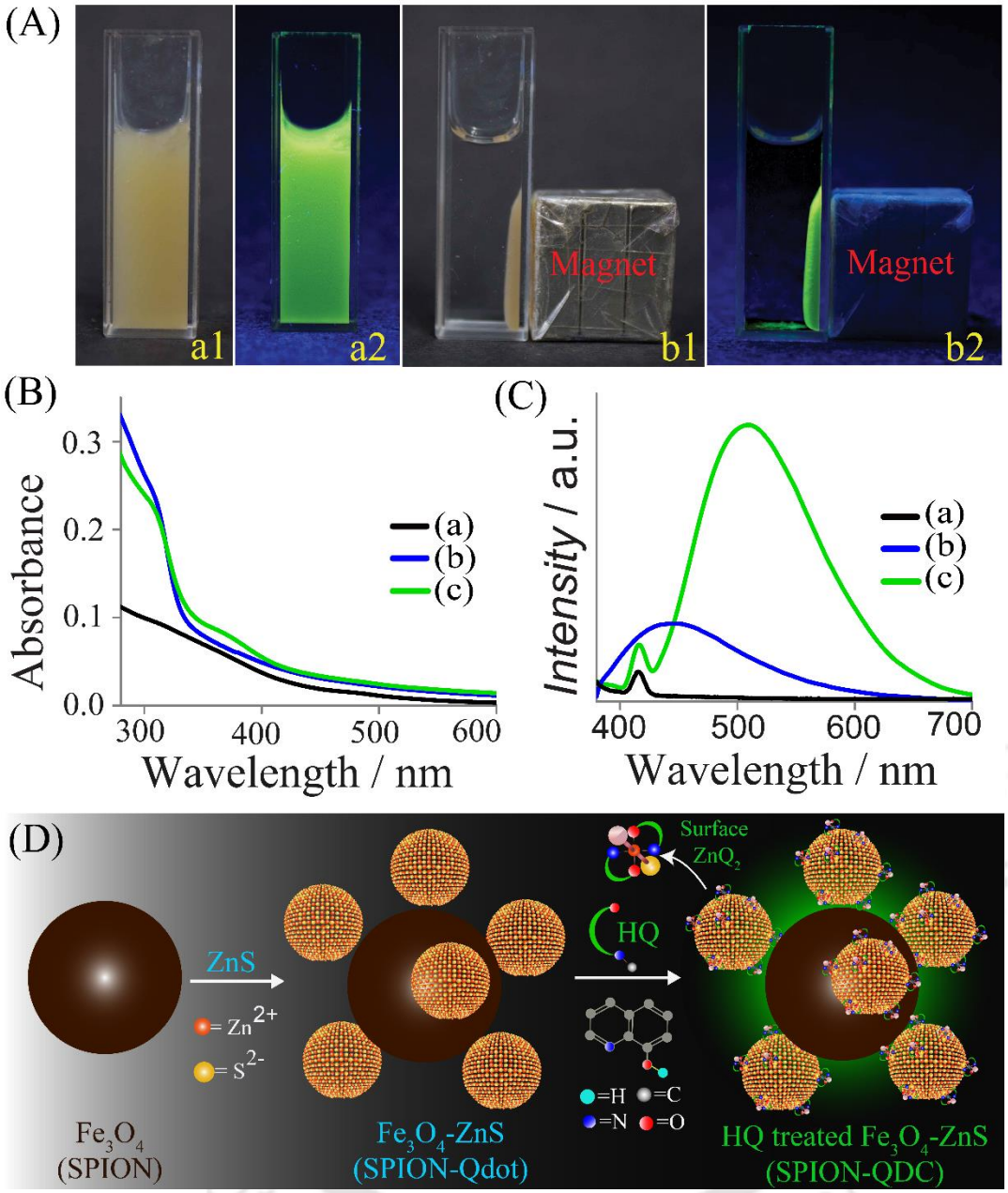

Figure 6.4. (**A**) Photographs of the aqueous dispersion of SPION-QDC in (a) absence and (b) presence of an external magnetic field under (1) white and (2) UV light (365 nm). (**B**) UV-vis and (**C**) emission spectra of the aqueous dispersion of (a) Fe_3O_4 (pH-9.5; λ_{ex}-320 nm); (b) Fe_3O_4-ZnS (pH-6.8; λ_{ex}-320 nm); and (c) SPION-QDC (pH-6.8; λ_{ex}-365 nm). (**D**) Schematic representation of the formation of SPION-QDC composite.

The aqueous dispersion of Fe_3O_4-ZnS composite upon complexation reaction with HQ exhibited a strong green luminescent color (Figure 6.4A), following irraditaion with UV (365 nm) light. This was in contrast to the as-synthesized Fe_3O_4-ZnS composite and Fe_3O_4 NPs, which showed no such emission (Figure A.6.1, Appendix). On the other hand, dispersions of Fe_3O_4 NPs and Fe_3O_4-ZnS composite

(following HQ treatment too) were dark and light brown color respectively in daylight (Figure 6.4A and Figure A.6.1, Appendix). Importantly, the product of the reaction could be separated using a magnet (Figure 6.4A) and could again be redispersed in water with retention of luminescence (not shown).

The UV-vis spectrum of the composite following complexation consisted of an excitonic peak at 320 nm (due to the Qdot) and a peak at 365 nm, assigned to ZnQ_2 complex formed on the surface of the Qdot (Figure 6.4B).[175, 180, 193-194] The luminescent spectrum of the Fe_3O_4-ZnS composite composite consisted of a single peak at 440 nm (upon excitation at 320 nm). On the other hand, following complexation the peak at 440 nm disappeared and a new and intense peak appeared at 500 nm (Figure 6.4.C). The excitation maximum for the peak at 500 nm appeared at 365 nm (Figure A.6.2, Appendix). However, Fe_3O_4 nanocrystals did not have any clear emision peak even in the presence of HQ, thus discounting the possibility of the peak at 500 nm due to any product (associated with Fe) from the reaction (Figure A.6.3, Appendix). The results are consistent with previous observations of formation of ZnQ_2 complex on the surface of ZnS Qdot.[175, 180, 193-194] Overall, the results suggest that several ZnS nanocrystals grew on each Fe_3O_4; the complexation reaction led to the formation of ZnQ_2 on the surface of the ZnS Qdots. Earlier results suggested the bonding of the complex with the dangling sulphide ions present on the surface, while the sixth coordinate my be occupied by H_2O. We define the new composite as SPION-QDC (SPION – Qdot – Complex), the formation of which is schematically shown in Figure 1D. It is to be mentioned here that the optimum amount of HQ required for the reaction was calculated by monitoring the saturation in emission intensity at 500 nm (Figure A.6.4, Appendix). It was found to require 0.03 mM HQ for a 2.0 mL of Fe_3O_4-ZnS composite dispersion (with an absorbance value of 0.20-0.25 at 320 nm). That the luminescence at 500 nm was due to the formaton of a complex was further supported by the retention of emission following centrifugation of the product and redispersion into the same medium (Figure A.6.4, Appendix). Furthermore, there was no significant change in pH of the reaction medium after complexation, which ruled out the effect of pH on the changes in the luminescence.

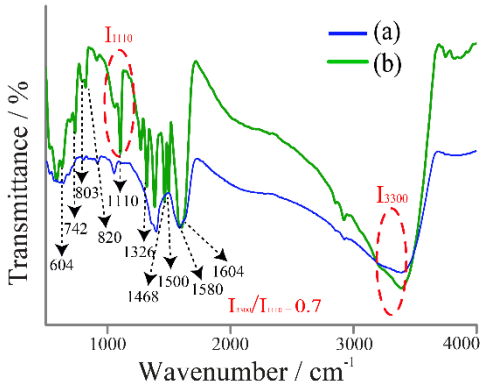

Figure 6.5. Fourier transform infrared (FTIR) spectra of the solid particles of (a) Fe_3O_4-ZnS and (b) HQ treated Fe_3O_4-ZnS. The intensity of the peak at 1110 cm^{-1} (due to C-O-Zn coordination) was 0.7 times that of the peak at 3300 cm^{-1}, clearly indicating the formation of octahedral ZnQ_2 complexes on the surface of the Fe_3O_4-ZnS composite.[152, 175, 180, 193-194] Similarly, the presence of the peaks at 604 and 742 cm^{-1} (in-plane ring deformation), at 742, 803, and 820 cm^{-1} (C−H out-of-plane wagging), at 1326 cm^{-1} (C−H bending), at 1500 and 1468 cm^{-1} (pyridyl and phenyl rings) and at 1580 and 1604 cm^{-1} (C−C/ C−N stretching) demonstrated the facile incorporation of ZnQ_2 complexes on the surface of Fe_3O_4-ZnS. [152, 175, 180, 193-194]

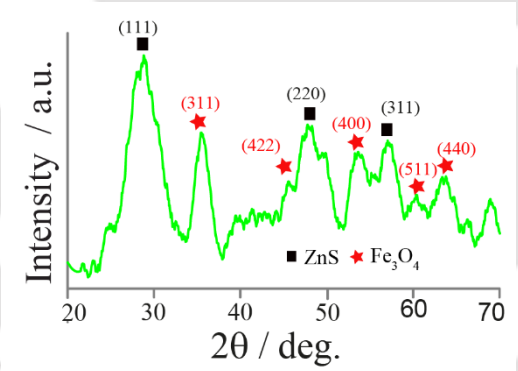

Figure 6.6. Powder x-ray diffraction (XRD) pattern of solid HQ treated Fe_3O_4-ZnS.

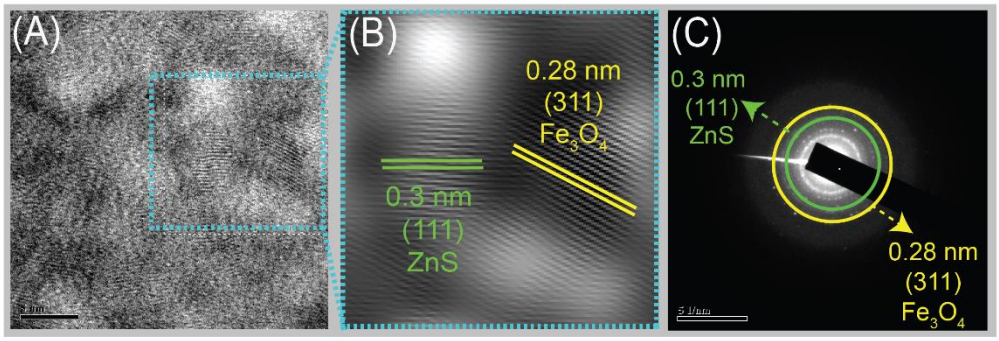

Figure 6.7. (**A**) High resolution TEM (HRTEM; scale bar- 5 nm) and (**B**) corresponding inverse fast Fourier transform (IFFT) images and (**C**) selected area electron diffraction (SAED) pattern (scale bar: 5 nm^{-1}) of the aqueous dispersion of HQ treated Fe_3O_4-ZnS.

Fourier transform infrared (FTIR) spectroscopy results showed that SPION-QDC contained the functional groups corresponding to the octahedral ZnQ_2 complexes, which were absent in Fe_3O_4-ZnS (SPION-Qdot) composite. [152, 175, 180, 193-194] The details are described in the Figure 6.5. Additionally, the elemental analysis, from atomic absorption spectroscopy (AAS), showed constancy of Fe:Zn content, thus indicating that there was no discernible depletion of metal ions from the composite due to complexation reaction (Table A.6.2, Appendix). However, the changes in the zeta potential indicated modification of the SPION-Qdot surface following complexation (Table A.6.1, Appendix). Also, the preservation of morphological characteristics of the Fe_3O_4-ZnS composite following complexation with HQ was confirmed by XRD, TEM and SAED analyses (Figure 6.6-6.7). [175, 188-190]

The as-synthesized Fe_3O_4-ZnS (SPION-Qdot) composite had a photoluminescence QY of 0.6 % (at 320 nm excitation). On the other hand, the SPION-QDC resulted in a QY of 5.9 % (with excitation at 365 nm) and 0.8 % (with excitation at 320 nm, Table A.6.3, Appendix). The significant enhancement of QY and the red-shift of the excitation maximum, due to the formation of complex on the surface of Qdot is expected to make the SPION-QDC more attractive for bioimagning, especially against the background of strong cellular autofluorescence.[195-196] Additionally, the average excited-state lifetime of the SPION-QDC was measured to be 12.54 ns, also enhancing their potential for bioimaging (Figure A.6.5 and Table A.6.4, Appendix). [195-196] Furthermore, the HQ treated Fe_3O_4-ZnS composite was found 5 times more photostable than an organic dye (here rhodamine 6G). For example, the decrease in luminescence intensity for HQ treated Fe_3O_4-ZnS and rhodamine 6G were observed to be 0.003 and 0.016% per sec (Figure 6.8A and Table A.6.5, Appendix), supporting the superiority of the composite. Moreover, the stability of the luminescence (at λ_{ex}-365 nm and λ_{em}-500 nm) of the SPION-QDC in human blood serum (as measured for 24 h) indicated its clinical application potential (Figure 6.8B). Additionally, the zeta potential of the aqueous dispersion of the SPION-QDC was measured to be –25.5 ± 0.6 mV, indicating its colloidal stability in water, which is required for biological applications (Table A.6.1, Appendix).[193-194] Furthermore, the stability and long-term storage in solid forms were confirmed by preservation of the bright green fluorescence, even after 15 days, as observed under fluorescence microscope (Figure A.6.6, Appendix).

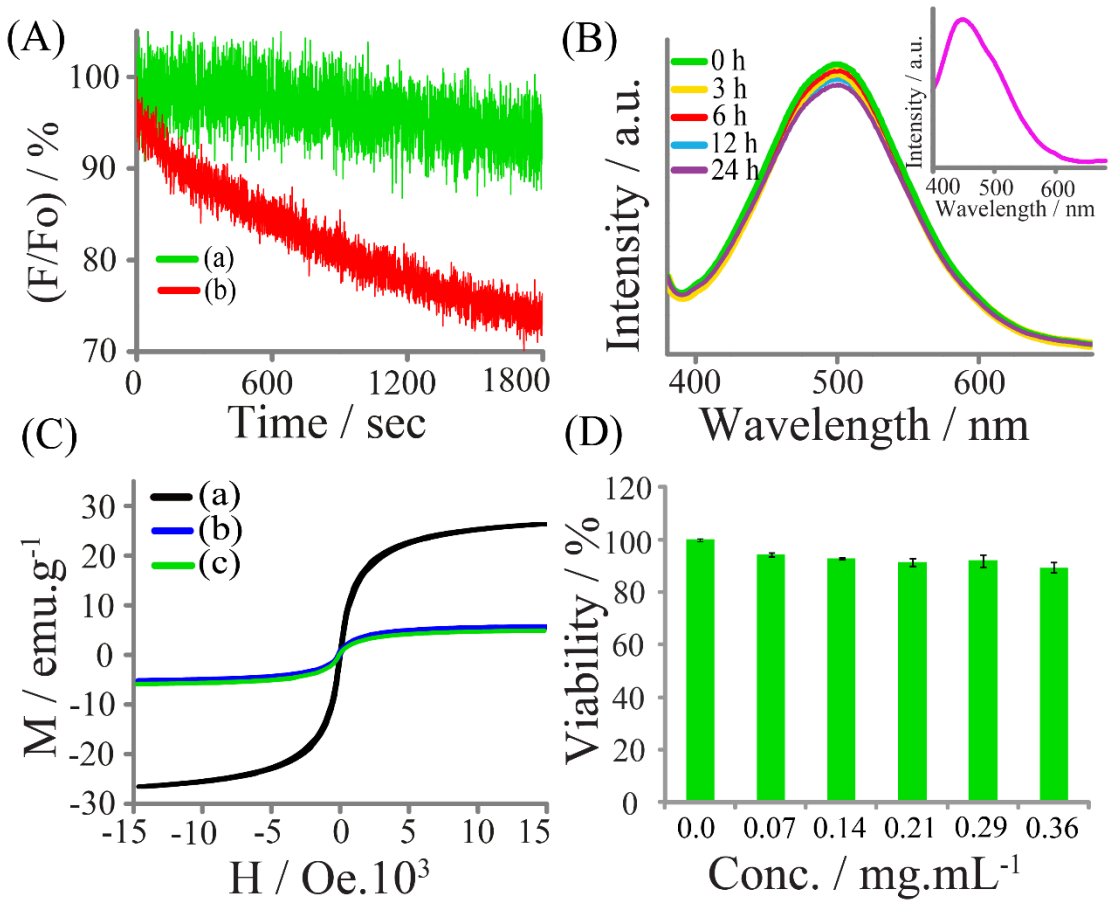

Figure 6.8. (**A**) Photostability (λ_{ex}-365 nm) - under continuous irradiation of light - of (a) SPION-QDC (in water; λ_{em}-500 nm) and (b) rhodamine 6G organic dye (in ethanol; λ_{em}-570 nm). (**B**) Luminescence (λ_{ex}-365 nm) stability of SPION-QDC composite in human blood serum as measured at different time intervals; Inset- emission spectrum (λ_{ex}-365 nm) of only human blood serum. (**C**) M–H hysteresis curves of the solid particles of (a) Fe_3O_4, (b) Fe_3O_4-ZnS (SPION-Qdot), and (c) SPION-QDC. (**D**) MTT based cell viability assay of HeLa cells after 24 h treatment with varying concentrations of SPION-QDC composite.

The vibrating sample magnetometric (VSM) analysis of Fe_3O_4, Fe_3O_4-ZnS and SPION-QDC showed magnetization saturation values of 26.4, 3.88 and 3.81 emu/g, respectively and the measurements supported their super paramagnetic nature at room temperature (Figure 6.8C and Table A.6.6, Appendix).[188-189, 197] The decrease in magnetic saturation of Fe_3O_4-ZnS from (only) Fe_3O_4 (per unit weight) may be due to the contribution of diamagnetic ZnS nanocrystals formed on the Fe_3O_4 NPs. Additionally, the treatment of HQ to Fe_3O_4-ZnS composite did not significantly change

its magnetic saturation. Furthermore, the SPION-QDC showed magnetic saturation, which is sufficient for magnet guided imaging applications. [188-189, 197]

The MTT based cell viability assay, performed using different concentrations (with a maximum 0.36 mg/mL) of the SPION-QDC, showed that more than 90% of the cervical cancer HeLa cells were viable after 24 h of incubation (Figure 6.8D). This clearly indicated that the composite was nontoxic to the mammalian cells and thus makes it suitable for biological applications.

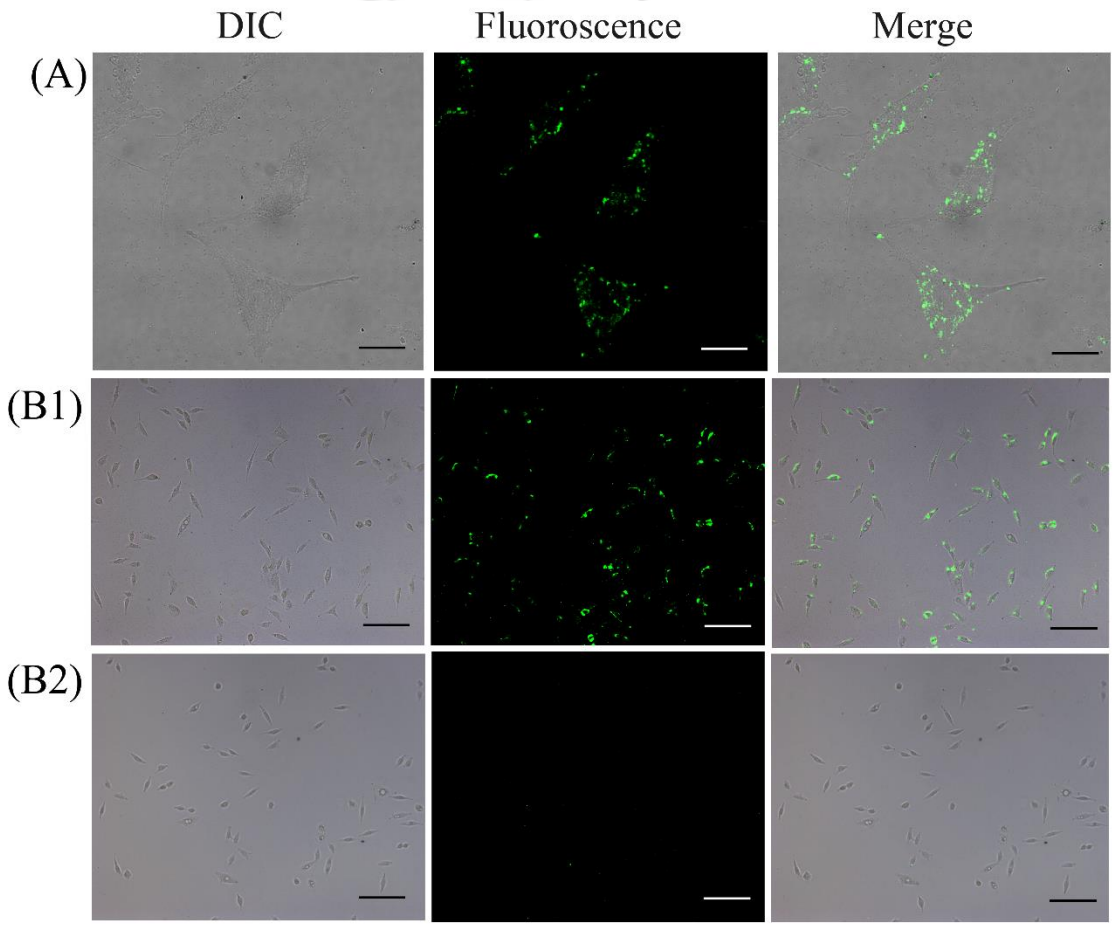

Figure 6.9. (**A**) Confocal laser scanning microscopic images (scale bar - 25 μm) of HeLa cells following 4 h incubation with SPION-QDC. (**B**) Fluorescence microscopic images (scale bar - 100 μm) of HeLa cells – which were cultured on two cover slips placed inside a petri plate and incubated with SPION-QDC for 4 h. A magnet was placed below one cover slip during incubation. The images are for cells on the cover slip (1) closer to external magnet and (2) the other one away from the magnet.

Additionally, the SPION-QDC composite exhibited bright green luminescence under confocal microscope, using 405 nm diode laser (Figure 6.9A), while no such

green fluorescence was observed in control HeLa cells (Figure A.6.7, Appendix). Importantly, the magnetic property of the composite offered the opportunity for labelling of cells with spatial control, by using external magnetic field. In order to achieve this, HeLa cells were cultured onto two cover slips - placed inside a cell culture petri plate and then were incubated with the SPION-QDC composite for 4 h. A small magnet was placed below the petri plate and closer to one of the cover slips (Figure 6.10). When viewed using a microscope, strong green luminescence was observed for the cells on the cover slip which was near to magnet, while the cells on the other one (away from the magnet) showed negligible luminescence (Figure 6.9B). On the other hand, in the absence of any magnet strong green luminescence from the cells attached to both the cover slips could be observed (Figure A.6.8, Appendix). This means that the magnetic property of the composite could be used to direct the same for cell labelling with spatial control. This may auger well for targeted cellular imaging and drug delivery.

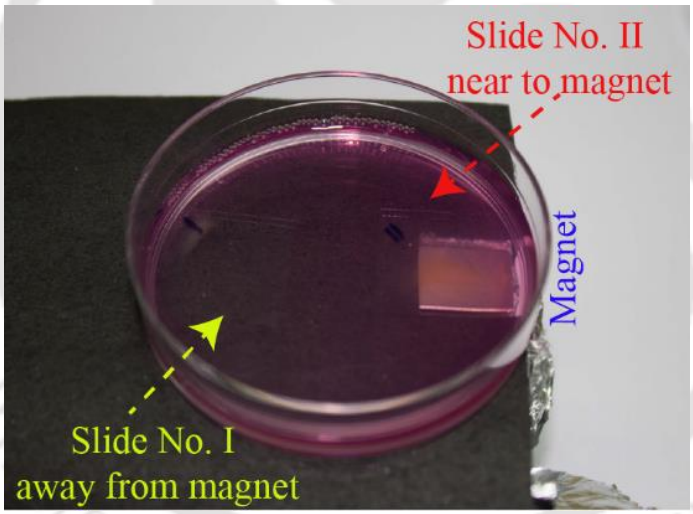

Figure 6.10. Digital image of the set up used for magnet driven cellular imaging of HeLa cells using HQ treated Fe_3O_4-ZnS composite. The petridis contains two glass slides; Slide No. I is away from the magnet placed below the petridis and slide no. II is near and above the magnet.

6.3. Conclusion

In conclusion, a new composite has been developed based on the complexation reaction of Fe_3O_4-ZnS composite nanocrystals with HQ, leading to the formation of luminescent ZnQ_2 on the surface of the Qdot. The high photoluminescence QY, photo-stability and superparamgnetism of the SPION-QDC composite was used to demonstrate cellular labelling with spatial control using an external magnetic field. Furthermore, the luminescence stability in human blood serum, non-toxicity and magnet guided specific cell imaging properties of the biocompatible SPION-QDC would make it a suitable candidate for targeted bioimaging. Moreover, the complexation based QY enhancement of multifunctional materials can be expected to bring new excitement in biodiagnostics in near future.

Chapter 7

Summary and Future Prospects

7.1 Summary

The present thesis has been able to address partly the role of the surface ions in the emission characteristics of Qdots, synthesized at comparatively low temperatures. This has been achieved by using a simple cation exchange route; while on the other hand, based on their chemical reactivity, the surface metal ions formed inorganic complexes with an external organic ligand and the complexed Qdot - which was called herein as quantum dot complex (QDC) -exhibited superior optical properties such high QY and longer emissive life time and extra-ordinary thermal stability in comparison to bare inorganic complexes. In addition, the complexation reaction on the surface of Qdots has also demonstrated their uses to make the hydrophobic Qdots biologically amenable following their transfer into water, to create a single component redox active double channel emitting platform – in which the properties of Qdots and surface complexes are retained, and to fabricate an excellent bio imaging probe – in combination with super-paramagnetic iron oxide nanoparticle (SPION) – for the purpose of magnet guided imaging of the cervical cancer HeLa cells and thus their potential clinical applications. Finally, the chemical reactions such ion exchange and complexation on the surface of Qdots provide platforms for understanding the surface chemistry of the Qdots and pave way for the formation of newer composite with superior properties in order to have better applications of Qdots.

7.2 Future Prospects

The presented chemical reactions on the surface of Qdots will bring a newer paradigm towards understanding their surface chemistry – which is important for achieving their desired applications in biodiagnostics and optoelectronics. This is also expected to open new avenues in optical materials with superior roles of principles of chemistry. Moreover, the formation of inorganic complexes on the surface of Qdots will provide a new regime to have their applications in white light generation, sensing of different chemical and biological entities, catalyze chemical reactions. Further, the

understanding and establishing chemistry of complexes on the surface is important in opening new vistas utilizing the full repertoire of traditional metal–organic complexes. The present thesis can be expected to have a significant impact on technology involving optical and optoelectronic devices, energy harvesting, chemical and biological sensing, and bioimaging and targeted drug delivery.

Appendix

A2: Chapter 2

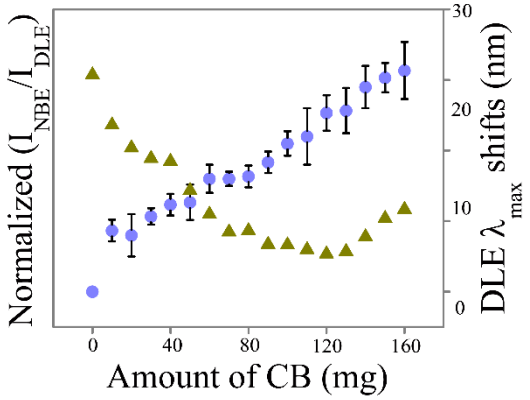

Figure A.2.1. Dependence of wavelength shifts and NBE/DLE intensity ratio on the amount of CB added (recorded at 3 h after addition).

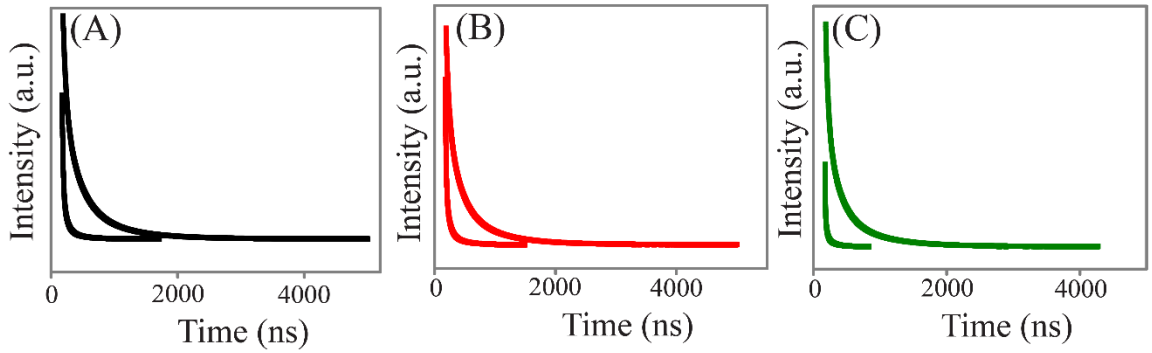

Figure A.2.2. Photoluminescence decay curves of (A) $Zn_xCd_{1-x}S$ NCs; (B) 50 mg CB added NCs and (C) 150 mg of CB added NCs.

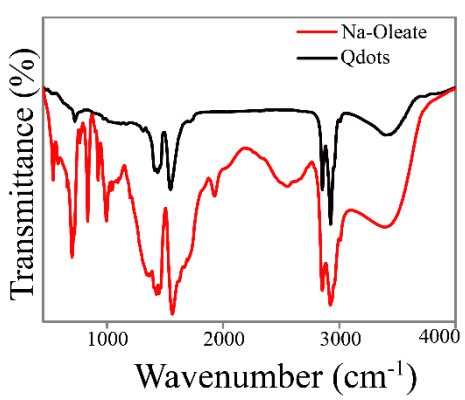

Figure A.2.3. FTIR spectra of (A) sodium oleate and oleate capped $Zn_xCd_{1-x}S$.

Planes	$d_{spacing}$ (nm)					
	Wurtzite CdS	$Zn_xCd_{1-x}S$			Wurtzite ZnS	Present case
		x= 0.0	x= 0.5	x= 1.0		
(002)	`0.3367	0.335	0.326	0.312	0.3128	0.32
(110)	0.2068	0.207	0.193	-	0.1911	-
(112)	-	-	-	-	-	-

Table A.2.1. Interplanar distances of as prepared $Zn_xCd_{1-x}S$ NCs measures from HRTEM image (reported) and observed.

Amount of CB added (mg)	Quantum Yield (%)
0	12.0
10	10.4
20	10.2
30	9.2
40	7.5
50	7.3
60	6.3
70	6.1
80	5.6
90	4.7
100	4.5
110	4.3
120	3.1
130	2.5
140	2.4
150	1.7
160	1.5

Table A.2.2. Variation of quantum yield of $Zn_xCd_{1-x}S$ NCs with the amount of CB.

Amount of CB added (mg)	A_1 (%)	τ_1 (ns)	A_2 (%)	τ_2 (ns)	A_3 (%)	τ_3 (ns)	τ_{av} (ns)	$\chi 2$
0	20.7	14.7	41.4	58.0	37.9	235.0	192.6	0.993
50	19.6	13.5	39.5	55.3	40.9	211.8	176.3	0.998
150	11.7	5.0	31.8	23.9	56.5	113.8	103.5	0.999

Table A.2.3. (A) Decay parameters of $Zn_xCd_{1-x}S$ NCs and CB added NCs: Near Band Edge Emission (monitored at 420 nm).

Amount of CB added (mg)	A_1 (%)	τ_1 (ns)	A_2 (%)	τ_2 (ns)	A_3 (%)	τ_3 (ns)	τ_{av} (ns)	$\chi 2$
0	8.7	53.1	46.5	248.4	44.8	711.8	583.0	1.044
50	7.7	46.8	40.5	209.4	51.8	635.2	543.6	1.065
150	12.6	40.8	39.4	188.2	48.0	589.8	499.8	0.999

Table A.2.3. (B) Decay parameters of $Zn_xCd_{1-x}S$ NCs and CB added NCs: Deep Level Emission (monitored at 539 nm (as synthesized), 555 nm (50 mg CB added) and 564 nm (150 mg CB added).

Peak position (cm^{-1})	Functional groups
3430	O-H Stretching
2930	-C-H Asymmetric Stretching
2845	-C-H Symmetric Stretching
1560	$-COO^-$ Asymmetric Stretching
1440	-C-H Bending
1123	-C-O Stretching

Table A.2.4. FTIR Peak positions of various functional groups observed with samples as in Figure 2.6.

A3: Chapter 3

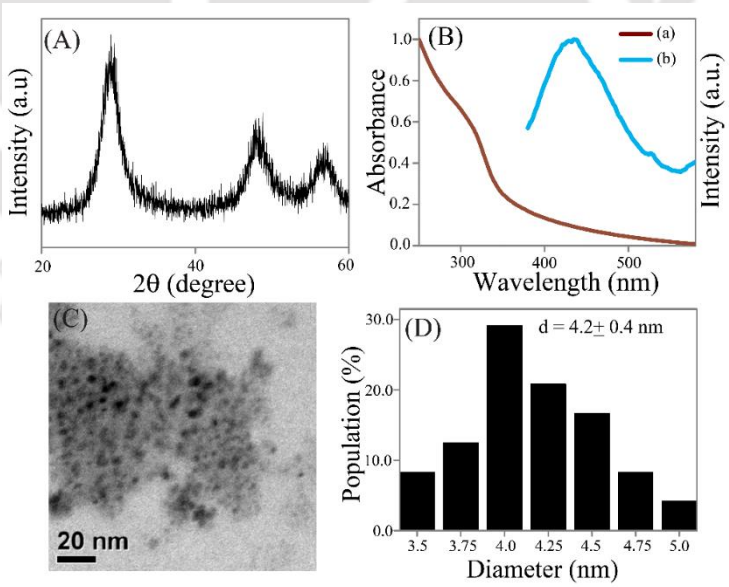

Figure A.3.1. (A) Powder X-ray diffraction pattern, **(B)** uv-vis and emission (λ_{ex}-322 nm; in water), **(C)** transmission electron microscopic (TEM) image (scale bar-20 nm), and **(D)** corresponding particle size distributionof uncapped ZnS Qdots.

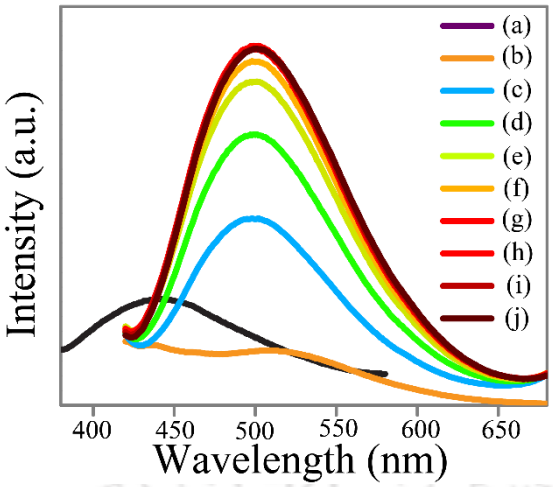

Figure A.3.2. Emission spectra (λ_{ex}= 361nm) of (a) Qdots (λ_{ex}= 322 nm) in water, (b) 5.0 mM of 8-HQ in methanol and (c) 5.0 µL, (d) 10.0 µL, (e) 15.0 µL, (f) 20.0 µL, (g) 25.0 µL, (h) 30.0 µL, (i) 35.0 µL and (j) 40.0 µL of 5.0 mM 8-HQ (in methanol) added ZnS Qdots (2 mL) dispersion . The absorbance of the Qdots was 0.03 at 361 nm.

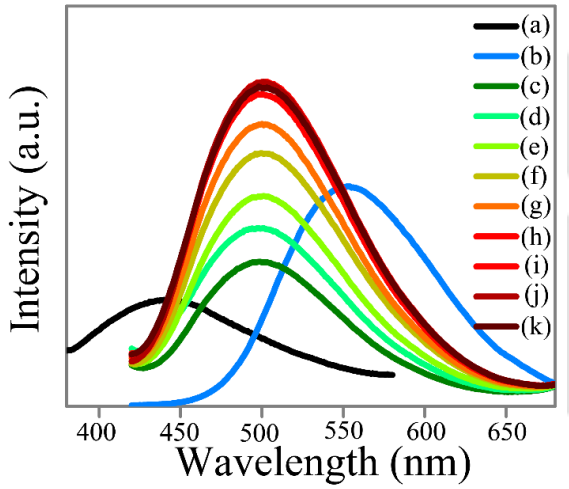

Figure A.3.3. Emission spectra (λ_{ex}= 361nm) of (a) Qdots (λ_{ex}= 322 nm) in water, (b) 0.5 mM of ZnQ2 in methanol and different amount (c) 10.0 µL, (d) 20.0 µL, (e) 30.0 µL, (f) 40.0 µL, (g) 60.0 µL, (h) 80.0 µL, (i) 100.0 µL, (j) 120.0 µL and (k) 140.0 µL of 0.5 mM of ZnQ2 (in methanol) added ZnS Qdots (2 mL) dispersion. The absorbance of the Qdots was 0.03 at 361 nm.

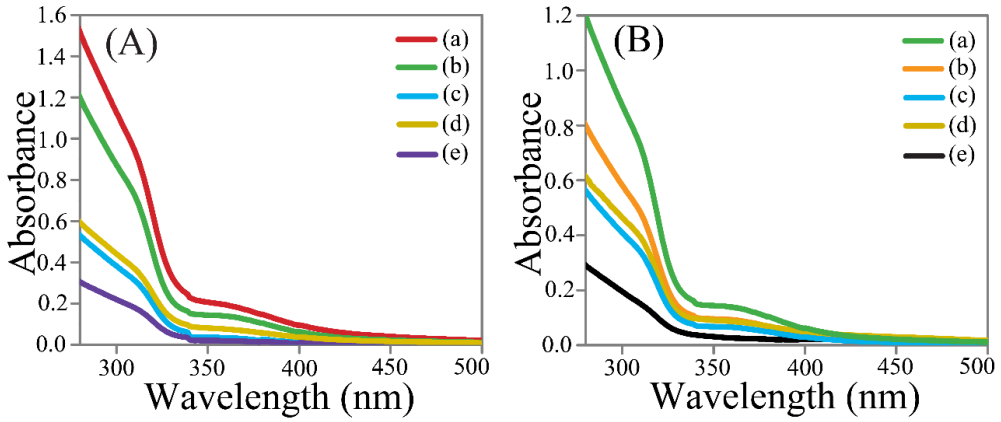

Figure A.3.4. UV-Vis spectra of (A) HQ added ZnS Qdots (B) ZnQ_2 added ZnS Qdots (a) before centrifugation; (b) pellet (re-dispersed into same amount of solvent) and (c) supernatant after first centrifugation; (d) pellet (re-dispersed into same amount of solvent) and (e) supernatant after second centrifugation.

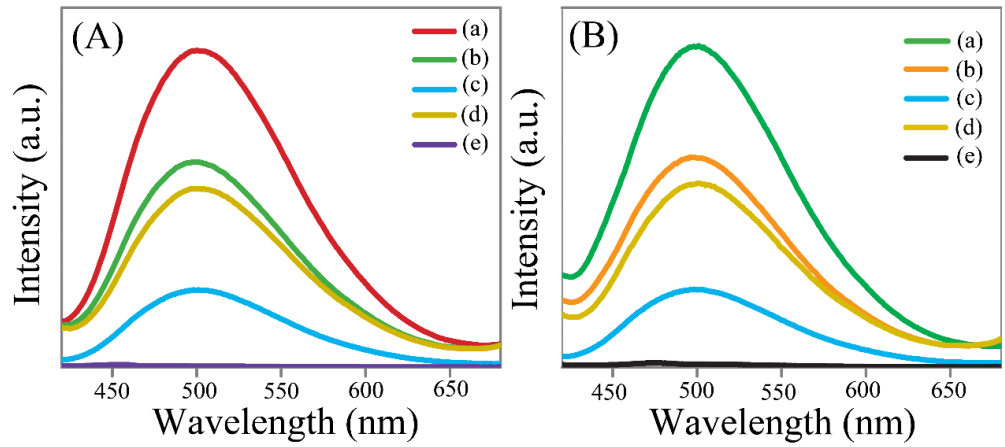

Figure A.3.5. Emission spectra (λ_{ex} = 361nm) of (A) HQ added ZnS Qdots (B) ZnQ_2 added ZnS Qdots (a) before centrifugation; (b) pellet (re-dispersed into same amount of solvent) and (c) supernatant after first centrifugation; (d) pellet (re-dispersed into same amount of solvent) and (e) supernatant after second centrifugation.

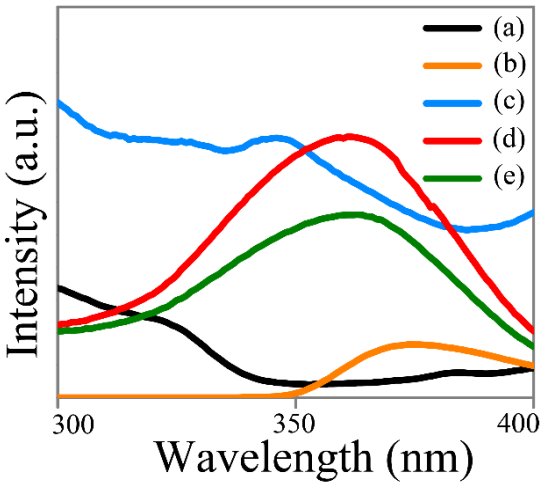

Figure A.3.6. Excitation spectra of (a) cysteine capped ZnS Qdots (λ_{em} = 440 nm); (b) HQ (λ_{em} = 520 nm); (c) ZnQ_2 (λ_{em} = 550 nm); (d) HQ added ZnS Qdots (λ_{em} = 500 nm) and (e) ZnQ_2 added ZnS Qdots and (λ_{em} = 500 nm).

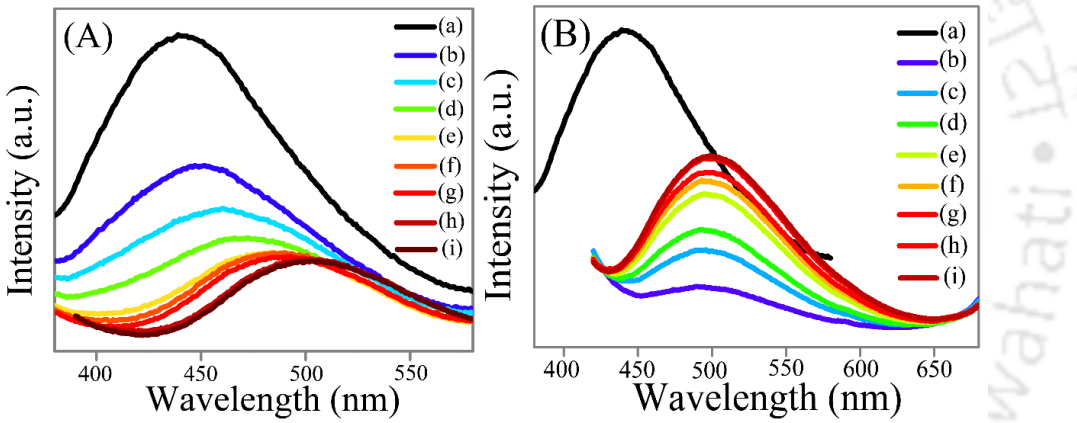

Figure A.3.7. Emission spectra (A) at λ_{ex} = 322 nm and (B) at λ_{ex} = 361 nm of 2.0 mL Qdot dispersion in water in the presence of different amounts: (a) 0.0 µL ; (b) 2.0 µL, (c) 4.0 µL, (d) 8.0 µL, (e) 12.0 µL, (f) 16.0 µL, (g) 20.0 µL, (h) 25.0 µL and (i) 30.0 µL respectively, of 1.0 mM HQ (methanol).

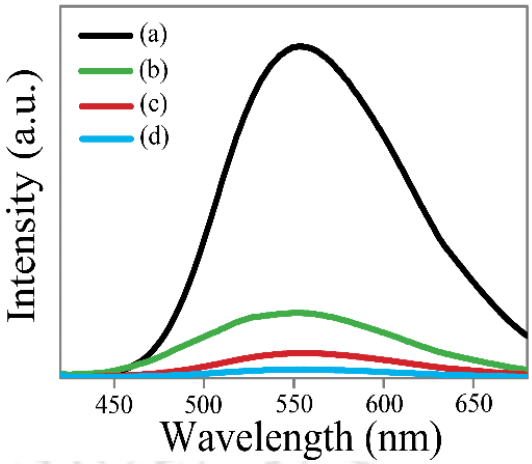

Figure A.3.8. Emission spectra (λ_{ex} = 361 nm) of (a) 0.5 mM of ZnQ_2 complex in methanol; (b) 0.5 mL, (c) 0.2 mL, and (d) 0.1 mL ZnQ_2 complex (in methanol) added to 2 mL of Mili Q water.

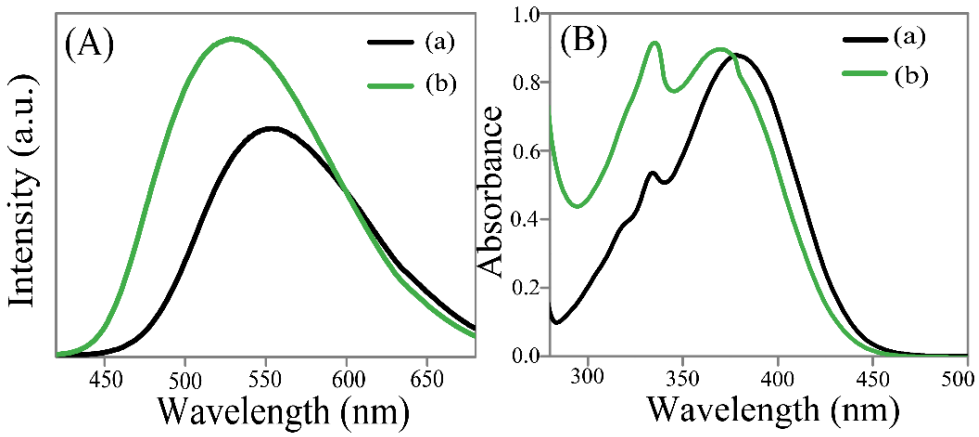

Figure A.3.9. (A) Emission and **(B)** UV-Vis (λ_{ex} = 361 nm) spectra of (a) 0.5 mM of ZnQ2 complex solution in methanol (pH- 7.4) and (b) that after addition of Na_2S (pH-7.8).

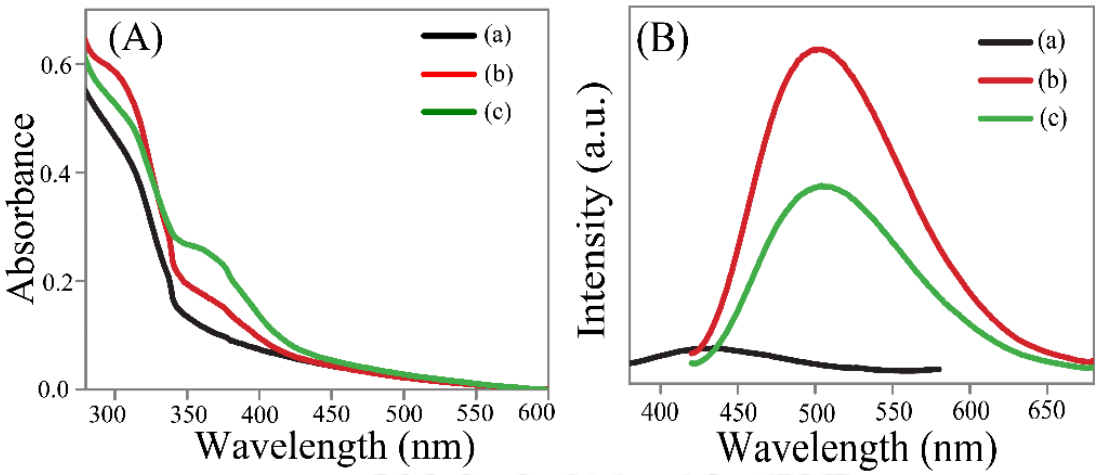

Figure A.3.10. (A) UV-Vis and **(B)** emission spectra of (a) uncapped ZnS Qdots, and of those following addition of (b) 30.0 µL 5.0 mM HQ (in methanol) and (c) 100.0 µL of 0.5 mM of ZnQ_2 complex (in methanol) to a 2.0 mL dispersion in water (emission was monitored at 361nm).

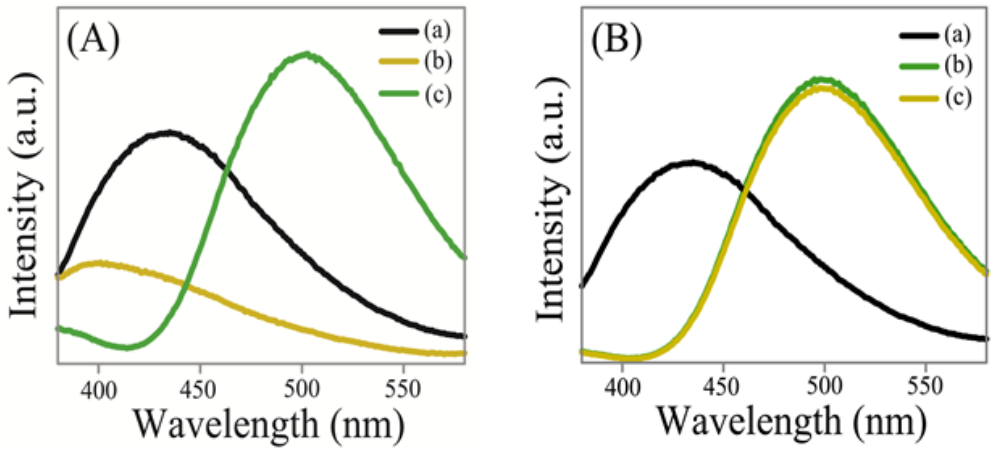

Figure A.3.11. (A) Emission spectra (λ_{ex} = 322 nm) of (a) cysteine stabilized ZnS Qdots (in water), (b) 2.0 mL of ZnS Qdots following addition of 30.0 µL of 5.0 mM BQ and (c) BQ-containing ZnS Qdots to which 30.0 µL of 5.0 mM HQ was then added. **(B)** Emission spectra of (a) cysteine stabilized ZnS Qdots, (b) 2.0 mL of ZnS Qdots following addition of 30.0 µL of 5.0 mM HQ and (c) HQ-containing ZnS Qdots to which 30.0 µL of 5.0 mM BQ was then added.

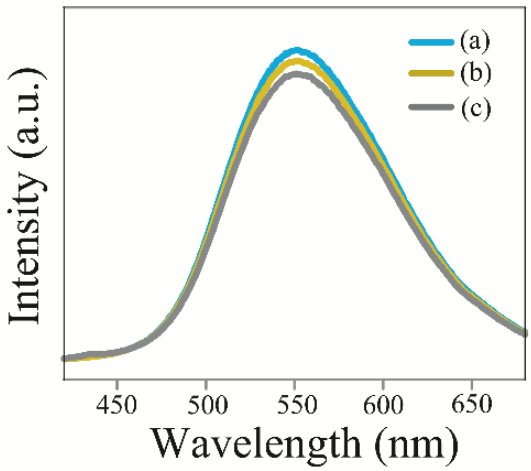

Figure A.3.12. Emission spectra (λ_{ex} = 361 nm) of (a) 2 mL of 0.5 mM ZnQ_2 complex (in methanol) and following addition of (b) 30.0 µL and (c) 60.0 µL 5.0 mM BQ.

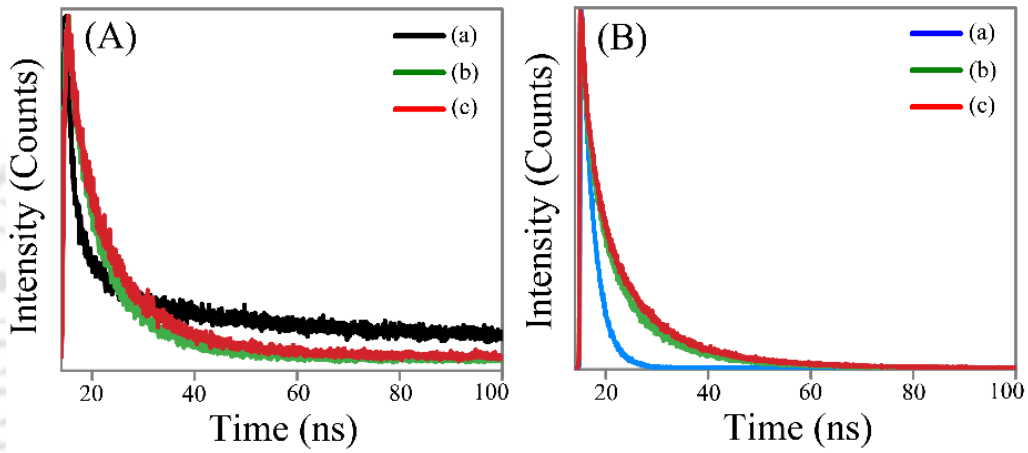

Figure A.3.13. (A) Time-resolved photoluminescence spectra of (a) cysteine capped ZnS Qdots; (b) HQ-added ZnS Qdots and (c) ZnQ_2 added ZnS Qdots. The spectra were recorded using LED (308 nm). **(B)** Time-resolved photoluminescence spectra of (a) ZnQ2; (b) HQ-added ZnS Qdots and (c) ZnQ_2 added ZnS Qdots. The spectra were recorded using LASER (375 nm).

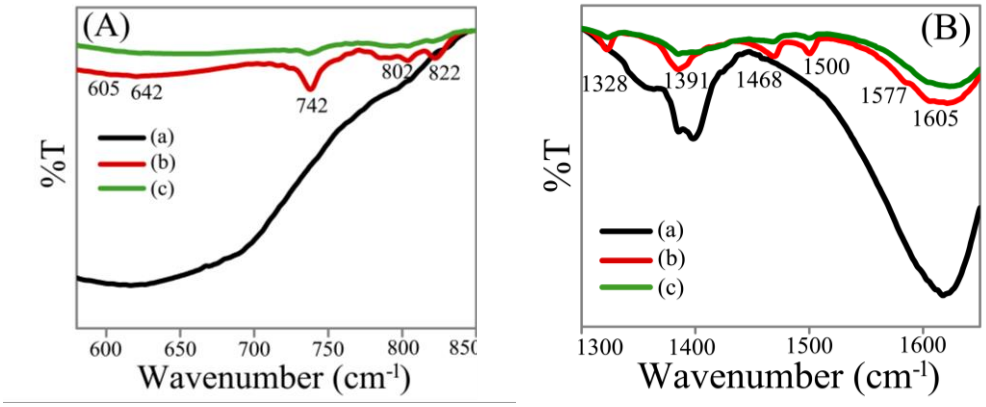

Figure A.3.14. FTIR spectra in the (**A**) range: 580-850 cm^{-1} and (**B**) range: 1300-1620 cm^{-1} of (a) ZnS Qdots (b) HQ added ZnS Qdots and (c) ZnQ_2 added ZnS Qdots.

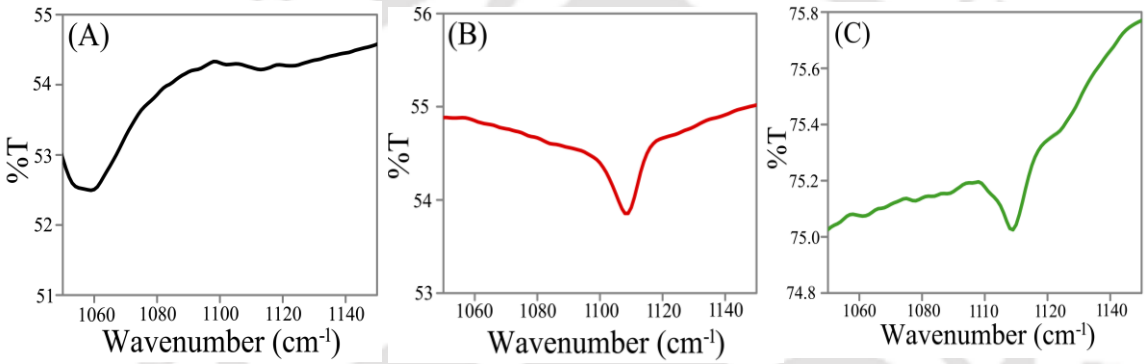

Figure A.3.15. FTIR (range: 1050-1150 cm^{-1}) spectra of (**A**) ZnS Qdots, (**B**) HQ added ZnS Qdots and (**C**) ZnQ_2 added ZnS Qdots.

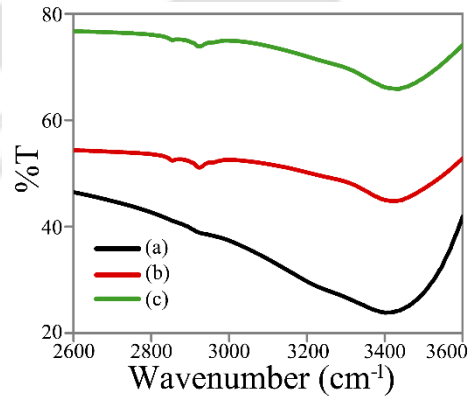

Figure A.3.16. FTIR (range: 2600-3600 cm^{-1}) spectra of (a) ZnS Qdots, (b) HQ added ZnS Qdots and (c) ZnQ_2 added ZnS Qdots.

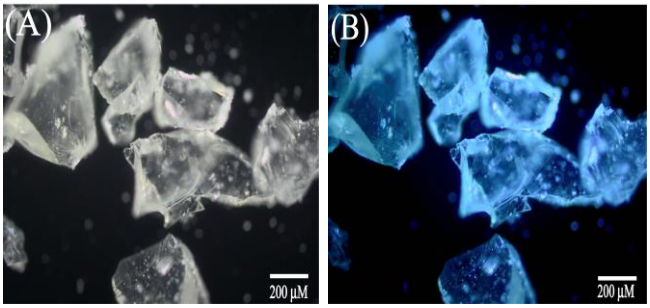

Figure A.3.17. Microscopic images of cysteine capped ZnS Qdots in presence of **(A)** white and **(B)** UV light (λ_{ex} = 350 nm).

Samples	Q.Y (%) with excitation at	
	322 nm	361 nm
(a) ZnS Qdots	0.3	-
(b) HQ	-	0.2
(c) ZnQ_2	-	0.9
(c) HQ added ZnS Qdots	0.16	3.2
(d) ZnQ_2 added ZnS Qdots	0.14	3.0

Table A.3.1. Quantum yield (%) of (a) cysteine capped ZnS Qdots, (b) HQ, (c) ZnQ_2, (d) (c) HQ added ZnS Qdots and (d) ZnQ_2 added ZnS Qdots.

Samples	A_1 (%)	τ_1 (ns)	A_2 (%)	τ_2 (ns)	A_3 (%)	τ_3 (ns)	τ_{av} (ns)	χ^2
ZnS Qdots	16.25	3.35	83.75	33.63	-	-	33.1	1.03
HQ added ZnS Qdots	3.88	2.178	43.59	6.05	52.54	13.49	11.4	1.02
ZnQ_2 added ZnS Qdots	3.93	0.789	40.56	5.88	55.52	14.18	12.2	1.04

Table A.3.2.A. Decay parameters of the product following complexation between cysteine capped ZnS Qdots and 8-HQ or ZnQ_2, monitored at 308 nm (using LED).

Samples	A_1 (%)	τ_1 (ns)	A_2 (%)	τ_2 (ns)	A_3 (%)	τ_3 (ns)	τ_{av} (ns)	χ^2
ZnQ_2	100	2.47	-	-	-	-	2.47	1.03
HQ added ZnS Qdots	5.72	1.31	42.39	5.05	51.89	12.36	10.5	1.06
ZnQ_2 added ZnS Qdots	6.87	1.55	40.51	6.06	52.62	14.11	11.9	1.02

Table A.3.2.B. Decay parameters of complexation between cysteine capped ZnS Qdots and 8-HQ or ZnQ_2 monitored at 375 nm (using LASER).

Samples	Fluorescence decrease rate (I/I_0) (% per sec)
Rhodamine 6G	0.013
HQ treated ZnS Qdots	0.003
ZnQ_2 treated ZnS Qdots	0.004
ZnQ_2	0.004

Table A.3.3. Fluorescence decrease rate (% per sec) of (a) Conventional organic dye (Rhodamine 6G) (b) HQ added ZnS Qdots (c) ZnQ2 added ZnS Qdots and (d) ZnQ_2 complex.

Wave number (Cm^{-1})	Functional groups	(a) ZnQ_2	(b) ZnS Qdots	(c) HQ added ZnS Qdots	(d) ZnQ_2 added ZnS Qdots
1605	C-C/C-N stretching	P	A	P	P
1577	C-C/C-N stretching	P	A	P	P
1500	Pyridyl group of HQ	P	A	P	P
1468	Phenyl group of HQ	P	A	P	P
1328	C-H bending	P	A	P	P
1110	-C-O-Zn Stretching	P	A	P	P
822	C-H out plane wagging	P	A	P	P
802	C-H out plane wagging	P	A	P	P
742	C-H out plane wagging, in plane ring deformation	P	A	P	P
642	in-plane ring deformation	P	A	P	P
605	in-plane ring deformation	P	A	P	P

Table A.3.4. Tabulated FTIR wave number vs functional groups of (a) ZnQ_2, (b) cysteine capped ZnS Qdots, (c) HQ added ZnS Qdots and (d) ZnQ_2 added ZnS Qdots.
In table A.3.4, P and A indicates the presence and absence of the functional groups.

Samples	**I_{3300} : I_{1110}**
cysteine capped ZnS Qdots	No significant peak at 1110 cm^{-1}
ZnQ_2	0.70
HQ added ZnS Qdots	0.88
ZnQ_2 added ZnS Qdots	0.92

Table A.3.5. Tabulated intensity ratio of 3333 cm^{-1} band to 1110 cm^{-1} band of (a) cysteine capped ZnS Qdots, (b) ZnQ_2, (c) HQ added ZnS Qdots and (d) ZnQ_2 added ZnS Qdots.

A4: Chapter 4

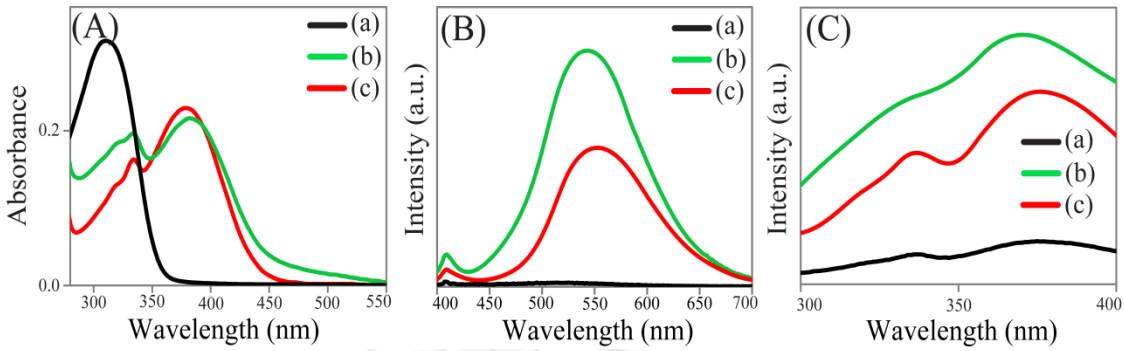

Figure A.4.1. (A) UV-Vis spectra, **(B)** emission spectra (λ_{ex}=365 nm) and **(C)** excitation spectra (at their individual emission maxima) of methanolic solution of (a) HQ (λ_{em}=520 nm), (b) ZnQ_2 (λ_{em}= 550 nm) and (c) CdQ_2 (λ_{em}= 545 nm).

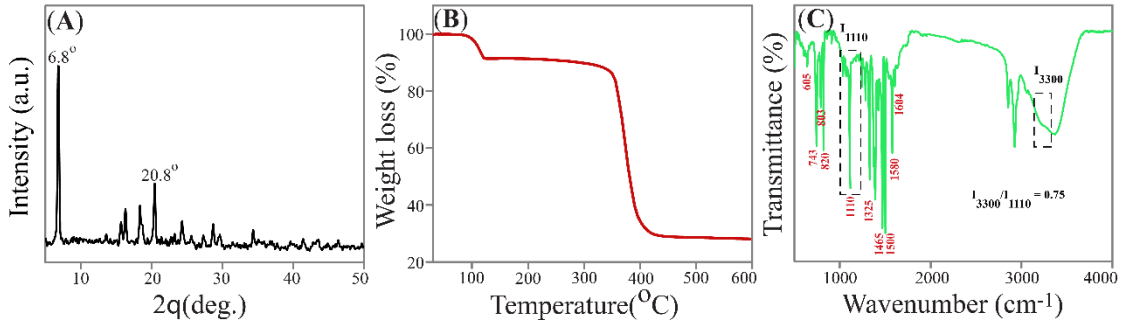

Figure A.4.2. (A) Powder X-ray diffraction pattern, **(B)** thermo gravimetric analysis (TGA) and **(C)** FTIR spectrum of solid $CdQ_2.2H_2O$.

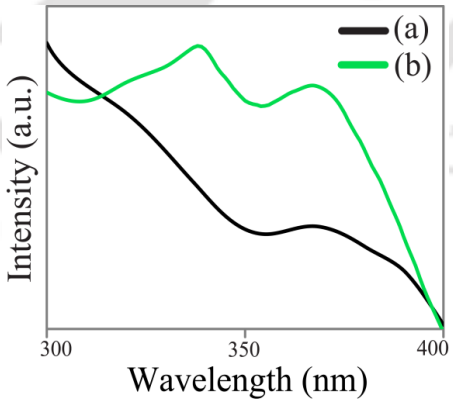

Figure A.4.3. Excitation spectra of (a) oleate capped $Zn_xCd_{1-x}S$ Qdots (in hexane; at λ_{em}- 539 nm), (b) Qdots transferred into water following complexation with HQ (at λ_{em}- 505 nm).

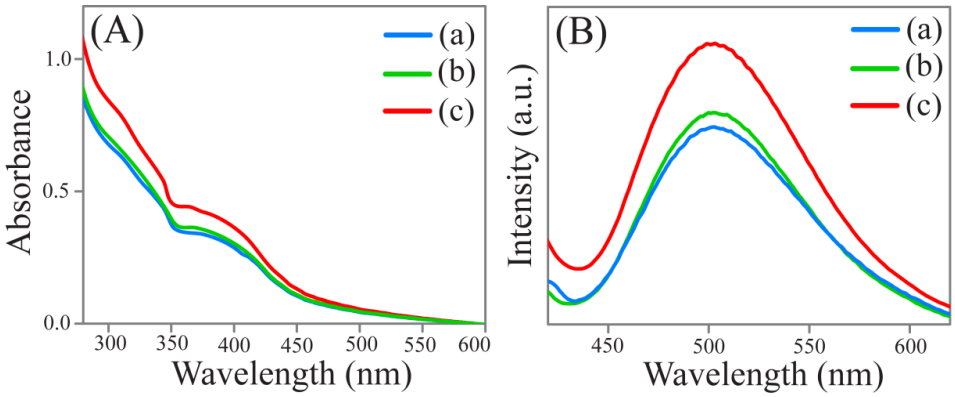

Figure A.4.4. (**A**) UV-Vis and (**B**) emission spectra (λ_{ex} =365 nm) of phase transferred Qdots (in water) following complexation with (a) 0.1 mM ZnQ_2 (pH-5.58), (c) 0.1 mM CdQ_2 (pH-5.62) and (d) mixture of 0.1 mM ZnQ_2 and 0.1 mM CdQ_2 (pH-5.6) in water phase (with which the reaction was started).

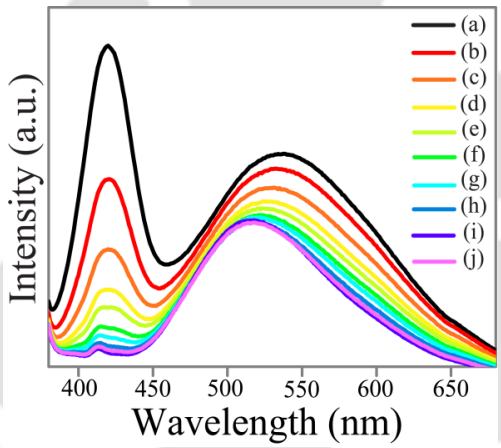

Figure A.4.5. Emission spectra (λ_{ex}= 369 nm) of (a) oleate capped $Zn_xCd_{1-x}S$ Qdots (in hexane), (b) (b) 5.0 µL, (c) 10.0 µL, (d) 15.0 µL, (e) 20.0 µL, (f) 25.0 µL, (g) 30.0 µL, (h) 35.0 µL, (i) 40.0 µL and (j) 45.0 µL of 1.0 mM 8-HQ (in hexane) added Qdots (2.0 ml) dispersion . The absorbance of the Qdots was 0.54 at 369 nm.

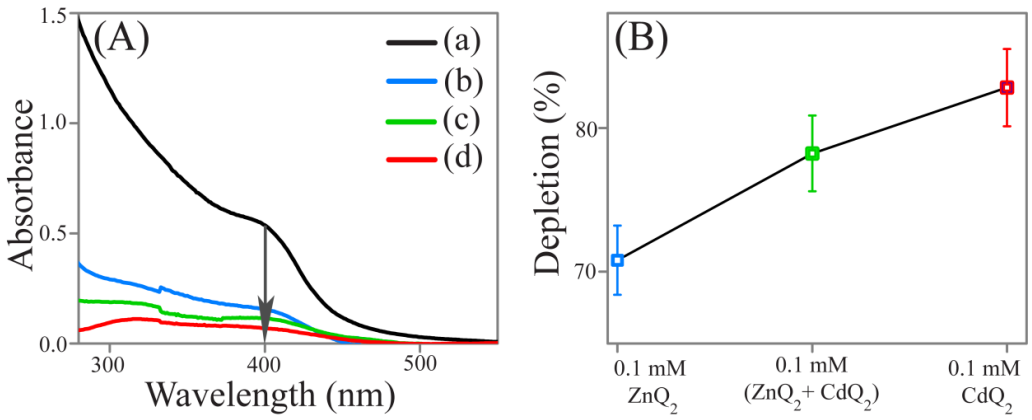

Figure A.4.6. (**A**) UV-Vis spectra of (a) oleate capped $Zn_xCd_{1-x}S$ Qdots (in hexane) and the rest part in hexane after phase transfer of Qdots into water following complexation with (b) 0.1 mM ZnQ_2, (c) 0.1 mM CdQ_2 and (d) mixture of (0.05 mM ZnQ_2 + 0.05 mM CdQ_2) in water phase (with which the reaction was started), (**B**) corresponding of their depletion (%) of Qdots in hexane.

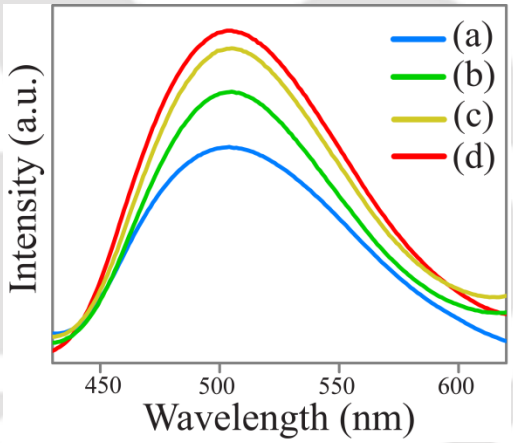

Figure A.4.7. Emission spectra (λ_{ex}= 365 nm) of the transferred Qdots into water following complexation with (**A**) HQ having (a) 0.25 mM (pH-5.66), (b) 0.5 mM (pH-5.62), (c) 0.75 mM (pH-5.73), and (d) 1.0 mM (pH-5.65) concentration in water phase (with which the reaction was started).

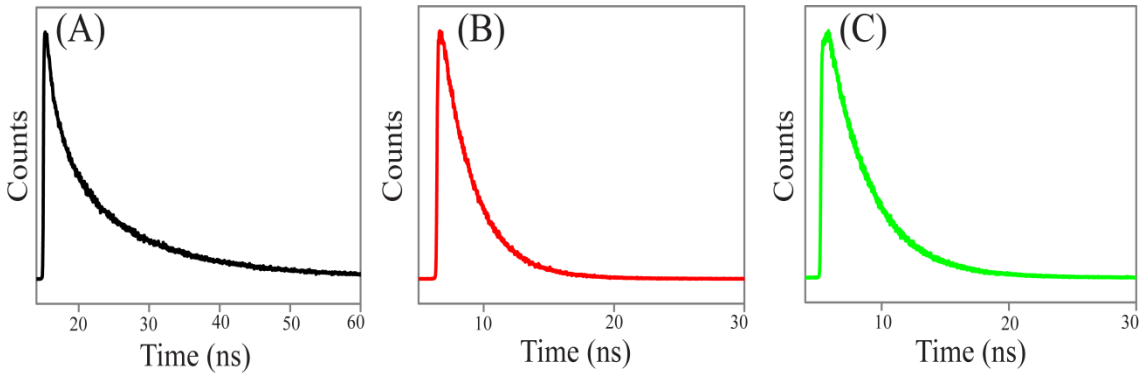

Figure A.4.8. Time-resolved photoluminescence spectra (using 375 nm LASER) of (**A**) Qdots transferred into water following complexation with HQ (at λ_{em}= 505 nm), (**B**) ZnQ_2 (in methanol; at λ_{em} = 550 nm) and (**C**) CdQ_2 (in methanol; at λ_{em} = 545 nm).

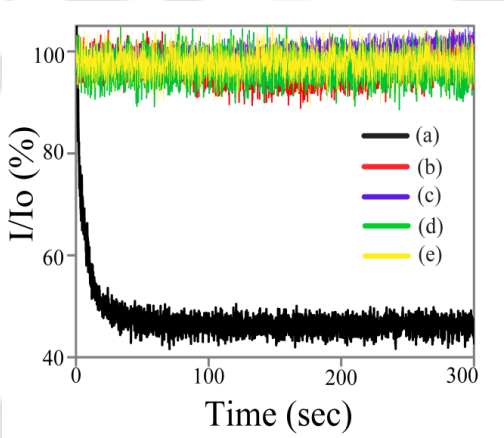

Figure A.4.9. Effect of photo irradiation with time on the emission (λ_{ex} = 365 nm) intensity of (a) conventional dye (Rhodamine- 6G in ethanol at λ_{em} = 570 nm); (b) oleate capped $Zn_xCd_{1-x}S$ Qdots (in hexane; at λ_{em} = 539 nm) and (c) Transferred Qdots (in water; at λ_{em} = 505 nm) and (d) ZnQ_2 (in methanol; at λ_{em} = 550 nm) and (e) CdQ_2 (in methanol; at λ_{em} = 545 nm).

Phase Transfer System	Hexane Phase Composition		Water Phase Composition			
	Conc. of Qdots	Total volume (mL)	Water (mL)	MeOH (mL)	Total volume (mL)	Conc. of HQ (mM)
(I)	0.2mg/mL	5.0	4.0	1.0	5.0	0.25
(II)	0.2mg/mL	5.0	4.0	1.0	5.0	0.50
(III)	0.2mg/mL	5.0	4.0	1.0	5.0	0.75
(IV)	0.2mg/mL	5.0	4.0	1.0	5.0	1.00

Table A.4.1. The details of phase transfer systems for transferring oleate capped $Zn_xCd_{1-x}S$ Qdots form hexane phase to water phase following complexation with different amount of HQ.

Phase Transfer System	Hexane Phase Composition		Water Phase Composition				
	Conc. of Qdots	Total volume (mL)	Water (mL)	MeOH (mL)	Total volume (mL)	MQ_2 complex	Conc. (mM)
(I)	0.2mg/mL	5.0	4.0	1.0	5.0	ZnQ_2	0.1
(II)	0.2mg/mL	5.0	4.0	1.0	5.0	CdQ_2	0.1
(III)	0.2mg/mL	5.0	4.0	1.0	5.0	ZnQ_2 + CdQ_2	0.05 +0.05

Table A.4.2. The details of phase transfer systems for transferring oleate capped $Zn_xCd_{1-x}S$ Qdots form hexane phase to water phase following complexation with MQ_2 complexes.

Conc. of HQ (mM)	Depletion (%)
0.25	68.5±5.5
0.50	75.3±2.8
0.75	85.4±3.3
1.00	91.4±3.9

Table A.4.3. The dependence of % of depletion (or transfer efficiency) on the amount of HQ used for surface complexation reaction during transfer of oleate capped $Zn_xCd_{1-x}S$ Qdots from hexane phase to water phase.

Complex used	Conc.(mM)	Depletion (%)
ZnQ_2	0.1	70.8±2.4
ZnQ_2 + CdQ_2 (1:1)	0.1	78.2±2.6
CdQ_2	0.1	82.8±2.7

Table A.4.4. The dependence of % of depletion (or transfer efficiency) on different complexes which were used for surface complexation reaction during transfer of oleate capped $Zn_xCd_{1-x}S$ Qdots from hexane phase to water phase.

Samples	λ_{ex} (nm)	Q.Y (%)
(a) $Zn_xCd_{1-x}S$ Qdots (in hexane)	369	10.8%
(b) Transferred Qdots (in water)	365	4.9%
(c) ZnQ_2 (in methanol)	365	1.1%
(d) CdQ_2 (in methanol)	365	1.3%

Table A.4.5. Quantum yield (%) w.r.t. quinine sulphate (in 0.1 M H_2SO_4) of (a) $Zn_xCd_{1-x}S$ Qdots (in hexane), (b) transferred Qdots (in water), (c) ZnQ_2 (in MeOH), (d) CdQ_2 (in MeOH).

Samples	A_1 (%)	τ_1 (ns)	A_2 (%)	τ_2 (ns)	A_3 (%)	τ_3 (ns)	τ_{av} (ns)	χ^2
(A) Transferred Qdots	5.5	1.8	34.5	6.9	59.9	16.9	14.9	1.03
(B) ZnQ_2 (in MeOH)	100	2.5	-	-	-	-	2.5	1.03
(C) CdQ_2 (in MeOH)	100	3.3	-	-	-	-	3.3	1.05

Table A.4.6. Decay parameters (using 375 nm LASER) of (A) transferred Qdots in water (λ_{em}= 505 nm), (B) ZnQ_2 (in MeOH; λ_{em}= 550 nm), (C) CdQ_2 (in MeOH; λ_{em}= 545 nm).

Samples	Monitored at		Fluorescence decease rate (I/I_0) (% per sec)
	λ_{ex} (nm)	λ_{em} (nm)	
(a) Rhodamine 6 G	365	560	0.11
(b) $Zn_xCd_{1-x}S$ Qdots	369	539	0.02
(c) Transferred Qdots	365	505	0.01
(d) ZnQ_2	365	550	0.03
(e) CdQ_2	365	545	0.02

Table A.4.7. Fluorescence decrease rate (% per sec) of (a) Conventional organic dye (Rhodamine 6G); (b) $Zn_xCd_{1-x}S$ Qdots (in hexane), (c) transferred Qdots (in Water), (d) ZnQ_2 (in methanol), (e) CdQ_2 (in methanol).

A5: Chapter 5

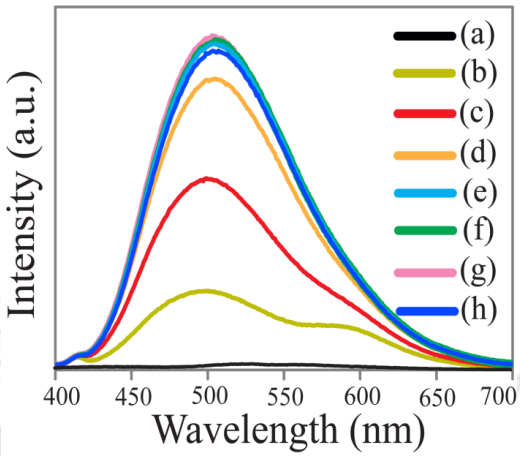

Figure A.5.1. Emission spectra (with λ_{ex}= 364 nm) with different amount - (a) 0.0 µL, (b) 5.0 µL, (c) 10.0 µL, (d) 15.0 µL, (e) 20.0 µL, (f) 25.0 µL, (g) 30.0 µL and (h) 35.0 µL - of 5.0 mM HQ (in methanol) added to 2.0 mL aqueous dispersion of AcAc capped 5.6% Mn^{2+} doped ZnS Qdots.

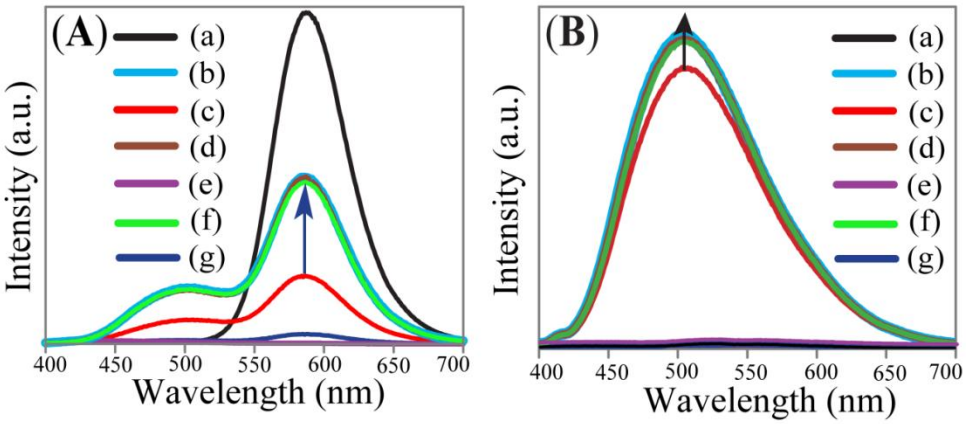

Figure A.5.2. Emission spectra (**A**) with λ_{ex} = 330 nm and (**B**) with λ_{ex} = 364 nm of (a) AcAc capped 5.6% Mn^{2+} doped ZnS Qdot; (b) optimum (30.0 µL) and (c) excess (100.0 µL) of 5.0 mM HQ added AcAc capped 5.6% Mn^{2+} doped ZnS Qdot before centrifugation; (d) pellet (following redispersion) and (e) supernatant of optimum HQ added AcAc capped 5.6% Mn^{2+} doped ZnS Qdot after centrifugation; (f) pellet (following redispersion) and (g) supernatant of excess HQ added AcAc capped 5.6% Mn^{2+} doped ZnS Qdot after centrifugation .

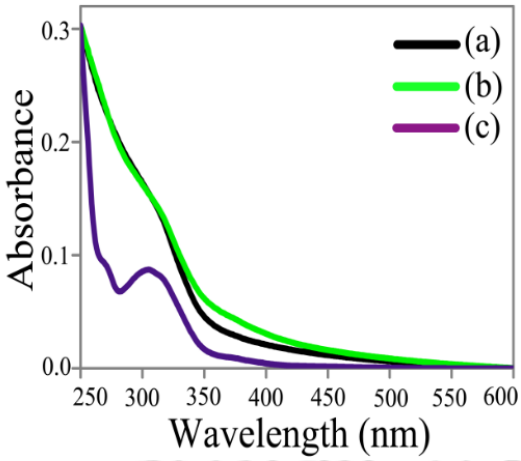

Figure A.5.3. UV-vis spectra of (a) AcAc capped 5.6% Mn^{2+} doped ZnS Qdot; (b) pellet (following redispersion) and (c) supernatant of excess (100.0 µL) 5.0 mM HQ added AcAc capped 5.6% Mn^{2+} doped ZnS Qdot (2.0 mL) after centrifugation.

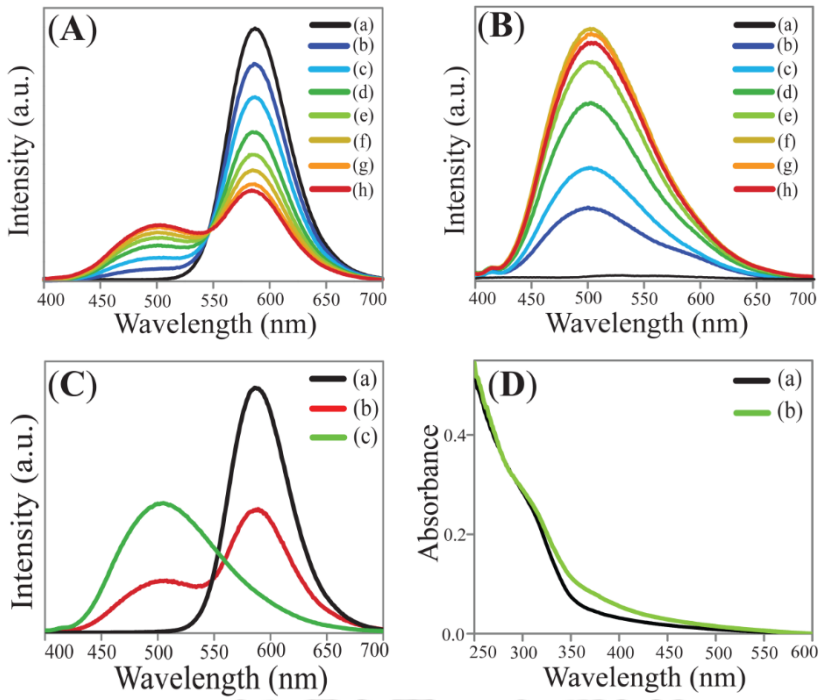

Figure A.5.4. Emission spectra at (**A**) λ_{ex} =330 nm and **(B)** λ_{ex} =364 nm with different amount - (a) 0.0 µL, (b) 20.0 µL, (c) 40.0 µL, (d) 60.0 µL, (e) 80.0 µL, (f) 100.0 µL, (g) 120.0 µL and (h) 140.0 µL - of 0.5 mM ZnQ_2 (in methanol) added to 2.0 mL aqueous dispersion of AcAc capped 5.6% Mn^{2+} doped ZnS Qdots; (**C**) emission spectra of (a) Qdots (λ_{ex} =330 nm) and (b, c) excess (200.0 µL) of 0.5 mM ZnQ_2 added Qdots (2.0 mL) (recorded following centrifugation and redispersion) monitored with λ_{ex} =330 and 364 nm light respectively and (**D**) UV-vis spectra of (a) Qdots and (b) excess (200.0 µL) of 0.5 mM ZnQ_2 added Qdots (recorded following centrifugation and redispersion).

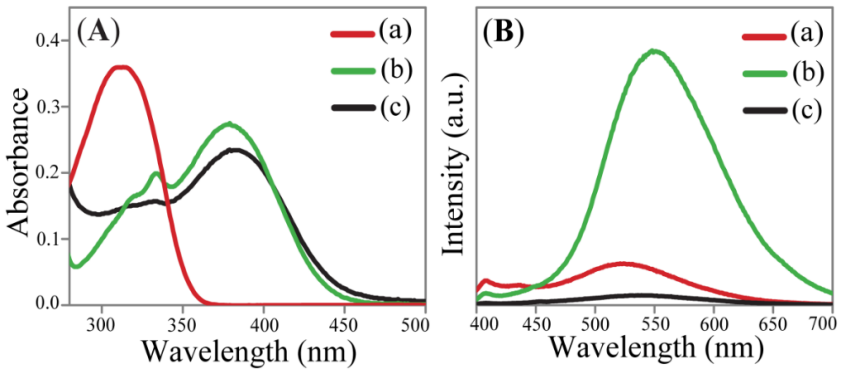

Figure A.5.5. (**A**) UV-Vis and (**B**) emission spectra (λ_{ex} =364 nm) of (a) HQ, (b) ZnQ_2, and (c) MnQ_2 in methanol.

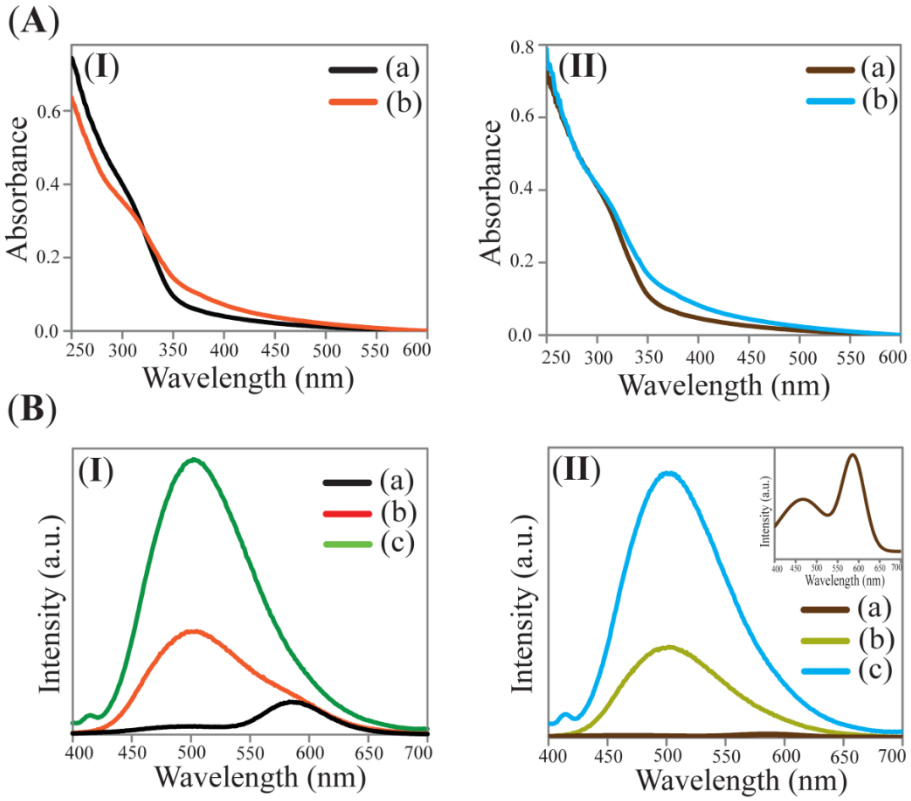

Figure A.5.6. (**A**) UV-vis spectra of (a) AcAc capped Qdots with different amount of Mn^{2+} concentrations: (I) medium (3.4%) content and (II) low content (2.7%) and (b) excess (100.0 µL of 5.0 mM) HQ added Qdots (2.0 mL) (recorded following centrifugation and redispersion) and (**B**) emission spectra of (a) AcAc capped Qdots (λ_{ex} =330 nm) with different amount of Mn^{2+} concentrations: (I) medium (3.4%) content and (II) low content (2.7%) and (b, c) excess (100 µL of 5.0 mM) HQ added Qdots (2.0 mL) (recorded following centrifugation and redispersion) with λ_{ex} =330 and 364 nm, respectively; (inset; shows the two emission peaks due to Mn^{2+} and host ZnS of 2.7% Mn^{2+} doped ZnS).

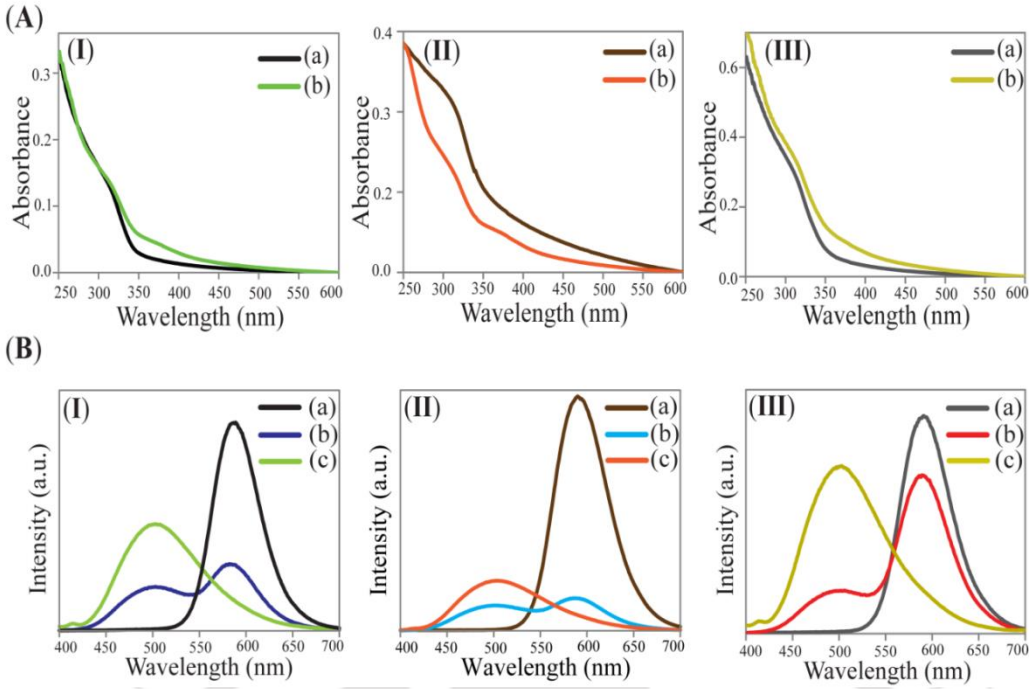

Figure A.5.7. (**A**) UV-Vis spectra of (**I**) uncapped, (**II**) citrate capped and (**III**) chitosan capped (a) 5.0-6.0% Mn^{2+} doped ZnS Qdot and (b) the centrifuged product obtained from excess (100 μL of 5.0 mM) HQ added to 2.0 mL of 5.0-6.0% Mn^{2+} doped ZnS Qdot (**B**) emission spectra of (**I**) uncapped, (**II**) citrate capped and (**III**) chitosan capped (a) 5.0-6.0% Mn^{2+} doped ZnS Qdot with (a) λ_{ex} = 330 nm; and the centrifuged product obtained from excess (100 μL of 5.0 mM) HQ added to 2.0 mL of 5.0-6.0% Mn^{2+} doped ZnS Qdot with (b) λ_{ex} = 330 nm and (c) λ_{ex} = 364 nm.

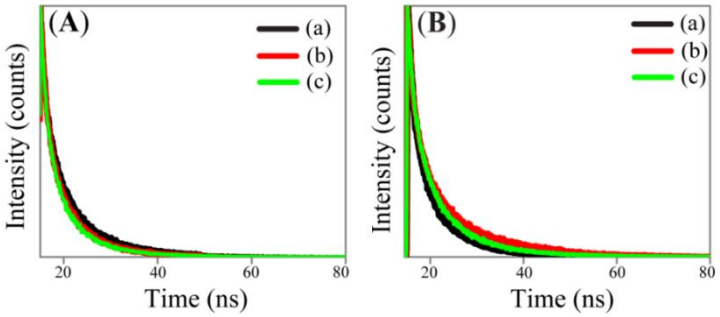

Figure A.5.8. Time-resolved photoluminescence spectra of (**A**) the product following complexation between HQ and AcAc capped Mn^{2+} doped ZnS Qdots with different dopant concentration (a) 5.6%, (b) 3.4% and (c) 2.7%; (**B**) the product following complexation between HQ and 5.0-6.0% Mn^{2+} doped ZnS Qdots with different capping environment using (a) no capping agents (uncapped), (b) citrate and (c) chitosan as capping agents.

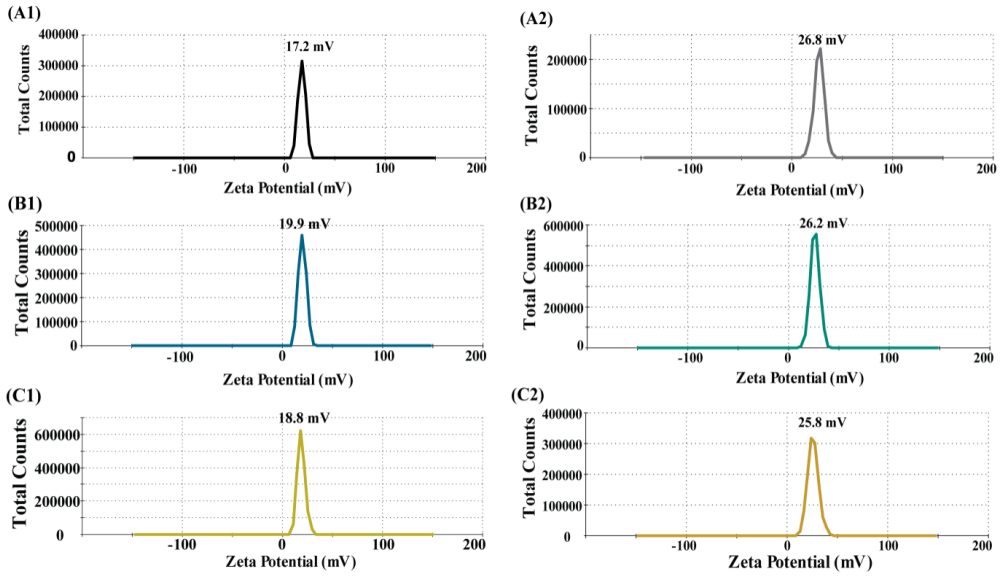

Figure A.5.9. Zeta potential curves of (**A**) 5.6%, (**B**) 3.4% and (**C**) 2.7% Mn^{2+} doped AcAc capped ZnS Qdots (**1**) and (**2**) their products following complexation with HQ.

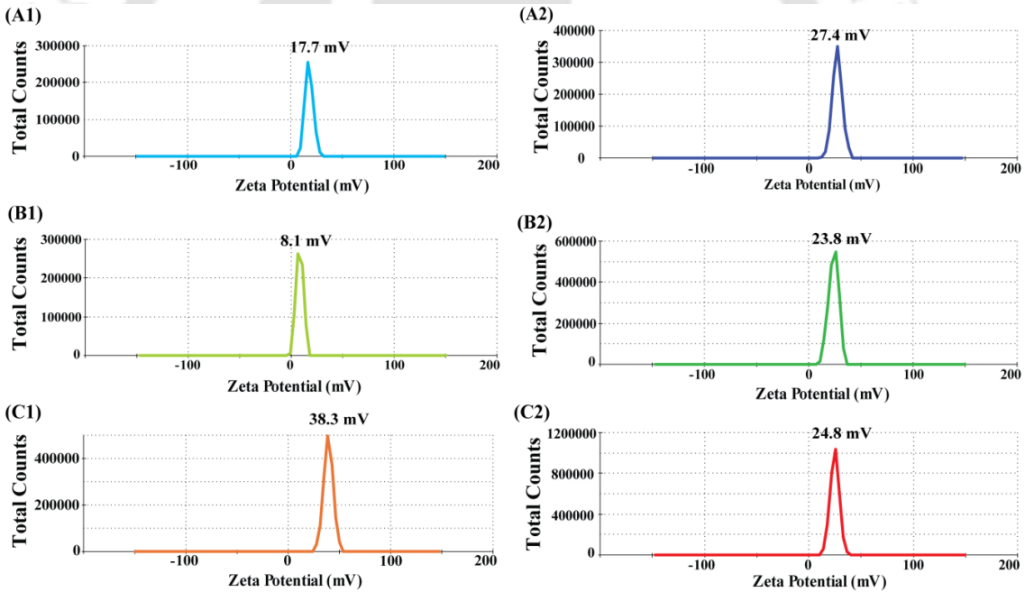

Figure A.5.10. Zeta potential curves of (**A**) bare (without capping agent), (**B**) citrate and (**C**) chitosan stabilized (**1**) 5.0-6.0% Mn^{2+} doped ZnS Qdots and (**2**) their products following complexation with HQ.

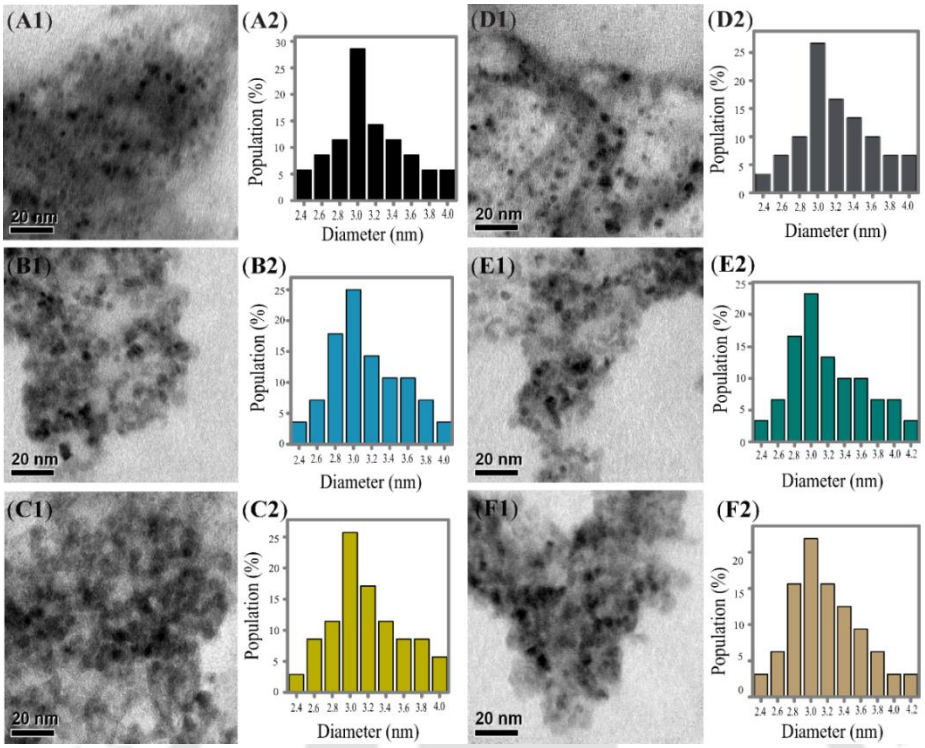

Figure A.5.11.TEM images (**1**) and corresponding particle size (**2**) distributions of AcAc capped (**A**) 5.6 %, (**B**) 3.4% and (**C**) 2.7% Mn^{2+} doped ZnS Qdots and (**D, E** and **F**) of their respective product following complexation with HQ.

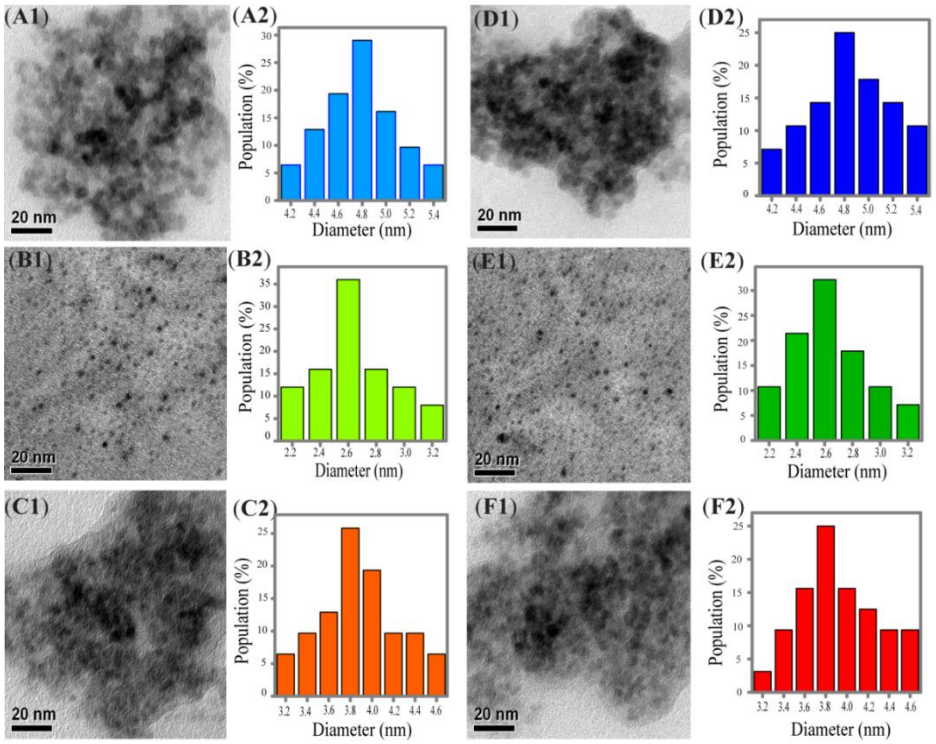

Figure A.5.12. TEM images (**1**) and corresponding particle size (**2**) distribution of 5.0-6.0% Mn^{2+} doped ZnS Qdots with different capping environment: (**A**) no capping agents, (**B**) citrate capped and (**C**) chitosan capped and (**D**, **E** and **F**) of their respective product following complexation with HQ.

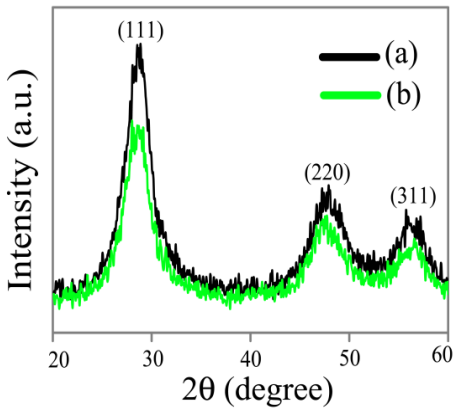

Figure A.5.13. Powder X-ray diffraction pattern of (a)AcAc capped 5.6% Mn^{2+} doped ZnS Qdot; (b) of the sample obtained following centrifugation of excess HQ added AcAc capped 5.6% Mn^{2+} doped ZnS Qdots.

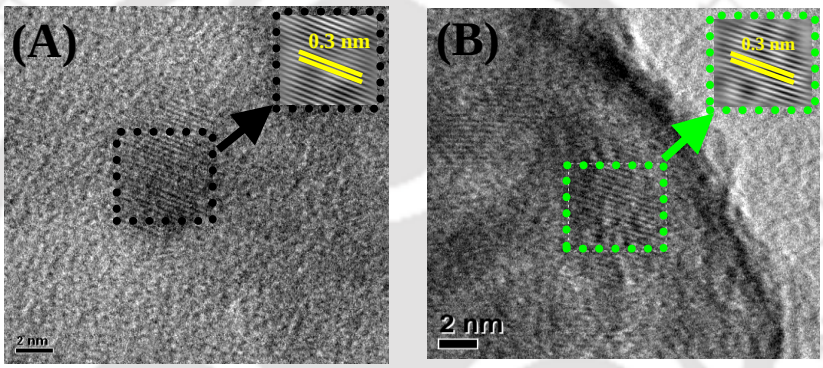

Figure A.5.14. HRTEM (scale bar- 2 nm) and corresponding IFFT (inset square boxes) of (**A**) AcAc capped 5.6% Mn^{2+} doped ZnS Qdot; (**B**) of the sample obtained following centrifugation of excess HQ added AcAc capped 5.6% Mn^{2+} doped ZnS Qdots.

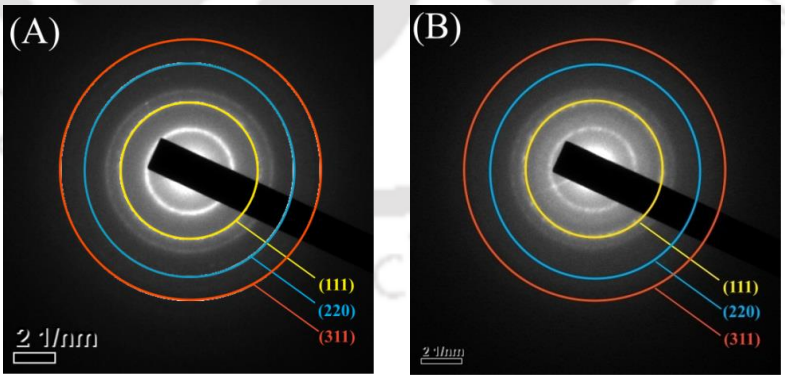

Figure A.5.15. Selected Area Electron Diffraction (SAED) (inset; scale bar: 2 nm^{-1}) images of (**A**) AcAc capped 5.6% Mn^{2+}doped ZnS Qdot; (**B**) of the sample obtained following centrifugation of excess HQ added AcAc capped 5.6% doped Mn^{2+}doped ZnS Qdots.

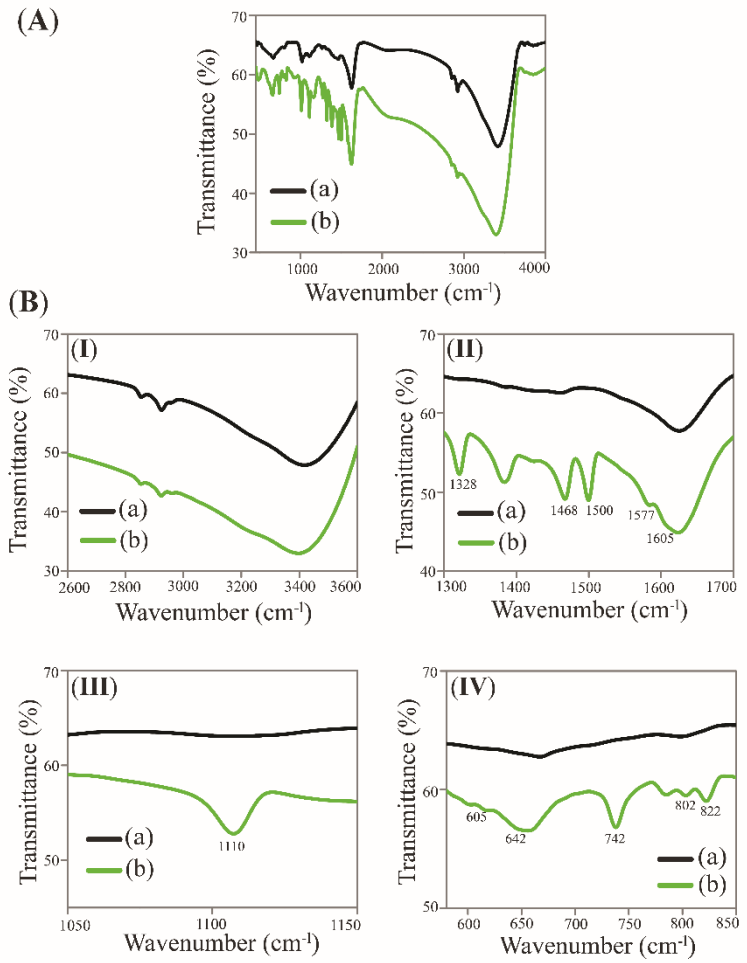

Figure A.5.16. **(A)** FTIR spectra of (a) AcAc capped Mn^{2+} ZnS Qdot; (b) of the sample obtained following centrifugation of excessHQ added AcAc capped 5.6% Mn^{2+}doped ZnS Qdots, and **(B)** their **e**xpanded forms in the (**I**) range 2600 -3600 cm^{-1}, (**II**) range 1300 -1700 cm^{-1}, (**III**) range 1050 -1150 cm^{-1}, and (**IV**) range 580 -850 cm^{-1}.

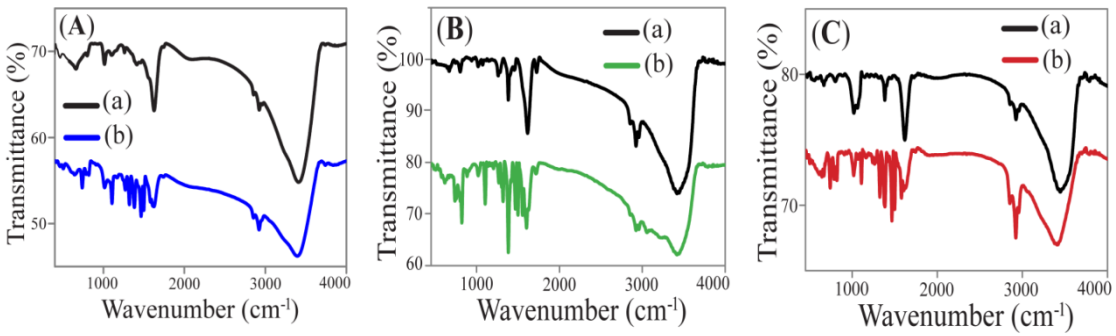

Figure A.5.17. FTIR spectra of (a) 5.0-6.0% Mn^{2+}doped ZnS Qdot (λ_{ex} = 330 nm); (b) pellet from excess (100.0 µl) 5.0 mM HQ added Mn^{2+} doped ZnS Qdot (2.0 mL) obtained after centrifugation: with (**A**) no capping agents; (**B**) citrate; and (**C**) chitosan as capping agents.

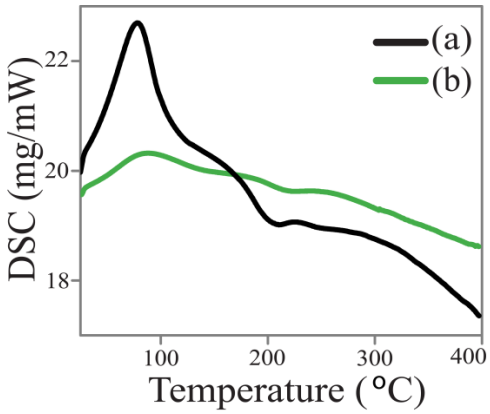

Figure A.5.18. Differential scanning calorimetric analysis of (a) Qdot and (b) QDC.

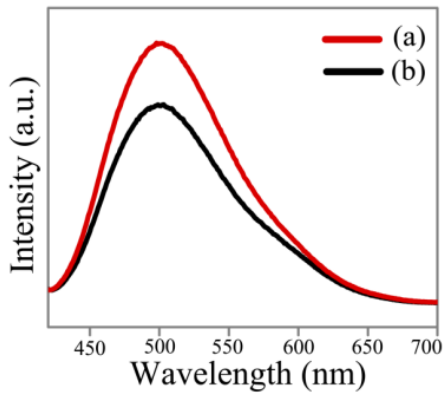

Figure A.5.19. Emission spectra (λ_{ex}=364 nm) of QDC (redispersed in methanol) (a) before and (b) after heating at 370 ^{o}C.

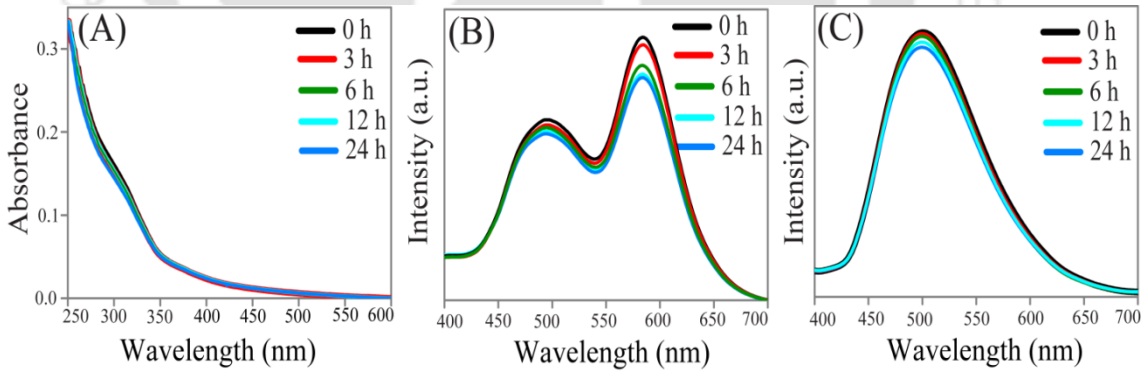

Figure A.5.20. (A) UV-Vis and emission spectra (B) at λ_{ex}-330 nm and (C) at λ_{ex}-365 nm of QDC in liquid phase at different time intervals.

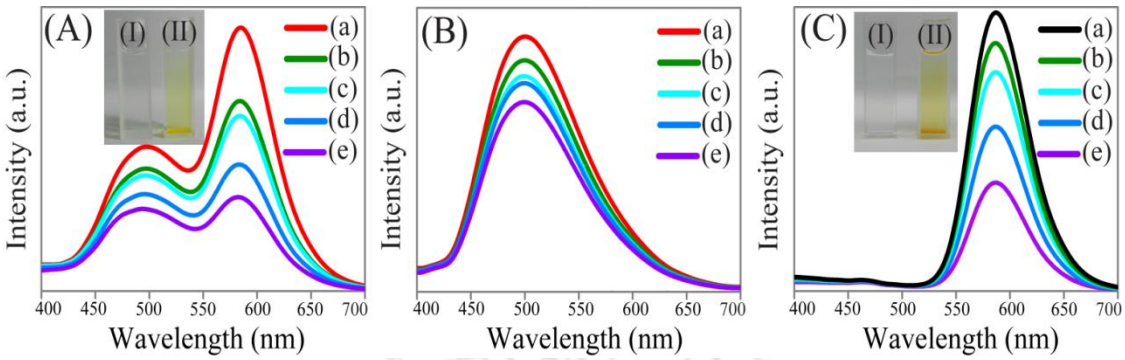

Figure A.5.21. Emission spectra (A) at λ_{ex}-330 nm (B) at λ_{ex}-365 nm of (a) 0.0 µL (b) 10.0 µL (c) 20.0 µL (d) 30.0 µL and (e) 40.0 µL of 5.0 mM Hg^{2+} treated 2.0 mL QDC (inset: (I) QDC and 40.0 µL of 5.0 mM Hg^{2+} treated QDC) and (C) emission spectra at λ_{ex}-330 nm of (a) 0.0 µL (b) 10.0 µL (c) 20.0 µL (d) 30.0 µL and (e) 40.0 µL of 5.0 mM Hg^{2+} treated 2.0 ml Qdots (inset: (I) Qdots and 40.0 µL of 5.0 mM Hg^{2+} treated Qdots) .

Sl. No.		Stabilizer	Mn (%)	QY (%)			(d) QY_c/QY_a
				Qdots (a) at 330 nm	QDC		
					(b) at 330 nm	(c) at 330 nm	
A	I	AcAc	5.6	6.2	3.0	4.2	0.68
	II	AcAc	3.4	0.6	-	4.4	-
	III	AcAc	2.7	0.04	-	4.5	-
B	I	Bare	5.8	9.2	3.3	7.0	0.76
	II	Citrate	6.0	25.4	4.8	20.0	0.79
	III	Chitosan	5.3	16.6	10.2	12.8	0.77

Table A.5.1. QY (using quinine sulphate as a standard) of (a) Qdots (λ_{ex} = 330 nm) (**A**) with different dopant concentration [(**I**) 5.6%, (**II**) 3.4% and (**III**) 2.7%], keeping AcAc as the capping agent and (**B**) with different capping agents [(**I**) no capping agents, (**II**) chitosan and (**III**) citrate as capping agents], keeping same dopant concentration (5.0-6.0%) and their corresponding product obtained following complexation with HQ, with (b) λ_{ex} = 330 nm and (c) 364 nm, respectively; (d) the QY ratio of the formed surface complex (at λ_{ex}= 364 nm) and their parent 5.0-6.0% Mn^{2+} doped ZnS Qdots (at λ_{ex}= 330 nm) having different stabilizers.

QDC				Tri exponentially fitted data							
Sl No.		Stabilizer	Mn (%)	A_1 (%)	τ_1 (ns)	A_2 (%)	τ_2 (ns)	A_3 (%)	τ_3 (ns)	τ_{av} (ns)	χ^2
A	I	AcAc	5.6	6.06	0.94	42.25	4.27	51.69	10.41	8.81	0.99
	II	AcAc	3.4	7.79	0.90	44.09	3.71	48.12	8.94	7.42	1.03
	III	AcAc	2.7	8.53	0.93	45.63	3.61	45.84	8.84	7.24	1.01
B	I	Bare	5.8	10.8	1.19	48.18	4.53	41.07	10.58	8.42	1.00
	II	Citrate	6.0	6.60	1.06	32.06	4.60	61.34	14.71	13.2	1.01
	III	Chitosan	5.3	6.67	1.13	43.25	4.53	50.08	11.15	9.35	1.04

Table A.5.2. Decay parameters (monitored using 375 nm laser) of the product following complexation between HQ and Mn^{2+} doped ZnS Qdots where the as-prepared Qdot has different synthetic environment: (**A**) with different dopant concentration [(**I**) 5.6%, (**II**) 3.4% and (**III**) 2.7%], keeping AcAc as capping agents and (**B**) with different capping agents [(**I**) bare (no capping agents), (**II**) chitosan and (**III**) citrate as capping agents], keeping same dopant concentration (5.0-6.0%).

Sl No.		Stabilizer	Mn (%)	pH at 23 °C	
				Qdots	QDC
A	I	AcAc	5.6	5.85	5.78
	II	AcAc	3.4	5.76	5.69
	III	AcAc	2.7	5.78	5.73
B	I	Bare	5.8	5.69	5.67
	II	Citrate	6.0	6.12	6.08
	III	Chitosan	5.3	5.62	5.60

Table A.5.3. pH measurement of the product following complexation between HQ and Mn^{2+} doped ZnS Qdots where the as-prepared Qdot has different synthetic environment: (**A**) with different dopant concentration [(**I**) 5.6%, (**II**) 3.4% and (**III**) 2.7%], keeping AcAc as capping agents and (**B**) with different capping agents [(**I**) no capping agents, (**II**) chitosan and (**III**) citrate as capping agents], keeping same dopant concentration (5.0-6.0%).

Sl No.		Capping molecules	% of dopants	Zeta Potential (mV)		Mobility (μmcm/Vs)	
				Qdots	QDC	Qdots	QDC
A	(I)	AcAc	5.6	17.2	26.8	1.4	2.1
	(II)	AcAc	3.4	19.9	26.2	1.6	2.0
	(III)	AcAc	2.7	18.8	25.8	1.5	2.0
B	(I)	Uncapped	5.8	17.7	27.4	1.4	2.1
	(II)	Citrate	6.0	8.1	23.8	0.6	1.9
	(III)	Chitosan	5.3	38.3	24.8	3.0	1.9

Table A.5.4. Measurement of zeta potential and mobility of Mn^{2+} doped ZnS Qdots with different synthetic environment: (**A**) with different dopant concentration [(**I**) 5.6%, (**II**) 3.4% and (**III**) 2.7%], keeping AcAc as capping agents and (**B**) with different capping agents [(**I**) no capping agents, (**II**) chitosan and (**III**) citrate as capping agents], keeping same dopant concentration (5.0-6.0%) and their products following complexation with HQ.

Sl No.		Capping molecules	% of dopants	Mn^{2+}doped ZnS Qdot			HQ added Mn^{2+} doped ZnS Qdot		
				$[Zn^{2}]$ (ppm)	$[Mn^{2+}]$ (ppm)	$[Mn^{2+}]$:$[Zn^{2+}]$	$[Zn^{2+}]$ (ppm)	$[Mn^{2+}]$ (ppm)	$[Mn^{2+}]$:$[Zn^{2+}]$
A	(I)	AcAc	5.6%	74.7	4.5	0.06	74.3	4.5	0.06
	(II)	AcAc	3.4%	74.1	2.7	0.04	73.7	2.6	0.04
	(III)	AcAc	2.7%	71.3	2.1	0.03	71.1	2.0	0.03
B	(I)	Uncapped	5.8%	75.3	4.7	0.06	75.0	4.5	0.06
	(II)	Citrate	6.0%	75.5	4.8	0.06	75.3	4.6	0.06
	(III)	Chitosan	5.3%	72.5	4.0	0.06	71.9	3.9	0.06

Table A.5.5. Tabulated Mn/Zn ratio of the product following complexation between HQ and Mn^{2+} doped ZnS Qdots where the as-prepared Qdot has different synthetic environment: (**A**) with different dopant concentration [(**I**) 5.6%, (**II**) 3.4% and (**III**) 2.7%], keeping AcAc as capping agent and (**B**) with different capping agents [(**I**) no capping agents, (**II**) chitosan and (**III**) citrate as capping agents], keeping same dopant concentration(5.0-6.0%).

Sl No	Capping molecules	% of dopants	Mn^{2+}doped ZnS Qdot		HQ added Mn^{2+} doped ZnS Qdots	
			Total No. of particles	Diameter (nm)	Total No. of particles	Diameter (nm)
(a)	AcAc	5.6%	245	3.1 ±0.4	210	3.1 ±0.4
(b)	AcAc	3.4%	198	3.1 ±0.4	180	3.1 ±0.5
(c)	AcAc	2.7%	175	3.1 ± 0.4	155	3.1 ±0.4

Table A.5.6. Change in average diameter (nm)of the AcAc capped Mn^{2+} doped ZnS Qdots, having different dopant concentrations [(**a**) 5.6%, (**b**) 3.4% and (**c**) 2.7%], following complexation with HQ .

Sl No.	Capping molecules	% of dopants	Mn^{2+}doped ZnS Qdot		HQ added Mn^{2+} doped ZnS Qdots	
			Total No. of particles	Diameter (nm)	Total No. of particles	Diameter (nm)
(a)	uncapped	5.8%	124	4.8 ±0.3	140	4.8 ±0.3
(b)	citrate	6.0%	200	2.6 ±0.3	224	2.6 ±0.3
(c)	chitosan	5.3%	155	3.9 ±0.4	160	3.9 ±0.4

Table A.5.7. Change in average diameter (nm) of the 5.0-6.0% Mn^{2+} doped ZnS Qdots, for different capping environment of the Qdots [(**a**) no capping agents, (**b**) citrate and (**c**) chitosan as capping agents], following complexation with HQ.

Stabilizer	Samples	Wavenumber (cm^{-1})										
		1605	1577	1500	1468	1328	1110	822	802	742	642	605
AcAc	Qdots	A	A	A	A	A	A	A	A	A	A	A
	QDC	P	P	P	P	P	P	P	P	P	P	P
Bare	Qdots	A	A	A	A	A	A	A	A	A	A	A
	QDC	P	P	P	P	P	P	P	P	P	P	P
Citrate	Qdots	A	A	A	A	A	A	A	A	A	A	A
	QDC	P	P	P	P	P	P	P	P	P	P	P
Chitosan	Qdots	A	A	A	A	A	A	A	A	A	A	A
	QDC	P	P	P	P	P	P	P	P	P	P	P

Table A.5.8. Presence (P) and absence (A) of the above functional groups in the product following complexation between HQ and 5.0-6.0% Mn^{2+} doped ZnS Qdots with different capping agents.

Wave number (Cm^{-1})	Functional groups	Wave number (Cm^{-1})	Functional groups
1605	C-C/C-N stretching	1110	-C-O-Zn Stretching
1577	C-C/C-N stretching	822	C-H out plane wagging
1500	Pyridyl group of HQ	802	C-H out plane wagging
1468	Phenyl group of HQ	742	C-H out plane wagging, in plane ring deformation
1328	C-H bending	642	in-plane ring deformation
605	in-plane ring deformation	-	-

Table A.5.9. Tabulated FTIR wavenumber vs functional groups of the product following complexation between HQ and 5.0-6.0% Mn^{2+} doped ZnS Qdots with different capping agents.

Stabilizer	Mn (%)	$I_{3300\ cm-1}$: $I_{1110cm-1}$	
		Qdots	QDC
AcAc	5.6	No significant peak at 1110 cm^{-1}	0.73
Uncapped	5.8	No significant peak at 1110 cm^{-1}	0.68
Citrate	6.0	No significant peak at 1110 cm^{-1}	0.81
Chitosan	5.3	No significant peak at 1110 cm^{-1}	0.84

Table A.5.10. Tabulated intensity ratio of 3333 cm^{-1} band to 1110 cm^{-1} band of the product following complexation between HQ and 5.0-6.0% Mn^{2+} doped ZnS Qdots with different capping environment.

Samples	PL decrease rate (% per sec) excited at	
	330 nm	364 nm
(a) Rhodamine 6G	0.10	0.11
(b) Qdot	0.02	-
(c) QDC	0.02	0.03
(d) ZnQ_2 complex	-	0.02

Table A. 5.11. Photoluminescence decrease rate (% per sec) of (a) organic dye (Rhodamine 6G at λ_{em}- 570 nm; in ethanol) (b) AcAc capped 5.6% Mn^{2+} doped ZnS Qdots (at λ_{em}- 588 nm; in water) (c) HQ added AcAc capped 5.6% Mn^{2+} doped ZnS Qdots (QDC at λ_{em}- 588 and 500 nm; in water) and (d) ZnQ_2 complex (at λ_{em}- 500 nm; in methanol) being monitored at two different excitation wavelengths (330 nm and 364 nm).

A6: Chapter 6

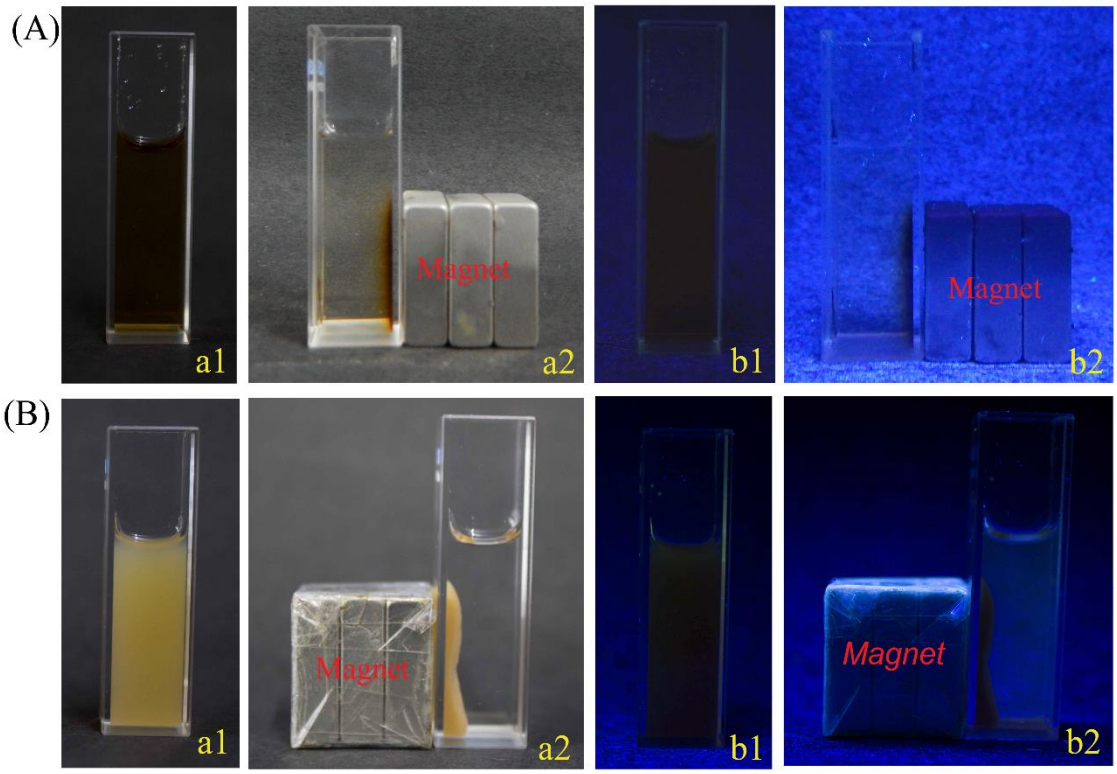

Figure A.6.1. Optical images of the aqueous dispersion of (**A**) Fe_3O_4 and (**B**) Fe_3O_4-ZnS recorded under (a) white and (b) UV light (365 nm), in the (1) absence and (2) presence of external magnetic field. Due to lack of absorbance ZnS Qdots did not show any fluorescence at the excitation wavelength of 365 nm.

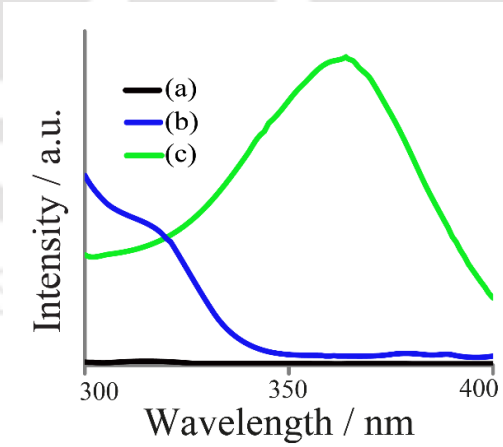

Figure A.6.2. Excitation spectra of the aqueous dispersion of (a) Fe_3O_4 (λ_{em}= 440 nm), (b) Fe_3O_4-ZnS (λ_{em}= 440 nm) and (c) HQ treated Fe_3O_4-ZnS (λ_{em}=500 nm).

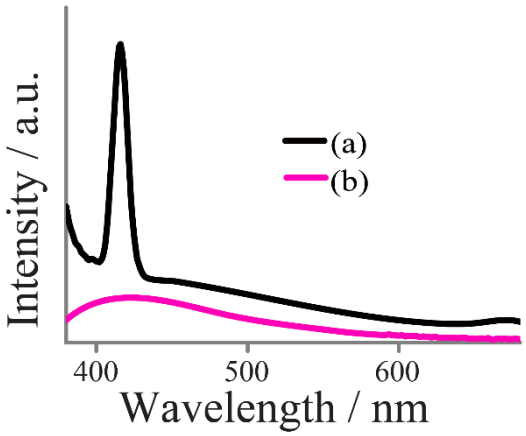

Figure A.6.3. Emission spectra (λ_{ex}=365 nm) of the aqueous dispersion of (a) Fe_3O_4 and (b) HQ treated Fe_3O_4.

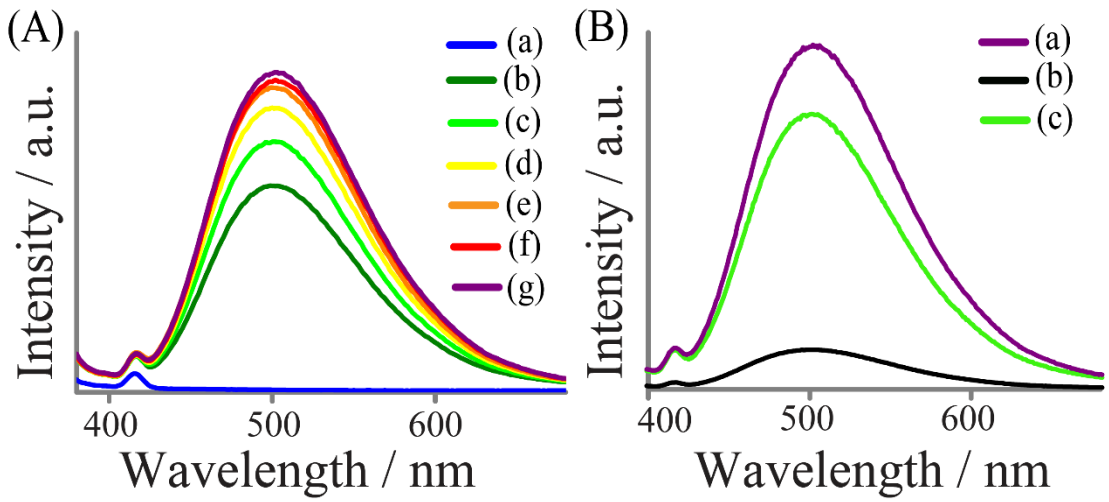

Figure A.6.4. (**A**) Emission spectra (λ_{ex}= 365 nm) of the medium resulting from addition of (a) 0.0 µL, (b) 2.0 µL, (c) 4.0 µL, (d) 6.0 µL, (e) 8.0 µL, (f) 10.0 µL, (g) 12.0 µL of 5.0 mM of HQ (in ethanol) to the aqueous dispersion of 2.0 mL of Fe_3O_4-ZnS (pH-6.8; with absorbance 0.2 at 320 nm); (**B**) emission spectra(λ_{ex}= 365 nm) of the medium when (a) 12.0 µL (optimum) of 5.0 mM of HQ was added to the aqueous dispersion of 2.0 mL of Fe_3O_4-ZnS before centrifugation, (b) supernatant and (c) pellets obtained following centrifugation and redispersion into same amount of solvent.

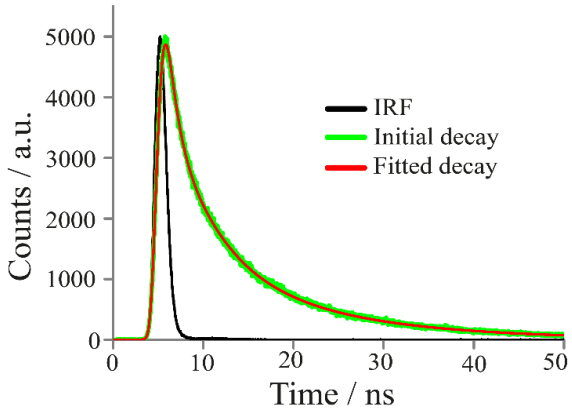

Figure A6.5. Decay profiles (using 340 nm LED as excitation source) of the aqueous dispersion of HQ treated Fe_3O_4-ZnS (λ_{em} =500 nm), which were fitted by tri exponential function. Where IRF stands for instrument response function.

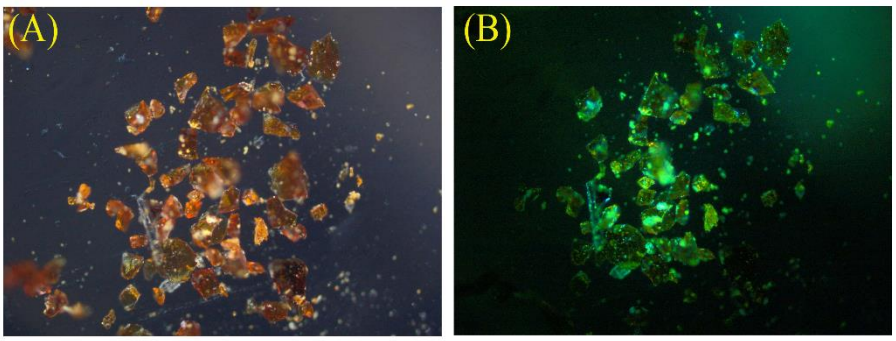

Figure A.6.6. Microscopic images of solid samples of HQ treated Fe_3O_4-ZnS in presence of (**A**) white and (**B**) UV light (λ_{ex} = 350 nm).The solids of the particles were placed on a glass slide and then imaged under fluorescence microscope.

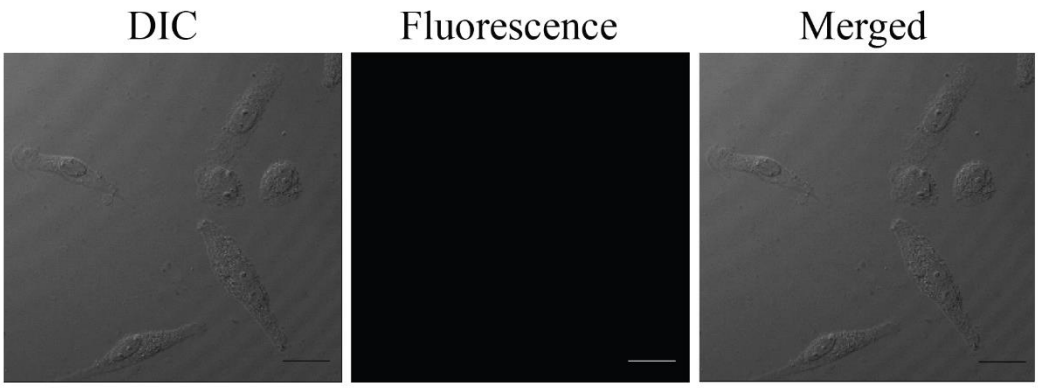

Figure A.6.7. Fluorescence image of only HeLa cells under confocal laser scanning microscope (scale bar – 25 μm).

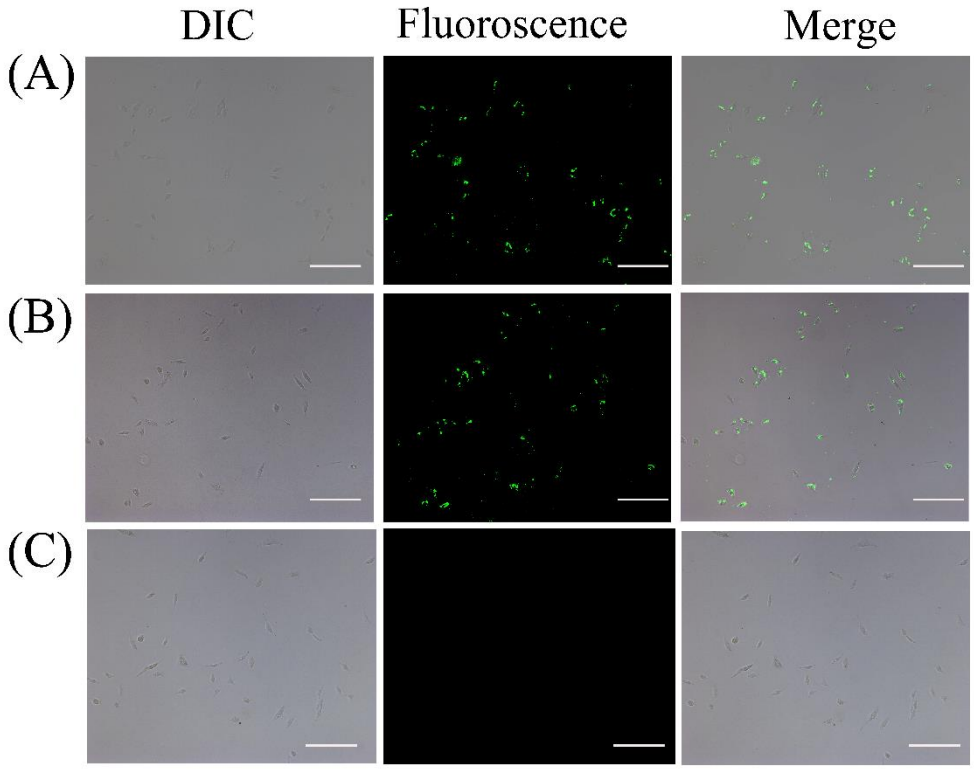

Figure A.6.8. Fluorescence images (scale bar – 100 μm) of HeLa cells – which were grown in a petridis containing on two glass slide (**A** and **B**) - following 4 h incubation with HQ treated Fe_3O_4/ZnS. Each glass slide was monitored under fluorescence microscope. (**C**) Fluorescence image (scale bar-100 μm) of only HeLa cells.

Samples	Zeta Potential (mV)
Fe_3O_4	-52.0 ± 0.5
Fe_3O_4/ZnS	-31.0 ± 0.1
HQ treated Fe_3O_4/ZnS	-25.5 ± 0.6

Table A.6.1. Zeta potential values of the aqueous dispersion of (a) Fe_3O_4, (b) Fe_3O_4-ZnS and (b) HQ treated Fe_3O_4-ZnS.

Samples	Conc. of Fe ions (ppm)	Conc. of Zn ions (ppm)	Fe/Zn ratio
Fe_3O_4-ZnS	2.32	12.1	0.192
SPION-QDC	2.20	11.7	0.188

Table A.6.2. Tabulated Fe/Zn ratio of the aqueous dispersion of (a) Fe_3O_4-ZnS and (b) HQ treated Fe_3O_4-ZnS.

Samples	Monitored λ_{ex} at	
	320 nm	365 nm
Fe_3O_4/ZnS	0.7%	-
HQ treated Fe_3O_4/ZnS	0.8%	5.9%

Table A.6.3. Quantum yield (%) w.r.t. quinine sulphate (in 0.1 M H_2SO_4) of the aqueous dispersion of (a) Fe_3O_4-ZnS (λ_{ex} =365 nm; λ_{em} =440 nm) and (b) HQ treated Fe_3O_4-ZnS (λ_{ex} =320 and 365 nm; λ_{em} =500 nm).

Samples	α_i(%)	τ_i (ns)	τ_{av} (ns)	χ^2
HQ treated Fe_3O_4/ZnS	33.54	4.68	12.54	1.10
	8.75	0.84		
	57.71	14.16		

Table A.6.4. Decay parameters (using 340 nm LED as excitation source) obtained following tri-exponential fitting of TRPL of the aqueous dispersion of HQ treated Fe_3O_4-ZnS (λ_{em} =500 nm).

Samples	λ_{ex} (nm)	λ_{em} (nm)	Fluorescence decrease rate (% per sec)
HQ treated Fe_3O_4-ZnS	365	500	0.015
Rhodamine-6G	365	570	0.003

Table A.6.5. Fluorescence decrease rate (% per sec) of (a) HQ treated Fe_3O_4-ZnS (in water) and (b) rhodamine 6 G (in ethanol).

Samples	Magnetic saturation value (emu. g^{-1})
Fe_3O_4	26.34
Fe_3O_4/ZnS	3.88
HQ treated Fe_3O_4/ZnS	3.81

Table A.6.6. Magnetic saturation value of the solid particles of (a) Fe_3O_4, (b) Fe_3O_4-ZnS and (b) HQ treated Fe_3O_4-ZnS.

Instruments.

Chapter 2. UV-Vis and PL spectra (using λ_{ex} = 369 nm) were recorded on a Perkin Elmer Lambda 45 UV-Vis spectrophotometer and Horiba Fluoromax-4 spectrofluorimeter respectively. Time-resolved photoluminescence (TRPL) intensity decays of the Qdots both in absence and presence of CB were recorded using a Life Spec II spectrofluorimeter (Edinburgh Instrument). The sample was excited by Pico Quant 375 nm LED source. The decay curves were analyzed by FAST software, provided by Edinburgh Instrument along with the fluorescence instrument. The XRD patterns for the powder NCs were recorded by a Brucker D2 Phaser X-ray diffractometer (having CuKα radiation 1.5418A0). A JEOL JEM 2100 transmission electron microscope (operated at a maximum accelerating voltage of 200 kV) was used to analyze size and structure of alloyed NCs deposited on Formvar carbon-coated copper grids. FTIR spectra of NC samples were recorded in a Perkin-Elmer (Model: Spectrum One) spectrophotometer. Elemental analysis was carried out using a fast sequential absorption spectrophotometer (Varian AA240FS model).

Chapter 3. The XRD patterns for the samples were recorded in a Brucker D2 Phaser X-ray diffractometer (having CuKα radiation at 1.5418Å). UV-Vis and PL spectra recordings were carried out with Hitachi U-2900 spectrophotometer and HORIBA-Fluorolg3 spectrofluorimeter respectively. A JEOL JEM-2100 transmission electron microscope (operated at a maximum accelerating voltage of 200 kV) was used to analyze size, structure (from high resolution TEM images) and nature of samples deposited on formvar-carbon-coated copper grids. Inverse fast Fourier transform (IFFT) images were obtained by using Gatan Digital Micrograph software. FT-IR spectra of solid samples were recorded in a Perkin-Elmer (Model: Spectrum One) spectrophotometer. Time-resolved photoluminescence (TRPL) analyses were performed using Life-Spec-II spectrofluorimeter (Edinburgh Instrument, using Pico Quant 375 nm LASER and 308 LED source). The decay curves were analyzed by FAST software, provided by Edinburgh Instrument along with the fluorescence instrument. Quantum yields of samples were measured using quinine sulphate (in 0.1 M H_2SO_4) as a standard. Photostability experiments were carried out in a Perkin Elmer LS 55 instrument for ½ h, using Rhodamine 6G as standard. TGA and DSC were recorded by using Perkin Elmer 4000 and Perkin Elmer 6000 instruments respectively. Optical

microscopy images under white and UV light (at an excitation wavelength of 350 nm) were recorded by OLYMPUS BX 51 microscope fitted with a digital camera. The pH of the dispersions of QDCs and Qdots was measured using a JENWAY 3510- pH meter.

Chapter 4. A Hitachi U-2900 spectrophotometer and a HORIBA-Fluorolog 3 spectrofluorometer were used to record the UV−vis and PL spectra. Quantum yield and photostabilty of samples were measured using standard solutions of quinine sulfate (in 0.1 M H_2SO_4) and rhodamine 6G, respectively. Time-resolved photoluminescence (TRPL) analyses were carried out using Life-Spec-II spectrofluorometer (Edinburgh Instrument, using Pico Quant 375 nm LASER source), and the decay curves were analyzed by FAST software. The pH of the dispersions of the sample was measured using a JENWAY 3510 pH meter. A PerkinElmer (Model: Spectrum One) spectrophotometer was used for recording the FT-IR spectra of solid samples. The transmission electron microscopic (TEM), high resolution TEM (HRTEM), and selected area electron diffraction (SAED) pattern of the samples deposited on formvar-carbon-coated copper grids were recorded in a JEOL JEM-2100 transmission electron microscope (operated at a maximum accelerating voltage of 200 kV). The particle size distribution and inverse fast Fourier transform (IFFT) images were obtained by using Gatan Digital Micrograph software. A Bruker D2 Phaser X-ray diffractometer (having Cu Kα radiation at 1.5418 Å) was used to measure the XRD patterns of the powder samples. Thermal gravimetric analysis (TGA) was recorded by using a Mettler Toledo TGA/SDTA851e thermal analyzer in a nitrogen atmosphere, with a heating rate of 7 °C/min.

Chapter 5. Photoluminescence spectra were recorded using HORIBA-Fluorolg3 spectrofluorimeter. UV-Vis spectra were recorded with Hitachi U-2900 spectrophotometer.The pH of the dispersions of QDCs and Qdots was measured using a JENWAY 3510- pH meter. Quantum yield (Q.Y.) of sample was calculated by using quinine sulphate (Q.Y.= 54% in 0.1 M H_2SO_4) as a reference sample. Time resolved PL studies were performed by using Life-Spec-II spectrofluorimeter (Edinburgh Instrument, using Pico Quant 375 nm LASER and 308 LED source) and the decay patterns of the samples were analyzed by FAST software with the same instruments. Rhodamine 6G was used as a standard for time dependent (up to 500 sec) photo

irradiation experiments.4 ESR (Electron Spin Resonance) spectra of the powder samples were recorded using JEOL FA 200 ESR spectrophotometer. FT-IR spectrophotometer (model: Spectrum Two) was used to analyze the solid samples. Zeta potential measurements of the colloidal dispersion were done using Malvern Zetasizer Nano ZS instruments. The XRD patterns of solid samples were measured using Brucker D2 Phaser X-ray diffractometer (having CuKα radiation at 1.5418Å). TEM, high resolution TEM and SAED (selected area electron diffraction) analyses were done with JEOL JEM-2100 transmission electron microscope (operated at a maximum accelerating voltage of 200 kV).Using Gatan Digital Micrograph software inverse fast Fourier transform (IFFT) images were obtained from the same sample used for TEM analysis. TGA and DSC were recorded by using Perkin Elmer 4000 and Perkin Elmer 6000 instruments, respectively. OLYMPUS BX 51 microscope fitted with a digital camera was used to capture the images of solid samples under white and UV (with 350 nm excitation wavelength) light.

Chapter 6. The digital photographs of the samples were taken under UV light (365 nm) using a UV-lamp (Spectroline). The UV-Vis and PL spectra were recorded using Perkin Elmer Lambda-750 spectrometer and HORIBA-Fluoromax4 spectrofluorimeter, respectively. The JENWAY 3510- pH meter was used to measure the pH of the samples. The XRD patterns of the powder samples were measured using Brucker D8Advance X-ray diffractometer. The TEM, HRTEM and SAED pattern of the samples were recorded in a JEOL JEM-2100 transmission electron microscope (operated at a maximum accelerating voltage of 200 kV) following deposition of the aqueous dispersion on formvar-carbon-coated copper grids. The inverse fast Fourier transform (IFFT) images and particle size distribution were obtained by using Gatan Digital Micrograph software. The photostability of the samples were measured in Perkin-Elmer spectrofluorimeter with continuous irradiation of light and 0.1 sec data intervals. Time-resolved photoluminescence (TRPL) analyses were performed using HORIBA-JOBIN YVON FLUOROLOG spectrofluorimeter and using 340 nm LED excitation source with pulse width <1ns. To capture the images of the solid samples under white and UV (with 350 nm excitation wavelength) light, OLYMPUS BX 51 microscope fitted with a digital camera was used. The atomic absorption spectrometer (Varian AA240FS model) was used for elemental analysis of the aqueous dispersion of

the samples following their acid digestion. The FTIR spectra of the solid samples were recorded using Perkin-Elmer (Model: Spectrum One) spectrophotometer. Magnetic measurement of the samples was performed using a vibrating sample magnetometer (VSM; Model No. 7410 series). HeLa cells incubated with samples were imaged under an epi-fluorescence microscope (Nikon Eclipse TS100, Tokyo) using a Qdot 525 nm filter. Using Leica TCS SP8 STED (405 nm diode laser; magnification-60x oil immersion objective) microscope the confocal images of the samples were recorded.

Quantum Yield Determination. The quantum yield (QY) of the samples were calculated using quinine sulphate (in 0.1 M H_2SO_4) as standard and following equation:

$$Q_s = Q_R \times \frac{I_s}{I_R} \times \frac{A_R}{A_S} \times \frac{\eta_S^2}{\eta_R^2} \qquad (1)$$

Where, Q_S = sample's QY; Q_R = standard's QY (0.54 in 0.1 M H_2SO_4); I_S = area under the emission curve of sample; I_R = area the emission curve of standard; A_R = standard's absorbance; A_S = sample's absorbance; η_S = refractive index of solvent which is used for dispersion of sample; η_R = refractive index of solvent which is used for dispersion of standard. The concentration of all samples and the standard were fixed followed by adjusting their absorbance to 0.1 $\pm$ 0.01 at 369 nm.

Life time calculation. The decay profile was fitted to a multi-exponential model using following equation

$$I(t) = \sum_i \alpha_i \exp\left(-t/\tau_i\right) \qquad (2)$$

Where, single, bi and tri exponential functions were used to fit respective emission with obtaining χ^2 close to 1.0. The averaged life times (τ_{av}) in Table S2, determined from the results of three exponential model using

$$\tau_{av} = \frac{\sum_i \alpha_i \tau_i^2}{\sum_i \alpha_i \tau_i} \qquad (3$$

Where, α_i and τ_i are the pre-exponential factors and excited-state luminescence decay time associated with the *i*-th component, respectively.

Bibliography

1) https://en.wikipedia.org/?title=Wassily_Kandinsky
2) http://blog.donorperfect.com/2009/08/everything-starts-from-a-dot/
3) Murphy, C. J.; Coffer, J. L. Quantum Dots: A Primer *Applied Spectroscopy* **2002**, *56*, 16A-27A.
4) Alivisatos, A. P. Semiconductor Clusters, Nanocrystals, and Quantum Dots *Science*, **1996**, *271*, 933–937.
5) Ekimov A. I.; Onushchenko A. A. Quantum Size Effect in Three-dimensional Microscopic Semiconductor Crystals *JETP Lett.* **1981**, *6*, 345–349.
6) Rossetti, R.; Nakahara, S.; Brus, L. E. Quantum Size Effects in the Redox Potentials, Resonance Raman Spectra, and Electronic Spectra of CdS Crystallites in Aqueous Solutions *J. Chem. Phys*. **1983**, *79*, 1086-1088.
7) Reed, M. A.; Randall, J. N.; Aggarwal, R. J.; Matyi, R. J.; Moore, T. M.; Wetsel, A. E. Observation of Discrete Electronic States in a Zero-dimensional Semiconductor Nanostructure *Phys Rev Lett.* **1988**, *60*, 535–537.
8) Hines, D. A.; Kamat, P. V. Excited State Reactions at the Quantum Dot Surface *University of Notre Dame PhD Thesis*, **2015**, 5-6.
9) Kippeny, T.; Swafford, L. A.; Rosenthal, S. J. Semiconductor nanocrystals: A Powerful Visual Aid for Introducing the Particle in a Box *J. Chem. Ed.* **2002,** *79*, 1094-1100.
10) Kambhampati, P. Fundamentals of the Quantum Confinement Effect, Book chapter in *Handbook of Photoluminescent Semiconductor Materials – Taylor & Francis*, **2011**.
11) Kambhampati, P. Unraveling the Structure and Dynamics of Excitons in Semiconductor Quantum Dots *Acc. Chem. Res.* **2011**, *44*, 1– 13.
12) Dabbousi, B. O.; RodriguezViejo, J.; Mikulec, F. V.; Heine, J. R.; Mattoussi, H.; Ober, R.; Jensen, K. F.; Bawendi, M. G. (CdSe)ZnS Core−Shell Quantum Dots: Synthesis and Characterization of a Size Series of Highly Luminescent Nanocrystallites *J. Phys. Chem. B* **1997**, 101, 9463-9475.
13) Murray, C. B.; Norris, D. J.; Bawendi, M. G. Synthesis and Characterization of Nearly Monodisperse CdE (E = Sulfur, Selenium, Tellurium) Semiconductor Nanocrystallites *J. Am. Chem. Soc.* **1993**, 115, 8706-8715.
14) Somers, R. C.; Bawendi, M. G.; Nocera, D. G. CdSe Nanocrystal based Chem-/Bio-Sensors *Chem. Soc. Rev*. **2007**, *36*, 579-591.
15) Moreels, I.; Justo, Y.; De Geyter, B.; Haustraete, K.; Martins, J. C.; Hens, Z. Size-Tunable, Bright, and Stable PbS Quantum Dots: A Surface Chemistry Study *ACS Nano* **2011**, 5,2004– 2012.
16) Moreels, I.; Lambert, K.; Smeets, D.; De Muynck, D.; Nollet, T.; Martins, J. C.; Vanhaecke,F.; Vantomme, A.; Delerue, C.; Allan, G.; Hens, Z.Size-Dependent Optical Properties of Colloidal PbS Quantum Dots *ACS Nano* **2009**, 3, 3023– 3030
17) Ho, M. Q.; Alan Esteves, R. J.; Kedarnath, G.; Arachchige, I. U. Size-Dependent Optical Properties of Luminescent Zn_3P_2 Quantum Dots *J. Phys. Chem. C*, **2015**, *119*, 10576–10584.
18) Nag, A.; Cherian, R.; Mahadevan, P.; Gopal, A. V.; Hazarika, A.; Mohan, A.; Vengurlekar,A.; Sarma, D. Size-Dependent Tuning of Mn^{2+} d Emission in Mn^{2+}-Doped CdS Nanocrystals: Bulk vs Surface *J. Phys. Chem. C* **2010**, *114*, 18323–18329.

19) El-Sayed, M. A. Small Is Different: Shape-, Size-, and Composition-Dependent Properties of Some Colloidal Semiconductor Nanocrystals *Acc. Chem. Res*. **2004**, *37*, 326– 333.
20) Boatman, E. M.; Lisensky, G. C.; Nordell, K. J. A Safer, Easier, Faster Synthesis for CdSe Quantum Dot Nanocrystals *J. Chem. Educ.* **2005**, 82, 1697-1699.
21) Brus, L. Electronic Wave Functions in Semiconductor Clusters: Experiment and Theory *J. Phys. Chem.*, **1986**, *90*, 2555–2560.
22) Kamat, P. V. Semiconductor Nanocrystals: *To Dope or Not to Dope J. Phys. Chem. Lett.*, **2011**, *2*, 2832–2833.
23) Vlaskin, V. A.; Janssen, N.; van Rijssel, J.; Beaulac, R. m.; Gamelin, D. R. Tunable Dual Emission in Doped Semiconductor Nanocrystals *Nano Lett.* **2010**, *10*, 3670– 3674.
24) Karan, N. S.; Sarma, D. D.; Kadam, R. M.; Pradhan, N. Doping Transition Metal (Mn or Cu) Ions in Semiconductor Nanocrystals *J. Phys. Chem. Lett.* **2010**, *1*, 2863– 2866.
25) Srivastava, B. B.; Jana, S.; Pradhan, N. Doping Cu in Semiconductor Nanocrystals: Some Old and Some New Physical Insights *J. Am. Chem. Soc.* **2011**, *133*, 1007– 1015.
26) Srivastava, B. B.; Jana, S.; Karan, N. S.; Paria, S.; Jana, N. R.; Sarma, D. D.; Pradhan, N. Highly Luminescent Mn-Doped ZnS Nanocrystals: Gram-Scale Synthesis *J. Phys. Chem. Lett.* **2010**, *1*, 1454– 1458.
27) Hazarika, A.; Pandey, A.; Sarma, D. D. Rainbow Emission from an Atomic Transition in Doped Quantum Dots *J. Phys. Chem. Lett.* **2014**, *5*, 2208– 2213.
28) Pradhan, N.; Sarma, D. D. Advances in Light-Emitting Doped Semiconductor Nanocrystals *J. Phys. Chem. Lett.* **2011**, *2*, 2818– 2826.
29) Nag, A.; Sarma, D. White Light from Mn^{2+}-doped CdS Nanocrystals: A New Approach *J. Phys. Chem. C* **2007**, *111*, 13641– 13644.
30) Santra, P. K.; Kamat, P. V. Mn-Doped Quantum Dot Sensitized Solar Cells. A Strategy to Boost Efficiency over 5%. *J. Am. Chem. Soc.* **2012**, *134*, 2508–2511.
31) Nag, A.; Chakraborty, S.; Sarma, D. D. To Dope Mn^{2+} in a Semiconducting Nanocrystal *J. Am. Chem. Soc*. **2008**, *130*, 10605– 10611.
32) Grandhi, G. K.; Viswanatha, R. Tunable Infrared Phosphors Using Cu Doping in Semiconductor Nanocrystals: Surface Electronic Structure Evaluation *J. Phys. Chem. Lett.* **2013**, *4*, 409-415.
33) Pradhan, N.; Peng, X. Efficient and Color-Tunable Mn-Doped ZnSe Nanocrystal Emitters: Control of Optical Performance via Greener Synthetic Chemistry *J. Am. Chem. Soc.* **2007**, *129*, 3339– 3347.
34) Bol, A. A.; Meijerink, A. Luminescence Quantum Efficiency of Nanocrystalline ZnS: Mn^{2+}.1.Surface Passivation and Mn^{2+} Concentration *J. Phys. Chem. B* **2001**, *105*, 10197– 10202.
35) Zhang, W.; Zhou, X.; Zhong, X. One-Pot Noninjection Synthesis of Cu-Doped $Zn_xCd_{1-x}S$ Nanocrystals with Emission Color Tunable over Entire Visible Spectrum *Inorg. Chem.* **2012**, *51*, 3579– 3587.
36) Begum, R.; Chattopadhyay, A. Redox-Tuned Three-Color Emission in Double (Mn and Cu) Doped Zinc Sulfide Quantum Dots *J. Phys. Chem. Lett.* **2014**, *5*, 126– 130.
37) Nag, A.; Sapra, S.; Nagamani, C.; Sharma, A.; Pradhan, N.; Bhat, S. V.; Sarma, D. D. A Study of Mn^{2+} Doping in CdS Nanocrystals *Chem. Mater*. **2007**, *19*, 3252– 3259.

38) Hines, D. A.; Kamat, P. V. Recent Advances in Quantum Dot Surface Chemistry *ACS Appl. Mater. Interfaces* **2014**, *6*, 3041– 3057.
39) Owen, J. The Coordination Chemistry of Nanocrystal Surfaces. *Science* **2015**, *347*, 615-616.
40) Anderson, N. C.; Hendricks, M. P.; Choi, J. J.; Owen, J. S. Ligand Exchange and the Stoichiometry of Metal Chalcogenide Nanocrystals: Spectroscopic Observation of Facile Metal-Carboxylate Displacement and Binding *J. Am. Chem. Soc.* **2013**, *135*, 18536– 18548.
41) Bae, W. K.; Joo, J.; Padilha, L. a; Won, J.; Lee, D. C.; Lin, Q.; Koh, W.; Luo, H.; Klimov, V. I.; Pietryga, J. M. Highly Effective Surface Passivation of PbSe Quantum Dots through Reaction with Molecular Chlorine *J. Am. Chem. Soc.* **2012**, *134*, 20160–20168.
42) Wheeler, L. M.; Levij, L. M.; Kortshagen, U. R. Tunable Band Gap Emission and Surface Passivation of Germanium Nanocrystals Synthesized in the Gas Phase. *J. Phys. Chem. Lett.* **2013**, *4*, 3392.
43) Teunis, M. B.; Dolai, S.; Sardar, R. Effects of Surface-Passivating Ligands and Ultrasmall CdSe Nanocrystal Size on the Delocalization of Exciton Confinement. *Langmuir* **2014**, *30*, 7851– 7858.
44) Zherebetskyy, D.; Scheele, M.; Zhang, Y. J.; Bronstein, N.; Thompson, C.; Britt, D.; Salmeron, M.; Alivisatos, P.; Wang, L. W. Hydroxylation of the Surface of PbS Nanocrystals Passivated with Oleic Acid *Science* **2014**, *344*, 1380-1384.
45) Jin, T.; Fuji, F.; Yamada, E.; Nodasaka, Y.; Kinjo, M. Control of the optical properties of quantum dots by surface coating with calix[n]arene carboxylic acids *J. Am. Chem. Soc.***2006**, *128*, 9288– 9289.
46) Baker, D. R.; Kamat, P. V. Tuning the Emission of CdSe Quantum Dots by Controlled Trap Enhancement *Langmuir* **2010**, *26*, 11272– 11276.
47) Wang, G.; Ji, J.; Zhang, X.; Zhang, Y.; Wang, Q.; You, X.; Xu, X. Colloidal Nanocrystals Fluoresced by Surface Coordination Complexes *Sci. Rep.* **2014**, 4, 5084-5092.
48) Tang, J.; Kemp, K.; Hoogland, S.; Jeong, K. S.; Liu, H.; Levina, L.; Furukawa, M.; Wang, X.; Debnath, R.; Cha, D.; Chou, K. W.; Fischer, A.; Amassian, A.; Asbury, J. B.; Sargent, E. H. Colloidal-Quantum-Dot Photovoltaics using Atomic-Ligand Passivation *Nature Materials* **2011**, *10*, 765-771.
49) Kim, S.; Bawendi, M. G. Oligomeric Ligands for Luminescent and Stable Nanocrystal Quantum Dots *J. Am. Chem. Soc.* **2003**, 125, 14652– 14653.
50) Karakoti, A. S.; Shukla, R.; Shanker, R.; Singh, S.Surface functionalization of quantum dots for biological applications *Adv. Colloid Interface Sci.* **2015**, 215, 28– 45.
51) Palui, G.; Avellini, T.; Zhan, N.; Pan, F.; Gray, D.; Alabugin, I.; Mattoussi, H. Photoinduced Phase Transfer of Luminescent Quantum Dots to Polar and Aqueous Media *J. Am. Chem. Soc.* **2012**, *134*, 16370– 16378.
52) Zhan, N.; Palui, G.; Grise, H.; Tang, H.; Alabugin, I.; Mattoussi, H.Combining Ligand Design with Photoligation to Provide Compact, Colloidally Stable, and Easy to Conjugate Quantum Dots *ACS Appl. Mater. Interfaces* **2013**, *5*, 2861– 2869.
53) Zhan, N.; Palui, G.; Safi, M.; Mattoussi, H. Multidentate Zwitterionic Ligands Provide Compact and highly biocompatible Quantum Dots *J. Am. Chem. Soc*. **2013**, *135*, 13786-13795.

54) Zhan, N.; Palui, G.; Grise, H.; Tang, H.; Alabugin, I.; Mattoussi, H. Combining Ligand Design with Photo-ligation to Provide Compact, Colloidally Stable and Easy to Conjugate Quantum Dots *ACS Appl. Mater. Interfaces* **2013,** *5*, 2861-2869.

55) Dennis, A. M.; Sotto, D.; Mei, B. C.; Medintz, I. L.; Mattoussi, H.; Bao, G. Surface Ligand Effects on Metal-affinity Coordination to Quantum Dots: Implications for Nanoprobe Self-Assembly *Bioconjugate Chem*. **2010**, *21*, 1160-1170.

56) Fanizza, E.; Urso, C.; Pinto, V.; Cardone, A.; Ragni, R.; Depalo, N.; Curri, M. L.; Agostiano,A.; Farinola, G. M.; Striccoli, M.Single White Light Emitting Hybrid Nanoarchitectures Based on Functionalized Quantum Dots *J. Mater. Chem. C* **2014**, *2*, 5286–5291.

57) Depalo, N.; Comparelli, R.; Huskens, J.; Ludden, M. J. W.; Perl, A.; Agostiano, A.; Striccoli,M.; Curri, M. L. Phase Transfer of CdS Nanocrystals Mediated by Heptamine β-Cyclodextrin *Langmuir* **2012**, *28*, 8711– 8720.

58) Zezza, F.; Comparelli, R.; Striccoli, M.; Curri, M. L.; Tommasi, R.; Agostiano, A.; Della Monica, M. High quality CdS nanocrystals: Surface Effects *Synth. Met.* **2003**, *139*, 597–600.

59) Depalo, N.; Comparelli, R.; Curri, M. L.; Striccoli, M.; Agostiano, A. Cyclodextrin Mediated Phase Transfer in Water of Organic Capped CdS Nanocrystals *Synth. Met.* **2005**, *148*, 43–46.

60) Fini, P.; Depalo, N.; Comparelli, R.; Curri, M. L.; Striccoli, M.; Castagnolo, M.; Agostiano,A. Interactions Between Surfactant Capped CdS Nanocrystals And Organic Solvent *J. Therm. Anal. Calorim.* **2008**, *92*, 271– 277.

61) Jara, D. H.;Yoon, S.; Stamplecoskie, K. G.; Kamat, P. V. Size-Dependent Photovoltaic Performance of CuInS2 Quantum Dots Sensitized Solar Cells *Chem. Mater*. **2014**, *26*, 7221–7228.

62) P.V. Kamat, Photochemistry on Nonreactive and Reactive (Semiconductor) Surfaces. *Chem. Rev.* **1993**, *93*, 267-300.

63) Hines, D. A.; Kamat, P. V. Quantum Dot Surface Chemistry: Ligand Effects and Electron Transfer Reactions. *J. Phys. Chem. C* **2013**, *117*, 14418–14426.

64) Hines, D. A.; Becker, M. A.; Kamat, P. V. Photoinduced Surface Oxidation and Its Effect on the Exciton Dynamics of CdSe Quantum Dots *J. Phys. Chem. C* **2012,** *116*,13452–13457.

65) Krause, M. M.; Mooney, J.; Kambhampati, P. Chemical and Thermodynamic Control of the Surface of Semiconductor Nanocrystals for Designer White Light Emitters *ACS Nano* **2013**, *7*, 5922-5929.

66) Nag, A.; Kovalenko, M. V.; Lee, J.-S.; Liu, W.; Spokoyny, B.; Talapin, D. V. Metal-Free Inorganic Ligands for Colloidal Nanocrystals: S^{2-}, HS^{-}, Se^{2-}, HSe^{-}, Te^{2-}, HTe^{-}, TeS_3^{2-}, OH^{-} and NH_2^{-} as Surface Ligands *J. Am. Chem. Soc.* **2011**, *133*, 10612– 10620.

67) Zhang, H.; Jang, J.; Liu, W.; Talapin, D. V. Colloidal Nanocrystals with Inorganic Halide, Pseudohalide, and Halometallate Ligands *ACS Nano* **2014**, *8*, 7359– 7369.

68) Uyeda, H. T.; Medintz, I. L.; Jaiswal, J. K.; Simon, S. M.; Mattoussi, H. Synthesis of Compact Multidentate Ligands to Prepare Stable Hydrophilic Quantum Dot Fluorophores *J. Am. Chem. Soc.* **2005**, *127*, 3870– 3878.

69) Begum, R.; Chattopadhyay, A. In Situ Reversible Tuning of Photoluminescence of Mn^{2+}Doped ZnS Quantum Dots by Redox Chemistry *Langmuir* **2011**, *27*, 6433– 6439.

70) Tang, J.; Kemp, K. W.; Hoogland, S.; Jeong, K. S.; Liu, H.; Levina, L.; Furukawa, M.; Wang, X.; Debnath, R.; Cha, D.; Chou, K. W.; Fischer, A.;

Amassian, A.; Asbury, J. B.; Sargent, E. H. Colloidal-Quantum-Dot Photovoltaics using Atomic-Ligand Passivation *Nat. Mater.* **2011**, 10, 765– 771.

71) Resch-Genger, U.; Grabolle, M.; Cavaliere-Jaricot, S.; Nitschke, R.; Nann, T. Quantum Dots versus Organic Dyes as Fluorescent Labels *Nature Methods* **2008**, *5*, 763 – 775.
72) Klostranec, J. M.; Chan, W. C. W. Quantum Dots in Biological and Biomedical Research: Recent Progress and Present Challenges *Adv. Mater.* **2006**, 18, 1953– 1964
73) Alivisatos, P. The Use of Nanocrystals in Biological Detection. *Nature Biotechnology* **2004**, *22*, 47-52.
74) Alivisatos, A. P.; Gu, W. W.; Larabell, C., Quantum dots as cellular probes. *Annual Review of Biomedical Engineering* **2005**, *7*, 55-76.
75) Michalet, X.; Pinaud, F.; Lacoste, T. D.; Dahan, M.; Bruchez, M. P.; Alivisatos, A. P.; Weiss, S., Properties of Fluorescent Semiconductor Nanocrystals and Their Application to Biological Labeling. *Single Molecules* **2001**, *2*, 261-276.
76) Michalet, X.; Pinaud, F. F.; Bentolila, L. A.; Tsay, J. M.; Doose, S.; Li, J. J.; Sundaresan, G.; Wu, A. M.; Gambhir, S. S.; Weiss, S. Quantum Dots for Live Cells, in Vivo Imaging, and Diagnostics. *Science* **2005**, *307*, 538-544.
77) Mattoussi, H.; Palui, G.; Na, H. B. Luminescent Quantum Dots as Platforms for Probing *In Vitro* and *In Vivo* Biological Processes *Adv. Drug Delivery Rev.* **2012**, *64*, 138–166.
78) Gao, X.; Cui, Y.; Levenson, R. M.; Chung, L.W.; Nie, S. *In Vivo* Cancer Targeting and Imaging with Semiconductor Quantum Dots. *Nat Biotechnol.* **2004**, *22*, 969-976.
79) Mandal, A.; Dandapat, A.; De, G. Magic Sized ZnS Quantum Dots as a Highly Sensitive and Selective Fluorescence Sensor Probe for Ag^{+} Ions. *Analyst* **2012**, *137*, 765-772.
80) Kamat, P. V. Quantum Dot Solar Cells. Semiconductor Nanocrystals as Light Harvestors *J. Phys. Chem. C* **2008**, *112*, 18737-18753.
81) Kamat, P. V.; Christians, J. A.; Radich, J. G. Quantum Dot Solar Cells. Hole Transfer as a Limiting Factor in Boosting Photoconversion Efficiency. *Langmuir* **2014**, *30*, 5716-5725.
82) Bang, J. H.; Kamat, P. V. Quantum Dot Sensitized Solar Cells. A Tale of Two Semiconductor Nanocrystals: CdSe and CdTe *ACS Nano* **2009**, *3*, 1467-1476.
83) Gimbert-Surinach, C.; Albero, J.; Stoll, T.; Fortage, J.; Collomb, M.-N.; Deronzier, A.; Palomares, E.; Llobet, A. Efficient and Limiting Reactions in Aqueous Light-Induced Hydrogen Evolution Systems Using Molecular Catalysts and Quantum Dots *J. Am. Chem. Soc.* **2014**, *136*, 7655– 7661.
84) Basu, M.; Garg, N.; Ganguli, A. K. A Type-II Semiconductor (ZnO/CuS heterostructure) for Visible Light Photocatalysis *J. Mater. Chem. A* **2014**, *2*, 7517-7525.
85) Dubois, F.; Mahler, B.; Dubertret, B.; Doris, E.; Mioskowski, C. A Versatile Strategy for Quantum Dot Ligand Exchange *J. Am. Chem. Soc.* **2007**, *129*, 482– 483.
86) Palui, G.; Avellini, T.; Zhan, N.; Feng, P.; Gray, D.L.; Alabugin, I.; Mattoussi, H. Photo-induced Ligand Exchange and Phase Transfer of Luminescent Quantum Dots to Aqueous Media *J. Am. Chem. Soc.* **2012,** *134*, 16370–16378.

87) Aldeek, F.; Hawkins, D.; Safi, M.; Palomo, V.; Palui, G.; Dawson, P. E.; Alabugin, I.; Mattoussi, H. UV and Sunlight Driven Photochemical Reduction of Lipoic Acid-Based Ligands to Promote Cap Exchange on Luminescent Quantum Dots *J. Am. Chem. Soc.* **2015**, *137*, 2704-2714.
88) Comparelli, R.; Zezza, F.; Striccoli, M.; Curri, M. L.; Tommasi, R.; Agostiano, A. Improved Optical Properties of CdS Quantum Dots by Ligand Exchange *Mater. Sci. Eng., C* **2003**, *23*, 1083– 1086.
89) Brown, P. R.; Kim, D.; Lunt, R. R.; Zhao, N.; Bawendi, M. G.; Grossman, J. C.; Bulović, V. Energy Level Modification in Lead Sulfide Quantum Dot Thin Films through Ligand Exchange *ACS Nano* **2014**, *8*, 5863– 5872.
90) Dai, M.-Q.; Yung, L.-Y. L. Ethylenediamine-Assisted Ligand Exchange and Phase Transfer of Oleophilic Quantum Dots: Stripping of Original Ligands and Preservation of Photoluminescence *Chem. Mater.* **2013**, *25*, 2193– 2201.
91) Liu, D.; Snee, P. T. Water-Soluble Semiconductor Nanocrystals Cap Exchanged with Metalated Ligands *ACS Nano* **2011**, *5*, 546– 550.
92) Owen, J. S.; Park, J.; Trudeau, P. E.; Alivisatos, A. P. Reaction Chemistry and Ligand Exchange at Cadmium-Selenide Nanocrystal Surfaces *J. Am. Chem. Soc.* **2008**, *130*, 12279– 12281.
93) Dong, A. G.; Ye, X. C.; Chen, J.; Kang, Y. J.; Gordon, T.; Kikkawa, J. M.; Murray, C. B. A Generalized Ligand-Exchange Strategy Enabling Sequential Surface Functionalization of Colloidal Nanocrystals *J. Am. Chem. Soc.* **2011**, *133*, 998– 1006.
94) Lingley, Z.; Lu, S.; Madhukar, A. A High Quantum Efficiency Preserving Approach to Ligand Exchange on Lead Sulfide Quantum Dots and Interdot Resonant Energy Transfer *Nano Lett.* **2011**, *11*, 2887– 2891.
95) Lu, C.; Gao, J.; Fu, Y.; Du, Y.; Shi, Y.; Su, Z. A Ligand Exchange Route to Highly Luminescent Surface-Functionalized ZnS Nanoparticles and Their Transparent Polymer Nanocomposites *Adv. Funct. Mater.* **2008**, *18*, 3070– 3079.
96) Bohle, D. S.; C. Spina, J. Chelating the Surface of Zinc in Zinc Oxide Nanocrystals: Spectroscopic Characterization of ZnO Surface-Bound Eriochrome Black T and 8-Hydroxyquinoline *J. Phys. Chem. C* **2009**, *113*, 14435– 14439.
97) Feng, L.; Wang, C.; Ma, Z.; Lu, C. 8-Hydroxyquinoline Functionalized ZnS Nanoparticles Capped with Amine Groups: A Fluorescent Nano Sensor for the Facile and Sensitive Detection of TNT Through Fluorescence Resonance Energy Transfer *Dyes Pigm.* **2013**, *97*, 84– 91.
98) Liu, B.; Lu, X.; Tong, C.; Wang, C.; Feng, L.; He, Y.; Lu, C. 8-Hydroxyquinoline and Its Derivatives Functionalized $Cd_{1-x}Zn_xSe_{1-y}S_y$ Alloyed NCs: Optical and Photophysical Properties *RSC Adv.* **2013**, *3*, 21298– 21301.
99) Lu, X.; Yang, J.; Fu, Y.; Liu, Q.; Qi, B.; Lu, C.; Su, Z. White Light Emission from Mn^{2+}Doped ZnS Nanocrystals Through The Surface Chelating of 8-Hydroxyquinoline-5-sulfonic acid *Nanotechnology.* **2010**, *21*, 115702– 115712.
100) Ma, W.; Qin, L.; Liu, F.; Gu, Z.; Wang, J.; Pan, Z. G.; James, T. D.; Long, Y. Ubiquinone-Quantum Dot Bioconjugates for In Vitro and Intracellular Complex I Sensing *Sci. Rep.***2013**, *3*, 1537– 1544.
101) Medintz, I. L.; Uyeda, H. T.; Goldman, E. R.; Mattoussi, H. Quantum Dot Bioconjugates for Imaging, Labelling and Sensing, *Nat. Mater.* **2005**, *4*, 435-446.
102) Zrazhevskiy, P.; Sena, M.; Gao, X. H. Designing Multifunctional Quantum Dots for Bioimaging, Detection, and Drug Delivery *Chem. Soc. Rev.* **2010**, *39*, 4326–4354.

103) Delehanty, J. B.; Medintz, I. L.; Pons, T.; Brunel, F. M.; Dawson, P. E.; Mattoussi, H. Self-Assembled Quantum Dot-Peptide Bioconjugates for Selective Intracellular Delivery *Bioconjugate Chem.* **2006**, *17*, 920– 927.
104) Medintz, I. L.; Stewart, M. H.; Trammell, S. A.; Susumu, K.; Delehanty, J. B.; Mei, B. C.; Melinger, J. S.; Blanco-Canosa, J. B.; Dawson, P. E.; Mattoussi, H. Quantum-Dot/Dopamine Bioconjugates Function as Redox Coupled Assemblies for *in Vitro* and Intracellular pH Sensing *Nat. Mater.* **2010**, *9*, 676– 684.
105) Erogbogbo, F.; Yong, K.-T.; Roy, I.; Hu, R.; Law, W.-C.; Zhao, W.; Ding, H.; Wu, F.; Kumar,R.; Swihart, M. T.; Prasad, P. N. *In Vivo* Targeted Cancer Imaging, Sentinel Lymph Node Mapping and Multi-Channel Imaging with Biocompatible Silicon Nanocrystals *ACS Nano* **2011**, *5*, 413– 423.
106) Susumu, K.; Uyeda, H. T.; Medintz, I. L.; Pons, T.; Delehanty, J. B.; Mattoussi,H. Enhancing the Stability and Biological Functionalities of Quantum Dots *via* Compact Multifunctional Ligands *J. Am. Chem. Soc.* **2007**, *129*, 13987– 13996.
107) Clapp, A. R.; Goldman, E. R.; Mattoussi, H. Capping of CdSe-ZnS Quantum Dots with DHLA and Subsequent Conjugation with Proteins *Nat. Protoc.* **2006**, *1*, 1258– 1266.
108) Depalo, N.; Carrieri, P.; Comparelli, R.; Striccoli, M.; Agostiano, A.; Bertinetti, L.; Innocenti,C.; Sangregorio, C.; Curri, M. L. Bio-functionalization of Anisotropic Nanocrystalline Semiconductor-Magnetic Heterostructures *Langmuir* **2011**, *27*, 6962– 6970.
109) Wang, W.; Kapur, A.; Ji, X.; Safi, M.; Palui, G.; Palomo, V.; Dawson, P. E.; Mattoussi, H. Photoligation of an Amphiphilic Polymer with Mixed Coordination Provides Compact and Reactive Quantum Dots," *J. Am. Chem. Soc.* **2015**, *137*, 5438-5451.
110) Palui, G.; Aldeek, F.; Wang, W.; Mattoussi, H. Strategies for Interfacing Inorganic Nanocrystals with Biological Systems based on Polymer-Coating *Chem. Soc. Rev.*, **2015**, *44*, 193-227.
111) Mukthavaram, R.; Wrasidlo, W.; Hall, D.; Kesari, S.; Makale, M. Assembly and Targeting of Liposomal Nanoparticles Encapsulating Quantum Dots *Bioconjugate Chem.* **2011**, *22*, 1638– 1644.
112) Wang, W.; Aldeek, F.; Ji, X.; Zeng, B.; Mattoussi, H. A Multifunctional Amphiphilic Polymer as a Platform for Surface-Functionalizing Metallic and Other Inorganic Nanostructures *Faraday Discussions* **2014**, *175*, 137-151.
113) Foda, M. F.; Huang, L.; Shao, F.; Han, H. Biocompatible and Highly Luminescent Near-Infrared $CuInS_2$/ZnS Quantum Dots Embedded Silica Beads for Cancer Cell Imaging *ACS Appl. Mater. Interfaces*, **2014**, *6*, 2011–2017.
114) Sohn, I. S.; Unithrattil, S.; Im, W. B. Stacked Quantum Dot Embedded Silica Film on a Phosphor Plate for Superior Performance of White Light-Emitting Diodes *ACS Appl. Mater. Interfaces* **2014**, *6*, 5744– 5748.
115) Gerion, D.; Pinaud, F.; Williams, S. C.; Parak, W. J.; Zanchet, D.; Weiss, S.; Alivisatos, A. P.Synthesis and Properties of Biocompatible Water-Soluble Silica-Coated CdSe/ZnS Semiconductor Quantum Dots *J. Phys. Chem. B* **2001**, *105*, 8861– 8871.
116) Rawalekar, S.; Kaniyankandy, S.; Verma, S.; Ghosh, H. N. Effect of Surface States on Charge-Transfer Dynamics in Type II CdTe/ZnTe Core–Shell Quantum Dots: A

Femtosecond Transient Absorption Study *J. Phys. Chem. C* **2011**, *115*, 12335–12342.

117) Vinayakan, R.; Shanmugapriya, T.; Nair, P. V.; Ramamurthy, P.; Thomas, K. G. An Approach for Optimizing the Shell Thickness of Core-Shell Quantum Dots Using Photoinduced Charge Transfer *J. Phys. Chem. C* **2007**, *111*, 10146– 10149.
118) Khanchandani, S.; Srivastava, P. K.; Kumar, S.; Ghosh, S.; Ganguli A. K. Band Gap Engineering of ZnO using Core/Shell Morphology with Environmentally Benign Ag_2S Sensitizer for Efficient Light Harvesting and Enhanced Visible-Light Photocatalysis *Inorg. Chem.*, **2014**, *53*, 8902–8912.
119) Khanchandani, S.; Kundu, S.; Patra, A.; Ganguli, A. K. Shell Thickness Dependent Photocatalytic Properties of ZnO/CdS Core–Shell Nanorods. *J. Phys. Chem. C* **2012**, *116*, 23653.
120) Thomas, A.; Nair, P. V.; George Thomas, K. InP Quantum Dots: An Environmentally Friendly Material with Resonance Energy Transfer Requisites *J. Phys. Chem. C* **2014**, *118*, 3838– 3845.
121) Chen, G.; Agren, H.; Ohulchanskyy, T. Y.; Prasad P. N. Light Upconverting Core–Shell Nanostructures: Nanophotonic Control for Emerging Applications *Chem. Soc. Rev.*, **2015**, *44*, 1680-1713.
122) Ramakrishna, G.; Jose, D. A.; Kumar, D. K.; Das, A.; Palit, D. K.; Ghosh, H. N. Strongly Coupled Ruthenium-Polypyridyl Complexes for Efficient Electron Injection in Dye-Sensitized Semiconductor Nanoparticles *J. Phys. Chem. B* **2005**, *109*, 15445– 15453.
123) Stewart, M. H.; Huston, A. L.; Scott, A. M.; Efros, A. L.; Melinger, J. S.; Gemmill, K. B.; Trammell, S. A.; Balnco-Canosa, J. B.; Dawson, P. E.; Medintz, I. L.Complex Förster Energy Transfer Interactions between Semiconductor Quantum Dots and a Redox-Active Osmium Assembly *ACS Nano* **2012**, *6*, 5330– 5347.
124) Sato, S.; Arai, T.; Morikawa, T.; Uemura, K.; Suzuki, T. M.; Tanaka, H.; Kajino, T. Selective CO_2 Conversion to Formate Conjugated with H_2O Oxidation Utilizing Semiconductor/Complex Hybrid Photocatalysts *J. Am. Chem. Soc.* **2011**, *133*, 15240–15243.
125) Debnath, T.; Maity, P.; Banerjee, T.; Das, A.; Ghosh, H. N. Ultrafast Electron Injection, Hole Transfer, and Charge Recombination Dynamics in CdSe QD Super-Sensitized Re(I)–Polypyridyl Complexes with Catechol and Resorcinol Moiety: Effect of Coupling *J. Phys. Chem. C*, **2015**, *119*, 3522–3529.
126) Cho, M.; Contreras, E. Q.; Lee, S. S.; Jones, C. J.; Jang, W.; Colvin, V. L. Characterization and Optimization of the Fluorescence of Nanoscale Iron Oxide/Quantum Dot Complexes. *J. Phys. Chem. C* **2014**, *118*, 14606-14616.
127) Selvan, S. T.; Patra, P. K.; Ang, C. Y.; Ying J. Y. Synthesis of Silica-Coated Semiconductor and Magnetic Quantum Dots and Their Use in the Imaging of Live Cells. *Angew. Chem. Int. Ed*. **2007**, *46*, 2448-2452.
128) Gu, H.; Zheng, R.; Zhang, X.; Xu, B. Facile One-Pot Synthesis of Bifunctional Heterodimers of Nanoparticles: A Conjugate of Quantum Dot and Magnetic Nanoparticles. *J. Am. Chem. Soc*. **2004**, *126*, 5664-5665.
129) Erogbogbo, F.; Yong, K.; Hu, R.; Law, W.; Ding, H.; Chang, C.; Prasad, P. N.; Swihart, M. T. Biocompatible Magnetofluorescent Probes: Luminescent Silicon Quantum Dots Coupled with Superparamagnetic Iron(III) Oxide. *ACS Nano* **2010**, *4*, 5131-5138.
130) Corato, R. D.; Bigall, N. C.; Ragusa, A.; Dorfs, D.; Genovese, A.; Marotta, R.; Manna, L.; Pellegrino T. Multifunctional Nanobeads Based on Quantum Dots and

Magnetic Nanoparticles: Synthesis and Cancer Cell Targeting and Sorting. *ACS Nano* **2011**, *5*, 1109-1121.

131) Fan, Y.; Liu, H.; Han, R.; Huang, L.; Shi, H.; Sha, Y.; Jiang, Y. Extremely High Brightness from Polymer-Encapsulated Quantum Dots for Two-photon Cellular and Deep-tissue Imaging *Sci. Rep*. **2014**, *5*, 9908.
132) Coropceanu, I.; Bawendi, M. G.Core/Shell Quantum Dot Based Luminescent Solar Concentrators with Reduced Reabsorption and Enhanced Efficiency *Nano Lett.* **2014**, *14*, 4097– 4101.
133) Huang, J.; Mulfort, K. L.; Du, P.; Chen, L. Photodriven Charge Separation Dynamics in CdSe/ZnS Core/Shell Quantum Dot/Cobaloxime Hybrid for Efficient Hydrogen Production *J. Am. Chem. Soc.* **2012**, *134*, 16472– 16475
134) http://chemistry.about.com/od/chemicalreactions/ss/10-Examples-of-Chemical-Reactions-in-Everyday-Life.htm.
135) Pittala, S.; Kittilstved, K. R. Cation Exchange in Small ZnS and CdS Molecular Analogues *Inorg. Chem.*, **2015**, *54*, 5757–5767.
136) Beberwyck, B. J.; Surendranath, Y.; Alivisatos, A. P. Cation Exchange: A Versatile Tool for Nanomaterials Synthesis. *J. Phys. Chem. C* **2013**, 117, 19759–19770.
137) Son, D. H.; Hughes, S. M.; Yin, Y.; Alivisatos, A. P. Cation Exchange Reactions in Ionic Nanocrystals *Science* **2004**, *306*, 1009– 1012.
138) Luther, J. M.; Zheng, H.; Sadtler, B.; Alivisatos, A. P. Synthesis of PbS Nanorods and Other Ionic Nanocrystals of Complex Morphology by Sequential Cation Exchange Reactions *J. Am. Chem. Soc.* **2009**, *131*, 16851– 16857.
139) Jain, P. K.; Amirav, L.; Aloni, S.; Alivisatos, A. P. Nanoheterostructure Cation Exchange: Anionic Framework Conservation *J. Am. Chem. Soc.* **2010**, *132*, 9997–9999.
140) Robinson, R. D.; Sadtler, B.; Demchenko, D. O.; Erdonmez, C. K.; Wang, L.-W.; Alivisatos,A. P. Spontaneous Superlattice Formation in Nanorods Through Partial Caiton Exchange *Science* **2007**, *317*, 355– 358.
141) Beberwyck, B. J.; Alivisatos, A. P. Ion Exchange Synthesis of III-V Nanocrystals *J. Am. Chem. Soc.* **2012**, *134*, 19977– 19980.
142) Miszta, K.; Dorfs, D.; Genovese, A.; Kim, M. R.; Manna, L. Cation Exchange Reactions in Colloidal Branched Nanocrystals *ACS Nano* 2011, 5, 7176
143) Justo, Y.; Sagar, L. K.; Flamee, S.; Zhao, Q.; Vantomme, A.; Hens, Z. Less Is More. Cation Exchange and the Chemistry of the Nanocrystal Surface *ACS Nano* **2014**, *8*, 7948– 7957.
144) Li, H. B.; Zanella, M.; Genovese, A.; Povia, M.; Falqui, A.; Giannini, C.; Manna, L. Sequential Cation Exchange in Nanocrystals: Preservation of Crystal Phase and Formation of Metastable Phases *Nano Lett.* **2011**, *11*, 4964– 4970.
145) Jaiswal, A.; Ghosh, S. S.; Chattopadhyay, A. Quantum Dot Impregnated-Chitosan Film for Heavy Metal Ion Sensing and Removal *Langmuir* **2012**, *28*, 15687- 15695.
146) Begum, R.; Bhandari, S.; Chattopadhyay, A. Surface Ion Engineering of Mn^{2+}-Doped ZnS Quantum Dots Using Ion-Exchange Resins *Langmuir* **2012**, *28*, 9722–9728.
147) https://en.wikipedia.org/wiki/Alfred_Werner
148) Kovalenko, M. V.; Bodnarchuk, M. I.; Zaumseil, J.; Lee, J. S.; Talapin, D. V. Expanding the Chemical Versatility of Colloidal Nanocrystals Capped with

Molecular Metal Chalcogenide Ligands *J. Am. Chem. Soc.* **2010**, *132*, 10085– 10092.

149) Liu, W.; Lee, J.-S.; Talapin, D. V. III-V Nanocrystals Capped with Molecular Metal Chalcogenide Ligands: High Electron Mobility and Ambipolar Photoresponse *J. Am. Chem. Soc.* **2013**, *135*, 1349– 1357.

150) Kovalenko, M. V.; Scheele, M.; Talapin, D. V. Colloidal Nanocrystals with Molecular Metal Chalcogenide Surface Ligands *Science* **2009**, *324*, 1417– 1420.

151) Kovalenko, M. V.; Schaller, R. D.; Jarzab, D.; Loi, M. A.; Talapin, D. V.Inorganically Functionalized PbS–CdS Colloidal Nanocrystals: Integration into Amorphous Chalcogenide Glass and Luminescent Properties *J. Am. Chem. Soc.* **2012**, 134, 2457– 2460.

152) Pan, H.; Liang, F.; Mao, C.; Zhu, J.; Chen, H. Highly Luminescent Zinc(II)-Bis(8-hydroxyquinoline) Complex Nanorods: Sonochemical Synthesis, Characterizations, and Protein Sensing *J. Phys. Chem. B* **2007**, *111*, 5767– 5772.

153) Sapochak, L. S.; Benincasa, F. E.; Schofield, R. S.; Baker, J. L.; Riccio, K. K. C.; Fogarty,D.; Kohlmann, H.; Ferris, K. F.; Burrows, P. E. Electroluminescent Zinc(II) Bis (8-hydroxyquinoline):Structural Effects on Electronic States and Device Performance *J. Am. Chem. Soc.* **2002**, *124*, 6119– 6125.

154) Pohl, R.; Anzenbacher, P., Jr Emission Color Tuning in AlQ_3 Complexes with Extended Conjugated Chromophores *Org. Lett.* **2003**, *5*, 2769– 2772.

155) Pohl, R.; Montes, V. A.; Shinar, J.; Anzenbacher, P., Jr Red–Green–Blue Emission from Tris(5-aryl-8-quinolinolate)Al(III) Complexes *J. Org. Chem.* **2004**, *69*, 1723– 1725.

156) Soroka, K.; Vithanage, R. S.; Phillips, D. A.; Walker, B.; Dasgupta, P. K. Fluorescence Properties of Metal Complexes of 8-Hydroxyquinoline-5-sulfonic acid and Chromatographic Applications *Anal. Chem.*, **1987**, *59*, 629–636.

157) Prachayasittikul, V. Prachayasittikul, S. Ruchirawat, S.; Prachayasittikul V. 8-Hydroxyquinolines: A Review of Their Metal Chelating Properties and Medicinal Applications *Drug Des Devel Ther*. **2013**, *7*, 1157–1178.

158) Hamada, Y.; Sano, T.; Fujita, N.; Fujii, T.; Nishio, Y.; Shibata, K.; *Jpn. J. Appl. Phys*., **1993**, *32*, 514-515.

159) Hopkins, T. A.; Meerholz, K.; Shaheen, S.; Anderson, M. L.; Schmidt, A.; Kippelen, B.; Padias, A. B.; Hall, H. K.; Peyghambarian, Jr. N.; Armstrong, N. R. Substituted Aluminum and Zinc Quinolates with Blue-Shifted Absorbance/Luminescence Bands: Synthesis and Spectroscopic, Photoluminescence, and Electroluminescence Characterization *Chem. Mater.*, **1996**, *8*, 344–351.

160) Ouyang, J.; Ratcliffe, C. I.; Kingston, D.; Wilkinson, B.; Kuijper, J.; Wu, X.; Ripmeester, J. A.; Yu, K. Gradiently Alloyed $Zn_xCd_{1-x}S$ Colloidal Photoluminescent Quantum Dots Synthesized via a Noninjection One-Pot Approach *J. Phys. Chem. C* **2008**, *112*, 4908– 4919.

161) Zanella, M.; Abbasi, A. Z.; Schaper, A. K.; Parak, W. J.Discontinuous Growth of II–VI Semiconductor Nanocrystals from Different Materials *J. Phys. Chem. C* **2010**, *114*, 6205–6215.

162) Weast, R. C.; Astle, M. J.; Beyer, W. H. *Hand book of Chemistry and Physics*, 64th ed, CRC Press, Inc., Boca Ratan, Fl, 1983, 50-51.

163) Resch, U.; Eychmueller, A.; Haase, M.; Weller, H. Absorption and Fluorescence Behavior of Redispersible Cadmium Sulfide Colloids in Various Organic Solvents *Langmuir* **1992**, *8*, 2215– 2218.

164) Dey, K. K.; Panda, B. R.; Paul, A.; Basu, S.; Chattopadhyay, A. Catalytic Gold Nanoparticle Driven pH Specific Chemical Locomotion. *J. Colloid Interface Sci.***2010**, *348*, 335-341.
165) Melhuish, W. H. Quantum Efficiencies of Fluorescence of Organic Substances: Effect of Solvent and Concentration of the Fluorescent Solute *J. Phys. Chem.* **1961**, *65*, 229–235.
166) Kim, M. R.; Park, S.-Y.; Jang, D.-J. Composition Variation and Thermal Treatment of $Zn_xCd_{1-x}S$ Alloy Nanoparticles to Exhibit Controlled and Efficient Luminescence *J. Phys. Chem. C* **2010**, *114*, 6452– 6457.
167) Wang, C.W.; Moffit, M. G. Surface-Tunable Photoluminescence from Block Copolymer-Stabilized Cadmium Sulfide Quantum Dots *Langmuir*, **2004**, *20*, 11784–11796.
168) Kumar, T. V. V.; Prabhakar, S.; Raju, G. B. Adsorption of Oleic Acid at Sillimanite/Water Interface *J. Colloid Interface Sci*., **2002**, *247*, 275–281.
169) I-Hsien, L.; Kuan, Y.; Chern. Equilibrium and Kinetics of Heavy Metal Ion Exchange *J.chin Inst. Chem. Eng.*, **2007**, *38*, 71–84.
170) Nanda, J.; Sapra, S.; Sarma, D. D.; Chandrasekharan, N.; Hodes, G. Size-Selected Zinc Sulfide Nanocrystallites: Synthesis, Structure, and Optical Studies**.** *Chem Mater*. **2000**, *12*, 1018- 1024.
171) Bing-she, X.; Yu-ying, H.; Hua, W.; He-feng, Z.; Xu-guang, L.; Ming-wei, C. *Solid State Commun.* **2005**, *136*, 318- 322.
172) Phillips, J. P.; Deye, J. F. Infrared Spectra of Oxine Chelates *Anal. Chim. Acta* **1957**, *17*, 231- 233.
173) Burda, C.; Link, S.; Mohamed, M.; El-Sayed, M.The Relaxation Pathways of CdSe Nanoparticles Monitored with Femtosecond Time-Resolution from the Visible to the IR: Assignment of the Transient Features by Carrier Quenching *J. Phys. Chem. B* **2001**, *105*,12286– 12292.
174) Bhandari, S.; Begum, R.; Chattopadhyay, A. Surface Ion Engineering for Tuning Dual Emission of $Zn_xCd_{1-x}S$ Nanocrystals *RSC Adv.* **2013**, *3*, 2885– 2888.
175) Bhandari, S.; Roy, S.; Chattopadhyay, A. Enhanced Photoluminescence and Thermal Stability of Zinc Quinolate Following Complexation on the Surface of Quantum Dot *RSC Adv.* **2014**, *4*, 24217– 24221.
176) Chen, W.; Peng, Q.; Li, Y. Luminescent Bis(8-hydroxyquinoline)cadmium Complex Nanorods *Cryst. Growth Des.* **2008**, *8*, 564– 567.
177) Khaorapapong, N.; Ogawa, M. Solid-State Intercalation of 8-Hydroxyquinoline into Li(I)-, Zn(II)- and Mn(II)-Montmorillonites *Appl. Clay Sci.* **2007**, *35*, 31– 38.
178) Soroka, K.; Vithanage, R. S.; Phillips, D. A.; Walker, B.; Dasgupta, P. K. Fluorescence Properties of Metal Complexes of 8-Hydroxyquinoline-5-sulfonic Acid and Chromatographic Applications *Anal. Chem.* **1967**, *59*, 629– 636.
179) Zeta Potential Analysis of Nanoparticles, http://www.nanocomposix.eu.
180) Bhandari, S.; Roy, S.; Pramanik, S.; Chattopadhyay, A. Surface Complexation Reaction for Phase Transfer of Hydrophobic Quantum Dot from Nonpolar to Polar Medium *Langmuir* **2014**, *30*, 10760– 10765.
181) Irving, H.; Williams, R. J. P. The Stability of Transition-Metal Complexes *J. Chem. Soc.***1953**, 3192– 3210.
182) Subha, R.; Nalla, V.; Yu, J. H.; Jun, S. W.; Shin, K.; Hyeon, T.; Vijayan, C.; Ji, W. Efficient Photoluminescence of Mn^{2+}-Doped ZnS Quantum Dots Excited by Two-

Photon Absorption in Near-Infrared Window II *J. Phys. Chem. C* **2013**, *117*, 20905– 20911.

183) Panda, S. K.; Hickey, S. G.; Demir, H. V.; Eychmuller, A. Bright White-Light Emitting Manganese and Copper Co-Doped ZnSe Quantum Dots *Angew. Chem., Int. Ed.* **2011**, *50*, 4432– 4436.

184) Rogach, A. L.; Gaponik, N.; Lupton, J. M.; Bertoni, C.; Gallardo, D. E.; Dunn, S.; Pira, N. L.; Paderi, M.; Repetto, P.; Romanov, S. G.; O'Dwyer, C.; Torres, C. M. S.; Eychmuller, A. Light-Emitting Diodes with Semiconductor Nanocrystals *Angew. Chem., Int. Ed.* **2008**, *47*, 6538– 6549.

185) Sharma, V. K.; Guzelturk, B.; Erdem, T.; Kelestemur, Y.; Demir, H. V.Tunable White-Light-Emitting Mn-Doped ZnSeNanocrystals *ACS Appl. Mater. Interfaces* **2014**, *6*, 3654–3660.

186) Xu, Z.; Hou, Y.; Sun, S.; Magnetic Core/Shell Fe_3O_4/Au and Fe_3O_4/Au/Ag Nanoparticles with Tunable Plasmonic Properties. *J. Am. Chem. Soc*. **2007**, *129*, 8698-8699.

187) Euliss, L. E.; Grancharov, S. G.; O'Brien, S.; Deming, T. J.; Stucky, G. D.; Murray, C. B.; Held, G. A. Cooperative Assembly of Magnetic Nanoparticles and Block Copolypeptides in Aqueous Media. *Nano Lett*. **2003**, *11*, 1489-1493.

188) Yu, X.; Wan, J.; Shan, Y.; Chen, K.; Han, X. A Facile Approach to Fabrication of Bifunctional Magnetic-Optical Fe_3O_4@ZnS Microspheres. *Chem. Mater*. **2009**, *21*, 4892-4898.

189) Wang, Z.; Wu, L.; Chen, M.; Zhou, S. Facile Synthesis of Superparamagnetic Fluorescent Fe_3O_4/ZnS Hollow Nanospheres. *J. Am. Chem. Soc*. **2009**, *131*, 11276-11277.

190) Beltran-Huarac, J.; Guinel, M. J-F.; Weiner, B. R.; Morell, G. Bifunctional Fe_3O_4/ZnS:Mn Composite Nanoparticles. *Mater. Lett.* **2013**, *98*, 108-111.

191) Rusakova, I.; Ould-Ely, T.; Hofmann, C.; Prieto-Centurion, D.; Levin, C. S.; Halas, N. J.; Luttge, A.; Whitmire, K. H. Nanoparticle Shape Conservation in the Conversion of MnO Nanocrosses into Mn_3O_4. *Chem. Mater*. **2007**, *19*, 1369-1375.

192) Han, S.; Li, C.; Liu, Z.; Lei, B.; Zhang, D.; Jin, W.; Liu, X.; Tang, T.; Zhou, C. Transition Metal Oxide Core-Shell Nanowires: Generic Synthesis and Transport Studies. *Nano Lett*. **2004**, *4*, 1241-1246.

193) Bhandari, S.; Roy, S.; Pramanik, S.; Chattopadhyay, A. Double Channel Emission from a Redox Active Single Component Quantum Dot Complex. *Langmuir* **2015**, *31*, 551-561.

194) Pramanik, S.; Bhandari, S.; Roy, S.; Chattopadhyay, A. Synchronous Tricolor Emission-Based White Light from Quantum Dot Complex. *J. Phys. Chem. Lett.*, **2015**, *6*, 1270-1274.

195) Mandal, G.; Darragh, M.; Wang, Y. A.; Heyes, C. D. Cadmium-free Quantum Dots as Time-gated Bioimaging Probes in Highly-autofluorescent Human Breast Cancer Cells. *Chem. Commun.*, **2013**, *49*, 624-626.

196) Fernandez-Moreira, V.; Thorp-Greenwood, F. L.; Coogan, M. P. Application of d^6 Transition Metal Complexes in Fluorescence Cell Imaging. *Chem. Commun*. **2010**, *46*, 186-202.

197) Gao, J.; Zhang, W.; Huang, P.; Zhang, B.; Zhang, X.; Xu, B. Intracellular Spatial Control of Fluorescent Magnetic Nanoparticles. *J. Am. Chem. Soc*. **2008**, *130*, 3710-3711.

List of Publications

In Peer Reviewed Journals:

1) **Bhandari, S.**; Pramanik, S.; Khandelia, R.; Chattopadhyay, A. Biofriendly White Light Emission from a Single Component Au Nanocluster-Quantum Dot Complex Nanocomposite **2015** (Submitted to *ACS Appl. Mater. Interfaces*).

2) **Bhandari, S.**; Khandelia, R.; Pan, U. N.; Chattopadhyay, A. Surface Complexation Based Biocompatible Magnetofluorescent Nanoprobe for Targeted Cellular Imaging *ACS Appl. Mater. Interfaces* **2015**, *7*, 17552–17557.

3) Roy, S.; **Bhandari, S.**; Chattopadhyay, A. Quantum Dot Surface mediated Unprecedented Reaction of Zn^{2+} and Copper Quinolate Complex *J. Phys. Chem. C* **2015**, *119*, 21191-21197.

4) Khandelia, R.; **Bhandari, S.**; Pan, U. N.; Ghosh, S. S.; Chattopadhyay, A. Gold Nanocluster Embedded Albumin Nanoparticles for Two-Photon Imaging of Cancer Cells Accompanying Drug Delivery *Small* **2015**, *11*, 4075-4081. (*This article has been appeared in Journal's* ***Frontispiece***).

5) Pramanik, S.; **Bhandari, S.**; Roy, S.; Chattopadhyay, A. Synchronous Tricolor Emission-Based White Light from Quantum Dot Complex *J. Phys. Chem. Lett.* **2015**, *6*, 1270–1274. (*This article has been featured in* ***C&E News*** *and* ***ACS Live Slides*** *presentation*).

6) **Bhandari, S.**; Roy, S.; Pramanik, S.; Chattopadhyay, A. Double Channel Emission from a Redox Active Single Component Quantum Dot Complex *Langmuir* **2015**, *31*, 551–561.

7) **Bhandari, S.**; Roy, S.; Pramanik, S.; Chattopadhyay, A. Surface Complexation Reaction for Phase Transfer of Hydrophobic Quantum Dot from Nonpolar to Polar Medium *Langmuir* **2014**, *30*, 10760–10765.

8) **Bhandari, S.**; Roy, S.; Chattopadhyay, A. Enhanced Photoluminescence and Thermal Stability of Zinc Quinolate Following Complexation on the Surface of Quantum Dot *RSC Adv.* **2014**, *4*, 24217- 24221.

9) **Bhandari, S.**; Begum, R.; Chattopadhyay, A. Surface Ion Engineering for Tuning Dual Emission of $Zn_xCd_{1-x}S$ Nanocrystals *RSC Adv*. **2013**, *3*, 2885-2888.

10) Dey, K. K.; **Bhandari, S.**; Bandyopadhyay, D.; Basu, S.; Chattopadhyay, A. The pH Taxis of an Intelligent Catalytic Microbot *Small* **2013**, *9*, 1916-1920.

11) Begum, R.; **Bhandari, S.**; Chattopadhyay, A. Surface Ion Engineering of Mn^{2+}-Doped ZnS Quantum Dots Using Ion-Exchange Resins *Langmuir* **2012**, *28*, 9722-9728.

In Conference Proceedings.

1) Presented an Oral Talk in **YSC-2015 (MRSI-Kolkata Chapter)** held at CGCRI, Kolkata, India.

2) Presented two posters in **Nano Sci-2014** held at Institute of Advanced Study in Science and Technology, Guwahati, India.

3) Presented a poster in DAE-BRNS 5th Interdisciplinary Symposium on Materials Chemistry, **ISMC-2014** held in Bhabha Atomic Research Centre, (BARC) Mumbai, India.

4) Presented a poster in International Conference on Nano Science and Technology, **ICONSAT-2014**, held at Institute of Nano Science and Technology (INST) in Mohali - 160062 (Punjab), India.

5) Presented a poster in DAE-BRNS 4th Interdisciplinary Symposium on Materials Chemistry, **ISMC-2012** held at Bhabha Atomic Research Centre, (BARC) Mumbai, India.

6) Presented a poster in Frontiers in Chemical Sciences, **FICS-2012** held at Indian Institute of Technology Guwahati, India.

7) Presented a poster in International Conference on Advanced Nanomaterials and Nanotechnology, **ICANN- 2011** held at Department of Physics and Centre for Nanotechnology, Indian Institute of Technology Guwahati, India.

Permissions

Title: (CdSe)ZnS Core–Shell Quantum Dots: Synthesis and Characterization of a Size Series of Highly Luminescent Nanocrystallites

Author: B. O. Dabbousi, J. Rodriguez-Viejo, F. V. Mikulec, et al

Publication: The Journal of Physical Chemistry B

Publisher: American Chemical Society

Date: Nov 1, 1997

PERMISSION/LICENSE IS GRANTED FOR YOUR ORDER AT NO CHARGE

This type of permission/license, instead of the standard Terms & Conditions, is sent to you because no fee is being charged for your order. Please note the following:

- Permission is granted for your request in both print and electronic formats, and translations.
- If figures and/or tables were requested, they may be adapted or used in part.
- Please print this page for your records and send a copy of it to your publisher/graduate school.
- Appropriate credit for the requested material should be given as follows: "Reprinted (adapted) with permission from (COMPLETE REFERENCE CITATION). Copyright (YEAR) American Chemical Society." Insert appropriate information in place of the capitalized words.
- One-time permission is granted only for the use specified in your request. No additional uses are granted (such as derivative works or other editions). For any other uses, please submit a new request.

If credit is given to another source for the material you requested, permission must be obtained from that source.

TH-1435_10612225

Title: Size-Tunable, Bright, and Stable PbS Quantum Dots: A Surface Chemistry Study

Author: Iwan Moreels, Yolanda Justo, Bram De Geyter, et al

Publication: ACS Nano

Publisher: American Chemical Society

Date: Mar 1, 2011

PERMISSION/LICENSE IS GRANTED FOR YOUR ORDER AT NO CHARGE

This type of permission/license, instead of the standard Terms & Conditions, is sent to you because no fee is being charged for your order. Please note the following:

- Permission is granted for your request in both print and electronic formats, and translations.
- If figures and/or tables were requested, they may be adapted or used in part.
- Please print this page for your records and send a copy of it to your publisher/graduate school.
- Appropriate credit for the requested material should be given as follows: "Reprinted (adapted) with permission from (COMPLETE REFERENCE CITATION). Copyright (YEAR) American Chemical Society." Insert appropriate information in place of the capitalized words.
- One-time permission is granted only for the use specified in your request. No additional uses are granted (such as derivative works or other editions). For any other uses, please submit a new request.

If credit is given to another source for the material you requested, permission must be obtained from that source.

Title:	Doping Transition Metal (Mn or Cu) Ions in Semiconductor Nanocrystals
Author:	Niladri S. Karan, D. D. Sarma, R. M. Kadam, et al
Publication:	Journal of Physical Chemistry Letters
Publisher:	American Chemical Society
Date:	Oct 1, 2010

PERMISSION/LICENSE IS GRANTED FOR YOUR ORDER AT NO CHARGE

This type of permission/license, instead of the standard Terms & Conditions, is sent to you because no fee is being charged for your order. Please note the following:

- Permission is granted for your request in both print and electronic formats, and translations.
- If figures and/or tables were requested, they may be adapted or used in part.
- Please print this page for your records and send a copy of it to your publisher/graduate school.
- Appropriate credit for the requested material should be given as follows: "Reprinted (adapted) with permission from (COMPLETE REFERENCE CITATION). Copyright (YEAR) American Chemical Society." Insert appropriate information in place of the capitalized words.
- One-time permission is granted only for the use specified in your request. No additional uses are granted (such as derivative works or other editions). For any other uses, please submit a new request.

If credit is given to another source for the material you requested, permission must be obtained from that source.

BACK | CLOSE WINDOW

Title:	Doping Cu in Semiconductor Nanocrystals: Some Old and Some New Physical Insights
Author:	Bhupendra B. Srivastava, Santanu Jana, Narayan Pradhan
Publication:	Journal of the American Chemical Society
Publisher:	American Chemical Society
Date:	Feb 1, 2011

PERMISSION/LICENSE IS GRANTED FOR YOUR ORDER AT NO CHARGE

This type of permission/license, instead of the standard Terms & Conditions, is sent to you because no fee is being charged for your order. Please note the following:

- Permission is granted for your request in both print and electronic formats, and translations.
- If figures and/or tables were requested, they may be adapted or used in part.
- Please print this page for your records and send a copy of it to your publisher/graduate school.
- Appropriate credit for the requested material should be given as follows: "Reprinted (adapted) with permission from (COMPLETE REFERENCE CITATION). Copyright (YEAR) American Chemical Society." Insert appropriate information in place of the capitalized words.
- One-time permission is granted only for the use specified in your request. No additional uses are granted (such as derivative works or other editions). For any other uses, please submit a new request.

If credit is given to another source for the material you requested, permission must be obtained from that source.

BACK | CLOSE WINDOW

Title: Control of the Optical Properties of Quantum Dots by Surface Coating with Calix[n]arene Carboxylic Acids

Author: Takashi Jin, Fumihiko Fujii, Eiji Yamada, et al

Publication: Journal of the American Chemical Society

Publisher: American Chemical Society

Date: Jul 1, 2006

PERMISSION/LICENSE IS GRANTED FOR YOUR ORDER AT NO CHARGE

This type of permission/license, instead of the standard Terms & Conditions, is sent to you because no fee is being charged for your order. Please note the following:

- Permission is granted for your request in both print and electronic formats, and translations.
- If figures and/or tables were requested, they may be adapted or used in part.
- Please print this page for your records and send a copy of it to your publisher/graduate school.
- Appropriate credit for the requested material should be given as follows: "Reprinted (adapted) with permission from (COMPLETE REFERENCE CITATION). Copyright (YEAR) American Chemical Society." Insert appropriate information in place of the capitalized words.
- One-time permission is granted only for the use specified in your request. No additional uses are granted (such as derivative works or other editions). For any other uses, please submit a new request.

If credit is given to another source for the material you requested, permission must be obtained from that source.

BACK | CLOSE WINDOW

Title:	Tuning the Emission of CdSe Quantum Dots by Controlled Trap Enhancement
Author:	David R. Baker, Prashant V. Kamat
Publication:	Langmuir
Publisher:	American Chemical Society
Date:	Jul 1, 2010

PERMISSION/LICENSE IS GRANTED FOR YOUR ORDER AT NO CHARGE

This type of permission/license, instead of the standard Terms & Conditions, is sent to you because no fee is being charged for your order. Please note the following:

- Permission is granted for your request in both print and electronic formats, and translations.
- If figures and/or tables were requested, they may be adapted or used in part.
- Please print this page for your records and send a copy of it to your publisher/graduate school.
- Appropriate credit for the requested material should be given as follows: "Reprinted (adapted) with permission from (COMPLETE REFERENCE CITATION). Copyright (YEAR) American Chemical Society." Insert appropriate information in place of the capitalized words.
- One-time permission is granted only for the use specified in your request. No additional uses are granted (such as derivative works or other editions). For any other uses, please submit a new request.

If credit is given to another source for the material you requested, permission must be obtained from that source.

Title: Energy Level Modification in Lead Sulfide Quantum Dot Thin Films through Ligand Exchange

Author: Patrick R. Brown, Donghun Kim, Richard R. Lunt, et al

Publication: ACS Nano

Publisher: American Chemical Society

Date: Jun 1, 2014

PERMISSION/LICENSE IS GRANTED FOR YOUR ORDER AT NO CHARGE

This type of permission/license, instead of the standard Terms & Conditions, is sent to you because no fee is being charged for your order. Please note the following:

- Permission is granted for your request in both print and electronic formats, and translations.
- If figures and/or tables were requested, they may be adapted or used in part.
- Please print this page for your records and send a copy of it to your publisher/graduate school.
- Appropriate credit for the requested material should be given as follows: "Reprinted (adapted) with permission from (COMPLETE REFERENCE CITATION). Copyright (YEAR) American Chemical Society." Insert appropriate information in place of the capitalized words.
- One-time permission is granted only for the use specified in your request. No additional uses are granted (such as derivative works or other editions). For any other uses, please submit a new request.

If credit is given to another source for the material you requested, permission must be obtained from that source.

Title: Ethylenediamine-Assisted Ligand Exchange and Phase Transfer of Oleophilic Quantum Dots: Stripping of Original Ligands and Preservation of Photoluminescence

Author: Meng-Qiao Dai, Lin-Yue Lanry Yung

Publication: Chemistry of Materials
Publisher: American Chemical Society
Date: Jun 1, 2013

PERMISSION/LICENSE IS GRANTED FOR YOUR ORDER AT NO CHARGE

This type of permission/license, instead of the standard Terms & Conditions, is sent to you because no fee is being charged for your order. Please note the following:

- Permission is granted for your request in both print and electronic formats, and translations.
- If figures and/or tables were requested, they may be adapted or used in part.
- Please print this page for your records and send a copy of it to your publisher/graduate school.
- Appropriate credit for the requested material should be given as follows: "Reprinted (adapted) with permission from (COMPLETE REFERENCE CITATION). Copyright (YEAR) American Chemical Society." Insert appropriate information in place of the capitalized words.
- One-time permission is granted only for the use specified in your request. No additional uses are granted (such as derivative works or other editions). For any other uses, please submit a new request.

If credit is given to another source for the material you requested, permission must be obtained from that source.

BACK | CLOSE WINDOW

Title:	Quantum-dot/dopamine bioconjugates function as redox coupled assemblies for in vitro and intracellular pH sensing
Author:	Igor L. Medintz, Michael H. Stewart, Scott A. Trammell, Kimihiro Susumu, James B. Delehanty, Bing C. Mei
Publication:	Nature Materials
Publisher:	Nature Publishing Group
Date:	Aug 1, 2010

Order Completed

Thank you very much for your order.

This is a License Agreement between Satyapriya Bhandari ("You") and Nature Publishing Group ("Nature Publishing Group"). The license consists of your order details, the terms and conditions provided by Nature Publishing Group, and the payment terms and conditions.

Get the printable license.

License Number	3645200958533
License date	Jun 10, 2015
Licensed content publisher	Nature Publishing Group
Licensed content publication	Nature Materials
Licensed content title	Quantum-dot/dopamine bioconjugates function as redox coupled assemblies for in vitro and intracellular pH sensing
Licensed content author	Igor L. Medintz, Michael H. Stewart, Scott A. Trammell, Kimihiro Susumu, James B. Delehanty, Bing C. Mei
Licensed content date	Aug 1, 2010
Type of Use	reuse in a dissertation / thesis
Volume number	9
Issue number	8
Requestor type	academic/educational
Format	print and electronic
Portion	figures/tables/illustrations
Number of figures/tables/illustrations	1
High-res required	no
Figures	Figure 1 b
Author of this NPG article	no
Your reference number	None
Title of your thesis / dissertation	Chemical Reactions on the Surface of Quantum Dots
Expected completion date	Jul 2015
Estimated size (number of pages)	None
Total	0.00 USD

Title: In Vivo Targeted Cancer Imaging, Sentinel Lymph Node Mapping and Multi-Channel Imaging with Biocompatible Silicon Nanocrystals

Author: Folarin Erogbogbo, Ken-Tye Yong, Indrajit Roy, et al

Publication: ACS Nano

Publisher: American Chemical Society

Date: Jan 1, 2011

PERMISSION/LICENSE IS GRANTED FOR YOUR ORDER AT NO CHARGE

This type of permission/license, instead of the standard Terms & Conditions, is sent to you because no fee is being charged for your order. Please note the following:

- Permission is granted for your request in both print and electronic formats, and translations.
- If figures and/or tables were requested, they may be adapted or used in part.
- Please print this page for your records and send a copy of it to your publisher/graduate school.
- Appropriate credit for the requested material should be given as follows: "Reprinted (adapted) with permission from (COMPLETE REFERENCE CITATION). Copyright (YEAR) American Chemical Society." Insert appropriate information in place of the capitalized words.
- One-time permission is granted only for the use specified in your request. No additional uses are granted (such as derivative works or other editions). For any other uses, please submit a new request.

If credit is given to another source for the material you requested, permission must be obtained from that source.

BACK | CLOSE WINDOW

Title:	Extremely High Brightness from Polymer-Encapsulated Quantum Dots for Two-photon Cellular and Deep-tissue Imaging
Author:	Yanyan Fan, Helin Liu, Rongcheng Han, Lu Huang, Hao Shi, Yinlin Sha
Publication:	Scientific Reports
Publisher:	Nature Publishing Group
Date:	Apr 24, 2015

Creative Commons

Title: Core/Shell Quantum Dot Based Luminescent Solar Concentrators with Reduced Reabsorption and Enhanced Efficiency

Author: Igor Coropceanu, Moungi G. Bawendi

Publication: Nano Letters

Publisher: American Chemical Society

Date: Jul 1, 2014

PERMISSION/LICENSE IS GRANTED FOR YOUR ORDER AT NO CHARGE

This type of permission/license, instead of the standard Terms & Conditions, is sent to you because no fee is being charged for your order. Please note the following:

- Permission is granted for your request in both print and electronic formats, and translations.
- If figures and/or tables were requested, they may be adapted or used in part.
- Please print this page for your records and send a copy of it to your publisher/graduate school.
- Appropriate credit for the requested material should be given as follows: "Reprinted (adapted) with permission from (COMPLETE REFERENCE CITATION). Copyright (YEAR) American Chemical Society." Insert appropriate information in place of the capitalized words.
- One-time permission is granted only for the use specified in your request. No additional uses are granted (such as derivative works or other editions). For any other uses, please submit a new request.

If credit is given to another source for the material you requested, permission must be obtained from that source.

Title: Photodriven Charge Separation Dynamics in CdSe/ZnS Core/Shell Quantum Dot/Cobaloxime Hybrid for Efficient Hydrogen Production

Author: Jier Huang, Karen L. Mulfort, Pingwu Du, et al

Publication: Journal of the American Chemical Society

Publisher: American Chemical Society

Date: Oct 1, 2012

PERMISSION/LICENSE IS GRANTED FOR YOUR ORDER AT NO CHARGE

This type of permission/license, instead of the standard Terms & Conditions, is sent to you because no fee is being charged for your order. Please note the following:

- Permission is granted for your request in both print and electronic formats, and translations.
- If figures and/or tables were requested, they may be adapted or used in part.
- Please print this page for your records and send a copy of it to your publisher/graduate school.
- Appropriate credit for the requested material should be given as follows: "Reprinted (adapted) with permission from (COMPLETE REFERENCE CITATION). Copyright (YEAR) American Chemical Society." Insert appropriate information in place of the capitalized words.
- One-time permission is granted only for the use specified in your request. No additional uses are granted (such as derivative works or other editions). For any other uses, please submit a new request.

If credit is given to another source for the material you requested, permission must be obtained from that source.

BACK | CLOSE WINDOW

Title:	Cation Exchange: A Versatile Tool for Nanomaterials Synthesis
Author:	Brandon J. Beberwyck, Yogesh Surendranath, A. Paul Alivisatos
Publication:	The Journal of Physical Chemistry C
Publisher:	American Chemical Society
Date:	Oct 1, 2013

PERMISSION/LICENSE IS GRANTED FOR YOUR ORDER AT NO CHARGE

This type of permission/license, instead of the standard Terms & Conditions, is sent to you because no fee is being charged for your order. Please note the following:

- Permission is granted for your request in both print and electronic formats, and translations.
- If figures and/or tables were requested, they may be adapted or used in part.
- Please print this page for your records and send a copy of it to your publisher/graduate school.
- Appropriate credit for the requested material should be given as follows: "Reprinted (adapted) with permission from (COMPLETE REFERENCE CITATION). Copyright (YEAR) American Chemical Society." Insert appropriate information in place of the capitalized words.
- One-time permission is granted only for the use specified in your request. No additional uses are granted (such as derivative works or other editions). For any other uses, please submit a new request.

If credit is given to another source for the material you requested, permission must be obtained from that source.

BACK | CLOSE WINDOW

Title: Less Is More. Cation Exchange and the Chemistry of the Nanocrystal Surface

Author: Yolanda Justo, Laxmi Kishore Sagar, Stijn Flamee, et al

Publication: ACS Nano

Publisher: American Chemical Society

Date: Aug 1, 2014

PERMISSION/LICENSE IS GRANTED FOR YOUR ORDER AT NO CHARGE

This type of permission/license, instead of the standard Terms & Conditions, is sent to you because no fee is being charged for your order. Please note the following:

- Permission is granted for your request in both print and electronic formats, and translations.
- If figures and/or tables were requested, they may be adapted or used in part.
- Please print this page for your records and send a copy of it to your publisher/graduate school.
- Appropriate credit for the requested material should be given as follows: "Reprinted (adapted) with permission from (COMPLETE REFERENCE CITATION). Copyright (YEAR) American Chemical Society." Insert appropriate information in place of the capitalized words.
- One-time permission is granted only for the use specified in your request. No additional uses are granted (such as derivative works or other editions). For any other uses, please submit a new request.

If credit is given to another source for the material you requested, permission must be obtained from that source.

Title: Surface Ion Engineering of Mn2+-Doped ZnS Quantum Dots Using Ion-Exchange Resins

Author: Raihana Begum, Satyapriya Bhandari, Arun Chattopadhyay

Publication: Langmuir

Publisher: American Chemical Society

Date: Jun 1, 2012

PERMISSION/LICENSE IS GRANTED FOR YOUR ORDER AT NO CHARGE

This type of permission/license, instead of the standard Terms & Conditions, is sent to you because no fee is being charged for your order. Please note the following:

- Permission is granted for your request in both print and electronic formats, and translations.
- If figures and/or tables were requested, they may be adapted or used in part.
- Please print this page for your records and send a copy of it to your publisher/graduate school.
- Appropriate credit for the requested material should be given as follows: "Reprinted (adapted) with permission from (COMPLETE REFERENCE CITATION). Copyright (YEAR) American Chemical Society." Insert appropriate information in place of the capitalized words.
- One-time permission is granted only for the use specified in your request. No additional uses are granted (such as derivative works or other editions). For any other uses, please submit a new request.

If credit is given to another source for the material you requested, permission must be obtained from that source.

BACK | CLOSE WINDOW

Title: Expanding the Chemical Versatility of Colloidal Nanocrystals Capped with Molecular Metal Chalcogenide Ligands

Author: Maksym V. Kovalenko, Maryna I. Bodnarchuk, Jana Zaumseil, et al

Publication: Journal of the American Chemical Society

Publisher: American Chemical Society

Date: Jul 1, 2010

PERMISSION/LICENSE IS GRANTED FOR YOUR ORDER AT NO CHARGE

This type of permission/license, instead of the standard Terms & Conditions, is sent to you because no fee is being charged for your order. Please note the following:

- Permission is granted for your request in both print and electronic formats, and translations.
- If figures and/or tables were requested, they may be adapted or used in part.
- Please print this page for your records and send a copy of it to your publisher/graduate school.
- Appropriate credit for the requested material should be given as follows: "Reprinted (adapted) with permission from (COMPLETE REFERENCE CITATION). Copyright (YEAR) American Chemical Society." Insert appropriate information in place of the capitalized words.
- One-time permission is granted only for the use specified in your request. No additional uses are granted (such as derivative works or other editions). For any other uses, please submit a new request.

If credit is given to another source for the material you requested, permission must be obtained from that source.

BACK | CLOSE WINDOW

Title: Inorganically Functionalized PbS–CdS Colloidal Nanocrystals: Integration into Amorphous Chalcogenide Glass and Luminescent Properties

Author: Maksym V. Kovalenko, Richard D. Schaller, Dorota Jarzab, et al

Publication: Journal of the American Chemical Society

Publisher: American Chemical Society

Date: Feb 1, 2012

PERMISSION/LICENSE IS GRANTED FOR YOUR ORDER AT NO CHARGE

This type of permission/license, instead of the standard Terms & Conditions, is sent to you because no fee is being charged for your order. Please note the following:

- Permission is granted for your request in both print and electronic formats, and translations.
- If figures and/or tables were requested, they may be adapted or used in part.
- Please print this page for your records and send a copy of it to your publisher/graduate school.
- Appropriate credit for the requested material should be given as follows: "Reprinted (adapted) with permission from (COMPLETE REFERENCE CITATION). Copyright (YEAR) American Chemical Society." Insert appropriate information in place of the capitalized words.
- One-time permission is granted only for the use specified in your request. No additional uses are granted (such as derivative works or other editions). For any other uses, please submit a new request.

If credit is given to another source for the material you requested, permission must be obtained from that source.

BACK | CLOSE WINDOW

RSC | Advancing the Chemical Sciences

Royal Society of Chemistry
Thomas Graham House
Science Park
Milton Road
Cambridge
CB4 0WF

Tel: +44 (0)1223 420 066
Fax: +44 (0)1223 423 623
Email: contracts-copyright@rsc.org

www.rsc.org

Acknowledgements to be used by RSC authors

Authors of RSC books and journal articles can reproduce material (for example a figure) from the RSC publication in a non-RSC publication, including theses, without formally requesting permission providing that the correct acknowledgement is given to the RSC publication. This permission extends to reproduction of large portions of text or the whole article or book chapter when being reproduced in a thesis.

The acknowledgement to be used depends on the RSC publication in which the material was published and the form of the acknowledgements is as follows:

- For material being reproduced from an article in *New Journal of Chemistry* the acknowledgement should be in the form:
  - [Original citation] - Reproduced by permission of The Royal Society of Chemistry (RSC) on behalf of the Centre National de la Recherche Scientifique (CNRS) and the RSC
- For material being reproduced from an article *Photochemical & Photobiological Sciences* the acknowledgement should be in the form:
  - [Original citation] - Reproduced by permission of The Royal Society of Chemistry (RSC) on behalf of the European Society for Photobiology, the European Photochemistry Association, and RSC
- For material being reproduced from an article in *Physical Chemistry Chemical Physics* the acknowledgement should be in the form:
  - [Original citation] - Reproduced by permission of the PCCP Owner Societies
- For material reproduced from books and any other journal the acknowledgement should be in the form:
  - [Original citation] - Reproduced by permission of The Royal Society of Chemistry

The acknowledgement should also include a hyperlink to the article on the RSC website.

The form of the acknowledgement is also specified in the RSC agreement/licence signed by the corresponding author.

Except in cases of republication in a thesis, this express permission does not cover the reproduction of large portions of text from the RSC publication or reproduction of the whole article or book chapter.

A publisher of a non-RSC publication can use this document as proof that permission is granted to use the material in the non-RSC publication.

VAT Registration Number: GB 342 1764 71 Registered Charity Number: 207890

Title:	Surface Complexation Reaction for Phase Transfer of Hydrophobic Quantum Dot from Nonpolar to Polar Medium
Author:	Satyapriya Bhandari, Shilaj Roy, Sabyasachi Pramanik, et al
Publication:	Langmuir
Publisher:	American Chemical Society
Date:	Sep 1, 2014

PERMISSION/LICENSE IS GRANTED FOR YOUR ORDER AT NO CHARGE

This type of permission/license, instead of the standard Terms & Conditions, is sent to you because no fee is being charged for your order. Please note the following:

- Permission is granted for your request in both print and electronic formats, and translations.
- If figures and/or tables were requested, they may be adapted or used in part.
- Please print this page for your records and send a copy of it to your publisher/graduate school.
- Appropriate credit for the requested material should be given as follows: "Reprinted (adapted) with permission from (COMPLETE REFERENCE CITATION). Copyright (YEAR) American Chemical Society." Insert appropriate information in place of the capitalized words.
- One-time permission is granted only for the use specified in your request. No additional uses are granted (such as derivative works or other editions). For any other uses, please submit a new request.

BACK | CLOSE WINDOW

Title: Double Channel Emission from a Redox Active Single Component Quantum Dot Complex

Author: Satyapriya Bhandari, Shilaj Roy, Sabyasachi Pramanik, et al

Publication: Langmuir

Publisher: American Chemical Society

Date: Jan 1, 2015

PERMISSION/LICENSE IS GRANTED FOR YOUR ORDER AT NO CHARGE

This type of permission/license, instead of the standard Terms & Conditions, is sent to you because no fee is being charged for your order. Please note the following:

- Permission is granted for your request in both print and electronic formats, and translations.
- If figures and/or tables were requested, they may be adapted or used in part.
- Please print this page for your records and send a copy of it to your publisher/graduate school.
- Appropriate credit for the requested material should be given as follows: "Reprinted (adapted) with permission from (COMPLETE REFERENCE CITATION). Copyright (YEAR) American Chemical Society." Insert appropriate information in place of the capitalized words.
- One-time permission is granted only for the use specified in your request. No additional uses are granted (such as derivative works or other editions). For any other uses, please submit a new request.

Title: Surface Complexation-Based Biocompatible Magnetofluorescent Nanoprobe for Targeted Cellular Imaging

Author: Satyapriya Bhandari, Rumi Khandelia, Uday Narayan Pan, et al

Publication: Applied Materials

Publisher: American Chemical Society

Date: Aug 1, 2015

PERMISSION/LICENSE IS GRANTED FOR YOUR ORDER AT NO CHARGE

This type of permission/license, instead of the standard Terms & Conditions, is sent to you because no fee is being charged for your order. Please note the following:

- Permission is granted for your request in both print and electronic formats, and translations.
- If figures and/or tables were requested, they may be adapted or used in part.
- Please print this page for your records and send a copy of it to your publisher/graduate school.
- Appropriate credit for the requested material should be given as follows: "Reprinted (adapted) with permission from (COMPLETE REFERENCE CITATION). Copyright (YEAR) American Chemical Society." Insert appropriate information in place of the capitalized words.
- One-time permission is granted only for the use specified in your request. No additional uses are granted (such as derivative works or other editions). For any other uses, please submit a new request.

TH-1435_10612225